

University of Nebraska - Lincoln

DigitalCommons@University of Nebraska - Lincoln

---

Engineering Mechanics Dissertations & Theses

Mechanical & Materials Engineering,  
Department of

12-2009

## Thermodynamically consistent large deformation constitutive model for glassy polymers

Ashwani Kumar Goel

University of Nebraska - Lincoln, ashwani@huskers.unl.edu

Follow this and additional works at: <https://digitalcommons.unl.edu/engmechdiss>



Part of the [Mechanical Engineering Commons](#)

---

Goel, Ashwani Kumar, "Thermodynamically consistent large deformation constitutive model for glassy polymers" (2009). *Engineering Mechanics Dissertations & Theses*. 4.

<https://digitalcommons.unl.edu/engmechdiss/4>

This Article is brought to you for free and open access by the Mechanical & Materials Engineering, Department of at DigitalCommons@University of Nebraska - Lincoln. It has been accepted for inclusion in Engineering Mechanics Dissertations & Theses by an authorized administrator of DigitalCommons@University of Nebraska - Lincoln.

**Thermodynamically consistent large deformation constitutive model for  
glassy polymers**

by

Ashwani Kumar Goel

A DISSERTATION

Presented to the Faculty of  
The Graduate College at the University of Nebraska  
In Partial Fulfillment of Requirements  
For the Degree of Doctor of Philosophy

Major: Engineering

Under the Supervision of Professor Mehrdad Negahban

Lincoln, Nebraska

December, 2009

Thermodynamically consistent large deformation constitutive model for glassy  
polymers

Ashwani Kumar Goel, Ph.D.

University of Nebraska, 2009

Adviser: Mehrdad Negahban

Polycarbonate(PC), like most glassy polymers when undergoing large deformations exhibits a very complex thermo-mechanical response. We look at PC as a model glassy polymer and examine its response to changes in loading rate, loading direction and temperature. We show that plastic flow in compression is accompanied by a change in the elastic response of PC from isotropic to anisotropic. This provides the necessity to introduce a new modeling method that can capture these changes. A finite deformation plasticity like thermodynamically consistent model is developed to capture this and the observed rate and temperature dependence. For this modeling method, we need to provide expressions for the elastic response, flow of the plastic deformation gradient and also provide methods to calculate the back stress. In an effort to mathematically capture the observed response of PC under a broad range of mechanical loads and thermal conditions, a protocol of experiments has been developed that can be used to systematically evaluate the parameters needed to characterize PC, and with potential for application to other glassy polymers. This experimental protocol combines traditional mechanical testing, ultrasonic wave speed measurements, dynamic kolsky bar methods and standard calorimetric studies to systematically construct a model for PC.

Polycarbonate (PC) is a tough transparent glassy polymer that is used for many structural applications, particularly as components of window and protective armor. Below its glass transition temperature of about  $150^{\circ}C$ , PC plastically flows under load, showing a rate dependent response and will not fully recover after removal of load, showing elements of plastic flow. As a result, the response of PC has been modeled using a rate dependent type model. When plastically deformed below the glass transition temperature, unlike PMMA, which is also a glassy polymer, PC will show very strong anisotropic elastic response. This can be seen from ultrasonic measurement of elastic wave-speed moduli after different levels of plastic compression. This is the first indication that traditional modeling methods based on plasticity will not work for capturing the response of PC if they are based on stress response models that only depend on the elastic deformation gradient. One needs to include additional history defining parameters in the stress response function, such as the plastic deformation gradient, to capture this development of anisotropy with plastic flow.

## Acknowledgements

I would like to take this opportunity to thank the people who supported me in different ways and made my stay enjoyable. First and foremost, I would like to express my sincere gratitude to my adviser, Dr. Mehrdad Negahban for his support and guidance over more than five years. It has definitely been his patience guidance and invaluable advice that have made this dissertation possible. His confidence in my work encouraged me to take on challenges and helped me solving the numerous problems which at all are not possible to include in one dissertation.

Next, I would like to express my sincere gratitude to Dr. Atarod Azizinamini for his support to develop large deformation finite element software which can be used for designing complex bridges. I would also like to express my thanks to Dr. Joseph Turner and Dr. Li Tan who have given me an opportunity to work related to biological and biomedical applications. I have not included any of this work in this dissertation but it keeps me wondering that how large deformation problems can be used in many different applications. The experience I got during these projects were enormous. I am also very grateful to Dr. Ruqiang Feng for his expert discussions related to Kolsky bar experiments and would like to thank him and Dr. Florin Bobaru to have accepted to be a part of the jury and for evaluating my dissertation work.

I would also like to acknowledge Dr. Jean-Marc Saiter for taking good care of me and my group in trip to Study Abroad in France. I will never forget that month which I spent in France.

I also wish to acknowledge Mr. Kyle Strabala, Mr. Jason Vogeler, Mr. Pierre De-

labarre, Mr. Jonathan Hein and Mr. Nathan Oliveira for carrying out valuable experiments on polycarbonate and providing me with the experimental results sooner than I expected. Their experimental efforts have been very helpful for me to analyze the data and use the analysis to develop a constitutive model.

I further would like to thank Mrs. Setareh Makinejad for inviting me and my family to her house over and over again and felt like I am at my home (I will always remember all the thanks giving dinner. I dont remember missing any of it.) I further would like to thank all of my colleagues for their friendship, namely, Ms. Lili Zhang, Dr. Philip Yuya, Dr. Goutam Ghoshal, Mr. Shailesh Ganpule, Mr. Roberto Soares, Dr. Mickael Arnoult, Mr. Ardalan Sherafati, Mr. Kittti Rattanadit, Mr. Ocelio Lima, Mr. Jianbin Zhu, Mr. Monchai Duangpanya and many others.

Now, at last but not a least, I would like to thank my family. My wife, Shipra, I love you and is very lucky to say that I am the one who got you. You are a very nice wife and a great Mom, which reminded me about our darling daughter, Siya. Siya, you are a very nice daughter and growing. Your kid-dish talk will always remain in my memory. I would also like to thank my parents, Mr. Vinod Kumar Goyal and Mrs. Sunita Goyal, I can never begin to repay you for the opportunity and encouragement you had given me. In spite of having the worst loss (departure of my brother) you insisted me to do Ph.D. and I know that I cannot be even half a good parent as you are. I would also like to thank my mother in law, Mrs. Sneh Gupta, for her support and always giving me encouragement in my work.

Finally, I would like to thank my brother, Anup Goyal, who has left me in this

world alone, but his memories will always be with me forever. I would like to dedicate my dissertation to him.

The research in this dissertation was partially supported by the U.S. Army Research Laboratory(ARL) under the RMAC-RTP Cooperative Agreement No. W911NF-04-2-0011.

# Contents

<b>List of Figures</b>	<b>x</b>
<b>List of Tables</b>	<b>xv</b>
<b>1 Introduction</b>	<b>1</b>
1.1 General introduction . . . . .	1
1.2 Background . . . . .	2
1.3 Hyperelastic constitutive modeling . . . . .	5
1.4 Polymer constitutive modeling . . . . .	7
1.5 Motivation of the thesis . . . . .	9
1.5.1 Modeling for stress . . . . .	10
1.5.2 Experimentally evaluating and modeling of equilibrium stress . . . . .	11
1.5.3 Conversion of plastic work to heat during high strain rate deformation of glassy polymer . . . . .	13
1.6 Outline . . . . .	14
<b>2 Kinematics, balance laws and notations</b>	<b>18</b>
2.1 Introduction . . . . .	18
2.2 Kinematics . . . . .	19
2.2.1 Elastic and plastic deformation gradient . . . . .	21
2.2.2 Incompressible plastic flow assumption . . . . .	23
2.3 Balance laws . . . . .	24
2.3.1 Conservation of mass . . . . .	25
2.3.2 Balance of linear momentum . . . . .	25
2.3.3 Balance of angular momentum . . . . .	26
2.3.4 Balance of work and energy . . . . .	26
2.3.5 Entropy and the entropy production inequality . . . . .	27
2.4 Finite deformation mechanical theory . . . . .	28
2.4.1 Rigid body motions . . . . .	29
2.4.2 Material symmetry . . . . .	31
2.5 Thermodynamic models with internal parameters . . . . .	32
2.6 Heat generation and flow . . . . .	37

2.7	Summary and conclusion . . . . .	39
<b>3</b>	<b>Constitutive modeling and assumptions</b>	<b>40</b>
3.1	Mechanical analog for the model . . . . .	40
3.2	Response of the mechanical analog for different tests . . . . .	43
3.2.1	Quasistatic loading . . . . .	43
3.2.2	Quasi-fast deformation at equilibrium . . . . .	44
3.2.3	Ultrasonic testing at constant load . . . . .	45
3.3	Constitutive model . . . . .	46
3.4	Assumed form of the free energy . . . . .	48
3.5	Summary and conclusion . . . . .	50
<b>4</b>	<b>Modeling the nonlinear thermo-elastic response of glassy polycarbonate</b>	<b>51</b>
4.1	Introduction . . . . .	51
4.2	Experimental measurements . . . . .	52
4.3	Modeling consideration . . . . .	53
4.4	Model used for free energy . . . . .	57
4.5	Fitting the model to experimental results . . . . .	57
4.6	Summary and conclusion . . . . .	60
<b>5</b>	<b>Modeling the development of elastic anisotropy with plastic flow</b>	<b>64</b>
5.1	Introduction . . . . .	65
5.2	Experimental measurements . . . . .	67
5.3	Modeling considerations . . . . .	70
5.4	Fitting the model to the results from compression . . . . .	76
5.5	Summary and conclusion . . . . .	81
<b>6</b>	<b>The development of elastic anisotropy at different temperature</b>	<b>84</b>
6.1	Abstract . . . . .	84
6.2	Experimental measurements . . . . .	85
6.3	Experimental results . . . . .	87
6.4	Fitting the model to results from compression at different temperature . . . . .	89
6.5	Introducing the effect of load . . . . .	91
6.6	Summary and conclusion . . . . .	95
<b>7</b>	<b>Experimentally evaluating equilibrium stress in uniaxial tests</b>	<b>98</b>
7.1	Introduction . . . . .	98
7.1.1	Background . . . . .	98
7.1.2	Method of approach . . . . .	99
7.1.3	Results presented . . . . .	99
7.1.4	Conclusions . . . . .	100
7.2	Literature review . . . . .	100
7.3	Theoretical foundation . . . . .	103
7.4	Proposed experimental method . . . . .	107
7.5	Materials and experimental setup . . . . .	109

7.6	Error analysis . . . . .	110
7.7	Results for polycarbonate at different temperatures . . . . .	115
7.8	Summary . . . . .	118
<b>8</b>	<b>Thermodynamically consistent model for back stress</b>	<b>119</b>
8.1	Background . . . . .	120
8.2	Partitioning the stress of the slow and fast elements . . . . .	121
8.3	Combining the models for free energy . . . . .	126
8.4	Constitutive model for back stress . . . . .	129
8.5	Free energy assumption of the back stress . . . . .	131
8.6	Fitting the model to experimental results from compression . . . . .	135
8.7	Summary and conclusion . . . . .	136
<b>9</b>	<b>Heat generation and heat capacity</b>	<b>138</b>
9.1	Heat capacity for the sample at zero stress and zero elastic and plastic strain	139
9.2	Experimental results and fitting the model . . . . .	142
9.3	Results and conclusion . . . . .	144
<b>10</b>	<b>Flow rule for glassy polycarbonate</b>	<b>145</b>
10.1	Flow rule and second law of thermodynamics . . . . .	145
10.2	Experimental results on monotonic compression . . . . .	147
10.3	Conversion of plastic work to heat . . . . .	151
10.4	Modeling the flow rules . . . . .	157
10.4.1	Models used for stress and back stress . . . . .	158
10.4.2	Calculation of plastic flow at low strain rates . . . . .	160
10.4.3	Calculation of plastic flow at high strain rates . . . . .	163
10.5	Summary and conclusion . . . . .	170
<b>11</b>	<b>Conclusion and scope for future work</b>	<b>173</b>
11.1	Conclusion . . . . .	173
11.2	Constitutive model . . . . .	176
11.2.1	Constitutive model for stress . . . . .	176
11.2.2	Constitutive model for back stress . . . . .	178
11.2.3	Over stress contribution for low and high strain rates . . . . .	179
11.2.4	Flow rule . . . . .	179
11.3	Future work . . . . .	180
<b>12</b>	<b>Appendix</b>	<b>182</b>
12.1	Appendix A: Calculation of derivatives of invariants . . . . .	183
12.2	Appendix B: Calculation of stress and its rate . . . . .	184
	<b>Bibliography</b>	<b>189</b>

# List of Figures

- 1.1 Stress strain curve for glassy polycarbonate at room temperature and 0.1 1/s strain rate. . . . . 3
- 1.2 Monotonic compression experiments (from [1, 2, 3]) for different strain rates at room temperature. . . . . 4
- 1.3 Monotonic compression experiments (from [2]) for different temperatures at 0.11s<sup>-1</sup>. . . . . 5
- 1.4 Axial and transverse modulus reported as a function of extent of plastic deformation in tension for PVC, PMMA, PS, and PC (from Ward [4]). The axial longitudinal modulus increases while the transverse longitudinal modulus decreases with plastic strain. . . . . 11
- 1.5 Stress buildup and stress relaxation seen in PMMA above its glass-transition temperature (from Negahban [5]). . . . . 13
  
- 2.1 Point P and Q changing from reference to current configuration. . . . . 20
- 2.2 Decomposition of the deformation gradient **F** into a plastic deformation gradient **F<sup>p</sup>** and an elastic deformation gradient **F<sup>e</sup>** (from Negahban [6]). . . . . 22
- 2.3 Two deformation histories that are identical but for the fact that each configuration in one is obtained by an arbitrary rigid body translation and rotation of the configuration of other is assumed to simply rotate the traction vector by the final amount of rotation (from Negahban [6]). . . . . 29
- 2.4 Schematic of the reorganization of the neighbourhood of influence of a point to get a new configuration that is materially equivalent (from Negahban [6]). . . . . 32
- 2.5 Reorganization of the initial configuration that is associated with the materials symmetry leaves the material indistinguishable from the original material so that the response to any history would result in identical stress for the original and reorganized configuration (from Negahban [6]). . . . . 33
  
- 3.1 Mechanical analog of proposed constitutive model for rate dependent thermal plasticity. . . . . 41
- 3.2 Mechanical analog corresponding to the quasistatic testing. . . . . 44
- 3.3 Mechanical analog corresponding to the quasi fast loading at equilibrium . . . . . 44

3.4	Mechanical analog corresponding to the rapid load $\Delta F$ superimposed with force $F_o$ for an ultrasonic testing. . . . .	45
3.5	Mechanical analog corresponding to an ultrasonic testing . . . . .	46
4.1	Specific volume for PC as a function of temperature at various pressure (Data extracted from [7]). . . . .	54
4.2	Longitudinal wave modulus for PC at different pressure and temperature (Data extracted from [7]). . . . .	54
4.3	Shear wave modulus for PC at different pressure and temperature (Data extracted from [7]). . . . .	55
4.4	Change of the bulk modulus $\kappa_\theta$ with temperature at different pressures and the fit from the model. . . . .	60
4.5	Change of the shear modulus $G_\theta$ with temperature at various pressures and the fit by the model. . . . .	61
4.6	Change of combined modulus at various pressures and the fit from the model. . . . .	61
4.7	Comparison of model results with experimentally measured longitudinal wave moduli (from Masubichi et al. [7]) at different temperature and pressure. . . . .	62
4.8	Comparison of model results with experimentally measured shear wave moduli (from Masubichi et al. [7]) at different temperature and pressure. . . . .	62
5.1	Axial and transverse modulus reported as a function of extent of plastic deformation in tension for PVC, PMMA, PS, and PC (from Ward [4]). The axial longitudinal modulus increases while the transverse longitudinal modulus decreases with plastic strain. . . . .	66
5.2	Description of the Pulse echo method (from Goel et al. [8]). . . . .	68
5.3	Plastically compressed PC sample after cutting for transverse wave speed measurements (from Goel et al. [8]). . . . .	69
5.4	Summary of testing: (a) original PC cylinder, (b) compressed PC cylinder, (c) ultrasonic testing in the axial direction, (d) sample cut and ultrasonically tested in transverse direction (from Goel et al. [8]). . . . .	70
5.5	Axial and transverse longitudinal wave modulus at different plastic strains (from Goel et al. [8]). . . . .	71
5.6	Axial and transverse shear wave modulus at different plastic strains (from Goel et al. [8]). . . . .	71
5.7	Change of the isotropic bulk modulus with plastic deformation. . . . .	78
5.8	Change of the isotropic shear modulus with plastic flow. . . . .	79
5.9	Change of $\rho_o \frac{\partial \psi}{\partial I_7^*}$ as a function of plastic flow. . . . .	79
5.10	Comparison of model results with experimentally measured wave moduli $E_a$ and $E_t$ (From Goel et al. [8]) for the given plastic strains. . . . .	80
5.11	Comparison of model results with experimentally measured wave moduli $G_a$ and $G_t$ (From Goel et al. [8]) for the given plastic strains. . . . .	80
5.12	Comparison between model predictions and results presented by Ward [4] for longitudinal modulus during after extension. . . . .	81
5.13	Comparison between model predictions and results presented by Ward [4] for shear modulus during after extension. . . . .	82

6.1	Density measured before plastic deformation as a function of temperature for PC using a weighing method at room temperature and the ARAMIS stereo optical system strain at higher temperatures (from Strabala et al. [9]). . . . .	86
6.2	Summary of testing: (a) original PC cylinder, (b) compressed PC cylinder, (c) ultrasonic testing in the axial direction, (d) sample cut and ultrasonically tested in transverse direction (from Strabala et al. [9]). . . . .	87
6.3	The axial longitudinal wave modulus (in MPa) at different plastic strains for different temperatures (from Strabala et al. [9]). . . . .	88
6.4	The transverse longitudinal wave modulus (in MPa) at different plastic strains for different temperatures (from Strabala et al. [9]). . . . .	88
6.5	Change of the isotropic factor $A_{iso}(\theta)$ with temperature. . . . .	91
6.6	Change of the anisotropic factor $A_{aniso}(\theta)$ with temperature. . . . .	92
6.7	Comparison of model results with experimentally measured wave moduli $E_a$ (from Strabala et al. [9]) for the given plastic strains at different temperatures. . . . .	92
6.8	Comparison of model results with experimentally measured wave moduli $E_t$ (from Strabala et al. [9]) for the given plastic strains at different temperatures. . . . .	93
6.9	Comparison of model results with experimentally measured longitudinal wave moduli by Masubichi et al [7] in confined compression at different temperature and pressure. . . . .	96
6.10	Comparison of model results with experimentally measured shear wave moduli Masubichi et al [7] in confined compression at different temperature and pressure. . . . .	96
7.1	Stress buildup and stress relaxation seen in PMMA above its glass-transition temperature (From Negahban [5]). . . . .	101
7.2	Schematic of proposed experiment to calculate the equilibrium stress and the associated tangent modulus (bottom), and a typical plot of the tangent modulus as a function of the axial stress in the cycle of unloading and loading for polycarbonate (top). . . . .	108
7.3	Typical cyclic loading in compression of polycarbonate at room temperature and the calculated back stress (from Goel et al. [10]) . . . . .	110
7.4	Typical transverse strain response obtained from the experiment (from Goel et al. [10]), the response that would result for an incompressible material, and the transverse strain measured at equilibrium. . . . .	111
7.5	Tangent modulus of polycarbonate at equilibrium in compression at room temperature. . . . .	111
7.6	Local Poisson's ratio of polycarbonate at equilibrium in compression at room temperature. . . . .	112
7.7	Strain history measured for polycarbonate in compression at room temperature (from Goel et al. [10]). . . . .	112
7.8	Comparison between calculated error for equilibrium stress and measurements calculated from multiple tests. . . . .	113
7.9	Comparison between calculated error for tangent modulus and measurements calculated from multiple tests. . . . .	113
7.10	Equilibrium stress and error for different temperatures (from [11]). . . . .	116

7.11	Local poisson's ratio at equilibrium for different temperatures (from [11]). . .	116
7.12	Tangent modulus at equilibrium for different temperatures (from [11]). . . .	117
8.1	Mechanical analog of proposed constitutive model for rate dependent thermal plasticity. . . . .	121
8.2	Mechanical analog corresponding to the quasi fast loading at equilibrium. .	122
8.3	Mechanical analog corresponding to the ultrasonic testing. . . . .	122
8.4	Comparison of tangent modulus from the ultrasonic model and measured from experimental cyclic loading. . . . .	125
8.5	Comparison of quasistatic stress model with the cyclic experiments. . . . .	126
8.6	In plane deformation for simple shear . . . . .	134
8.7	Stress strain curve response in shear from the model with $G_\infty = G_{\infty 1}$ and $G_{\infty 2} = 0$ . . . . .	134
8.8	The experimental (from Goel et al. [11]) and the model for back stress at room temperature . . . . .	136
8.9	Comparison of experiment (from [11]) with model for back stress at different temperature . . . . .	137
9.1	Specific heat for polycarbonate at different temperature (from [12]). . . . .	143
10.1	Monotonic compression experiments for different strain rates at room temperature (from [1, 2, 3]). . . . .	148
10.2	Monotonic compression experiments for different strain rates at $60^\circ C$ (from [1, 2, 3]). . . . .	148
10.3	Monotonic compression experiments for different strain rates at $100^\circ C$ (from [1, 2, 3]). . . . .	149
10.4	Monotonic compression experiments for different temperatures at $0.11s^{-1}$ (from [2]). . . . .	149
10.5	Monotonic compression experiments for different temperatures at $100s^{-1}$ (from [2]). . . . .	150
10.6	Monotonic compression experiments for different temperatures at $1120s^{-1}$ (from [3]). . . . .	150
10.7	Schematic of the stress and equilibrium stress. . . . .	153
10.8	Comparison of model prediction and experimentally evaluated temperature rise from Lerch et al. [13]. . . . .	153
10.9	Comparison of temperature rise from model at room temperature for different strain rates assuming adiabatic deformations. . . . .	154
10.10	Comparison of temperature rise from model at $60^\circ C$ for different strain rates assuming adiabatic deformations. . . . .	155
10.11	Comparison of temperature rise from model at $100^\circ C$ for different strain rates assuming adiabatic deformations. . . . .	155
10.12	Comparison of experimental (from [2]) and model under isothermal condition for 0.11 1/s and at room temperature. . . . .	156
10.13	Experimental (from [2]) and model isothermal monotonic compression results for 1.21 1/s and at different temperatures. . . . .	156

10.14	Experimental (from [2]) and model isothermal monotonic compression results for 108 1/s and at different temperatures. . . . .	157
10.15	Schematic for uniaxial compression for polycarbonate sample . . . . .	161
10.16	Experimental monotonic compression experiments (from [1, 2]) at room temperature. . . . .	161
10.17	The material parameter $\beta_{s1}$ with respect to $\Delta S_s$ at 20% axial strain for strain rates 0.00011/s, 0.11/s and 1.21 1/s. . . . .	164
10.18	The material parameter $\beta_{s2}$ with respect to $\varepsilon_s^p$ for strain rate 0.11 1/s. . . . .	164
10.19	Change of $\beta_{s3}$ with temperature. . . . .	165
10.20	Comparison between the experimental response (from [2]) and the model results at 0.11 1/s at different temperatures. . . . .	165
10.21	The material parameter $\beta_{f1}$ with respect to $\Delta S_f$ at 20% axial strain for strain rates 23 1/s, 108 1/s and 1120 1/s. . . . .	167
10.22	The material parameter $\beta_{f2}$ with respect to $\varepsilon_f^p$ for strain rate 1120 1/s. . . . .	167
10.23	Change of $\beta_{f3}$ with temperature. . . . .	168
10.24	Comparison between the correction of experimental response (from [3]) to get an isothermal response and the model results at 1194 1/s at different temperatures. . . . .	168
10.25	Comparison between experimental (from [2, 3]) and model results at room temperature and at different strain rates. . . . .	169
10.26	Tangent modulus from model at different strain rates under monotonic compression at two particular strains (0.3% strain and 0.5% strain). . . . .	170
11.1	Experimental protocol used to develop a large deformation constitutive model.	176

# List of Tables

# Chapter 1

## Introduction

### 1.1 General introduction

Amorphous glassy polymers such as poly (methyl methacrylate) (PMMA) and polycarbonate (PC) due to their light weight, high impact strength and other desirable characteristics are being continuously used in various engineering applications to resist high rates of impact. They are not only considered in many commercial products applications such as in electrical and electronics application, optical application, medical applications but also in structural application which includes windscreens and transparent armor. Due to the application of glassy polymers in a broad range of structural application it is important to analyze its mechanical behavior; hence the characterization of the response of such polymers is of importance. The ultimate goal of this research project is to develop a thermodynamically consistent large deformation constitutive modeling structure for amorphous polymers that can capture the response for large range of strain, strain rates and temperatures and can be used for determining the response in various applications and

under complex loading.

This dissertation provides a modeling structure that can be used to capture a diverse set of experimental observations for glassy polycarbonate spanning a large range of strain, strain rates and temperature. In an effort to mathematically capture the observed response under a broad range of mechanical loads and thermal conditions, a method of modeling and protocol for experiments has been developed that can be used to systematically evaluate the parameters needed for this characterization. This experimental protocol includes multiaxial monotonic compression experiments at different strain rates and temperatures, ultrasonic wave speed measurements in the axial and transverse directions, uniaxial cyclic tests to systematically construct a large deformation thermodynamically consistent model which could capture the responses at large strains and different strain rates and temperatures.

## 1.2 Background

This dissertation is primarily concerned with the rate dependent mechanical behavior of materials, in particular polymers, with a focus on predicting large strain behavior at low and at very high strain rates. The description of the stress strain response of an amorphous polymer under uniform tension/compression is very well understood. Figure 1.1 shows the stress strain behavior of PC in uniaxial compression at 0.1 1/s strain rate. Region 1 in the figure is a nonlinear elastic region with a small rate dependence, reaches to the peak which depends on the strain rate and temperature. As shown by Ravichandar and Lu [14] any unloading below this peak point does not result in significant hysteresis or permanent

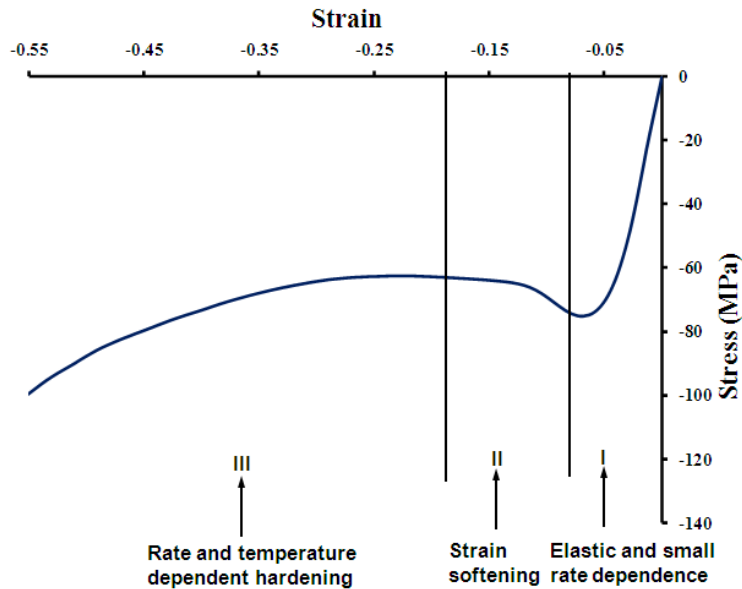


Figure 1.1: Stress strain curve for glassy polycarbonate at room temperature and 0.1 1/s strain rate.

strains. After yielding, the material possess an inelastic strain localization regions which appear in the form of micro shear bands causing the response of strain softening which is shown in Region 2 [14] and there is a drop in the true stress with plastic straining. These bands keep on accumulating and initiating plastic localization that in tension is associated with necking. The process in Region 3 is commonly called cold drawing and is a region where the active necking zone start to align plastically along the extension direction and this alignment give rise to strain hardening. Region 2 can also be explained as a transition from low plastic strain in Region 1 to high plastic strain in Region 3 which causes stress to drop.

The stress strain behavior explained in Figure 1.1 is strongly dependent on strain rate and temperature. Figure 1.2 shows the room temperature stress strain behavior for

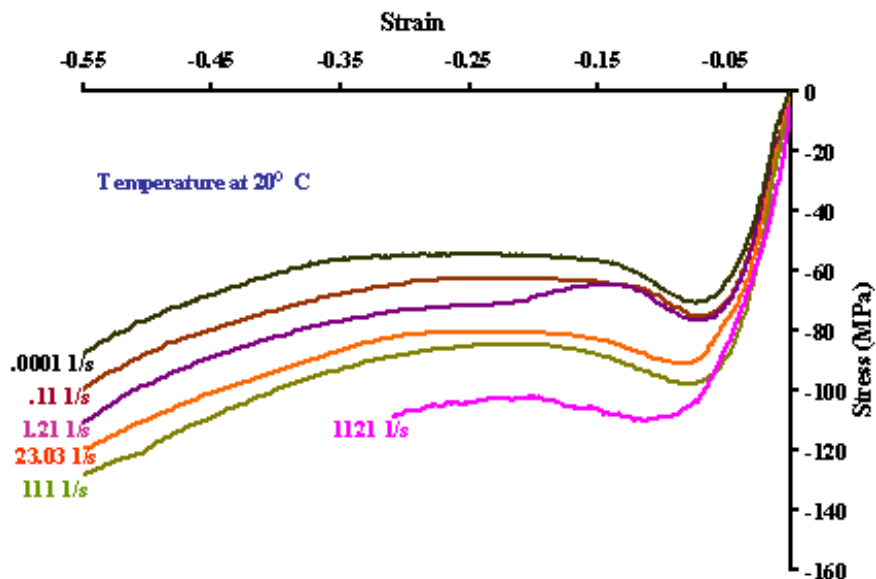


Figure 1.2: Monotonic compression experiments (from [1, 2, 3]) for different strain rates at room temperature.

glassy polycarbonate at different strain rates. As can be seen from the plot, with the increase in strain rate the stress level increases, but the effect is nonlinear such that if the rate is increased 100 times, the response does not increase by 100 times. This feature of amorphous polymer response is important to predict the behavior at very high strain rates. The same effect can be observed by comparing the response of PC at different temperatures but with the same strain rate. With the increase in temperature the response decreases due to thermal softening as shown in Figure 1.3 but again the effect is nonlinear. This is another factor which needs to be captured when modeling and predicting high rate behavior.

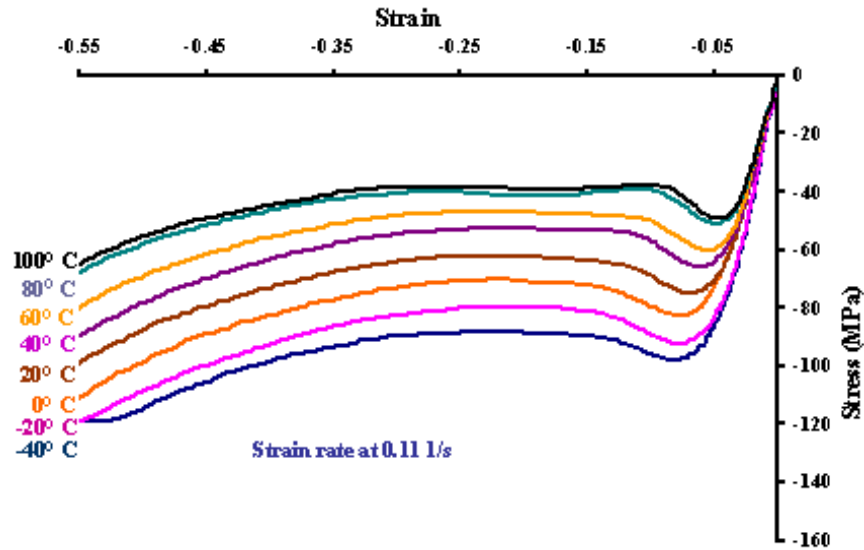


Figure 1.3: Monotonic compression experiments (from [2]) for different temperatures at  $0.11s^{-1}$ .

### 1.3 Hyperelastic constitutive modeling

Before discussing the constitutive models developed for a polymeric materials, let us discuss various modeling approaches that are used in the literature to develop hyperelastic constitutive models. The approaches based on hyperelastic models can then be used for polymeric materials. The modeling approaches can be classified into the three types depending upon the authors to develop a strain energy function.

The first kind of the models which are known as phenomenological models are the mathematical development of the free energy. The Mooney Model [15], Mooney Rivlin Model [16, 17], Biderman model [18], Haines-Wilson model [19], Ogden model [20] all comes under these form and the material parameters of these models are generally difficult to determine due to assumed form of the free energy.

The second type of model assumes the free energy of certain form which depends

on invariants and the derivative of free energy with respect to invariants are calculated from the experimental data. Rivlin and Saunders model [21] , Gent and Thomas model [22], Hart Smith model [23] are some of the examples of the model which fall into this form of modeling.

The third type of the model are developed from physical motivation. Such type of models are known as physics based models and are based on the physics of polymer chain network and statistical methods. It leads to a different strain energy function depending upon the microscopic response of polymer chains in the network. The Neo Hookean model [24] is the simplest physically based model and matches Mooney Rivlin model with only one material parameter but is derived from molecular chain statistics. It assumes that rubber material are constituted by a network of long flexible oriented chains linked by chemical bounds at junction points [25]. The 3 chain model used a non Gaussian chain elasticity. In 1942, Kuhn and Grun [26] used a non Gaussian theory to take into account the limiting extensibility of polymer chains and they derived the strain energy of the single chain. Later James and Guth [27], developed similar models where the network chains were distributed upon the principal stretches axis and Flory [28] and Treloar [29] assumed network chains are distributed upon four axis corresponding to the vertices of a regular tetrahedron. Later Arruda and Boyce [30] proposed a chain model with a distributed of chains upon eight directions corresponding to the vertices of a cube inscribed in the unit sphere. The model they developed was quite similar to three chain model but presents better agreement with experimental data for equibiaxial extension.

## 1.4 Polymer constitutive modeling

As discussed before, polymeric materials subjected to large strains have a rate dependent deformation response . There are many linear and nonlinear viscoelastic and viscoplastic constitutive models which have been developed to study the time dependent deformation of polymers, as well as the thermomechanical behavior of polymers under large deformation.

Traditionally, for an every small strain analysis, linear viscoelasticity has been used to simulate the material behavior [31]. In the linear viscoelastic models, combinations of springs and dashpots have been used to capture the rate dependent behavior. For the cases where the strains are large enough that the response is no longer linear, linear models are replaced by nonlinear viscoelastic models. For example, in a model developed by Cessna and Sternstein [32] used nonlinear dashpots instead on linear and were incorporated into the constitutive equations. The rate dependence observed in polymer deformation has also been modeled empirically by scaling the yield stress as a function of strain rate [33].

Another technique for polymer constitutive modeling has taken a molecular approach. In this method [4], the polymer deformation was assumed to be due to the motion of molecular chains over potential energy barriers. The molecular flow was due to applied stress, and the internal viscosity was assumed to decrease with increasing stress. The yield stress (the point where permanent deformation begins) was defined as the point where the internal viscosity decreased to the point where the applied strain rate is equal to the plastic strain rate. Internal stresses were also defined [4, 34]. These stresses represented the resistance to molecular flow that tends to drive the material back towards its original

configuration. A significant advancement in the modeling of polymers using a molecular approach has been made by Parks, Argon, Boyce, Arruda and their coworkers, by Wu and VanderGeissen and Anand and Gurtin. In order to capture the characteristics feature of the deformation behavior of glassy polymers, James and Guth [35] developed a model that account for the evolution of microstructure of the glassy polymer. Subsequently, a general three dimensional constitutive model was established based on the three chain model [36] using the generalized Argon double- kink model [37]. Further generalization of the model to the eight chain model [30] and the full network model [38] has been done. In these models, polymeric materials is approximated by a molecular chain network system defined by a cross links, which are assumed to be physically entangled points of molecular chains, whose number remains constant during the deformation. Therefore these types of model are refered as affine models. The constitutive equation obtained can well reproduce the tension and compression behavior, whereas the shear strength is likely to overestimate [38]. Indeed, the results of exerimental investigations implicitly suggest the possibility of a change in configuration of the entangled points due to deformation and a change in temperature [39], [40] which causes a change in the rigidity of th polymeric materials. Tomita and coworkers [41, 42] proposed the nonaffine model based on the molecular chain network theory, in which a change in the number of entangled points was taken into account.

In all these approaches, constitutive equations were developed [4, 34, 36, 43, 44]. In these equations, the polymer deformation was considered to be a function of parameters such as the activation energy, activation volume, molecular radius, molecular angle of rotation, and thermal constants. Furthermore, the deformation was assumed to be a function of

state variables that represented the resistance to molecular flow caused by a variety of mechanisms. The state variable values evolved with stress, inelastic strain and inelastic strain rate.

An alternative approach to the constitutive modeling of polymers has utilized, either directly or with some modifications, viscoplastic constitutive equations which have been developed for metals. For example, Bordonaro [45] modified the Viscoplasticity Theory Based on Overstress developed by Krempl [46]. In Bordonaro's model, the original theory was modified to attempt to account for phenomena encountered in polymer deformation that are not present in metals. For example, polymers behave differently from metals under conditions such as creep, relaxation and unloading. Other authors, such as Valisetty and Teply [47] and Zhang and Moore [48], also utilized viscoplastic constitutive equations developed to model the deformation of metals to analyze polymers. However, in these studies, only uniaxial tensile behavior was analyzed, and no attempt was made to consider phenomena such as unloading, creep or relaxation.

## 1.5 Motivation of the thesis

Many models that are developed to characterize the behavior of glassy polymers at large deformations are based on a modeling structure similar to that of plasticity, examples of such models are the models developed by Argon, Parks, Boyce, Arruda, and co-workers [49, 50, 51, 36, 52, 53, 54, 55, 56, 57, 58, 43, 59] and Krempl and co-workers [60, 61, 62, 63] and others. In most cases, a constitutive equation for stress is proposed, which depends on the elastic deformation gradient, supplemented by a flow rule for the plastic deformation,

which depends on the “over stress.” The over stress is a properly invariant difference between the stress and the back stress (related to equilibrium stress). The accuracy of the model depends upon the model used for stress and back stress along with the flow rule.

### 1.5.1 Modeling for stress

It is well known that the elastic response of many isotropic solid polymers become anisotropic as a result of plastic strain [4, 64, 65, 66, 67, 68, 69, 70]. This is clearly seen in Figure 1.4 that shows the axial and transverse wave moduli as a function of plastic strain in tension for poly vinyl chloride (PVC), poly(methyl methacrylate) (PMMA), polystyrene (PS) and bisphenol A polycarbonate (PC). As indicated in the figure, for each polymer the axial and transverse wave moduli are initially identical indicating the response is isotropic, and then gradually become different as the polymer is subjected to different extents of plastic deformation. Typically, as shown in the figure, for uniaxial tension the axial modulus increases and the transverse modulus decreases with the increase of plastic strain. The extent of this difference depends on the polymer. For the polymers shown in Figure 1.4, clearly PC is the most sensitive to plastic strain, developing very large differences in the moduli along the two directions, even at relatively small plastic strains. Also, it should be noted that this difference is in the order of the plastic strain (i.e., approximately 60% difference in modulus for approximately 60% plastic strain in tension).

Even though, as shown in Figure 1.4, there can develop a large difference between the axial and transverse moduli as a result of plastic flow, this fact is frequently ignored and not reflected in the models that are developed. Many models that are used to characterize the behavior of glassy polymers at large deformations are based on a modeling structure

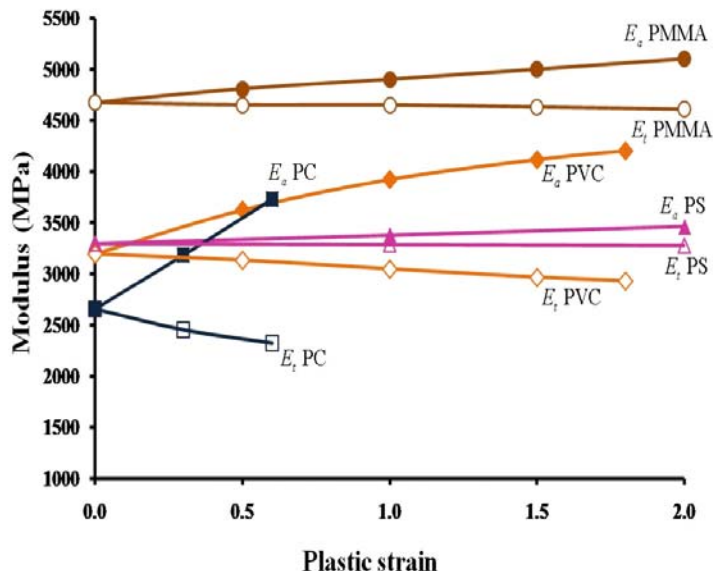


Figure 1.4: Axial and transverse modulus reported as a function of extent of plastic deformation in tension for PVC, PMMA, PS, and PC (from Ward [4]). The axial longitudinal modulus increases while the transverse longitudinal modulus decreases with plastic strain.

which describe the stress as a function of only the elastic deformation gradient. Without a parameter to characterize the anisotropy that develops as a result of plastic flow, these models preserve the initial symmetry (in most cases isotropy) of the elastic response. This is true even after plastic flow. We have developed a model for stress that depends both on the elastic and the plastic parts of the deformation and could capture the development of anisotropy with plastic flow.

### 1.5.2 Experimentally evaluating and modeling of equilibrium stress

The models which uses modeling structure similar to that of plasticity to characterize glassy polymers, all incorporates the idea of an equilibrium stress, that implies, thermodynamically, that there exist loading conditions under which the relaxation processes

stop so the load may be held at constant strain indefinitely, and which the material response tends towards these conditions. This is clearly observed above the glass-transition temperature, as is shown for PMMA in Figure 1.5, reproduced from Negahban [5]. This figure shows that at constant strain the stress either relaxes or increases toward the equilibrium response, depending on which side of the equilibrium response the process starts from, and then indefinitely stays there. Below the glass-transition temperature the relaxation processes slow down substantially, and identifying true equilibrium becomes more and more difficult, frequently resulting in the identification of a range of stresses which seem to exhibit the equilibrium conditions. Questions that arise in using these models are whether such equilibrium stresses exist, how can they be evaluated, and what experiments can be used to characterize the flow rule. One challenge in accurately evaluating the locus of equilibrium conditions is the fact that the relaxation process substantially slow down around these points, and, therefore, a method that does not directly require being at the equilibrium is desirable.

Several authors have looked at measuring the equilibrium stress. A review of the two main methods used for this can be found in an article by Neu and coworkers [71] and proposed by Ahlquist and Nix [72] and Onat [73], in which they use a model to characterize the equilibrium stress in 60Sn-40Pb soldering material. The disadvantage of the method is that it takes much longer time to evaluate the location of equilibrium stress. We have proposed a new method based on uniaxial tests which is a faster method to obtain the values for the equilibrium stress and it also provides with additional measurements of parameters at equilibrium that are normally not obtained. Later, we modeled the free energy as a

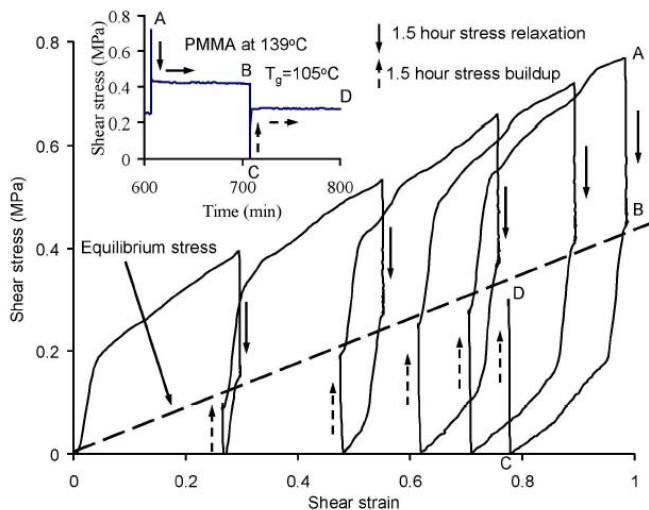


Figure 1.5: Stress buildup and stress relaxation seen in PMMA above its glass-transition temperature (from Negahban [5]).

function of invariants. The derivative of free energy with respect to the invariants were then calculated by fitting the experimental results for equilibrium stress measured from the method.

### 1.5.3 Conversion of plastic work to heat during high strain rate deformation of glassy polymer

Since the early work of Farren and Taylor [74] and Taylor and Quinny [75], it has been known that the mechanical energy of plastic deformation transform into heat which can cause temperature rise under adiabatic consideration. These authors measured the mechanical dissipation of energy in metals and showed that approximately 90% of plastic work was transformed instantaneously into heat. Hodowany et al.[76] showed that the fraction of plastic work converted into heat for an aluminium alloy AL2024-T3 varies

from 60 to 30% at high strain rates 3000 1/s. The nature of the thermal problem determines the temperature rise, if the generated heat flows away then little temperature rise will be noticed (isothermal condition) but under adiabatic condition the temperature can rise noticeably. The monotonic compression at a very low strain rate corresponds to an isothermal condition, but for a high strain rate curve corresponds to an adiabatic deformation due to which temperature increases during the experiments. The experimental results from Rittel [77] and Lerch [13] have performed a compression experiments under high strain rate and have indicated that temperature can increase as much as  $60^{\circ}C$  with 80% plastic strain. Since depending upon the strain rate the monotonic compression experiments undergoes isothermal and adiabatic condition, therefore a method is needed which could measure a temperature rise for such experiments and calculate a stress under isothermal condition for different rates and temperatures. We have calculated a temperature rise for a monotonic compression experiments and calculated the response under isothermal conditions for the high strain rate response.

## 1.6 Outline

For all the reasons given in the previous section, the synopsis of the present dissertation can be stated as follows.

In this dissertation, we present a large deformation thermodynamically consistent modeling structure whose primary objective is to capture the response of glassy PC at various ranges of strains, strain rates and temperatures. To achieve this objective, we address the observed development of elastic anisotropy with plastic strain and we introduce a new

method to evaluate the back stress using uniaxial cyclic tests. First, the constitutive model for stress is developed, which is assumed to depend upon the elastic and plastic deformation gradient and temperature. Then a constitutive model for back stress is developed based on the experimentally evaluated equilibrium stresses. Both these models are thermodynamically consistent and contribute to a single free energy. After developing the models for stress and back stress, the flow rule is developed which could capture the response at large strains and with different strain rates and temperature. In calculating the flow rule, the temperature rise for the monotonic compression experimental results at very high strain rates is calculated based on overstress and then the stress is interpolated under isothermal conditions for different temperatures. These corrected monotonic compression plots at high strain rates along with the low strain rates experimental plots at different temperatures were used to model the flow rule.

In **Chapter 2**, we present the basics of continuum mechanics, which includes kinematics and balance laws. After explaining the various terms related to continuum mechanics, finite deformation thermo-mechanically coupled viscoelasticity theory is presented and the constraints imposed on stress, back stress and plastic flow is discussed for a model to be thermodynamically consistent. Later, the heat generation and flow are described and the conditions for isothermal and adiabatic response are derived.

**Chapter 3** presents the one dimensional mechanical analog on which our modeling structure is based on, and this analog is used to develop a three dimensional constitutive model.

**Chapter 4** focuses on modeling the thermo-elastic response observed in PC at

different temperatures and pressures. Confined compression experiments were performed by Masubichi et al. [7] using a combined PVT test system with an ultrasonic velocity measurement system. They have reported longitudinal and shear wave speeds along with the PVT curve. A thermodynamically based large deformation thermo-elastic model is developed and was used to evaluate the wave moduli. The measured wave speeds were then used to model the thermo-elastic response of PC. The resulting model reproduces the correct longitudinal and shear wave speed moduli measured by the ultrasonic method under confined compression for glassy PC at different temperatures and higher loads.

In **Chapter 5 and 6**, the development of anisotropy as a result of plastic deformation below the glass-transition temperature is investigated and modeled for amorphous polycarbonate. Initially isotropic polycarbonate was subjected to different extents of plastic flow in uniaxial compression at zero load and the development of its anisotropic wave speed moduli were studied using ultrasonic wave speed measurements. Longitudinal and shear wave speed measurements were performed both in the axial and transverse direction. The measured moduli were then used to model the elastic response of polycarbonate using a model for stress that depends both on the elastic and plastic parts of the deformation. The constitutive model which reproduces the correct anisotropic wave moduli measured by the ultrasonic method at zero load was then combined with the large deformation thermoelastic model under confined compression developed in Chapter 4 at higher load to reproduce the anisotropic wave speed moduli at different temperatures below the glass transition temperatures and at higher load.

**Chapter 7 and 8** discusses the measuring and modeling of the equilibrium stress

(this is most commonly known as back stress but the back stress can be different from the equilibrium stress). A method based on uniaxial compression is proposed for evaluating the equilibrium stress of glassy polymers. The method is faster than other proposed methods for calculating the equilibrium stress, and provides additional measurements of parameters at equilibrium that are normally not obtained. Later, a model for back stress is developed that directly uses the free energy as a function of invariants. The derivative of free energy with respect to the invariants were then calculated by fitting the experimental results which require a new modeling structure to model the back stress.

**Chapter 9** discusses the free energy obtained such that it is consistent with both the stress and back stress model. This is augmented by a part that will just depend upon temperature, which is then calculated using the heat capacity at zero stress and zero elastic and plastic strains. The material parameter in the expression was then calculated using the experimental results from DSC.

In **Chapter 10** a flow rule is developed that can capture the monotonic compression response at large strains and at different temperatures. To do this we first correct the monotonic compression tests to obtain the isothermal response. In doing this, under the assumption of adiabatic flow and assuming the majority of heat is generated due to plastic flow, the temperature rise for uniaxial experiments is calculated. Interpolation is used to obtain the isothermal response from those results. The corrected stress for high strain rates along with low strain rate experimental results were used to model the flow rule.

**Chapter 11** summarize the main features of the constitutive model along with the future work needed to refine the proposed model.

## Chapter 2

# Kinematics, balance laws and notations

### 2.1 Introduction

In this chapter we introduce notation through the presentation of basic continuum mechanics. This includes descriptions of the kinematics and balance laws. Although the constitutive model developed in this dissertation is not necessarily the same as described in this chapter, but will be sufficient in describing the notation. After explaining the various terms, finite deformation thermo-mechanically coupled viscoelastic theory is presented and the constraints imposed on stress, back stress and on plastic flow is derived for a thermodynamically consistent model. Most of this development is based on Negahban [6]. For more comprehensive treatment the reader is referred to numerous monographs and books on the subject includes, for example Cristescu and Suliciu [78], Hill [79], Lubliner [80], Kachanov

[81], Cristescu [82], Maugin [83], Khan and Huang [84], Simo and Hughes [85], Lubarda [86], Bertram [87], Truesdell & Noll [88], Chadwick [89], Ferry [90] among others.

## 2.2 Kinematics

At each time, a material body occupies a physical region in space and each point in the body can be identified by its location. The mapping which identifies each point in the body by its location in space is the *configuration of the body*. The current configuration of the body is denoted by  $\kappa$ . It is common to take one configuration of the body as a *reference configuration*. This configuration serves as a means of distinguishing between material points in the body and identifies the relative placing of all points. The reference configuration will be denoted by  $\kappa_o$ . We will let  $\mathbf{X}$  denote the position vector of points in the reference configuration. The particle which occupied the location given by  $\mathbf{X}$  in the reference configuration will move to location  $\mathbf{x}(t)$  at time  $t$ . The body contains many particles and their motion can be given by a function  $\chi(\mathbf{X}, t)$  which gives the position at time  $t$  of the particle in location  $\mathbf{X}$  in the reference configuration. Therefore,

$$\mathbf{x}(t) = \chi(\mathbf{X}, t). \quad (2.1)$$

Consider point  $P$  and a point  $Q$  which is very close to  $P$  as shown in Figure 2.1. The vector going from  $P$  to  $Q$  in the reference configuration will be denoted by  $d\mathbf{X}$  and the vector going from  $P$  to  $Q$  in the current configuration will be denoted by  $d\mathbf{x}$ . The deformation gradient  $\mathbf{F}$  is a second-order tensor which relates  $d\mathbf{x}$  and  $d\mathbf{X}$  through the relation

$$d\mathbf{x} = \mathbf{F}d\mathbf{X}. \quad (2.2)$$

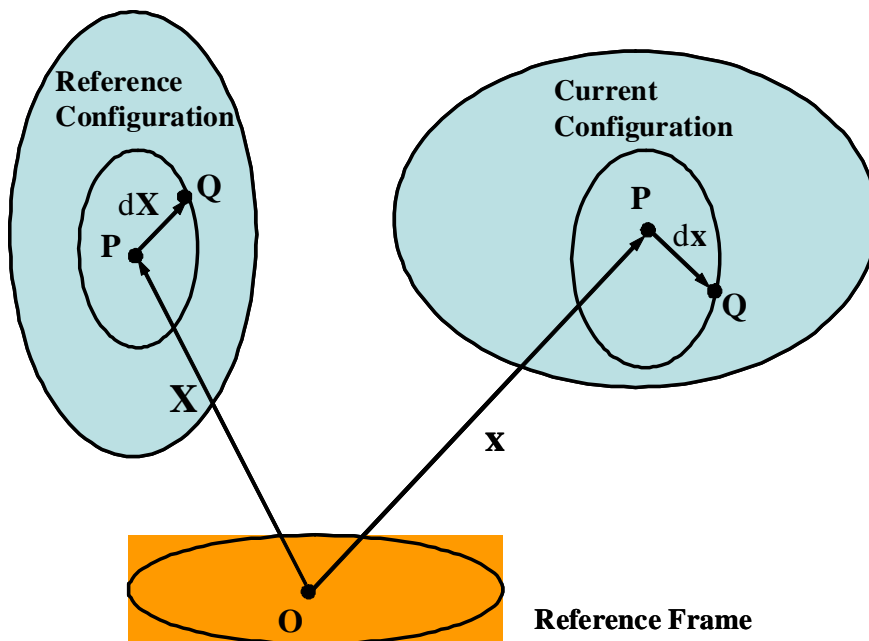


Figure 2.1: Point  $P$  and  $Q$  changing from reference to current configuration.

It is intuitive that one can find  $\mathbf{F}$  from the knowledge of the motion  $\chi(\mathbf{X}, t)$ . One can show that  $\mathbf{F}$  contains all the information needed to calculate both change in length and direction of line elements. Strain in a material is the amount line elements extend and the amount angles change between line elements. The right Cauchy stretch tensor  $\mathbf{C}$  and left Cauchy stretch tensor  $\mathbf{B}$  contains all the information needed to find how the length of any line element changes with respect to reference and current configuration respectively.  $\mathbf{C}$  and  $\mathbf{B}$  can be defined as

$$\mathbf{C} = \mathbf{F}^T \mathbf{F}, \quad (2.3)$$

$$\mathbf{B} = \mathbf{F} \mathbf{F}^T. \quad (2.4)$$

The polar decomposition theorem states that any deformation gradient  $\mathbf{F}$  can be

uniquely decomposed into

$$\mathbf{F} = \mathbf{R}\mathbf{U} = \mathbf{V}\mathbf{R}, \quad (2.5)$$

where  $\mathbf{R}$  is orthogonal (i.e.  $\mathbf{R}\mathbf{R}^T = \mathbf{R}^T\mathbf{R} = \mathbf{I}$ ), and  $\mathbf{U}$  and  $\mathbf{V}$  are symmetric positive definite (i.e.  $\mathbf{U} = \mathbf{U}^T$  and  $\mathbf{V} = \mathbf{V}^T$ ).  $\mathbf{R}$  represents a rigid body rotation and  $\mathbf{U}$  and  $\mathbf{V}$  represent pure deformation. Using polar decomposition one can show

$$\mathbf{C} = \mathbf{U}^2, \quad (2.6)$$

$$\mathbf{B} = \mathbf{V}^2.$$

The velocity gradient is denoted by  $\mathbf{L}$  and is defined as

$$\mathbf{L} = \nabla_{\mathbf{x}}(\mathbf{v}) = \dot{\mathbf{F}}\mathbf{F}^{-1}, \quad (2.7)$$

where  $\mathbf{v}$  is the velocity.  $\mathbf{L}$  is commonly separated into a symmetric tensor  $\mathbf{D}$  and a skew symmetric tensor  $\mathbf{W}$  such that

$$\mathbf{L} = \mathbf{D} + \mathbf{W}, \quad (2.8)$$

and where

$$\mathbf{D} = \frac{1}{2}(\mathbf{L} + \mathbf{L}^T), \quad (2.9)$$

$$\mathbf{W} = \frac{1}{2}(\mathbf{L} - \mathbf{L}^T), \quad (2.10)$$

for  $\mathbf{D}$  known as the rate of deformation or rate of strain tensor and  $\mathbf{W}$  is the spin or vorticity tensor.

### 2.2.1 Elastic and plastic deformation gradient

The separation of the deformation into elastic and plastic parts is shown in Figure 2.2. This separation is the classical Kroner [91]- Lee [92] decomposition which considers the

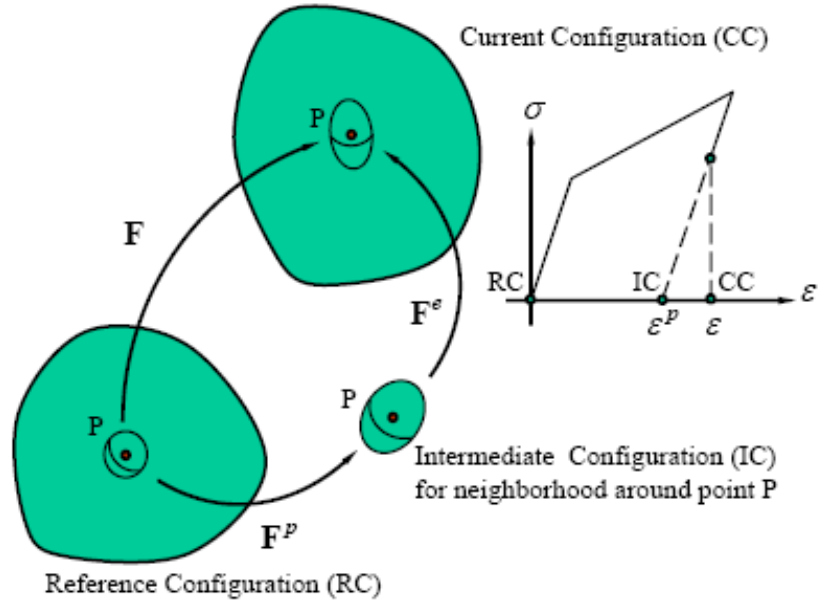


Figure 2.2: Decomposition of the deformation gradient  $\mathbf{F}$  into a plastic deformation gradient  $\mathbf{F}^p$  and an elastic deformation gradient  $\mathbf{F}^e$  (from Negahban [6]).

deformation gradient  $\mathbf{F}$  to separate into two parts

$$\mathbf{F} = \mathbf{F}^e \mathbf{F}^p, \quad (2.11)$$

where  $\mathbf{F}^e$  is the elastic deformation gradient and  $\mathbf{F}^p$  is the plastic deformation gradient [36, 54, 38, 93, 94]. At any stage of loading it is assumed that the neighbourhood of each material point can be unloaded (theoretically if not practically) leaving a stress free configuration. The deformation gradient describing comparison of this intermediate and fictitious stress free configuration to the reference configuration is taken as  $\mathbf{F}^p$ . As shown in Figure 2.2, the deformation gradient comparing the current configuration to the intermediate stress-free configuration is taken to be  $\mathbf{F}^e$ . Obviously, this definition has the characteristic of assigning information about the more permanent deformation to  $\mathbf{F}^p$ , while the portion that can be recovered by elastic unloading to  $\mathbf{F}^e$ . Also, this decomposition is not unique since many

intermediate configurations, each differing from the other by a rigid body motion, can be selected. As a result, in the modeling of  $\mathbf{F}^p$  we need to provide a description of how to select among these. In general, one can use polar decomposition to write

$$\mathbf{F}^e = \mathbf{R}^e \mathbf{U}^e = \mathbf{V}^e \mathbf{R}^e \quad , \quad \mathbf{F}^p = \mathbf{R}^p \mathbf{U}^p = \mathbf{V}^p \mathbf{R}^p. \quad (2.12)$$

For each of the elastic and plastic deformation gradients one can define the following strains

$$\begin{aligned} \mathbf{C}^e &= \mathbf{F}^{eT} \mathbf{F}^e \quad , \quad \mathbf{B}^e = \mathbf{F}^e \mathbf{F}^{eT}, \\ \mathbf{C}^p &= \mathbf{F}^{pT} \mathbf{F}^p \quad , \quad \mathbf{B}^p = \mathbf{F}^p \mathbf{F}^{pT}. \end{aligned} \quad (2.13)$$

For the total deformation we have

$$\begin{aligned} \mathbf{C} &= \mathbf{F}^T \mathbf{F} = \mathbf{F}^{pT} \mathbf{C}^e \mathbf{F}^p, \\ \mathbf{B} &= \mathbf{F} \mathbf{F}^T = \mathbf{F}^e \mathbf{B}^p \mathbf{F}^{eT}. \end{aligned} \quad (2.14)$$

Velocity gradient, deformation rate and spin tensor can be defined as

$$\begin{aligned} \mathbf{L}^e &= \dot{\mathbf{F}}^e \mathbf{F}^{e-1}, \quad \mathbf{D}^e = \frac{1}{2} (\mathbf{L}^e + \mathbf{L}^{eT}), \quad \mathbf{W}^e = \frac{1}{2} (\mathbf{L}^e - \mathbf{L}^{eT}), \\ \mathbf{L}^p &= \dot{\mathbf{F}}^p \mathbf{F}^{p-1}, \quad \mathbf{D}^p = \frac{1}{2} (\mathbf{L}^p + \mathbf{L}^{pT}), \quad \mathbf{W}^p = \frac{1}{2} (\mathbf{L}^p - \mathbf{L}^{pT}). \end{aligned} \quad (2.15)$$

The total velocity gradient can then be written as

$$\mathbf{L} = \dot{\mathbf{F}} \mathbf{F}^{-1} = \left( \dot{\mathbf{F}}^e \mathbf{F}^p + \mathbf{F}^e \dot{\mathbf{F}}^p \right) (\mathbf{F}^e \mathbf{F}^p)^{-1} = \left( \dot{\mathbf{F}}^e \mathbf{F}^p + \mathbf{F}^e \dot{\mathbf{F}}^p \right) \mathbf{F}^{p-1} \mathbf{F}^{e-1}. \quad (2.16)$$

### 2.2.2 Incompressible plastic flow assumption

We have made the standard assumption that the plastic flow is incompressible, so that

$$J^p = \det(\mathbf{F}^p) = 1. \quad (2.17)$$

Considering this assumption, the total volume ratio  $J$  can be written as

$$J = \det(\mathbf{F}) = J^e J^p = J^e = \det(\mathbf{F}^e). \quad (2.18)$$

## 2.3 Balance laws

The prediction of material response requires the combination of several elements. In general, these elements include mathematical models describing the material's response characteristics (constitutive equations), specific conditions describing the initial state of the matter (initial conditions), conditions describing how the specific body is being influenced by the surrounding (boundary conditions) and laws describing how to combine these elements (balance laws). The balance laws have a special place in the theory of material response since they are the same for all materials in contrast to constitutive equations that are different for each material. The five laws which are collectively called the balance laws include: the conservation of mass, the balance of linear momentum, the balance of angular momentum, the balance of work and energy, and the entropy production inequality. Each of the balance laws is a general statement on how all materials will respond over time, and can be used to calculate the specific response of a particular material body only when augmented by constitutive models for the specific material, and specific initial and boundary conditions describing the initial state of the material and the processing conditions.

### 2.3.1 Conservation of mass

The law of conservation of mass states that the mass in a body will not change if the particles in the body remain the same. The conservation of mass can be written as

$$\rho J = \rho_o, \quad (2.19)$$

where  $\rho$  is the current density and  $\rho_o$  is the density in reference configuration when  $J = 1$ , where  $J = \det(\mathbf{F})$  is the volume ratio.

### 2.3.2 Balance of linear momentum

The law of balance of linear momentum states that the resultant of all applied forces on a material body is equal to the rate of change of linear momentum for that material body. The law of balance of linear momentum can be written as

$$\int_{S(t)} \mathbf{t}^{(n)} dS + \int_{\mathbb{B}} \mathbf{b} dm = \frac{d}{dt} \int_{\mathbb{B}} \mathbf{v} dm, \quad (2.20)$$

where the first integral represents the resultant force due to traction on the surface of the body  $S(t)$ , the second integral represents the resultant body force, and the third integral represents the linear momentum of the body. In this expression  $\mathbf{t}^{(n)}$  is the traction vector on the surface of the current body,  $\mathbf{b}$  is the body force per unit mass of the body and  $m$  denotes the mass. In the expression for the balance of linear momentum, using the Cauchy relation for the traction vector given as  $\mathbf{t}^{(n)} = \mathbf{T}^T \mathbf{n}$ , where  $\mathbf{T}$  is the Cauchy stress tensor and  $\mathbf{n}$  is the unit normal to the current surface, replacing the integration over mass by integration over volume through the relation  $dm = \rho dV$  and assuming that the arguments

of the integrals are continuous, one can conclude that

$$\operatorname{div}_{\mathbf{x}}(\mathbf{T}^T) + \rho \mathbf{b} = \rho \mathbf{a}, \quad (2.21)$$

where  $\mathbf{a}$  is the particle acceleration.

### 2.3.3 Balance of angular momentum

The law of balance of angular momentum states that the resultant moment applied on a body must equal the rate of change of angular momentum of that material body. It has been shown that balance of angular momentum states that the Cauchy stress tensor is symmetric. That is,

$$\mathbf{T} = \mathbf{T}^T. \quad (2.22)$$

### 2.3.4 Balance of work and energy

The law of balance of work and energy states that the rate at which heat flows into a body  $\dot{Q}$  plus the rate at which work is being done on that body  $\dot{W}$  is equal to the rate at which the kinetic plus internal energy of the body changes. This can be written as

$$\dot{Q} + \dot{W} = \frac{d}{dt}(KE + IE), \quad (2.23)$$

where  $KE$  is the kinetic energy and  $IE$  is internal energy. The rate of doing work on the body  $\dot{W}$  is due to the rate of doing work by the traction on the surface and by the body forces. Since the power of a force to do work is given by the dot product of the force and the velocity of the particle of the body that the force is applied on, the rate of doing work

on the body is given by

$$\dot{W} = \int_{S(t)} \mathbf{t}^{(n)} \circ \mathbf{v} dS + \int_{\beta} \mathbf{b} \circ \mathbf{v} dm. \quad (2.24)$$

The rate of heat flow into the body is given by

$$\dot{Q} = - \int_{S(t)} \mathbf{q} \circ \mathbf{n} dS + \int_{\beta} r dm, \quad (2.25)$$

where  $\mathbf{q}$  is the heat flux vector and  $r$  is the radiation. Substituting the expression for  $\dot{Q}$  and  $\dot{W}$  in equation 2.23, using the definition of traction vector as  $\mathbf{t}^{(n)} = \mathbf{T}^T \mathbf{n}$ , replacing the integration over mass by integration over volume and assuming that the arguments of the integrals are continuous, one obtains the final form of the balance of energy as

$$-\operatorname{div}_{\mathbf{x}}(\mathbf{q}) + \rho r + \operatorname{tr}(\mathbf{T}\mathbf{L}) = \rho \dot{e}. \quad (2.26)$$

### 2.3.5 Entropy and the entropy production inequality

The entropy production inequality, also known as the second law of thermodynamics, states that the entropy in a material body of fixed mass increases at least as rapidly as entropy is added to the body through the addition of heat to the body, either by radiation directly into the body or by heat flow through the boundaries of the body. The total entropy in a body is given by  $\int_{\mathbb{B}} \eta dm$ , where  $\eta$  is the entropy per unit mass of the body, known as the specific entropy. The rate at which entropy is added to the body by heat is given by

$$\int_{\mathbb{B}} \frac{r}{\theta} dm - \int_{S(t)} \frac{1}{\theta} \mathbf{q} \circ \mathbf{n} dS, \quad (2.27)$$

where  $\theta$  denotes the particle temperature at each point in the body. Again replacing the integration over mass by integration over volume and assuming that the integrals are con-

tinuous, one can obtain the differential form of the law as

$$\rho \frac{r}{\theta} - \operatorname{div}_{\mathbf{x}} \left( \frac{1}{\theta} \mathbf{q} \right) \leq \rho \dot{\eta}. \quad (2.28)$$

Free-energy is defined by the relation  $e = \psi + \eta\theta$  where  $\psi$  is the free-energy per unit mass, also known as the specific free energy. Free-energy represents the portion of internal energy which is available for conversion into work or heat (not necessarily instantaneously). Through the expression relating internal energy, free-energy and entropy one can see that  $\eta\theta$  represent the portion of the energy which is not immediately accessible. One can introduce the relation  $e = \psi + \eta\theta$  into the entropy production inequality after differentiation and substitution for  $\dot{\eta}$ . Assuming a strictly positive temperature scale and use of the balance of energy results in the inequality

$$\rho \dot{\psi} - \operatorname{tr}(\mathbf{T}\mathbf{L}) + \rho \eta \dot{\theta} + \frac{1}{\theta} \mathbf{q} \circ \nabla_{\mathbf{x}}(\theta) \leq 0. \quad (2.29)$$

This inequality is also known as the Clausius-Duhem inequality.

## 2.4 Finite deformation mechanical theory

In this section we will study large deformations, including large rigid body motions. We will do this in the context of the multiplicative decomposition of the deformation gradient into an elastic part and a plastic part given by

$$\mathbf{F} = \mathbf{F}^e \mathbf{F}^p. \quad (2.30)$$

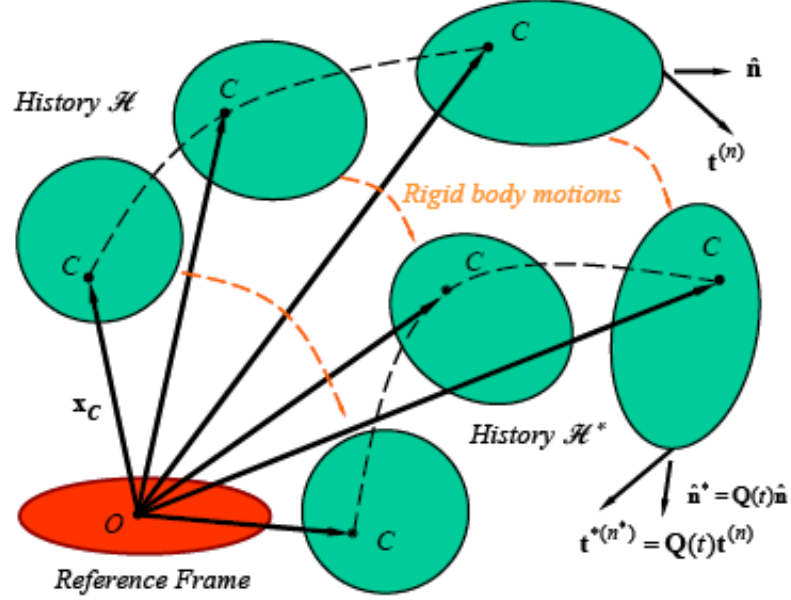


Figure 2.3: Two deformation histories that are identical but for the fact that each configuration in one is obtained by an arbitrary rigid body translation and rotation of the configuration of other is assumed to simply rotate the traction vector by the final amount of rotation (from Negahban [6]).

#### 2.4.1 Rigid body motions

The influence of rigid body motions on the stress is normally dictated by the influence of rigid body motions on the traction. Normally, a rigid body motion is assumed to reorient the traction by the amount of the rigid body rotation. As shown in Figure 2.3, if the body is rotated by a rigid body rotation given by the orthogonal transformation  $\mathbf{Q}$  such that the current deformation gradient changes from  $\mathbf{F}$  to  $\mathbf{F}^* = \mathbf{Q}\mathbf{F}$ , then any normal  $\mathbf{n}$  transforms to  $\mathbf{n}^* = \mathbf{Q}\mathbf{n}$  and the traction on the surface with the normal  $\mathbf{n}$  given by  $\mathbf{t}^{(n)}$  changes to  $\mathbf{t}^{*(n^*)} = \mathbf{Q}\mathbf{t}^{(n)}$ . This can be shown to require that the Cauchy stress  $\mathbf{T}$  changes to the Cauchy stress  $\mathbf{T}^* = \mathbf{Q}\mathbf{T}\mathbf{Q}^T$ . Consider the constitutive model for Cauchy stress as

$$\mathbf{T} = \mathbf{T}^+(\mathbf{F}^e, \mathbf{F}^p). \quad (2.31)$$

The requirement that  $\mathbf{T}^* = \mathbf{Q}\mathbf{T}\mathbf{Q}^T$  requires that

$$\mathbf{T}^+(\mathbf{F}^{*e}, \mathbf{F}^{*p}) = \mathbf{Q}\mathbf{T}^+(\mathbf{F}^e, \mathbf{F}^p)\mathbf{Q}^T. \quad (2.32)$$

Obviously, to impose this restriction we need to know what the effect of rigid body motions is on  $\mathbf{F}^e$  and  $\mathbf{F}^p$ . Since  $\mathbf{F}^* = \mathbf{Q}\mathbf{F}$ , we have

$$\mathbf{F}^* = \mathbf{F}^{*e}\mathbf{F}^{*p} = \mathbf{Q}\mathbf{F}^e\mathbf{F}^p. \quad (2.33)$$

Let us first consider how we expect plastic deformation gradient to change with rigid body rotation. It seems rational to take plastic deformation gradient to be unaffected by rigid body rotations since this is consistent with our idea that plastic deformation does not change with pure elastic deformation. Therefore, we will assume that

$$\mathbf{F}^{*p} = \mathbf{F}^p. \quad (2.34)$$

This then requires that

$$\mathbf{F}^{*e} = \mathbf{Q}\mathbf{F}^e, \quad (2.35)$$

so that the relation above is satisfied. Once imposed on the constitutive model for Cauchy stress, these assumptions result in

$$\mathbf{T}^+(\mathbf{Q}\mathbf{F}^e, \mathbf{F}^p) = \mathbf{Q}\mathbf{T}^+(\mathbf{F}^e, \mathbf{F}^p)\mathbf{Q}^T. \quad (2.36)$$

Selection of  $\mathbf{Q} = \mathbf{R}^{eT}$  and reorganization yields

$$\mathbf{T} = \mathbf{T}^+(\mathbf{F}^e, \mathbf{F}^p) = \mathbf{R}^e\mathbf{T}^+(\mathbf{U}^e, \mathbf{F}^p)\mathbf{R}^{eT}. \quad (2.37)$$

Since there is a one-to-one relation between  $\mathbf{U}^e$  and  $\mathbf{C}^e$ , one can create models with the arguments

$$\mathbf{T} = \mathbf{R}^e \mathbf{T}^+(\mathbf{U}^e, \mathbf{F}^p) \mathbf{R}^{eT} = \mathbf{R}^e \mathbf{T}^{++}(\mathbf{C}^e, \mathbf{F}^p) \mathbf{R}^{eT}. \quad (2.38)$$

### 2.4.2 Material symmetry

Material symmetry requires that the stress be the same for any two histories that are identical up to a reorganization of the reference configuration in ways that reflect symmetries of the material. This idea is schematically shown in Figure 2.4 where an alternate reference configuration is constructed which is materially identical to the original one since the change represents the symmetry of the material. Two configurations  $\kappa_o$  and  $\bar{\kappa}_o$  that are related through a transformation  $\mathbf{M}$  which represents the symmetry of the material are shown in Figure 2.5. If on each one of these two configurations we impose the same deformation history, the response should be the same. As can be seen in the figure 2.5, imposing a deformation on  $\kappa_o$  described by the deformation gradient  $\mathbf{F}$  should be equivalent to imposing the deformation gradient  $\bar{\mathbf{F}}$  on  $\bar{\kappa}_o$  since  $\bar{\mathbf{F}}$  represents imposing  $\mathbf{F}$  on  $\bar{\kappa}_o$ . It is easy to see that one can write

$$\bar{\mathbf{F}} = \mathbf{F} \mathbf{M}. \quad (2.39)$$

If the deformation  $\mathbf{F}$  is decomposed into an elastic and plastic part given by  $\mathbf{F} = \mathbf{F}^e \mathbf{F}^p$  and the deformation gradient  $\bar{\mathbf{F}}$  is decomposed into an elastic and plastic part given by  $\bar{\mathbf{F}} = \bar{\mathbf{F}}^e \bar{\mathbf{F}}^p$ , then we will have

$$\bar{\mathbf{F}} = \bar{\mathbf{F}}^e \bar{\mathbf{F}}^p = \mathbf{F} \mathbf{M} = \mathbf{F}^e \mathbf{F}^p \mathbf{M} = \mathbf{F}^e \mathbf{M} \mathbf{M}^{-1} \mathbf{F}^p \mathbf{M}. \quad (2.40)$$

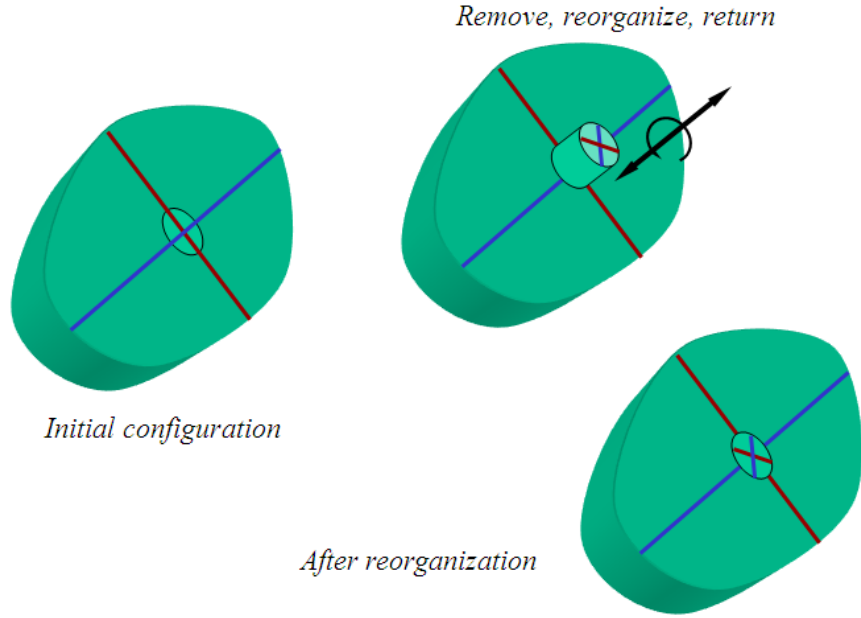


Figure 2.4: Schematic of the reorganization of the neighbourhood of influence of a point to get a new configuration that is materially equivalent (from Negahban [6]).

We will concentrate on symmetries that are described by orthogonal transformations and select

$$\bar{\mathbf{F}}^e = \mathbf{F}^e \mathbf{M}, \quad \bar{\mathbf{F}}^p = \mathbf{M}^{-1} \mathbf{F}^p \mathbf{M}. \quad (2.41)$$

The assumption that the stress remains unchanged under such changes can be written as  $\bar{\mathbf{T}} = \mathbf{T}$  and imposes the following condition on the constitutive model for Cauchy stress written as

$$\mathbf{T} = \mathbf{T}^+(\mathbf{F}^e, \mathbf{F}^p) = \mathbf{T}^+(\mathbf{F}^e \mathbf{M}, \mathbf{M}^T \mathbf{F}^p \mathbf{M}). \quad (2.42)$$

## 2.5 Thermodynamic models with internal parameters

The viscoelasticity model we have used is developed based on a modeling structure for plasticity. The model is a special case of a general first-gradient thermomechanical

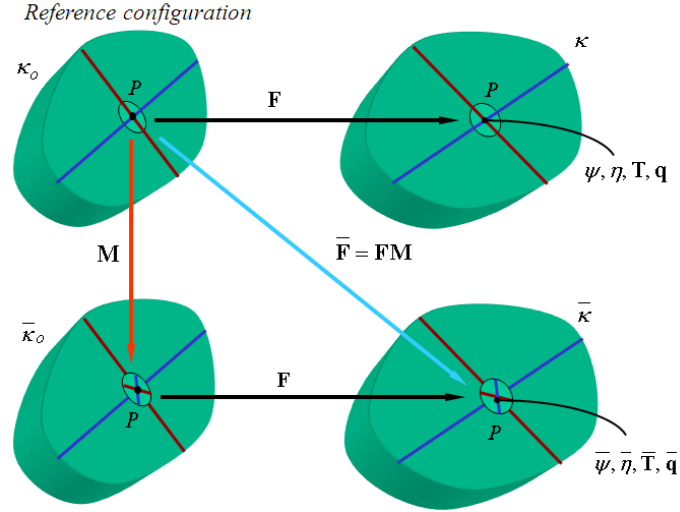


Figure 2.5: Reorganization of the initial configuration that is associated with the materials symmetry leaves the material indistinguishable from the original material so that the response to any history would result in identical stress for the original and reorganized configuration (from Negahban [6]).

material. To construct this model we will decompose the deformation gradient  $\mathbf{F}$  into three parts. These parts will be the elastic deformation gradient  $\mathbf{F}^e$ , the plastic deformation gradient  $\mathbf{F}^p$  and the thermal deformation gradient  $\mathbf{F}^\theta$ , and will assume they combine to give the deformation gradient through the equation

$$\mathbf{F}(t) = \mathbf{F}^e(t) \mathbf{F}^p(t) \mathbf{F}^\theta(t). \quad (2.43)$$

This decomposition is not unique and becomes meaningful only after providing constitutive assumptions and expressions for calculating  $\mathbf{F}^p$  and  $\mathbf{F}^\theta$  from the history. For our plasticity model we will assume that the state of the material is given by the following set of variables

$$S(t) = \left\{ \mathbf{F}^e(t), \mathbf{F}^p(t), \mathbf{F}^\theta(t), \theta(t), \mathbf{G}(t) \right\}, \quad (2.44)$$

where  $\theta$  is the temperature and  $\mathbf{G}$  is the temperature gradient. The assumption of the response depending on the state of the material can be written as

$$\begin{aligned}
\psi(\mathbf{X}, t) &= \psi^+ \left\{ \mathbf{F}^e(t), \mathbf{F}^p(t), \mathbf{F}^\theta(t), \theta(t), \mathbf{G}(t) \right\}, \\
\eta(\mathbf{X}, t) &= \eta^+ \left\{ \mathbf{F}^e(t), \mathbf{F}^p(t), \mathbf{F}^\theta(t), \theta(t), \mathbf{G}(t) \right\}, \\
\mathbf{T}(\mathbf{X}, t) &= \mathbf{T}^+ \left\{ \mathbf{F}^e(t), \mathbf{F}^p(t), \mathbf{F}^\theta(t), \theta(t), \mathbf{G}(t) \right\}, \\
\mathbf{q}(\mathbf{X}, t) &= \mathbf{q}^+ \left\{ \mathbf{F}^e(t), \mathbf{F}^p(t), \mathbf{F}^\theta(t), \theta(t), \mathbf{G}(t) \right\},
\end{aligned} \tag{2.45}$$

where a superscript “+” will denote the function for evaluating the dependent variables which are free energy  $\psi$ , entropy  $\eta$ , Cauchy stress tensor  $\mathbf{T}$  and heat flux vector  $\mathbf{q}$ . The entropy production inequality introduces constraints on the constitutive response functions.

This law in the form of the Clausius- Duhem inequality is written as

$$\rho \dot{\psi} - \text{tr}(\mathbf{T}\mathbf{L}) + \rho \eta \dot{\theta} + \frac{1}{\theta} \mathbf{q} \circ \nabla_{\mathbf{x}}(\theta) \leq 0, \tag{2.46}$$

and must be satisfied for all possible processes. The current assumptions on the constitutive dependence of the specific free energy result in the expression for  $\dot{\psi}$  given as

$$\dot{\psi} = \partial_{\mathbf{F}^e}(\psi) : \dot{\mathbf{F}}^e + \partial_{\mathbf{F}^p}(\psi) : \dot{\mathbf{F}}^p + \partial_{\mathbf{F}^\theta}(\psi) : \dot{\mathbf{F}}^\theta + \partial_{\theta}(\psi) \dot{\theta} + \partial_{\mathbf{G}}(\psi) \circ \dot{\mathbf{G}}. \tag{2.47}$$

The rate of the deformation gradient can be written as

$$\dot{\mathbf{F}} = \dot{\mathbf{F}}^e \mathbf{F}^p \mathbf{F}^\theta + \mathbf{F}^e \dot{\mathbf{F}}^p \mathbf{F}^\theta + \mathbf{F}^e \mathbf{F}^p \dot{\mathbf{F}}^\theta. \tag{2.48}$$

This provides an expression for the rate of elastic deformation gradient as

$$\dot{\mathbf{F}}^e = \dot{\mathbf{F}} \mathbf{F}^{\theta-1} \mathbf{F}^{p-1} - \mathbf{F}^e \dot{\mathbf{F}}^p \mathbf{F}^{p-1} - \mathbf{F}^e \mathbf{F}^p \dot{\mathbf{F}}^\theta \mathbf{F}^{\theta-1} \mathbf{F}^{p-1}. \tag{2.49}$$

We can introduce this into the equation of  $\dot{\psi}$  and substitute it into the Clausius Duhem inequality to get

$$\begin{aligned} & \left[ \rho \partial_{\mathbf{F}^e} (\psi) \mathbf{F}^{p-T} \mathbf{F}^{\theta-T} - \mathbf{T}^T \mathbf{F}^{-T} \right] : \dot{\mathbf{F}} + \rho [\eta + \partial_{\theta} (\psi)] \dot{\theta} \\ + \rho & \left[ \partial_{\mathbf{F}^{\theta}} (\psi) - \mathbf{F}^{pT} \mathbf{F}^{eT} \partial_{\mathbf{F}^e} (\psi) \mathbf{F}^{p-T} \mathbf{F}^{\theta-T} \right] : \dot{\mathbf{F}}^{\theta} + \rho \left[ \partial_{\mathbf{F}^p} (\psi) - \mathbf{F}^{eT} \partial_{\mathbf{F}^e} (\psi) \mathbf{F}^{p-T} \right] : \dot{\mathbf{F}}^p \\ & + \rho \partial_{\mathbf{G}} (\psi) \circ \dot{\mathbf{G}} + \frac{1}{\theta} \mathbf{q} \circ \partial_{\mathbf{x}} (\theta) \leq 0. \end{aligned}$$

This must hold for all admissible processes. We will focus on thermal deformation gradients that can be represented in the rate form by a constitutive expression of the form

$$\dot{\mathbf{F}}^{\theta}(t) = \boldsymbol{\alpha}(t) \dot{\theta}(t), \quad (2.50)$$

where  $\boldsymbol{\alpha}$  is a second order tensor coefficient of thermal expansion. To manipulate this restriction and obtain relations between the unknown functions, one needs to establish the independence of the different terms of this equation. This can only be done after the establishment of an evolution equation (“flow rule”) for the internal parameter  $\mathbf{F}^p$ . The evolution equation for  $\dot{\mathbf{F}}^p$  will be assumed to be given by the following relation

$$\dot{\mathbf{F}}^p = \dot{\mathbf{F}}^{p+}(\mathbf{F}^e, \mathbf{F}^p, \theta). \quad (2.51)$$

As a result of this, the flow rule cannot be made time independent and therefore a rate dependence will appear in the final response. In theory one can select  $\dot{\mathbf{F}}$  and  $\dot{\theta}$  arbitrary and each may take any arbitrary value. Under the current assumption the only way to satisfy the entropy production inequality is that the following relations will always be satisfied.

These relations can be written as

$$\mathbf{T}^T = \rho \partial_{\mathbf{F}^e} (\psi) \mathbf{F}^{eT}, \quad (2.52)$$

$$\eta = -\partial_{\theta}(\psi) - \left[ \partial_{\mathbf{F}^{\theta}}(\psi) - \mathbf{F}^{pT} \mathbf{F}^{eT} \partial_{\mathbf{F}^e}(\psi) \mathbf{F}^{p-T} \mathbf{F}^{\theta-T} \right] : \boldsymbol{\alpha}, \quad (2.53)$$

$$\rho \left[ \partial_{\mathbf{F}^p}(\psi) - \mathbf{F}^{eT} \partial_{\mathbf{F}^e}(\psi) \mathbf{F}^{p-T} \right] : \dot{\mathbf{F}}^p \leq 0, \quad (2.54)$$

$$\partial_{\mathbf{G}}(\psi) = 0, \quad (2.55)$$

$$\frac{1}{\theta} \mathbf{q} \circ \partial_{\mathbf{x}}(\theta) \leq 0. \quad (2.56)$$

Examination of these expressions reveals that the Cauchy stress and the specific entropy cannot be functions of  $\mathbf{G}$  either, leaving only the heat flux vector with a possible dependence on the temperature gradient. Introducing the back stress defined by

$$\mathbf{T}^b = \rho \partial_{\mathbf{F}^p}(\psi) \mathbf{F}^{pT}, \quad (2.57)$$

and substituting along with equation of stress in equation 2.54 gives

$$- \left[ \left( \mathbf{T}^{bT} - \mathbf{F}^{eT} \mathbf{T}^T \mathbf{F}^{e-T} \right) \mathbf{F}^{p-T} \right] : \dot{\mathbf{F}}^p \leq 0. \quad (2.58)$$

This expression suggest the introduction of an overstress  $\Delta \mathbf{T}$  defined by

$$\Delta \mathbf{T} = \mathbf{F}^{e-1} \mathbf{T} \mathbf{F}^e - \mathbf{T}^b. \quad (2.59)$$

The restriction imposed by the Clausius Duhem inequality on the plastic flow can now be written as

$$-\Delta \mathbf{T}^T : \mathbf{L}^p \leq 0, \quad (2.60)$$

or  $\Delta \mathbf{T}^T : \mathbf{L}^p \geq 0$ . This is the constraint on the flow rule which needs to be satisfied at all times for a model to be thermodynamically consistent.

## 2.6 Heat generation and flow

The heat generation and flow at a point can be calculated using the expression of balance of work and energy given by

$$\rho \dot{e} = -\operatorname{div}_{\mathbf{x}}(\mathbf{q}) + \rho r + \operatorname{tr}(\mathbf{T}\mathbf{L}) . \quad (2.61)$$

If we define

$$\rho \dot{h} = \rho r - \operatorname{div}_{\mathbf{x}}(\mathbf{q}), \quad (2.62)$$

where  $h$  is the specific heat added to the point, then the balance of work and energy can be written as

$$\dot{h} = \dot{e} - \frac{1}{\rho} \operatorname{tr}(\mathbf{T}\mathbf{L}) . \quad (2.63)$$

In terms of specific free-energy and entropy, using the relationship  $e = \psi + \eta\theta$ , the equation 2.63 can be written as

$$\dot{h} = \dot{\psi} + \dot{\eta}\theta + \eta\dot{\theta} - \frac{1}{\rho} \operatorname{tr}(\mathbf{T}\mathbf{L}). \quad (2.64)$$

To calculate  $\dot{h}$ , let us first consider the terms we have already calculated. For a thermodynamically consistent model one can show that

$$\rho \dot{\psi} + \rho \eta \dot{\theta} - \operatorname{tr}(\mathbf{T}\mathbf{L}) = -\Delta \mathbf{T}^T : \mathbf{L}^p. \quad (2.65)$$

Therefore, the expression for the rate of change of the heat added can be written as

$$\dot{h} = \dot{\eta}\theta - \frac{1}{\rho} \Delta \mathbf{T}^T : \mathbf{L}^p. \quad (2.66)$$

The equation for  $\dot{\eta}$  can then be written as

$$\dot{\eta} = \dot{\eta}_{\mathbf{L}} : \mathbf{L} + \dot{\eta}_{\theta} \dot{\theta} + \dot{\eta}_{\mathbf{L}^p} : \mathbf{L}^p, \quad (2.67)$$

where

$$\begin{aligned}
\dot{\eta}_{\mathbf{L}} &= \frac{1}{\rho} \partial_{\theta} (\mathbf{T}^T), \\
\dot{\eta}_{\dot{\boldsymbol{\theta}}} &= \partial_{\theta} (\boldsymbol{\eta}) - \left[ \partial_{\mathbf{F}^{\theta}} (\psi) - \frac{1}{\rho} \mathbf{F}^{pT} \mathbf{F}^{eT} \partial_{\theta} (\mathbf{T}^T) \mathbf{F}^{p-T} \mathbf{F}^{\theta-T} \right] : \partial_{\theta} (\boldsymbol{\alpha}), \\
\dot{\eta}_{\mathbf{L}^p} &= - \left\{ \frac{1}{\rho} \partial_{\theta} (\mathbf{T}^T) \right\}.
\end{aligned} \tag{2.68}$$

Plastic flow would normally contribute to both the rising of temperature and the flowing of heat from the point. If we consider a process that is adiabatic (i.e., we thermally isolate the point) then  $\dot{h}$  must be set to zero, and we should see the rising of the temperature. In the adiabatic case, during plastic flow we have

$$0 = \theta \dot{\eta}_{\mathbf{L}} : \mathbf{L} + \boldsymbol{\theta} \dot{\eta}_{\dot{\boldsymbol{\theta}}} : \dot{\boldsymbol{\theta}} + \theta \dot{\eta}_{\mathbf{L}^p} : \mathbf{L}^p - \frac{1}{\rho} \Delta \mathbf{T}^T : \mathbf{L}^p. \tag{2.69}$$

Therefore the rate of temperature rise due to plastic flow under adiabatic conditions is given by

$$\dot{\boldsymbol{\theta}} = \frac{1}{\boldsymbol{\theta} \dot{\eta}_{\dot{\boldsymbol{\theta}}}} \left[ \frac{1}{\rho} \Delta \mathbf{T}^T : \mathbf{L}^p - \theta \dot{\eta}_{\mathbf{L}} : \mathbf{L} - \theta \dot{\eta}_{\mathbf{L}^p} : \mathbf{L}^p \right]. \tag{2.70}$$

If on the other hand the process is happening under isothermal conditions, one can calculate the heat that needs to be removed from the point. This is given by setting  $\dot{\boldsymbol{\theta}} = 0$  to get

$$\dot{h} = \theta \dot{\eta}_{\mathbf{L}} : \mathbf{L} + \boldsymbol{\theta} \dot{\eta}_{\mathbf{L}^p} : \mathbf{L}^p - \frac{1}{\rho} \Delta \mathbf{T}^T : \mathbf{L}^p.$$

The expression of  $\dot{h}$  can also be used to calculate specific heat capacity  $c$  to get

$$c = \frac{\dot{h}}{\dot{\theta}} = \frac{\dot{\eta}}{\dot{\theta}} - \frac{1}{\rho \dot{\theta}} \Delta \mathbf{T}^T : \mathbf{L}^p. \tag{2.71}$$

## 2.7 Summary and conclusion

In this chapter we have discussed the basic notation. After presenting the kinematics and balance laws, the large deformation thermodynamically consistent theory is discussed for viscoelastic solids based on thermo-plasticity like models. Based upon that theory it is shown that a model for stress and back stress can be calculated by taking the derivative of free energy with respect to elastic and plastic deformation gradient respectively are given by the equations

$$\mathbf{T}^T = \rho \partial_{\mathbf{F}^e} (\psi) \mathbf{F}^{eT}, \quad (2.72)$$

and

$$\mathbf{T}^b = \rho \partial_{\mathbf{F}^p} (\psi) \mathbf{F}^{pT}. \quad (2.73)$$

The restriction imposed on the flow rule is also discussed which is given by the relation

$$-\Delta \mathbf{T}^T : \mathbf{L}^p \leq 0, \quad (2.74)$$

for a model to be thermodynamically consistent. Finally, the heat generation and flow at the point is discussed and conditions for the adiabatic and isothermal conditions are derived.

Later, the expression for the specific heat capacity is calculated which is given by

$$c = \frac{\dot{h}}{\dot{\theta}} = \frac{\dot{\eta}}{\dot{\theta}} \theta - \frac{1}{\rho \dot{\theta}} \Delta \mathbf{T}^T : \mathbf{L}^p. \quad (2.75)$$

## Chapter 3

# Constitutive modeling and assumptions

In the previous chapter we have discussed the framework for developing the large deformation thermodynamically consistent viscoelastic model. In this chapter we will discuss the one-dimensional mechanical analog which will be used to develop the constitutive model to capture the response from very low to very high strain rates. The idea of the mechanical analog will then be used to develop a three-dimensional constitutive model.

### 3.1 Mechanical analog for the model

The constitutive model that will be developed has similar ideas incorporated as those given by Boyce et al. [36], Arruda and Boyce [54, 56, 36, 52, 53, 57, 58] and Krempl and co-workers [60, 61, 62, 63] which require a model for stress, back stress and a flow rule. These models were extended by Anand et al. [94] and Mulliken et al. [95]. The model

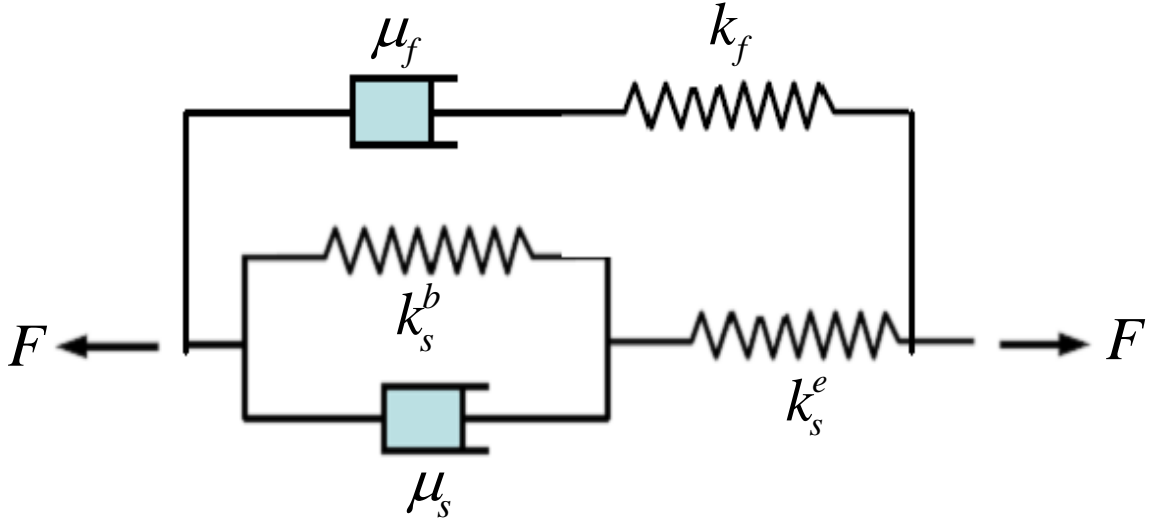


Figure 3.1: Mechanical analog of proposed constitutive model for rate dependent thermal plasticity.

developed here is based on the mechanical analog shown in Figure 3.1. This analog contains a standard linear solid in parallel with a fast relaxation rate element. The standard solid element consists of an elastic spring  $k_s^e$  in series with viscoelastic element consisting of a back stress spring  $k_s^b$  in parallel to dashpot with viscosity  $\mu_s$ . The fast rate element consists of the spring  $k_f$  and dashpot  $\mu_f$ . The subscript "s" and "f" denote, respectively, the "slow" and "fast" relaxation rates.

If we construct a constitutive model based on the mechanical analog shown in the Figure 3.1, the total load  $F$  is given by the sum of the loads  $F_s$  and  $F_f$ , where load  $F_s$  corresponds to the load from standard linear solid and the load  $F_f$  corresponds to the load from fast relaxation element. For a linear solid element the load  $F_s$  can be calculated as  $F_s = k_s^e \varepsilon_s^e$  where  $k_s^e$  represents the stiffness in the elastic spring and  $\varepsilon_s^e$  represents the strain in this spring. The backstress spring is modeled by the equation  $F_s^b = k_s^b \varepsilon_s^p$  where

$k_s^b$  represents the stiffness in the back stress spring and  $\varepsilon_s^p$  represents the strain in the back stress spring. The load  $F_{\mu s}$  is the load in the viscous element and modeled by the equation  $F_{\mu s} = \mu_s \dot{\varepsilon}_s^p$  where  $\mu_s$  represents the viscosity and  $\dot{\varepsilon}_s^p$  represents the rate of straining of the element. Similarly, for the fast relaxation element, the load  $F_f$  can be calculated as  $F_f = k_f \varepsilon_f^e$  and the load  $F_{\mu f} = \mu_f \dot{\varepsilon}_f^p$ . The total strain in the system is given by

$$\varepsilon = \varepsilon_s^e + \varepsilon_s^p = \varepsilon_f^e + \varepsilon_f^p . \quad (3.1)$$

The applied load  $F$  on the system is given by

$$F = F_s + F_f , \quad (3.2)$$

$$F_s = F_s^b + F_{\mu s} ,$$

$$F_f = F_{\mu f} .$$

Under these conditions, the spring  $k_s^e$  carries the load  $F_s$ , which is distributed between the back stress spring  $k_s^b$  and the damper  $\mu_s$ . From the constitutive equation we have

$$F_{\mu s} = F_s - F_s^b = \mu_s \dot{\varepsilon}_s^p ,$$

giving the rate of extension of the viscous damper and back stress element through the relation

$$\dot{\varepsilon}_s^p = \frac{1}{\mu_s} [F_s - F_s^b] = \frac{1}{\mu_s} \Delta F_s , \quad (3.3)$$

where  $\Delta F_s = F_s - F_s^b$  is the overstress. This is the difference between load carried by elastic spring  $k_s^e$  and back stress spring  $k_s^b$ . Considering load  $F_f$ , this load is carried by spring  $k_f$  and by the damper  $\mu_f$ . The extension of the viscous damper  $\mu_f$  is given by

$$\dot{\varepsilon}_f^p = \frac{1}{\mu_f} F_f . \quad (3.4)$$

This material model is defined by the values of  $k_s^e$ ,  $k_s^b$ ,  $\mu_s$ ,  $k_f$  and  $\mu_f$ . Considering the case where  $\mu_s \gg \mu_f$ , there will be fast relaxation in damper  $\mu_f$  compared to  $\mu_s$ . Therefore, for very low strain rates the relaxations are faster in the damper  $\mu_f$  therefore giving  $F_f \approx 0$ , and the whole of the response will come from the standard linear solid and is given by  $F_s$ . But for high strain rates, in which the time is not sufficient enough for the stress  $F_f$  to relax out, the total load will be the summation of  $F_s$  and  $F_f$ . Therefore, the additional spring  $k_f$  and dashpot  $\mu_f$  gives the flexibility of capturing the high rate response without contributing to the low rate response characterized in slow tests by the standard solid model.

## 3.2 Response of the mechanical analog for different tests

In this dissertation a diverse set of experiments which includes monotonic compression experiments at different strain rates and temperatures, ultrasonic wave speed measurement and uniaxial cyclic tests are used to determine the material parameters in a constitutive model. In this section let us see how the mechanical analog will behave under different experimental conditions.

### 3.2.1 Quasistatic loading

Quasistatic loading corresponds to a very slow loading rate. If the loading rate is slow enough so that we can assume that the high speed element is relaxed at all times, then the quasistatic response measures the behavior of the standard linear solid element as shown in Figure 3.2.

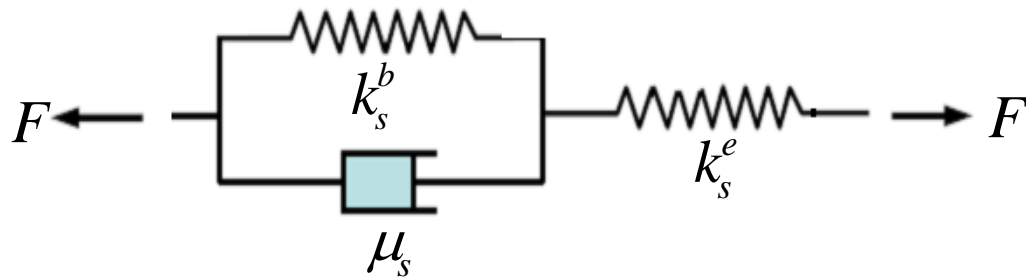


Figure 3.2: Mechanical analog corresponding to the quasistatic testing.

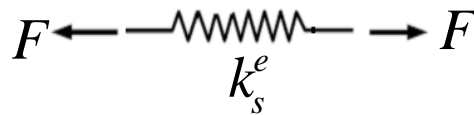


Figure 3.3: Mechanical analog corresponding to the quasi fast loading at equilibrium

### 3.2.2 Quasi-fast deformation at equilibrium

Quasi-fast tests corresponds to loading rates faster than the quasistatic loading, but slower than the high rate loading, such that the high speed element is relaxed at all times. If we do a Quasi-fast deformation at equilibrium then  $\mu_s$  will be large such that  $\dot{\varepsilon}_s^p$  will be slow, so that whole of the response will come from the spring  $k_s^e$  while the spring-dashpot part is close to locked as shown in Figure 3.3. This type of deformation at equilibrium gives a good measure of  $k_s^e$  as a function of elastic deformation.

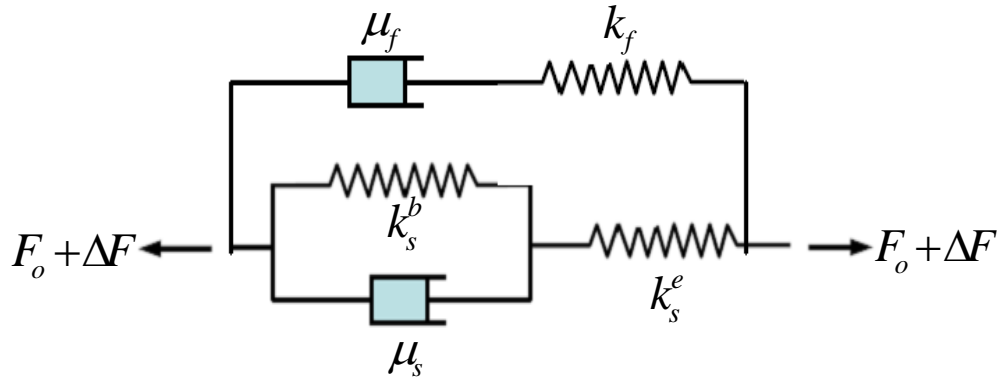


Figure 3.4: Mechanical analog corresponding to the rapid load  $\Delta F$  superimposed with force  $F_o$  for an ultrasonic testing.

### 3.2.3 Ultrasonic testing at constant load

Ultrasonic testing corresponds to a rapid loading rate superposed on a slow loading. In most cases ultrasonic testing is done in two steps, firstly a constant load  $F_o$  is applied for a relatively large time period followed by a rapid superimposed force  $\Delta F$ . This is shown in Figure 3.4.

For the initial force  $F_o$  the time of application is large. As a result the force in friction element  $F_{\mu_f} = 0$ , which also gives  $F_f = 0$ . When the rapid load  $\Delta F$  is applied for a very short amount of time, the  $\mu_s$  and  $\mu_f$  elements will initially seem locked and so elements  $k_s^e$  and  $k_f$  only deforms under load  $\Delta F$  and the entire system will behave as two springs in parallel. As a result, ultrasonics measures the response of the system shown in Figure 3.5.

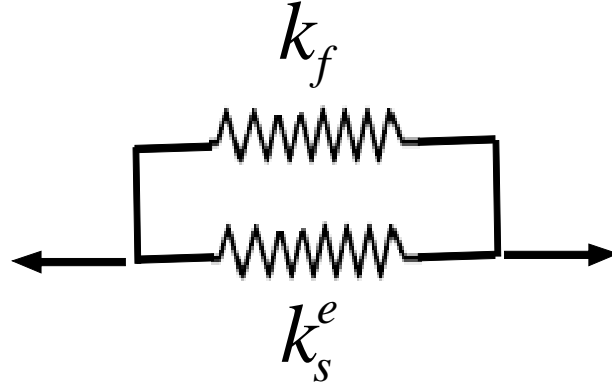


Figure 3.5: Mechanical analog corresponding to an ultrasonic testing

### 3.3 Constitutive model

The idea of the mechanical analog presented in the previous section can be used to develop a three-dimensional nonlinear constitutive model. As in the mechanical analog, the total deformation gradient  $\mathbf{F}$  is assumed to decompose into two parts for each element such that

$$\mathbf{F} = \mathbf{F}_s^e \mathbf{F}_s^p = \mathbf{F}_f^e \mathbf{F}_f^p, \quad (3.5)$$

where  $\mathbf{F}_s^e$  and  $\mathbf{F}_s^p$  are, respectively, the elastic and plastic deformation gradient corresponding to the slow strain rate response given by standard linear solid element and  $\mathbf{F}_f^e$  and  $\mathbf{F}_f^p$  are, respectively, the elastic and plastic deformation gradient corresponding to the high strain rate response of the high relaxation element. Since the two elements are in parallel, the total Cauchy stress  $\mathbf{T}$  can be written as

$$\mathbf{T} = \mathbf{T}_s + \mathbf{T}_f, \quad (3.6)$$

where  $\mathbf{T}_s$  is the stress corresponding to the low strain rate element (standard solid) and  $\mathbf{T}_f$  is the stress that comes from the higher strain rate element. The overstress  $\Delta\mathbf{T}_s$ , which is the properly invariant difference between stress and back stress, can be written as

$$\Delta\mathbf{T}_s = \mathbf{F}_s^{e-1} \mathbf{T}_s \mathbf{F}_s^e - \mathbf{T}_s^b, \quad (3.7)$$

where  $\mathbf{T}_s^b$  is the back stress for the standard linear solid.  $\Delta\mathbf{T}_f$  can be defined by

$$\Delta\mathbf{T}_f = \mathbf{F}_f^{e-1} \mathbf{T}_f \mathbf{F}_f^e, \quad (3.8)$$

since there is no back stress in the fast relaxation element. The restriction imposed on the flow rule due to thermodynamically consistency condition can be satisfied by setting

$$-\Delta\mathbf{T}_s^T : \mathbf{L}_s^p \leq 0, \quad (3.9)$$

$$-\Delta\mathbf{T}_f^T : \mathbf{L}_f^p \leq 0, \quad (3.10)$$

where  $\mathbf{L}_s^p$  and  $\mathbf{L}_f^p$  are, respectively, the plastic velocity gradient corresponding to  $\mathbf{F}_s^p$  and  $\mathbf{F}_f^p$ , and are given by the equations

$$\mathbf{L}_s^p = \dot{\mathbf{F}}_s^p \mathbf{F}_s^{p-1}, \quad (3.11)$$

$$\mathbf{L}_f^p = \dot{\mathbf{F}}_f^p \mathbf{F}_f^{p-1}. \quad (3.12)$$

In the remaining of the dissertation we will develop models to characterize the three dimensional model based on this analog by providing specific experimental results and developing models for  $\mathbf{T}_s, \mathbf{T}_s^b, \dot{\mathbf{F}}_s^p$  for the standard linear solid element and  $\mathbf{T}_f, \dot{\mathbf{F}}_f^p$  for high relaxation element.

### 3.4 Assumed form of the free energy

The constitutive model for the stress and back stress can be tied together by assuming these are part of a consistent thermodynamic formulation. As discussed in the previous chapter, once the free energy is known, the stress and back stress can be calculated using, respectively, the derivative of free energy with respect to elastic and plastic deformation gradient. The constitutive model developed in the literature assumes the form to be separable into additive parts of the free energy and is given by

$$\psi = \psi^e(\mathbf{F}^e, \theta) + \psi^b(\mathbf{F}^p, \theta), \quad (3.13)$$

where  $\psi^e$  is the free energy which depends on the elastic deformation gradient and temperature and  $\psi^b$  is the free energy which depends on the plastic deformation gradient and temperature. From this form of the free energy the constitutive model for stress and back stress can be calculated as

$$\mathbf{T}^T = \rho \partial_{\mathbf{F}^e} (\psi^e) \mathbf{F}^{eT}, \quad (3.14)$$

$$\mathbf{T}^{bT} = \rho \partial_{\mathbf{F}^p} (\psi^b) \mathbf{F}^{pT}. \quad (3.15)$$

Such a type of free energy has the advantage that the model for stress and back stress come from different parts of the free energy that do not depend on one another. But, this form of free energy, as will be explained in Chapter 5, cannot capture the development of anisotropy seen with plastic flow. As was shown in Figure 1.4, glassy polymers are sensitive to plastic strain, developing very large differences in the moduli along the two directions, even at relatively small plastic strains. Therefore, to capture this development of anisotropy, the constitutive model developed in this dissertation is based on the form

$$\psi = \psi_s(\mathbf{F}_s^e, \mathbf{F}_s^p, \theta) + \psi_f(\mathbf{F}_f^e, \theta) + \psi_\theta(\theta), \quad (3.16)$$

where  $\psi_s(\mathbf{F}_s^e, \mathbf{F}_s^p, \theta)$  and  $\psi_f(\mathbf{F}_f^e, \theta)$  are, respectively, the free energy terms contributed from the slow and fast response and  $\psi_\theta(\theta)$  is the free energy term contributed from the pure thermal behavior. The part of the free energy from very low strain rates  $\psi_s(\mathbf{F}_s^e, \mathbf{F}_s^p, \theta)$  is assumed to be given by three terms

$$\psi_s(\mathbf{F}_s^e, \mathbf{F}_s^p, \theta) = \psi_{s1}(\mathbf{F}_s^e, \theta) + \psi_{s2}(\mathbf{F}_s^p, \theta) + \psi_{s3}(\mathbf{F}_s^e, \mathbf{F}_s^p, \theta), \quad (3.17)$$

where  $\psi_{s1}$  and  $\psi_{s2}$  are terms which only depend upon the elastic or plastic deformation gradient along with the temperature, and  $\psi_{s3}$  is free energy term that depends upon all three terms of  $\mathbf{F}_s^e$ ,  $\mathbf{F}_s^p$  and  $\theta$ . The free energy contribution from very high strain rates are given by one term  $\psi_f(\mathbf{F}_f^e, \theta)$ . It should be noted that this separation is not unique or well defined at this time since  $\psi_{s1}$  and  $\psi_{s2}$  can simply be included as different parts of  $\psi_{s3}$ . Yet, this separation of terms is convenient in the following development since it helps separate the process of fitting the model. From this form of the constitutive model for free energy the stress and back stress can be calculated as

$$\mathbf{T} = \mathbf{T}_s + \mathbf{T}_f = \rho \partial_{\mathbf{F}_s^e} (\psi_{s1}) \mathbf{F}_s^{eT} + \rho \partial_{\mathbf{F}_s^e} (\psi_{s3}) \mathbf{F}_s^{eT} + \rho \partial_{\mathbf{F}_f^e} (\psi_f) \mathbf{F}_f^{eT}, \quad (3.18)$$

$$\mathbf{T}_s^b = \rho \partial_{\mathbf{F}_s^p} (\psi_{s2}) \mathbf{F}_s^{pT} + \rho \partial_{\mathbf{F}_s^p} (\psi_{s3}) \mathbf{F}_s^{pT}. \quad (3.19)$$

This form of the model for the free energy shows that the expression for stress and back stress both contain  $\psi_{s3}$  since it depends upon both  $\mathbf{F}_s^e$  and  $\mathbf{F}_s^p$ . The calculation of this type of free energy from values of stress and back stress is more difficult than the separable free

energy given by equation 3.13. This proposed type of free energy results in additional terms in stress and back stress that help to capture the development of anisotropy with the plastic flow, and the models constructed are at the same time thermodynamically consistent.

### 3.5 Summary and conclusion

In this chapter we have presented a one dimensional mechanical analog which is used to capture the response at both low and high strain rates. This analog is based on two elements, one having faster relaxation compared to the other, such that its effect dies out for low strain rates and is active only at high strain rates. In the remaining of the dissertation we will develop models to characterize the three dimensional model constructed based on this analog by providing specific experimental results and developing models for  $\psi$ ,  $\mathbf{T}_s$ ,  $\mathbf{T}_f$ ,  $\mathbf{T}_s^b$ ,  $\dot{\mathbf{F}}_s^p$  and  $\dot{\mathbf{F}}_f^p$ .

## Chapter 4

# Modeling the nonlinear thermo-elastic response of glassy polycarbonate

### 4.1 Introduction

In this chapter and the next two chapters we will be using ultrasonic experiments to calculate the response of PC. During ultrasonic testing, as discussed in the previous chapter, the responses are approximately given by a mechanical analog constructed by the slow and fast element elastic springs in parallel as shown in Figure 3.5. In such a case we assume  $\mathbf{F}_s^e \approx \mathbf{F}_f^e = \mathbf{F}^e$  and  $\mathbf{F}_s^p = \mathbf{F}^p$ . Therefore, we will be using  $\mathbf{F}^e$  and  $\mathbf{F}^p$  instead of concentrating on individual components. In Chapter 8, we will provide a way to separate the response of the standard linear solid from the high relaxation element. This is done

using the results at equilibrium.

In this chapter, we construct a nonlinear thermo-elastic model for polycarbonate under load based on a set of experiments conducted at different temperatures in confined compression by Masubichi et al. [7]. These authors have proposed a measurement method under confined compression for calculating the longitudinal and shear wave velocities for PC under high pressure and temperature using ultrasonic wave speed measurements. The model developed in this chapter is a thermodynamically based large deformation thermo-elastic model of this data.

Many models that are used to characterize the thermo-elastic behavior of glassy polymers at large deformations are based on a modeling structure [49, 50, 51, 36, 52, 53, 54, 55, 56, 57, 58, 43, 59, 60, 61] which describe the stress as a function of the elastic deformation gradient along with bulk and shear moduli that depend upon temperature. The bulk and shear moduli are usually fitted using the initial slope of uniaxial compression or tension experiments at different temperatures. In the current work we have used the confined compression experimental results at different temperatures and pressures to make a large deformation thermo-elastic model for stress. The resulting model reproduces the correct longitudinal and shear wave speed moduli measured by the ultrasonic method under confined compression for glassy PC at different temperatures and higher loads.

## 4.2 Experimental measurements

The experimental measurements discussed here were performed by Masubichi et al. [7]. These authors have combined a pressure-volume-temperature (PVT) test system

with an ultrasonic velocity measurement system to calculate the longitudinal and shear wave speed of PC under high pressure using a closed and sealed system. The samples were processed into a cylindrical shape (with 100% ceiling area and 3 mm height) and were set into a PVT system (since the temperature and pressure need to be controlled during the test) and they have measured the longitudinal and shear wave velocities for this PC. The description of the experimental procedure is provided in [7, 96, 97, 98]. The compression and shear wave moduli were calculated using the standard wave equations

$$E = \rho v_l^2, \quad (4.1)$$

$$G = \rho v_s^2, \quad (4.2)$$

where  $E$  is the longitudinal (compression/tension) wave modulus,  $G$  is the shear wave modulus,  $\rho$  is the density,  $v_l$  is the wave speed for longitudinal waves, and  $v_s$  is the wave speed for shear waves. Figure 4.1 shows the specific volume as a function of temperature (T) with various pressures (P). The density can be calculated as the reciprocal of the specific volume using the PVT curves shown in Figure 4.1. Figure 4.2 and 4.3 shows the wave modulus at different temperatures and pressures.

### 4.3 Modeling consideration

In developing a model to characterize the observed changes in the elastic moduli, we will consider an expression for the Cauchy stress  $\mathbf{T}$  that is a function of the elastic deformation gradient and temperature. We first start by constructing a standard thermodynamic thermo-elastic model. Specifically, we will construct a model based on a specific

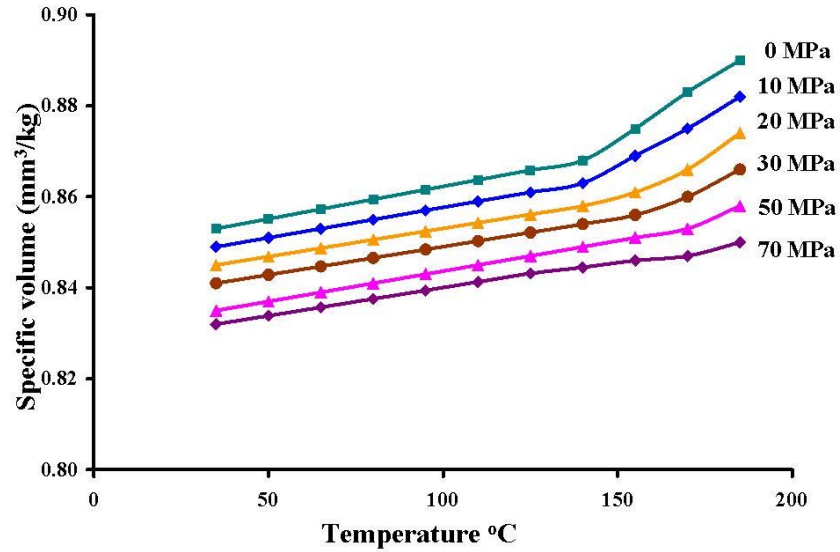


Figure 4.1: Specific volume for PC as a function of temperature at various pressure (Data extracted from [7]).

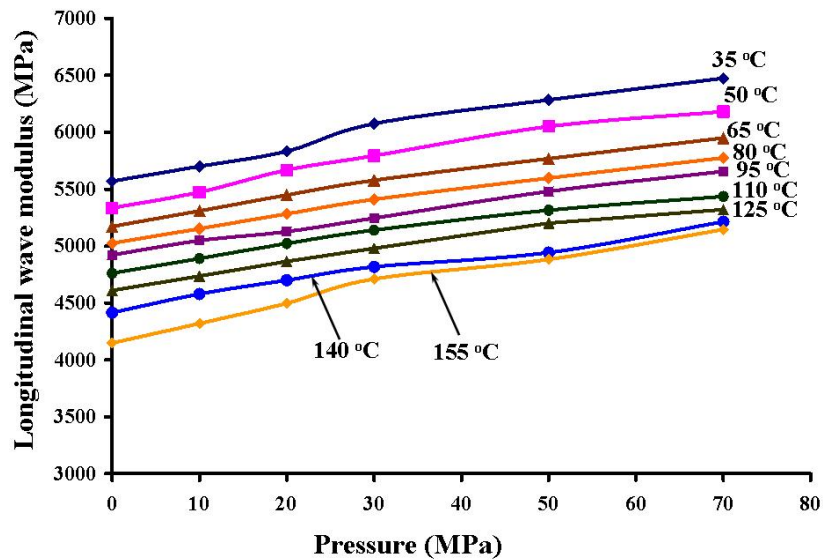


Figure 4.2: Longitudinal wave modulus for PC at different pressure and temperature (Data extracted from [7]).

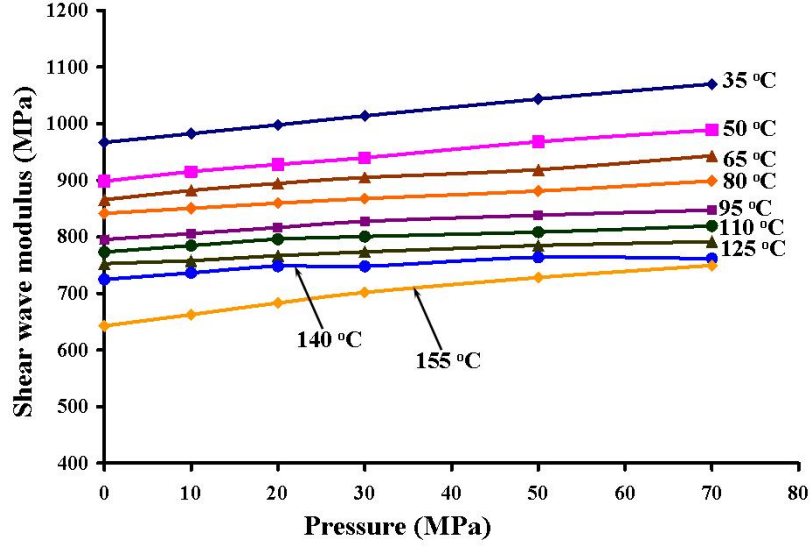


Figure 4.3: Shear wave modulus for PC at different pressure and temperature (Data extracted from [7]).

free energy  $\psi$  given by a function of elastic deformation gradient  $\mathbf{F}^e$ , thermal deformation gradient  $\mathbf{F}^\theta$ , temperature gradient  $\mathbf{G}$  and temperature  $\theta$ . That is, we select a model of the form

$$\psi = \psi^+(\mathbf{F}^e, \mathbf{F}^\theta, \mathbf{G}, \theta), \quad (4.3)$$

where the superscript “+” indicates the function used to model the variable, and we assume that the deformation gradient  $\mathbf{F}$  is decomposed through the multiplicative decomposition  $\mathbf{F} = \mathbf{F}^e \mathbf{F}^\theta$ . The thermodynamic restrictions remove the dependence of the free energy on  $\mathbf{G}$ . We also assume that the free energy does not depend on  $\mathbf{F}^\theta$ . As a result, from this point on we work with a free energy given by a constitutive equation written in the form

$$\psi = \psi^+(\mathbf{F}^e, \theta). \quad (4.4)$$

Without any loss of generality, we can replace this form by one that depends on the elastic right Cauchy stretch tensor where  $\mathbf{C}^e = \mathbf{F}^{eT} \mathbf{F}^e = \mathbf{U}^{e2}$ . This form will be written as

$$\psi = \psi^+(\mathbf{C}^e, \theta). \quad (4.5)$$

As given by Spencer [99], there are three isotropic scalar invariants for a symmetric tensor.

These are given by

$$I_1 = \text{tr}(\mathbf{C}^e), \quad I_2 = \text{tr}(\mathbf{C}^{e2}), \quad I_3 = \text{tr}(\mathbf{C}^{e3}). \quad (4.6)$$

Since the response of materials to volumetric deformations is normally vastly different from the response in shear, we construct a new, yet equivalent, set of invariants given by

$$I_1^* = \frac{I_1}{J^{e\frac{2}{3}}}, \quad I_2^* = \frac{I_2}{I_1^2}, \quad I_3^* = J^e = \det(\mathbf{F}^e), \quad (4.7)$$

where the effect of volume changes are removed from  $I_1$ ,  $I_2$  and explicitly expressed in the form of the volume ratio given by  $I_3^*$ . We, thus, have an expression for free energy of an isotropic material expressed by

$$\psi = \psi^+(I_1^*, I_2^*, I_3^*, \theta). \quad (4.8)$$

As is shown in Negahban [100], as a result of the second law of thermodynamics, the Cauchy stress  $\mathbf{T}$  can be expressed as

$$\mathbf{T}^T = \rho \partial_{\mathbf{F}^e}(\psi) \mathbf{F}^{eT}, \quad (4.9)$$

where  $\rho$  is the current density. Since the Cauchy stress is symmetric, we can remove the transpose from the Cauchy stress.

## 4.4 Model used for free energy

The specific model considered for free energy is described here. This model has the form

$$\psi = \frac{1}{\rho_o} \kappa_\theta \ln^2(J^e) + \frac{1}{\rho_o} G_\theta (I_1^* - 3) + \frac{1}{\rho_o} E_{comb} (I_1^* - 3) \ln^2(J^e) + \psi_\theta(\theta), \quad (4.10)$$

where we will assume that  $\kappa_\theta$ ,  $G_\theta$ ,  $E_{comb}$  and  $\psi_\theta(\theta)$  are functions only of temperature.

Considering this form of free energy and noting that

$$\begin{aligned} \partial_{\mathbf{F}^e} (I_1^* - 3) &= \frac{2}{J^{e\frac{2}{3}}} \left( \mathbf{F}^e - \frac{I_1}{3} \mathbf{F}^{e-T} \right), \\ \partial_{\mathbf{F}^e} [\ln^2(J^e)] &= 2 \ln(J^e) J^e \mathbf{F}^{e-T}, \end{aligned} \quad (4.11)$$

the Cauchy stress can then be calculated from equations 4.9 and 4.11 as

$$\begin{aligned} \mathbf{T} &= \frac{1}{J} \left[ G_\theta \frac{2}{J^{e\frac{2}{3}}} \left( \mathbf{B}^e - \frac{I_1}{3} \mathbf{I} \right) + 2\kappa_\theta J^e \ln(J^e) \mathbf{I} \right. \\ &\quad \left. E_{comb} \left\{ \frac{2}{J^{e\frac{2}{3}}} \left( \mathbf{B}^e - \frac{I_1}{3} \mathbf{I} \right) \ln^2(J^e) + 2 \ln(J^e) (I_1^* - 3) \mathbf{I} \right\} \right]. \end{aligned} \quad (4.12)$$

It should be noted that in this form the stress is automatically zero at zero elastic deformation (i.e.  $\mathbf{F}^e = \mathbf{I}$ ). For the model presented, there are three material parameters  $\kappa_\theta$ ,  $G_\theta$  and  $E_{comb}$  which needs to be calculated.

## 4.5 Fitting the model to experimental results

To fit the experimental data we need to first evaluate the wave moduli under load for the model. Once this is done, we can then use the experimental data to find the values of the three material parameters given in equation 4.12. We take  $\mathbf{e}_i$  to denote an orthonormal base with  $\mathbf{e}_3$  along the direction of compression. During confined compression at constant

temperature, the elastic stretch in the transverse directions will be taken to be unity, but along the direction of compression will be denoted by  $\lambda^e$ . The thermal deformation gradient is assumed to be the same in all the directions which makes the structure of elastic and thermal deformation gradient given by the forms

$$\mathbf{F}^e = \mathbf{e}_1 \otimes \mathbf{e}_1 + \mathbf{e}_2 \otimes \mathbf{e}_2 + \lambda^e \mathbf{e}_3 \otimes \mathbf{e}_3, \quad (4.13)$$

$$\mathbf{F}^\theta = \lambda^\theta \mathbf{e}_1 \otimes \mathbf{e}_1 + \lambda^\theta \mathbf{e}_2 \otimes \mathbf{e}_2 + \lambda^\theta \mathbf{e}_3 \otimes \mathbf{e}_3. \quad (4.14)$$

The deformation gradient  $\mathbf{F} = \mathbf{F}^e \mathbf{F}^\theta$  can then be calculated as

$$\mathbf{F} = \lambda^\theta \mathbf{e}_1 \otimes \mathbf{e}_1 + \lambda^\theta \mathbf{e}_2 \otimes \mathbf{e}_2 + \lambda \mathbf{e}_3 \otimes \mathbf{e}_3, \quad (4.15)$$

where  $\lambda$  is the total axial stretch and is given by the relationship

$$\lambda = \lambda^e \lambda^\theta. \quad (4.16)$$

As  $\mathbf{F}$  is given through the relationship  $\mathbf{F} = \mathbf{F}^e \mathbf{F}^\theta$ , the volume ratio in this homogeneous deformation is given by the relationship

$$J = J^e J^\theta, \quad (4.17)$$

where  $J^e = \det(\mathbf{F}^e)$  and  $J^\theta = \det(\mathbf{F}^\theta)$  are, respectively, the elastic and thermal volume ratios. For the confined compression in this experiment we will assume that the stress is given during the compression by

$$\mathbf{T} = T_t \mathbf{e}_3 \otimes \mathbf{e}_3 + T_t \mathbf{e}_3 \otimes \mathbf{e}_3 + T_a \mathbf{e}_3 \otimes \mathbf{e}_3, \quad (4.18)$$

where  $T_a$  is the axial stress and  $T_t$  is the transverse stress. For  $\mathbf{T} = \mathbf{0}$ ,  $\mathbf{F}^e = \mathbf{I}$ , which gives  $\lambda^e = 1$ , volume ratio  $J$  can then be expressed as

$$J = J^\theta = \lambda^{\theta^3}. \quad (4.19)$$

For  $\mathbf{T} \neq \mathbf{0}$

$$\lambda^e = \frac{\lambda}{\lambda^\theta} = \frac{J}{J^\theta}. \quad (4.20)$$

In evaluating the response we can take the volume  $V_o$  at a given temperature  $\theta_o$  and zero pressure as the reference. For any measured volume  $V$ , we will have

$$J = \frac{V}{V_o}. \quad (4.21)$$

First we focus on the response at zero pressure, which is characterized by  $J^e = 1$  so that  $J = J^\theta$ . For such a case  $J^\theta$  can be calculated for all temperatures. Once we have calculated  $J^\theta$ , then by changing the pressure, we can calculate  $\lambda^e$  using the above relationship. As a result, for all the data points below the glass transition temperature we can calculate  $\lambda^e$  and  $\lambda^\theta$ , so that by this process  $\mathbf{F}^e$  and  $\mathbf{F}^\theta$  can be calculated.

For a general deformation, the components of elastic deformation gradient and stress in the base  $\mathbf{e}_i$  are taken, respectively, as  $F_{ij}^e$  and  $T_{ij}$  so that

$$\mathbf{F}^e = F_{ij}^e \mathbf{e}_i \otimes \mathbf{e}_j, \quad (4.22)$$

$$\mathbf{T} = T_{ij} \mathbf{e}_i \otimes \mathbf{e}_j. \quad (4.23)$$

The wave moduli measured in the experiments can be evaluated from these components through calculating the relations

$$E_a = \frac{\partial T_{33}}{\partial F_{33}^e} \Big|_{\mathbf{F}^e}, \quad G_a = \frac{\partial T_{13}}{\partial F_{13}^e} \Big|_{\mathbf{F}^e}. \quad (4.24)$$

These moduli were evaluated for the model and fit to the two measured moduli through a least square fit. The results of this fit are shown in Figures 4.4, 4.5 and 4.6. The indicated curves were fit to the obtained variables using the functions

$$G_\theta = 1098 \times e^{-\left(\frac{\theta}{357.15}\right)} \text{ MPa}, \quad (4.25)$$

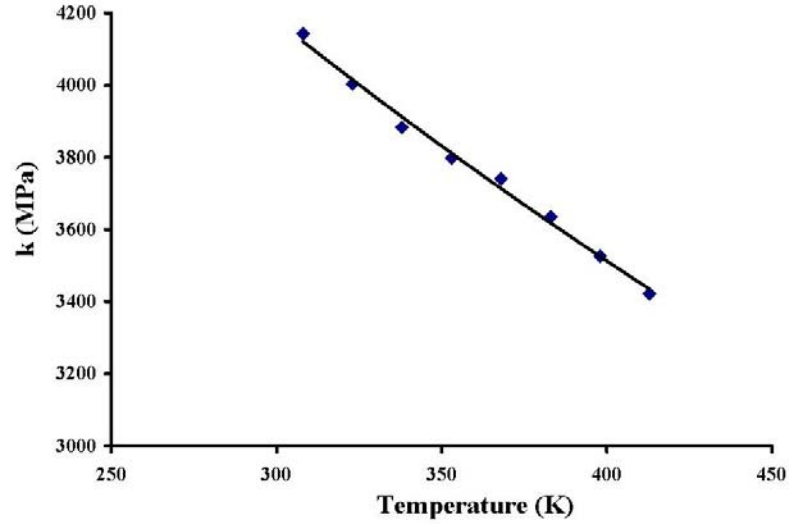


Figure 4.4: Change of the bulk modulus  $\kappa_\theta$  with temperature at different pressures and the fit from the model.

$$\kappa_\theta = 7034 \times e^{-\left(\frac{\theta}{588.23}\right)} \text{ MPa}, \quad (4.26)$$

$$E_{comb} = 60500 \text{ MPa}. \quad (4.27)$$

As can be seen from Figure 4.7 and 4.8, showing the comparison of the experimental results for the wave moduli and those obtained from this fit, the fitting process accurately reproduces the observe wave moduli.

## 4.6 Summary and conclusion

This chapter focuses on modeling the thermal elastic response observed in PC at different temperatures and pressures. Confined compression experiments were performed by Masubichi et al. using a combined PVT test system with an ultrasonic velocity measurement system. They have reported longitudinal and shear wave speeds along with the PVT curve.

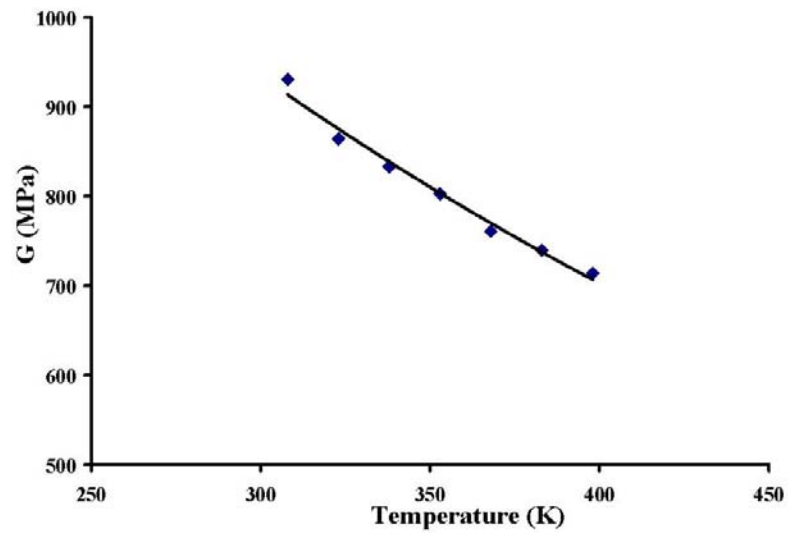


Figure 4.5: Change of the shear modulus  $G_\theta$  with temperature at various pressures and the fit by the model.

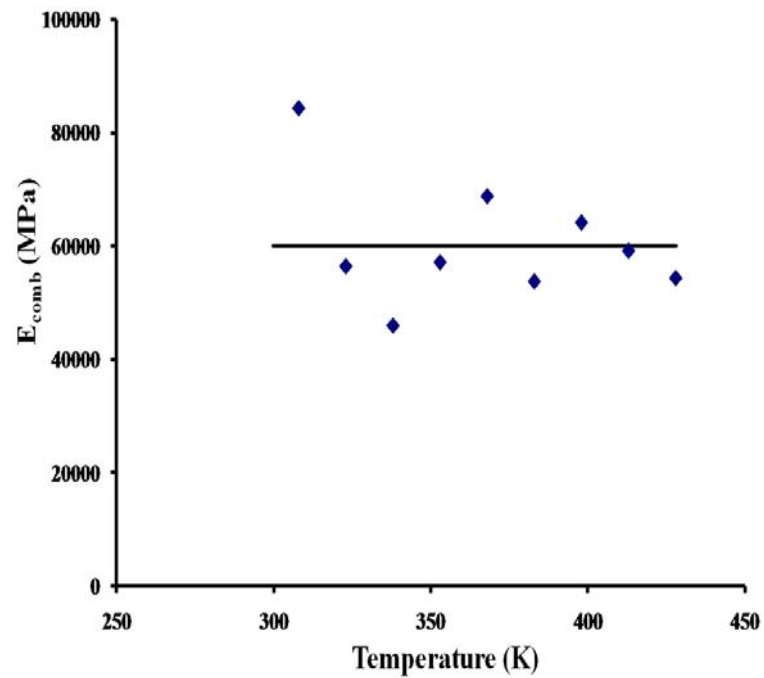


Figure 4.6: Change of combined modulus at various pressures and the fit from the model.

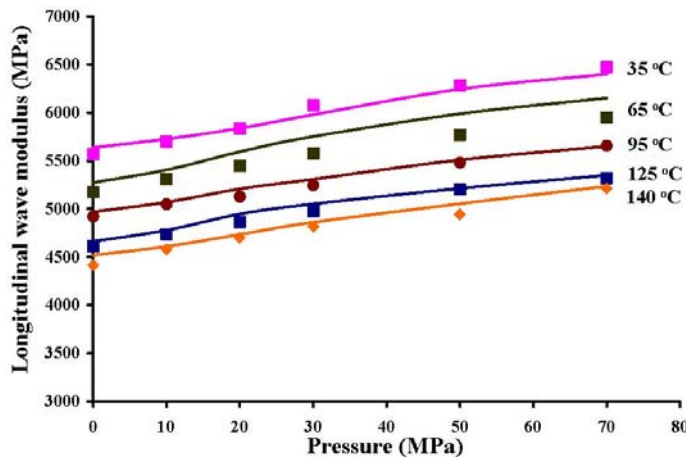


Figure 4.7: Comparison of model results with experimentally measured longitudinal wave moduli (from Masubichi et al. [7]) at different temperature and pressure.

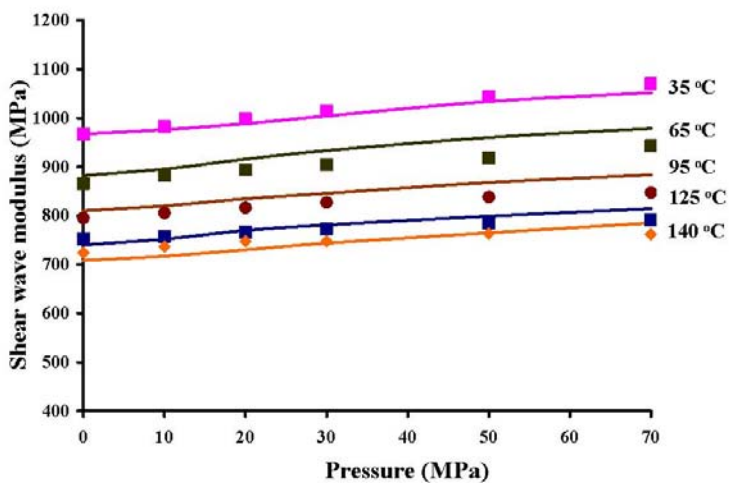


Figure 4.8: Comparison of model results with experimentally measured shear wave moduli (from Masubichi et al. [7]) at different temperature and pressure.

To capture the wave speed moduli at different temperatures and pressures, a model for the free energy based on the elastic deformation gradients was constructed. This model was then simplified and fit to the experimental data. The resulting fits were in good agreement with the experimentally observed moduli and provided the thermo-elastic response of PC at various temperatures and pressures. The large deformation thermo-elastic constitutive model for stress developed is given by

$$\begin{aligned} \mathbf{T} = & \frac{1}{J} \left[ G_{\theta} \frac{2}{J^{e\frac{2}{3}}} \left( \mathbf{B}^e - \frac{I_1}{3} \mathbf{I} \right) + 2\kappa_{\theta} J^e \ln(J^e) \mathbf{I} \right. \\ & \left. E_{comb} \left\{ \frac{2}{J^{e\frac{2}{3}}} \left( \mathbf{B}^e - \frac{I_1}{3} \mathbf{I} \right) \ln^2(J^e) + 2 \ln(J^e) (I_1^* - 3) \mathbf{I} \right\} \right], \end{aligned} \quad (4.28)$$

where the material parameters  $G_{\theta}$ ,  $\kappa_{\theta}$  and  $E_{comb}$  selected to fit the results of Masubichi et al. [7] are given by

$$G_{\theta} = 1098 \times e^{-\left(\frac{\theta}{357.15}\right)} \text{ MPa}, \quad (4.29)$$

$$\kappa_{\theta} = 7034 \times e^{-\left(\frac{\theta}{588.23}\right)} \text{ MPa}, \quad (4.30)$$

$$E_{comb} = 60500 \text{ MPa}, \quad (4.31)$$

where temperature  $\theta$  is in Kelvin.

## Chapter 5

# Modeling the development of elastic anisotropy with plastic flow

In the previous chapter we have developed a thermo-elastic model for stress that reproduces the longitudinal and shear wave moduli measured by the ultrasonic method under confined compression for glassy PC at different temperatures and under load. In doing this we have ignored any plastic flow assuming constrained compression does not induce much plastic flow. In this chapter the development of anisotropy as a result of plastic deformation at room temperature is investigated and modeled for PC. Initially isotropic polycarbonate was subjected to different extents of plastic flow in uniaxial compression and the wave speed moduli were studied using ultrasonic wave speed measurements. Longitudinal and shear wave speed measurements were performed both in the axial and transverse direction. The measured wave moduli clearly indicates the development of anisotropy as a result of plastic deformation. The measured moduli were then used to model the elastic

response of polycarbonate using a model for stress that depends both on the elastic and the plastic parts of the deformation. To simplify the modeling, in this chapter we only consider response at room temperature. The effect of temperature is then considered in the next chapter.

## 5.1 Introduction

As mentioned in Chapter 1, the elastic response of many isotropic solid polymers such as poly vinyl chloride (PVC), poly (methyl methacrylate) (PMMA), polystyrene (PS) and bisphenol A polycarbonate (PC) becomes anisotropic as a result of plastic strain [4, 64, 65, 66, 67, 68, 69, 70]. This is clearly seen in Figure 5.1 where at zero plastic strain the axial and transverse modulus are identical indicating that material is initially isotropic and then the axial modulus increases while the transverse modulus decreases with the increase plastic strain. The extent of difference between the two moduli with plastic strain depends on the polymer and it can be clearly seen from the figure that PC is the most sensitive to plastic strain (i.e. approximately 60% difference in modulus for approximately 60% of the plastic strain).

Even though a large difference can develop between the axial and transverse moduli as a result of plastic flow, as shown in Figure 5.1, this fact is frequently ignored and not reflected in the models that are developed. Many models that are used to characterize the behavior of glassy polymers at large deformations describe the stress as a function of only the elastic deformation. Without a parameter to characterize the anisotropy that develops as a result of plastic flow, these models preserve the initial symmetry (in most

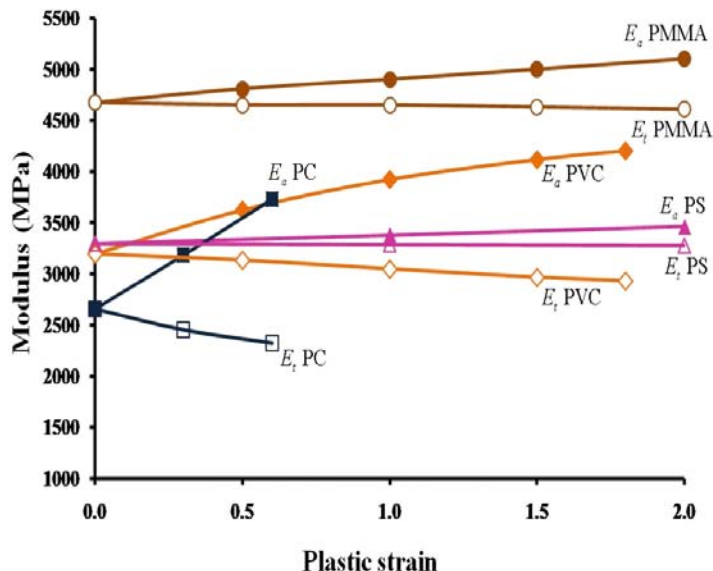


Figure 5.1: Axial and transverse modulus reported as a function of extent of plastic deformation in tension for PVC, PMMA, PS, and PC (from Ward [4]). The axial longitudinal modulus increases while the transverse longitudinal modulus decreases with plastic strain.

cases isotropy) of the elastic response. This is true even after plastic flow. To remedy this, in the modeling of stress one needs to introduce a structure parameter, such as the extent of plastic deformation, in addition to the extent of elastic deformation.

In the current work ultrasonic wave speed measurements are used to characterize the change in the elastic moduli of PC after compression to different extents of plastic strain. These are then used to make a model for the elastic response of PC, using a model for stress that depends on both the elastic and plastic deformation gradients. The resulting model is a finite deformation model that at the limit of zero elastic strain reproduces the correct anisotropic elastic moduli measured by the ultrasonic method.

## 5.2 Experimental measurements

All tests were performed on Lexan 9034. Samples were cut from 1.27 cm thick sheets and tested without any thermal conditioning.

The compression and shear wave moduli were calculated using the standard wave equations

$$E = \rho v_l^2, \quad (5.1)$$

$$G = \rho v_s^2, \quad (5.2)$$

where  $E$  is the longitudinal (compression/tension) wave modulus,  $G$  is the shear wave modulus,  $\rho$  is the density,  $v_l$  is the wave speed for longitudinal waves and  $v_s$  is the wave speed for shear waves. The density was measured through a standard method based on weighing the samples in air and water. The compression and shear wave speeds were evaluated by using a standard pulse-echo method for waves produced using ultrasonic transducers in the 1-5 MHz range [101]. Figure 5.2 shows a schematic of the wave speed measurement method, which is based on dividing the distance traveled by the travel time. The pulse echo method is based on using the same ultrasonic transducer to both produce and measure the wave profile. Once the signal is recorded using an oscilloscope, the time between two consecutive echoes is measured, noting that the impedance mismatch between the PC and transducer results in each echo being out of phase from the original signal, and the distance traveled being twice the thickness of the sample. Figure 5.2 shows a typical digitized signal, where one can see the initial pulse and its echoes. Note that the flat peaks on the initial pulse are due to saturation of the oscilloscope signal and not an actual flat peak in the signal. The initial pulse is not used, only the echoes are used since the interaction between the

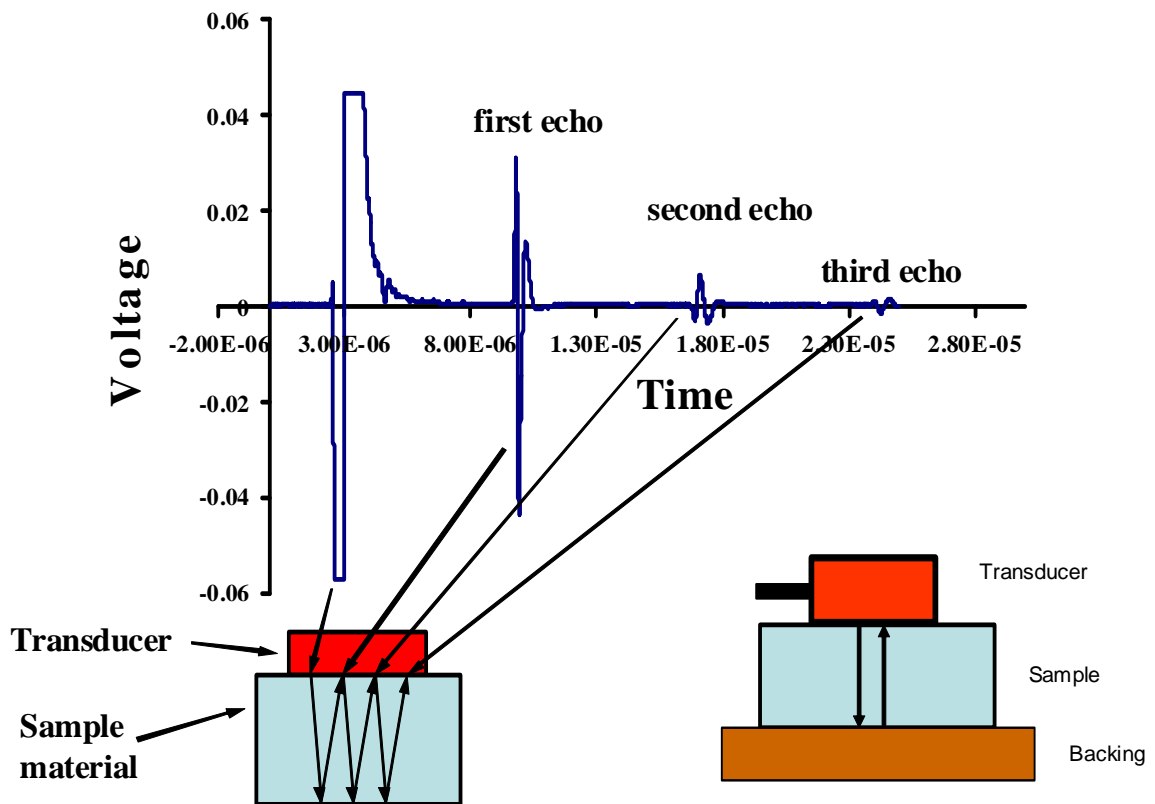


Figure 5.2: Description of the Pulse echo method (from Goel et al. [8]).

transducer and the surface creates an initially complex signal.

The experiments were performed on samples from a series of initially compressed PC cylinders. The PC cylinders were plastically strained to approximately 10%, 20%, 30% and 40% at a strain rate of 0.01 1/s, and then left unloaded for at least 1 day before further testing. The recovery at this temperature after 1 day was minimal, and a study of the samples after 1 day showed no noticeable changes either in the permanent strain or wave measurements. The samples were then ultrasonically tested in the axial direction to calculate the associated longitudinal and shear wave speeds. From these wave speeds the

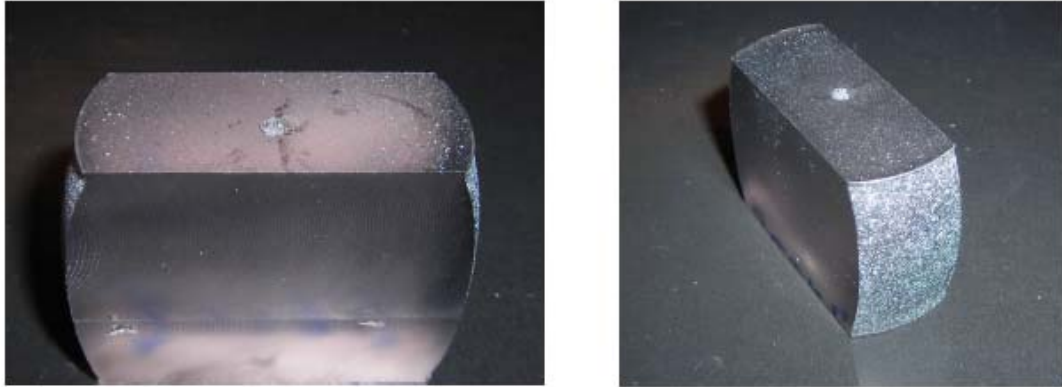


Figure 5.3: Plastically compressed PC sample after cutting for transverse wave speed measurements (from Goel et al. [8]).

axial longitudinal wave modulus  $E_a$  and axial shear wave modulus  $G_a$  were calculated. The samples were then cut as shown in Figure 5.3, and were ultrasonically tested to get the transverse longitudinal wave modulus  $E_t$  and transverse shear wave modulus  $G_t$ . The summary of the testing procedure is shown in Figure 5.4. As shown in the figure, the axial shear wave modulus was measured twice, once during axial wave speed measurements and again during transverse wave speed measurements (indicated as  $G'_a$ ) by orienting the transducer to produce waves that are similar. The two measurements were identical indicating the sample was truly transversely isotropic.

Figures 5.5 and 5.6 show, respectively, the longitudinal and shear moduli that were measured. As can be seen in Figure 5.5, the axial and transverse wave moduli are the same at zero plastic strain, indicating that the sample was initially isotropic. The difference between the axial and transverse moduli increases with increasing plastic strain, which indicates that the material develops more pronounced anisotropy with the increase of plastic strain. For the range of plastic strains considered, the axial wave modulus  $E_a$

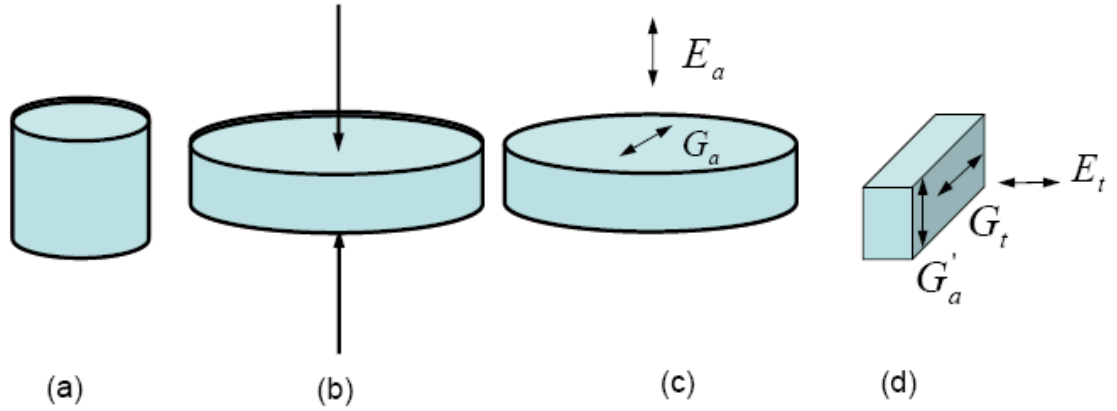


Figure 5.4: Summary of testing: (a) original PC cylinder, (b) compressed PC cylinder, (c) ultrasonic testing in the axial direction, (d) sample cut and ultrasonically tested in transverse direction (from Goel et al. [8]).

decreases and the transverse wave modulus  $E_t$  increases with the increase of the plastic strain in compression. The difference in these moduli is significant compared to the error in the measurement, indicated on the figure. Figure 5.6 shows the shear wave moduli along the different directions. As can be seen in the figure, the shear wave moduli  $G_a$  and  $G'_a$  are the same and different from  $G_t$ .  $G'_a$  and  $G_t$  are measured with the transducer oriented to produce shear along the two directions  $90^\circ$  apart, one along the axis and another perpendicular. The transverse shear wave modulus increases as a function of the plastic strain in compression, while the axial shear wave modulus seems to remain constant.

### 5.3 Modeling considerations

In developing a model to characterize the observed changes in the elastic moduli, we will consider an expression for the Cauchy stress  $\mathbf{T}$  that is a function of the elastic and the plastic deformation gradients. This is done since traditionally used expressions

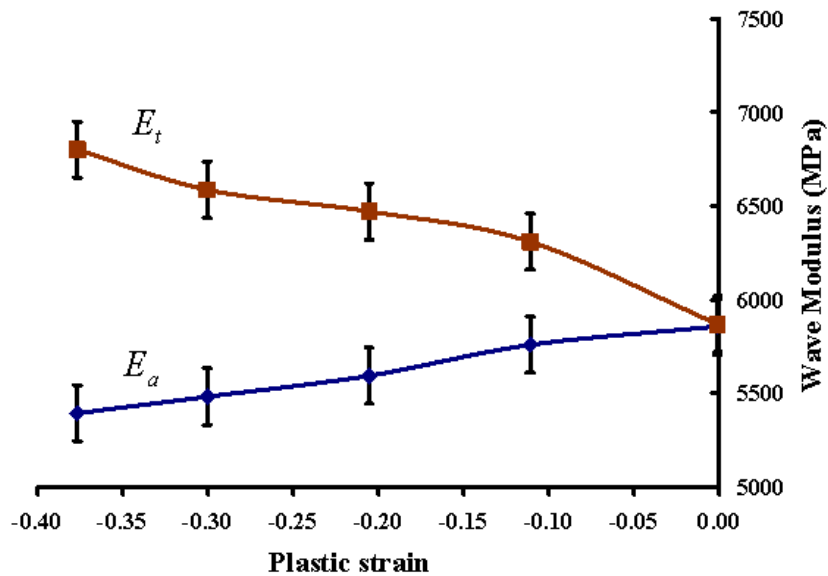


Figure 5.5: Axial and transverse longitudinal wave modulus at different plastic strains (from Goel et al. [8]).

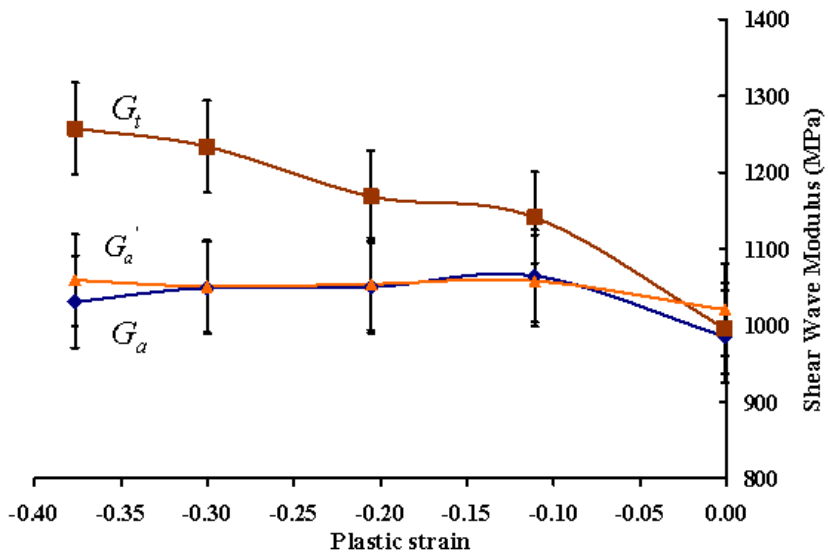


Figure 5.6: Axial and transverse shear wave modulus at different plastic strains (from Goel et al. [8]).

[49, 50, 51, 36, 52, 53, 54, 55, 56, 57, 58, 43, 59, 60, 61], that only depend on the elastic deformation, do not allow modeling of a change in material symmetry. Specifically, we will construct a model based on a specific free energy  $\psi$  given by a function of elastic deformation gradient  $\mathbf{F}^e$ , the plastic deformation gradient  $\mathbf{F}^p$ , and temperature  $\theta$ . That is, we select a model of the form

$$\psi = \psi^+(\mathbf{F}^e, \mathbf{F}^p, \theta), \quad (5.3)$$

where the superscript “+” indicates the function used to model the variable, and we assume that the deformation gradient  $\mathbf{F}$  is decomposed through the multiplicative decomposition  $\mathbf{F} = \mathbf{F}^e \mathbf{F}^p \mathbf{F}^\theta$  for  $\mathbf{F}^\theta$  denoting the thermal deformation gradient. Imposing invariance to rigid body motions allows one to write the model for free energy as

$$\psi = \psi^+(\mathbf{U}^e, \mathbf{F}^p, \theta), \quad (5.4)$$

where  $\mathbf{U}^e$  is the right symmetric factor in the polar decomposition of  $\mathbf{F}^e$ . It also follows that the plastic deformation gradient in this equation can be taken to indifferent to rigid body motions [100] if it is assumed that it can be calculated from the history of the deformation gradient. The initial symmetry of the material is characterized by a group of transformations containing members that reorganize the reference configuration [102, 103]. Each member  $\mathbf{M}$  in the material symmetry group  $\mathcal{G}$  is a transformation of the reference configuration that leaves the reorganized neighborhood of the material point thermodynamically indistinguishable from the original neighborhood. That is, transformation of  $\mathbf{F}$  to  $\mathbf{F}\mathbf{M}$ , and the associated transformations of  $\mathbf{F}^e$  to  $\mathbf{F}^e\mathbf{M}$  and  $\mathbf{F}^p$  to  $\mathbf{M}^{-1}\mathbf{F}^p\mathbf{M}$ , leave the value of the free energy unchanged. For an orthogonal transformation  $\mathbf{M}$ , this requires that

$$\psi = \psi^+(\mathbf{U}^e, \mathbf{F}^p, \theta) = \psi^+(\mathbf{M}^T \mathbf{U}^e \mathbf{M}, \mathbf{M}^T \mathbf{F}^p \mathbf{M}, \theta). \quad (5.5)$$

For an initially isotropic material, with the reference configuration selected appropriately such that all the symmetry transformations are orthogonal [102], the constraint given by equation 5.5 must be satisfied for all orthogonal transformations. Since the decomposition of  $\mathbf{F}^p$  into its symmetric and skew symmetric parts is unique, one can use results given for the scalar isotropic invariants of two symmetric tensors (  $\mathbf{U}^e$  and  $\mathbf{F}_{sym}^p = \frac{1}{2}(\mathbf{F}^p + \mathbf{F}^{pT})$  ) and one skew symmetric tensor (  $\mathbf{F}_{skew}^p = \frac{1}{2}(\mathbf{F}^p - \mathbf{F}^{pT})$  ), as given by Spencer [99] and, more recently in reduced form, by Zheng [104]. Therefore, one can, in general, construct a model for the specific free energy in terms of the 21 isotropic invariants of  $\mathbf{U}^e$ ,  $\mathbf{F}_{sym}^p$  and  $\mathbf{F}_{skew}^p$  which are given by

$$\begin{aligned}
I_1 &= tr(\mathbf{U}^e), & I_2 &= tr(\mathbf{U}^{e2}), & I_3 &= tr(\mathbf{U}^{e3}), \\
I_4 &= tr(\mathbf{F}_{sym}^p), & I_5 &= tr(\mathbf{F}_{sym}^{p2}), & I_6 &= tr(\mathbf{F}_{sym}^{p3}), \\
I_7 &= tr(\mathbf{U}^e \mathbf{F}_{sym}^p), & I_8 &= tr(\mathbf{U}^e \mathbf{F}_{sym}^{p2}), & I_9 &= tr(\mathbf{U}^{e2} \mathbf{F}_{sym}^p), \\
I_{10} &= tr(\mathbf{U}^{e2} \mathbf{F}_{sym}^{p2}), & I_{11} &= tr(\mathbf{F}_{skew}^{p2}), \\
I_{12} &= tr(\mathbf{U}^e \mathbf{F}_{skew}^{p2}), & I_{13} &= tr(\mathbf{U}^{e2} \mathbf{F}_{skew}^{p2}), & I_{14} &= tr(\mathbf{U}^{e2} \mathbf{F}_{skew}^{p2} \mathbf{U}^e \mathbf{F}_{skew}^p), \\
I_{15} &= tr(\mathbf{F}_{sym}^p \mathbf{F}_{skew}^{p2}), & I_{16} &= tr(\mathbf{F}_{sym}^{p2} \mathbf{F}_{skew}^{p2}), & I_{17} &= tr(\mathbf{F}_{sym}^{p2} \mathbf{F}_{skew}^{p2} \mathbf{F}_{sym}^p \mathbf{F}_{skew}^p), \\
I_{18} &= tr(\mathbf{U}^e \mathbf{F}_{sym}^p \mathbf{F}_{skew}^p), & I_{19} &= tr(\mathbf{U}^e \mathbf{F}_{sym}^{p2} \mathbf{F}_{skew}^p), & I_{20} &= tr(\mathbf{U}^{e2} \mathbf{F}_{sym}^p \mathbf{F}_{skew}^p), \\
I_{21} &= tr(\mathbf{U}^e \mathbf{F}_{skew}^{p2} \mathbf{F}_{sym}^p \mathbf{F}_{skew}^p).
\end{aligned} \tag{5.6}$$

Even though plausible, the number of invariants are too many to realistically be used in modeling the response, so we assume that the contribution of the plastic deformation gradient to the free energy is through the right Cauchy stretch tensor  $\mathbf{C}^p = \mathbf{F}^{pT} \mathbf{F}^p$ . We also use  $\mathbf{C}^e = \mathbf{U}^{e2}$  in place of  $\mathbf{U}^e$ , due to a convenience in calculation of the former relative to the latter, and the fact that there is a one-to-one relation between them. As given by

Spencer [99], there are ten isotropic scalar invariants of  $\mathbf{C}^e$  and  $\mathbf{C}^p$ . These are given by

$$\begin{aligned} I_1 &= tr(\mathbf{C}^e), & I_2 &= tr(\mathbf{C}^{e2}), & I_3 &= tr(\mathbf{C}^{e3}), \\ I_4 &= tr(\mathbf{C}^p), & I_4 &= tr(\mathbf{C}^{p2}), & I_6 &= tr(\mathbf{C}^{p3}), \\ I_7 &= tr(\mathbf{C}^e \mathbf{C}^p), & I_8 &= tr(\mathbf{C}^{e2} \mathbf{C}^p), & I_9 &= tr(\mathbf{C}^e \mathbf{C}^{p2}), & I_{10} &= tr(\mathbf{C}^{e2} \mathbf{C}^{p2}). \end{aligned} \quad (5.7)$$

Since the response of materials to volumetric deformations is normally vastly different from the response in shear, we construct a new, yet equivalent, set of invariants given by

$$\begin{aligned} I_1^* &= \frac{I_1}{J^{e\frac{2}{3}}}, & I_2^* &= \frac{I_2}{I_1^2}, & I_3^* &= J^e = \det(\mathbf{F}^e), \\ I_4^* &= \frac{I_4}{J^{p\frac{2}{3}}}, & I_5^* &= \frac{I_5}{I_4^2}, & I_6^* &= J^p = \det(\mathbf{F}^p), \\ I_7^* &= I_7 - I_1 - I_4 + 3, & I_8^* &= I_8 - I_2 - I_4 + 3, & I_9^* &= I_9 - I_1 - I_5 + 3, \\ I_{10}^* &= I_{10} - I_2 - I_5 + 3, \end{aligned} \quad (5.8)$$

where the effect of volume changes are removed from  $I_1$ ,  $I_2$ ,  $I_4$  and  $I_5$  and explicitly expressed in the form of the volume ratio in  $I_3^*$  and  $I_6^*$ . We, thus, have an the expression for the free energy given by

$$\psi = \psi^+(I_1^*, \dots, I_{10}^*, \theta). \quad (5.9)$$

As has been given in Negahban [100], as a result of the second law of thermodynamics, the Cauchy stress  $\mathbf{T}$  can be expressed as

$$\mathbf{T}^T = \rho \partial_{\mathbf{F}^e}(\psi) \mathbf{F}^{eT}, \quad (5.10)$$

where  $\rho$  is the current density. Since the Cauchy stress is symmetric, we can remove “ $T$ ” from the stress. Considering the form of the free energy given in equation 5.9, the Cauchy stress can then be expressed as

$$\mathbf{T} = \rho \sum_{i=1}^{10} \frac{\partial \psi}{\partial I_i^*} \partial_{\mathbf{F}^e}(I_i^*) \mathbf{F}^{eT}, \quad (5.11)$$

where from Appendix A we note that

$$\begin{aligned}
\partial_{\mathbf{F}^e}(I_1^*) &= \frac{2}{J^e \frac{2}{3}} \left( \mathbf{F}^e - \frac{I_1}{3} \mathbf{F}^{e-T} \right), \\
\partial_{\mathbf{F}^e}(I_2^*) &= \frac{4}{I_1^2} \mathbf{F}^e \left( \mathbf{C}^e - \frac{I_2}{I_1} \mathbf{I} \right), \\
\partial_{\mathbf{F}^e}(I_3^*) &= J^e \mathbf{F}^{e-T}, \\
\partial_{\mathbf{F}^e}(I_4^*) &= \partial_{\mathbf{F}^e}(I_5^*) = \partial_{\mathbf{F}^e}(I_6^*) = 0, \\
\partial_{\mathbf{F}^e}(I_7^*) &= 2\mathbf{F}^e (\mathbf{C}^p - \mathbf{I}), \\
\partial_{\mathbf{F}^e}(I_8^*) &= 2\mathbf{F}^e (\mathbf{C}^e \mathbf{C}^p + \mathbf{C}^p \mathbf{C}^e - 2\mathbf{C}^e), \\
\partial_{\mathbf{F}^e}(I_9^*) &= 2\mathbf{F}^e (\mathbf{C}^{p2} - \mathbf{I}), \\
\partial_{\mathbf{F}^e}(I_{10}^*) &= 2\mathbf{F}^e (\mathbf{C}^e \mathbf{C}^{p2} + \mathbf{C}^p \mathbf{C}^{e2} - 2\mathbf{C}^e).
\end{aligned} \tag{5.12}$$

Substituting 5.12 into 5.11 results in the expression for Cauchy stress given by

$$\begin{aligned}
\mathbf{T} &= \rho \left\{ \frac{2}{J^e \frac{2}{3}} \frac{\partial \psi}{\partial I_1^*} \left( \mathbf{B}^e - \frac{I_1}{3} \mathbf{I} \right) + \frac{4}{I_1^2} \frac{\partial \psi}{\partial I_2^*} \mathbf{B}^e \left( \mathbf{B}^e - \frac{I_2}{I_1} \mathbf{I} \right) + J^e \frac{\partial \psi}{\partial I_3^*} \mathbf{I} \right. \\
&\quad + 2 \frac{\partial \psi}{\partial I_7^*} \mathbf{F}^e (\mathbf{C}^p - \mathbf{I}) \mathbf{F}^{eT} + 2 \frac{\partial \psi}{\partial I_8^*} \mathbf{F}^e (\mathbf{C}^e \mathbf{C}^p + \mathbf{C}^p \mathbf{C}^e - 2\mathbf{C}^e) \mathbf{F}^{eT} \\
&\quad \left. + 2 \frac{\partial \psi}{\partial I_9^*} \mathbf{F}^e (\mathbf{C}^{p2} - \mathbf{I}) \mathbf{F}^{eT} + 2 \frac{\partial \psi}{\partial I_{10}^*} \mathbf{F}^e (\mathbf{C}^e \mathbf{C}^{p2} + \mathbf{C}^{p2} \mathbf{C}^e - 2\mathbf{C}^e) \mathbf{F}^{eT} \right\}.
\end{aligned} \tag{5.13}$$

The stress should be zero for zero elastic strain, irrespective of the value of the plastic deformation gradient. Therefore, we should have  $\mathbf{T} = \mathbf{0}$  for  $\mathbf{F}^e = \mathbf{R}^e$ , where  $\mathbf{R}^e$  can be any orthogonal tensor, and this should hold for all  $\mathbf{F}^p$ . This can be satisfied by setting

$$\begin{aligned}
\frac{\partial \psi}{\partial I_3^*} &= 0, \\
\frac{\partial \psi}{\partial I_7^*} + 2 \frac{\partial \psi}{\partial I_8^*} &= 0, \\
\frac{\partial \psi}{\partial I_9^*} + 2 \frac{\partial \psi}{\partial I_{10}^*} &= 0,
\end{aligned} \tag{5.14}$$

for  $\mathbf{F}^e = \mathbf{R}^e$ . One method to satisfy these conditions is to simply assume the last two conditions are always true (even when the elastic strain is not zero) and to take functions

for the free energy that have a derivative with respect to the third invariant that is zero at  $\mathbf{F}^e = \mathbf{R}^e$ . Under such a condition the expression for stress is given by

$$\begin{aligned} \mathbf{T} = & \rho \left\{ \frac{2}{J^{e\frac{2}{3}}} \frac{\partial \psi}{\partial I_1^*} \left( \mathbf{B}^e - \frac{I_1}{3} \mathbf{I} \right) + \frac{4}{I_1^2} \frac{\partial \psi}{\partial I_2^*} \mathbf{B}^e \left( \mathbf{B}^e - \frac{I_2}{I_1} \mathbf{I} \right) + J^e \frac{\partial \psi}{\partial I_3^*} \mathbf{I} \right. \\ & + \frac{\partial \psi}{\partial I_7^*} \mathbf{F}^e [2(\mathbf{C}^p - \mathbf{I}) - (\mathbf{C}^e \mathbf{C}^p + \mathbf{C}^p \mathbf{C}^e - 2\mathbf{C}^e)] \mathbf{F}^{eT} \\ & \left. + \frac{\partial \psi}{\partial I_9^*} \mathbf{F}^e [2(\mathbf{C}^{p2} - \mathbf{I}) - (\mathbf{C}^e \mathbf{C}^{p2} + \mathbf{C}^{p2} \mathbf{C}^e - 2\mathbf{C}^e)] \mathbf{F}^{eT} \right\}. \end{aligned} \quad (5.15)$$

Even with these simplifications, five material functions  $\frac{\partial \psi}{\partial I_1^*}$ ,  $\frac{\partial \psi}{\partial I_2^*}$ ,  $\frac{\partial \psi}{\partial I_3^*}$ ,  $\frac{\partial \psi}{\partial I_7^*}$  and  $\frac{\partial \psi}{\partial I_9^*}$  need to be evaluated at each loading point. Since we only have four elastic moduli measured per plastic strain, the fitting of all five would be impossible with the current experimental results. In addition, when confining the response to uniaxial compression, it can be shown that the expressions to fit the material functions result in a linear system with a singular coefficient matrix (see Appendix B), so only three conditions can be satisfied. As a result, we chose to set the derivative of the free energy with respect to  $I_2^*$  and  $I_9^*$  equal to zero, and to fit the three remaining derivatives to the four moduli using a least square fit. For the remainder of this chapter we will focus on using a model for stress given by

$$\begin{aligned} \mathbf{T} = & \left\{ \frac{2}{J J^{e\frac{2}{3}}} \rho_o \frac{\partial \psi}{\partial I_1^*} \left( \mathbf{B}^e - \frac{I_1}{3} \mathbf{I} \right) + \rho_o \frac{\partial \psi}{\partial I_3^*} \frac{J^e}{J} \mathbf{I} \right. \\ & \left. + \rho_o \frac{\partial \psi}{\partial I_7^*} \frac{1}{J} \mathbf{F}^e [2(\mathbf{C}^p - \mathbf{I}) - (\mathbf{C}^e \mathbf{C}^p + \mathbf{C}^p \mathbf{C}^e - 2\mathbf{C}^e)] \mathbf{F}^{eT} \right\}. \end{aligned} \quad (5.16)$$

## 5.4 Fitting the model to the results from compression

To fit the experimental data we need to evaluate the wave moduli from the model after plastic flow due to uniaxial compression. Once this is done, we can then use the experimental data to find the values of the three derivatives of the free energy given in

equation 5.16.

We take  $\mathbf{e}_i$  to denote an orthonormal base with  $\mathbf{e}_3$  along the direction of compression. During uniaxial compression, the plastic deformation gradient is given by the form

$$\mathbf{F}^p = \lambda^{p*} \mathbf{e}_1 \otimes \mathbf{e}_1 + \lambda^{p*} \mathbf{e}_2 \otimes \mathbf{e}_2 + \lambda^p \mathbf{e}_3 \otimes \mathbf{e}_3, \quad (5.17)$$

where  $\lambda^p$  is the plastic stretch in the axial compression direction and  $\lambda^{p*}$  is the plastic stretch in the transverse direction. These are taken to be the measured stretches of the sample after plastic deformation. The components of the elastic deformation gradient and the stress in the base  $\mathbf{e}_i$  are taken, respectively, as  $F_{ij}^e$  and  $T_{ij}$  so that

$$\mathbf{F}^e = F_{ij}^e \mathbf{e}_i \otimes \mathbf{e}_j, \quad (5.18)$$

$$\mathbf{T} = T_{ij} \mathbf{e}_i \otimes \mathbf{e}_j. \quad (5.19)$$

The wave moduli considered in the experiments can be evaluated from these components through the relations

$$E_a = \frac{\partial T_{33}}{\partial F_{33}^e} \Big|_{\mathbf{F}^e=\mathbf{I}}, \quad E_t = \frac{\partial T_{11}}{\partial F_{11}^e} \Big|_{\mathbf{F}^e=\mathbf{I}}, \quad G_a = G'_a = \frac{\partial T_{13}}{\partial F_{13}^e} \Big|_{\mathbf{F}^e=\mathbf{I}}, \quad G_t = \frac{\partial T_{12}}{\partial F_{12}^e} \Big|_{\mathbf{F}^e=\mathbf{I}}. \quad (5.20)$$

These moduli were evaluated for the model and fit to the four measured moduli through a least square fit. The result of this fit is shown in Figures 5.7, 5.8 and 5.9. The parameters  $\kappa$  and  $G$  in the figures, which, respectively, become associated with the isotropic bulk modulus and shear modulus, are defined in terms of the derivatives of the free energy given by  $G = 2\rho_o \frac{\partial \psi}{\partial I_1^*}$  and  $\kappa(1 - J^e) = \rho_o \frac{\partial \psi}{\partial I_3^*}$ . The indicated curves were fit to the obtained variables using the functions

$$\kappa = 4670 + 200 \times (I_4^* - 3) \quad MPa, \quad (5.21)$$

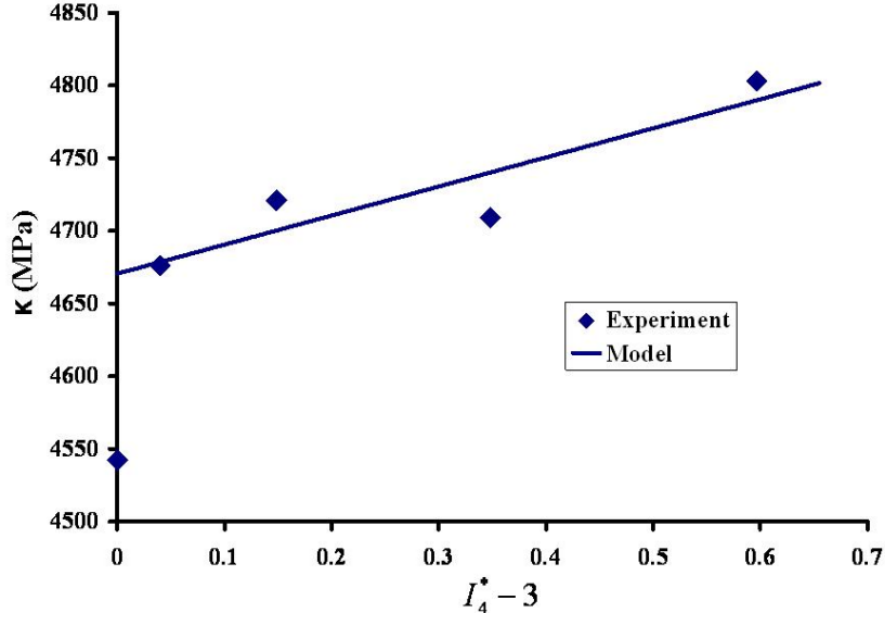


Figure 5.7: Change of the isotropic bulk modulus with plastic deformation.

$$G = 1072 - 159 \times (I_4^* - 3) \text{ MPa}, \quad (5.22)$$

$$\rho_o \frac{\partial \psi}{\partial I_7^*} = -283 - 150 \times e^{-\frac{(I_4^* - 3)}{0.125}} + 433 \times e^{-\frac{(I_4^* - 3)}{0.004}} \text{ MPa}. \quad (5.23)$$

In constructing these models we have assumed that these are only a function of the plastic deformation gradient. As can be seen from Figure 5.10 and 5.11, which show the comparison of the experimental results for the wave moduli and those obtained from this fit, the fit accurately reproduces the observed wave moduli, with better results for the longitudinal waves as opposed to the shear waves.

In Figure 5.12 and 5.13 we compare the model predictions with the results provided by Ward for PC after uniaxial tension [4], also shown in Figure 5.1. As can be seen, the model trends follow that reported by Ward, but the magnitudes are different. This might be attributed to the fact that the current results were for wave moduli measured using a 1 MHz

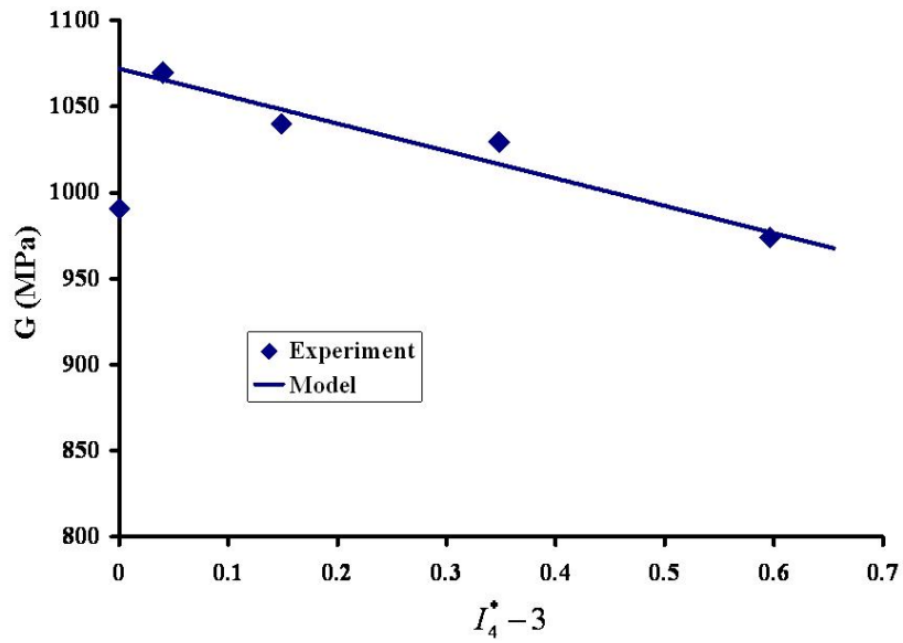


Figure 5.8: Change of the isotropic shear modulus with plastic flow.

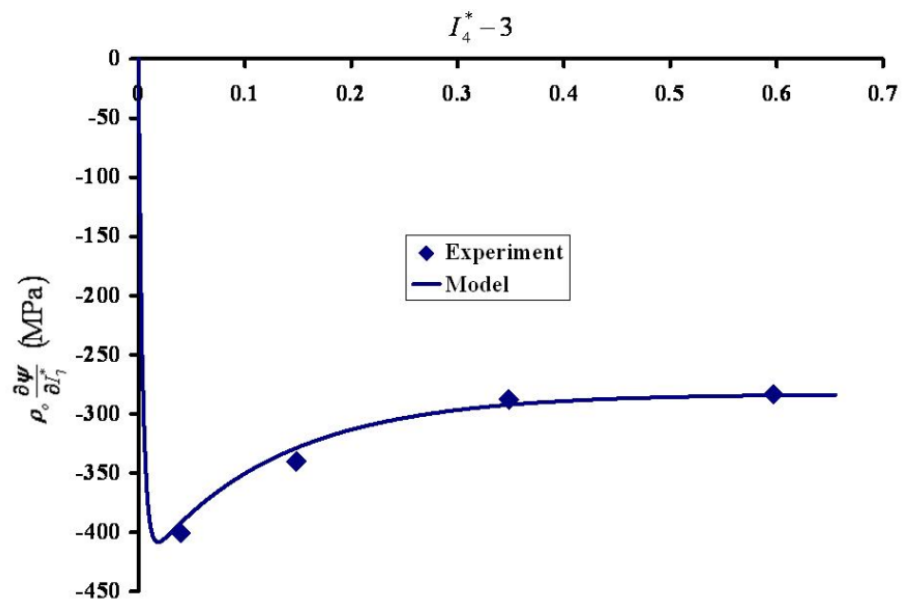


Figure 5.9: Change of  $\rho_o \frac{\partial \psi}{\partial I_7^*}$  as a function of plastic flow.

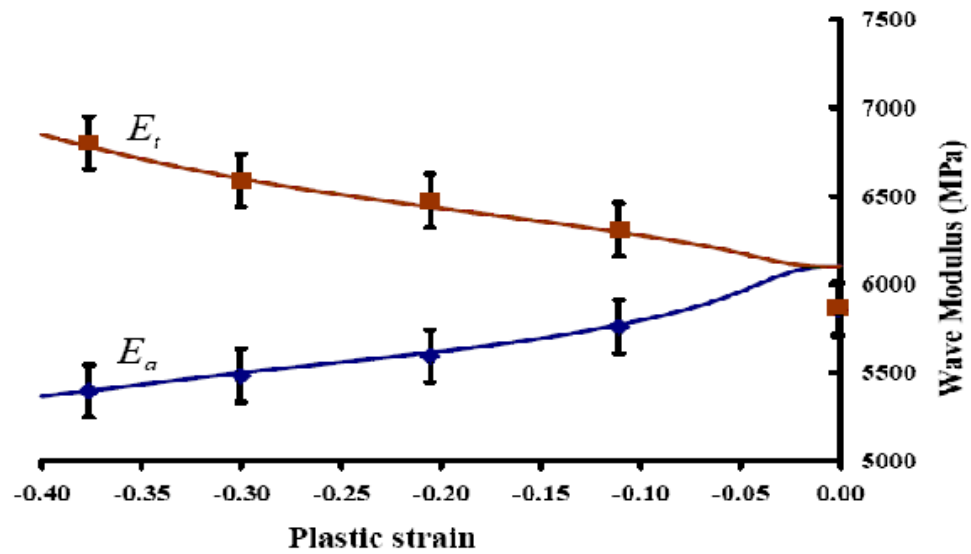


Figure 5.10: Comparison of model results with experimentally measured wave moduli  $E_a$  and  $E_t$  (From Goel et al. [8]) for the given plastic strains.

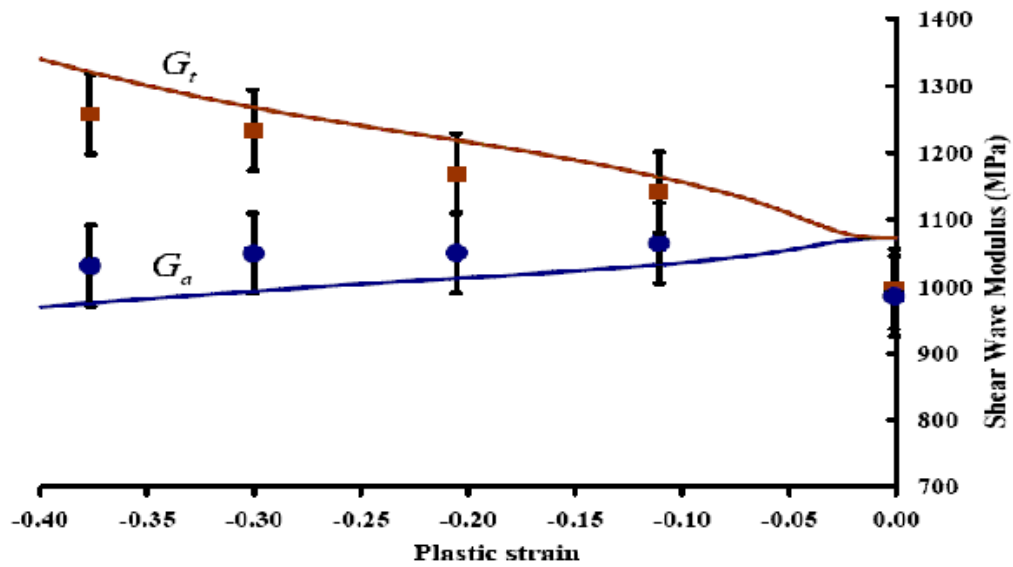


Figure 5.11: Comparison of model results with experimentally measured wave moduli  $G_a$  and  $G_t$  (From Goel et al. [8]) for the given plastic strains.

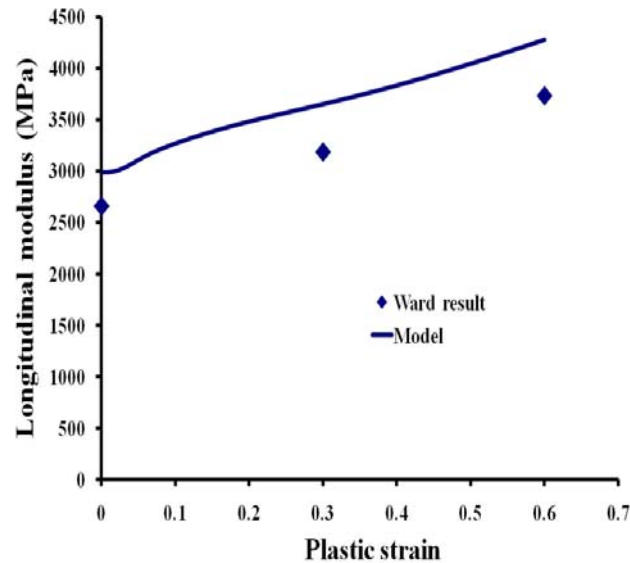


Figure 5.12: Comparison between model predictions and results presented by Ward [4] for longitudinal modulus during after extension.

transducer as opposed to the results reported by Ward that were measured using frequencies in the range of 100-400 Hz, or they might be due to the difference in the materials used here and by Ward.

## 5.5 Summary and conclusion

This chapter focuses on measuring and modeling the anisotropic elastic response observed in PC after plastic deformation at room temperature. Uniaxial compression was used to prepare samples with different extents of plastic deformation, up to approximately 40% compression (a logarithmic strain of approximately -0.5). Ultrasonic wave speed measurements were used to obtain the longitudinal and shear wave speed moduli along the axis of compression and perpendicular to this axis. The transverse wave moduli, both lon-

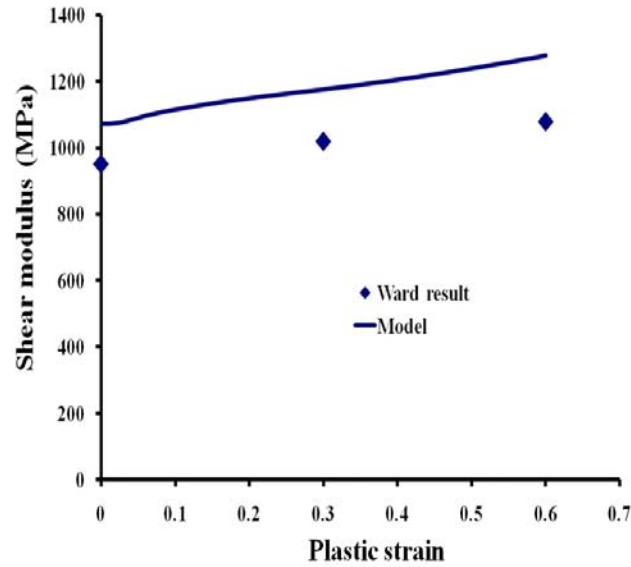


Figure 5.13: Comparison between model predictions and results presented by Ward [4] for shear modulus during after extension.

gitudinal and shear, increased with plastic compression, while in the axial direction the longitudinal wave modulus decreased and shear wave modulus stayed constant.

The extent of the difference in the wave moduli between axial and transverse directions for PC is substantial, indicating that ignoring this could result in substantial error in the predictions of the resulting models. These differences were in the same order as the imposed plastic strains (i.e., approximately 20% difference in moduli for 40% plastic compressive strain).

To capture the observed development of anisotropic elastic moduli, a model for the free energy based on the elastic and plastic deformation gradients was constructed. Since the PC used was initially isotropic, representations for this model were provided for an initially isotropic material. This model was then simplified and fit to the experimental data. The resulting fits were in good agreement with the experimentally observed moduli,

and predicted similar trends to experimental results reported in tension by Ward [4].

## Chapter 6

# The development of elastic anisotropy at different temperature

### 6.1 Abstract

The development of anisotropy as a result of plastic deformation below the glass transition temperature is investigated here for different temperatures. Initially isotropic polycarbonate is subjected to different extents of plastic strain in compression and the development of its anisotropic wave moduli are studied using ultrasonic wave speed measurements for plastic deformation at different temperatures. Longitudinal wave speed measurements were performed both in the axial and transverse directions at each temperature. To model the response, the anisotropic model for stress developed for the response at room temperature in the previous chapter was then modified to add temperature dependence. The temperature dependence was shown to be captured by separate Arrhenius equations

separately scaling the "initially isotropic" and "anisotropic" parts.

## 6.2 Experimental measurements

All tests were performed on Lexan 9034. Samples were cut from 1.27 cm thick sheets and tested without any thermal conditioning. The compression longitudinal wave moduli were calculated using the standard wave equations

$$E = \rho v_l^2, \quad (6.1)$$

where  $E$  is the longitudinal (compression/tension) wave modulus,  $\rho$  is the density and  $v_l$  is the wave speed for longitudinal waves. The density, mass, and dimensions of the uncompressed sample were recorded at room temperature. The density of the sample at room temperature was measured through a standard method based on weighing the samples in air and water. The oven was warmed up to the desired temperature and was allowed to reach thermal equilibrium. The uncompressed sample was then placed inside the oven and was allowed to reach thermal equilibrium to get a homogeneous temperature over the sample. The sample was compressed to the desired strain. The entire compression process was stereo optically recorded and then analyzed with ARAMIS. After reaching the desired plastic strain, the longitudinal ultrasonic wave speed, dimensions, and volume were recorded at the elevated temperature after unloading. The density at room temperature, volume at room temperature, and volume at the elevated temperature were used to calculate the density at the elevated temperature. The initial evaluated density is shown in Figure 6.1 for samples that were not yet plastically deformed. The experimental procedure for calculating the wave moduli is explained in the previous chapter. The experiments were performed

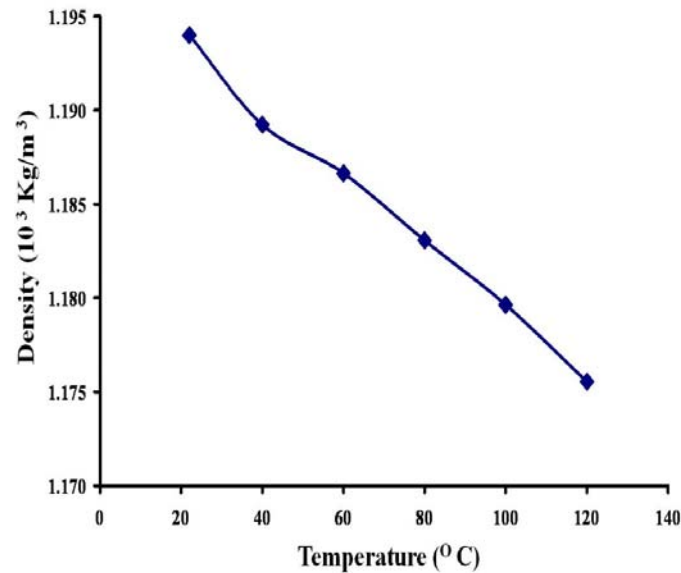


Figure 6.1: Density measured before plastic deformation as a function of temperature for PC using a weighing method at room temperature and the ARAMIS stereo optical system strain at higher temperatures (from Strabala et al. [9]).

on samples from a series of initially uncompressed PC cylinders. The PC cylinders were plastically strained to approximately 10%, 20%, 30% and 40% at a strain rate of 0.01 1/s. All tests were conducted in a convection oven. The samples were then ultrasonically tested in the axial direction to calculate the associated longitudinal wave speed. From this wave speed the axial longitudinal wave modulus was calculated. The samples were then cut as shown in Figure 5.3, and were placed in the oven and heated until they reached the temperature of the compression. The samples were then ultrasonically tested to get the transverse longitudinal wave modulus. The summary of the testing procedure is shown in Figure 6.2.

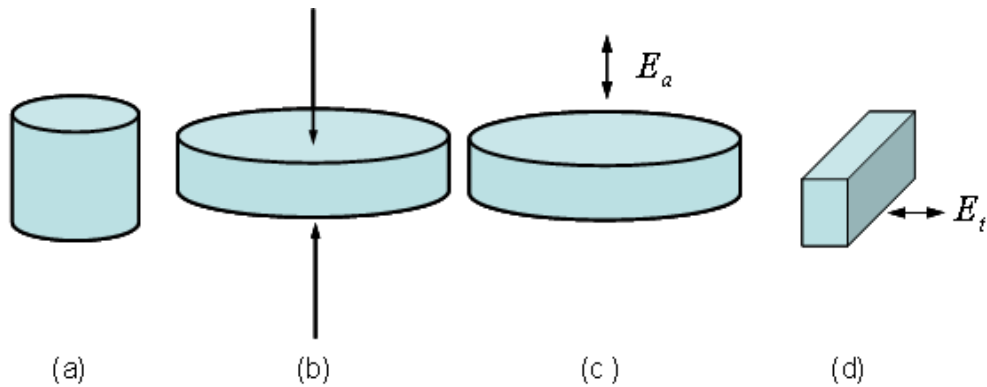


Figure 6.2: Summary of testing: (a) original PC cylinder, (b) compressed PC cylinder, (c) ultrasonic testing in the axial direction, (d) sample cut and ultrasonically tested in transverse direction (from Strabala et al. [9]).

### 6.3 Experimental results

The experiments were conducted at different temperatures below the glass transition temperature of PC. Figures 6.3 and 6.4 shows the longitudinal and transverse wave moduli as they were measured at these temperatures. The longitudinal wave moduli decrease while the transverse wave moduli increase with increase in plastic strain at constant temperature and the longitudinal and transverse wave moduli decrease with an increase in the temperature at constant plastic strain.

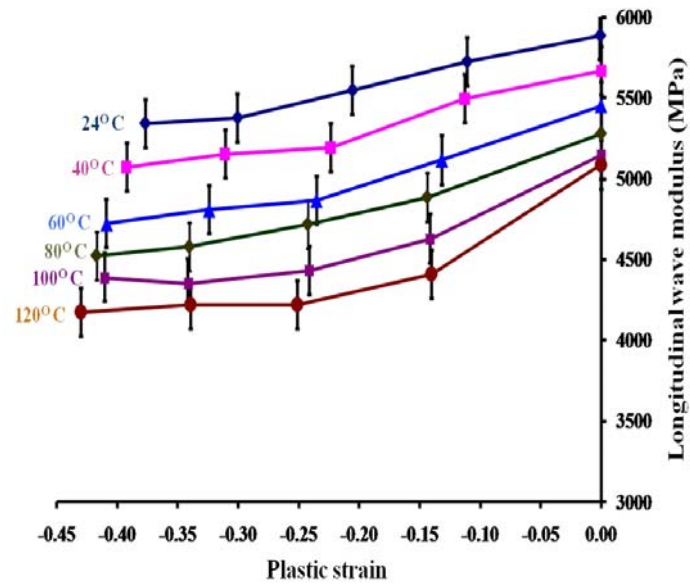


Figure 6.3: The axial longitudinal wave modulus (in MPa) at different plastic strains for different temperatures (from Strabala et al. [9]).

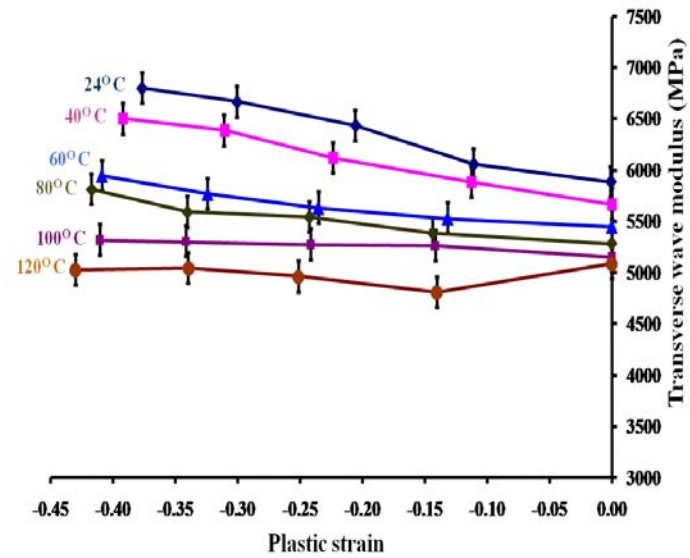


Figure 6.4: The transverse longitudinal wave modulus (in MPa) at different plastic strains for different temperatures (from Strabala et al. [9]).

## 6.4 Fitting the model to results from compression at different temperature

To include the effect of the temperature, the model presented in equation 5.16 can be modified and written as

$$\begin{aligned} \mathbf{T} = & A_{iso} \left[ G \frac{1}{J J^{e \frac{2}{3}}} \left( \mathbf{B}^e - \frac{I_1}{3} \mathbf{I} \right) + \kappa \frac{J^e \ln(J^e)}{J} \mathbf{I} \right] \\ & + A_{aniso} \left[ \rho_o \frac{\partial \psi}{\partial I_7^*} \frac{1}{J} \mathbf{F}^e \{ 2(\mathbf{C}^p - \mathbf{I}) - (\mathbf{C}^e \mathbf{C}^p + \mathbf{C}^p \mathbf{C}^e - 2\mathbf{C}^e) \} \right] \mathbf{F}^{eT}. \end{aligned} \quad (6.2)$$

In the above model  $(1 - J^e)$  is replaced by  $\ln(J^e)$ , since due to the fact that  $J^e$  is very close to 1 both the functions are the same. Additionally, as the volume of a body is compressed and tends to 0, the stresses should be very high which is expressed better by the function  $\ln(J^e)$  which tends to infinity as  $J^e$  tends to zero, rather than  $(1 - J^e)$  which tends to 1. The two material parameters  $A_{iso}$  and  $A_{aniso}$  are assumed to be only a function of temperature, and it is also assumed that the other material parameters do not depend upon temperature. To fit the experimental data, at different temperature we need to evaluate the wave moduli from the model, and to impose on the model the conditions of plastic flow during compression. Once this is done, we can then use the experimental data obtained at different temperatures to find the two factors  $A_{iso}$  and  $A_{aniso}$  in equation 6.2. We take  $\mathbf{e}_i$  to denote an orthonormal base with  $\mathbf{e}_3$  along the direction of compression. During uniaxial compression the plastic deformation gradient is given by the form

$$\mathbf{F}^p = \lambda^{p*} \mathbf{e}_1 \otimes \mathbf{e}_1 + \lambda^{p*} \mathbf{e}_2 \otimes \mathbf{e}_2 + \lambda^p \mathbf{e}_3 \otimes \mathbf{e}_3, \quad (6.3)$$

where  $\lambda^p$  is the plastic stretch in the axial direction and  $\lambda^{p*}$  is the plastic stretch in the transverse direction. The wave moduli considered in the experiments can be evaluated from

the components of stress through the relations

$$E_a = \frac{\partial T_{33}}{\partial F_{33}^e} \Big|_{\mathbf{F}^e=\mathbf{I}}, \quad E_t = \frac{\partial T_{11}}{\partial F_{11}^e} \Big|_{\mathbf{F}^e=\mathbf{I}}. \quad (6.4)$$

These moduli were evaluated using the model given in equation 6.2. A least square fit of the model to the experimental data was performed to calculate the temperature functions  $A_{iso}$  and  $A_{aniso}$ . In performing the least square fit, the experimental data points at zero plastic strain and 10% plastic strain are ignored because for the longitudinal wave moduli obtained at different temperatures the moduli are much higher at low plastic strains compared to the moduli at higher plastic strains. These high values might be due to aging which is removed with plastic flow. Therefore, in fitting the response only the experimental data points of 20% plastic strain and greater are considered in calculating  $A_{iso}$  and  $A_{aniso}$ . The plot fitting the isotropic and anisotropic factors are shown in figures 6.5 and 6.6. The indicated curves were fit to the obtained variables using the functions

$$A_{iso} = 2.28 \times e^{-\left(\frac{\theta}{357}\right)}, \quad (6.5)$$

$$A_{aniso} = 6.04 \times e^{-\left(\frac{\theta}{166}\right)}, \quad (6.6)$$

where  $\theta$  is given in degree Kelvin. Figure 6.7 and 6.8 shows the comparison of the experimental results for the wave moduli and those obtained from this fit at different temperatures from room temperature to  $120^\circ C$ . As can be seen, the fit reproduces the observe wave moduli within the error bar.

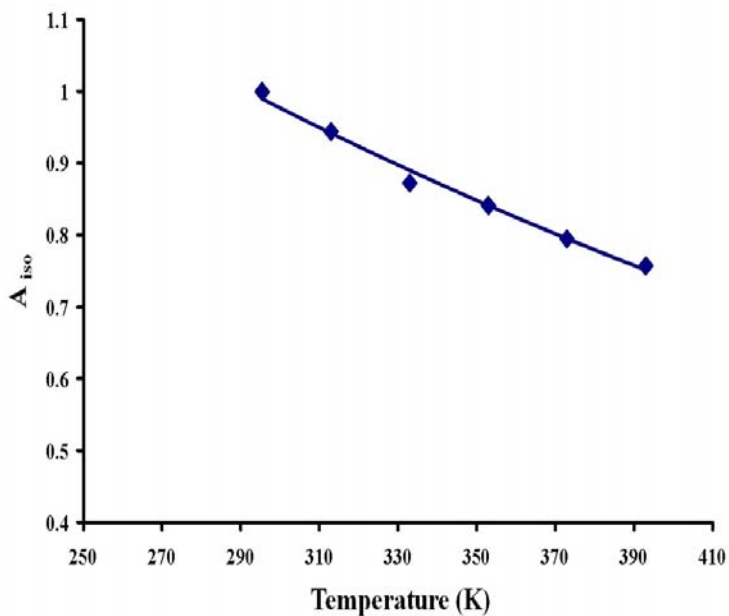


Figure 6.5: Change of the isotropic factor  $A_{iso}(\theta)$  with temperature.

## 6.5 Introducing the effect of load

In the previous section we have developed a constitutive model for stress which has the capability to predict the anisotropic wave moduli at different temperatures, but for zero load. The purpose of this section is to combine this model with the large deformation thermo-elastic model developed in Chapter 4. The resulting model will have both the capability to capture the development of anisotropy with plastic flow measured at zero load and include the nonlinear part of the effect of loading. The constitutive model to capture development of elastic anisotropy at zero load resulting from plastic flow is given by equation 6.2 where  $A_{iso}$  and  $A_{aniso}$  are function of temperatures and  $G$ ,  $\kappa$  and  $\rho_o \frac{\partial \psi}{\partial I_7^*}$  are functions of

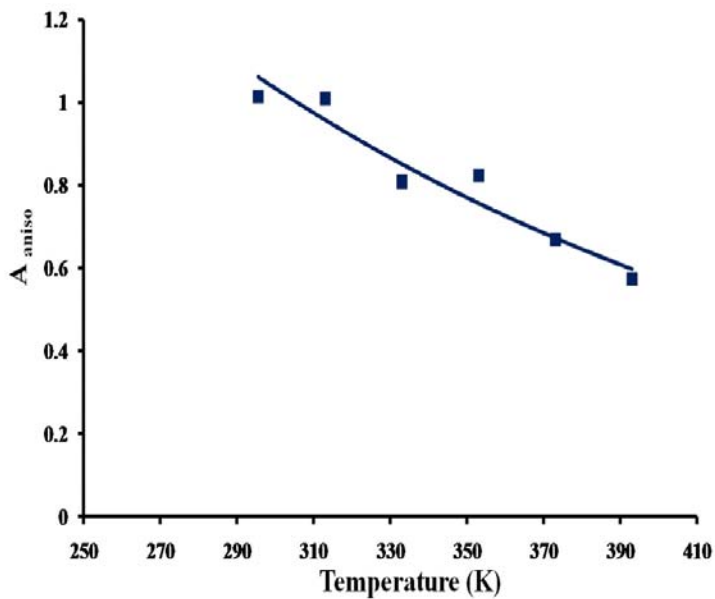


Figure 6.6: Change of the anisotropic factor  $A_{aniso}(\theta)$  with temperature.

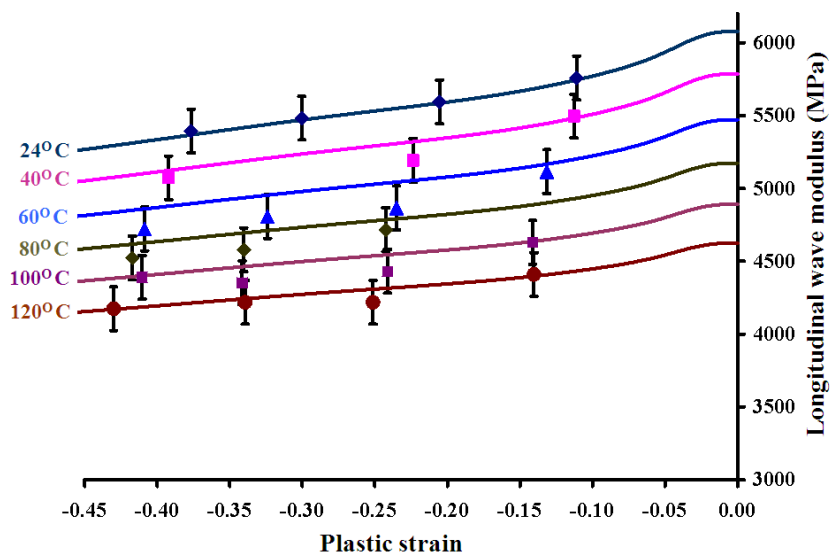


Figure 6.7: Comparison of model results with experimentally measured wave moduli  $E_a$  (from Strabala et al. [9]) for the given plastic strains at different temperatures.

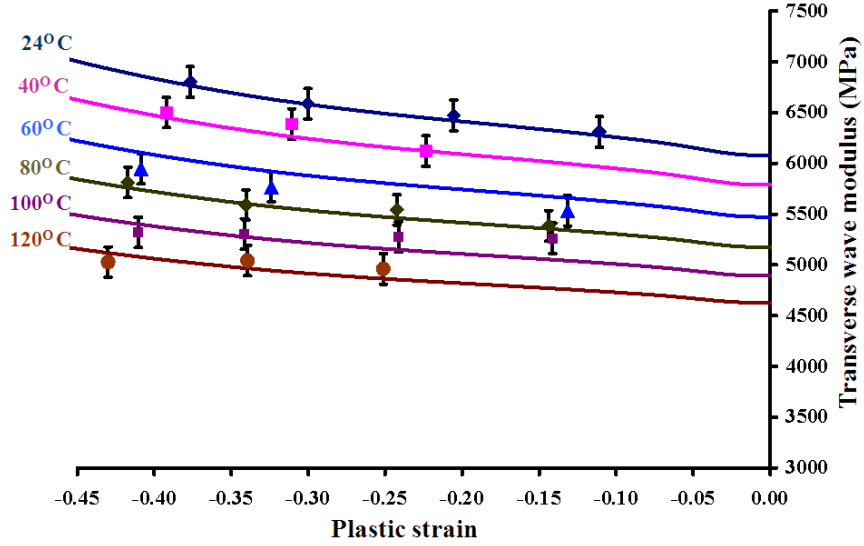


Figure 6.8: Comparison of model results with experimentally measured wave moduli  $E_t$  (from Strabala et al. [9]) for the given plastic strains at different temperatures.

plastic strain. The material parameters  $A_{iso}$ ,  $A_{aniso}$ ,  $G$ ,  $\kappa$  and  $\rho_o \frac{\partial \psi}{\partial I_7^*}$  are given by

$$A_{iso} = 2.28 \times e^{-\left(\frac{\theta}{357}\right)}, \quad (6.7)$$

$$A_{aniso} = 6.04 \times e^{-\left(\frac{\theta}{166}\right)}, \quad (6.8)$$

$$\kappa = 4670 + 200 \times (I_4^* - 3) \text{ MPa}, \quad (6.9)$$

$$G = 1072 - 159 \times (I_4^* - 3) \text{ MPa}, \quad (6.10)$$

$$\rho_o \frac{\partial \psi}{\partial I_7^*} = -283 - 150 \times e^{-\left(\frac{I_4^* - 3}{0.125}\right)} + 433 \times e^{-\left(\frac{I_4^* - 3}{0.004}\right)} \text{ MPa}. \quad (6.11)$$

for  $\theta$  given in degree Kelvin, and  $I_4^* = \frac{tr(\mathbf{C}^p)}{J^p \frac{2}{3}}$ . The nonlinear thermo-elastic constitutive

model for stress developed in Chapter 4 is given by

$$\begin{aligned} \mathbf{T} = & \rho \left[ G_\theta \frac{2}{J^e \frac{2}{3}} \left( \mathbf{B}^e - \frac{I_1}{3} \mathbf{I} \right) + 2\kappa_\theta J^e \ln(J^e) \mathbf{I} \right. \\ & \left. E_{comb} \left\{ \frac{2}{J^e \frac{2}{3}} \left( \mathbf{B}^e - \frac{I_1}{3} \mathbf{I} \right) \ln^2(J^e) + 2 \ln(J^e) (I_1^* - 3) \mathbf{I} \right\} \right], \end{aligned} \quad (6.12)$$

where  $G_\theta$ ,  $\kappa_\theta$  and  $E_{comb}$  are functions of temperature. These material parameters are given by

$$G_\theta = 1098 \times e^{-\left(\frac{\theta}{357.15}\right)} \text{ MPa}, \quad (6.13)$$

$$\kappa_\theta = 7034 \times e^{-\left(\frac{\theta}{588.23}\right)} \text{ MPa}, \quad (6.14)$$

$$E_{comb} = 60500 \text{ MPa}. \quad (6.15)$$

We would like to combine both of these models such that the final model reproduces both the effects of load and the development of anisotropy. A full combination of these two models is not possible since the data does not match at zero load. This might be due to several factors, one being the fact that these results are for different materials. We can still partially combine the two models. Since we would like to develop a model for the Lexan 9034, we do this combination by using the model developed here, and only adding terms from the thermo-elastic model, developed based on the experimental results of Masubichi et al. [7], that vanish at zero load. In this way we may add the nonlinear elastic contribution while retaining the ultrasonic response we have measured and fit for Lexan 9034. The expression for the stress rate for thermoelastic model 6.12 is given by

$$\begin{aligned} \dot{\mathbf{T}} = & \rho \left[ \frac{2}{J^{e\frac{2}{3}}} G_\theta \left( \overline{\mathbf{B}^e - \frac{I_1}{3} \mathbf{I}} \right) + 2\kappa_\theta \overline{J^e \ln(J^e)} \mathbf{I} \right. \\ & + \mathbf{E}_{comb} \left\{ \frac{2}{J^{e\frac{2}{3}}} \left( \overline{\mathbf{B}^e - \frac{I_1}{3} \mathbf{I}} \right) \ln^2(J^e) + \frac{2}{J^{e\frac{2}{3}}} \left( \mathbf{B}^e - \frac{I_1}{3} \mathbf{I} \right) \overline{\ln^2(J^e)} \right\} \\ & \left. + \mathbf{E}_{comb} \left\{ 2\ln(J^e)(I_1^* - 3) + 2\ln(J^e) \overline{(I_1^* - 3)} \right\} \right]. \end{aligned} \quad (6.16)$$

Calculating  $\dot{\mathbf{T}}$  at  $\mathbf{F}^e = \mathbf{I}$  gives,

$$\dot{\mathbf{T}} \big|_{\mathbf{F}^e = \mathbf{I}} = \rho \left[ \frac{2}{J^{e\frac{2}{3}}} G_\theta \left( \overline{\mathbf{B}^e - \frac{I_1}{3} \mathbf{I}} \right) + 2\kappa_\theta \overline{J^e \ln(J^e)} \mathbf{I} \right]. \quad (6.17)$$

Therefore, the terms with coefficient  $\mathbf{E}_{comb}$  will not have any effect in calculating the wave modulus at  $\mathbf{F}^e = \mathbf{I}$ . Therefore, we construct the final model for stress by adding this term to 6.2 to get

$$\begin{aligned} \mathbf{T} = & A_{iso} \left[ G \frac{1}{J J^{e\frac{2}{3}}} \left( \mathbf{B}^e - \frac{I_1}{3} \mathbf{I} \right) + \kappa \frac{\ln(J^e)}{J} \mathbf{I} \right] \\ & + A_{aniso} \left[ \rho_o \frac{\partial \psi}{\partial I_7^*} \frac{1}{J} \mathbf{F}^e [2(\mathbf{C}^p - \mathbf{I}) - (\mathbf{C}^e \mathbf{C}^p + \mathbf{C}^p \mathbf{C}^e - 2\mathbf{C}^e)] \right] \mathbf{F}^{eT} \\ & + E_{comb} \left\{ \frac{2}{J^{e\frac{2}{3}}} \left( \mathbf{B}^e - \frac{I_1}{3} \mathbf{I} \right) \ln^2(J^e) + 2 \ln(J^e) (I_1^* - 3) \mathbf{I} \right\}. \end{aligned} \quad (6.18)$$

The modification of 6.2 will not effect the modeling done to capture the development of anisotropy with plastic flow, but it will introduce elements of the confined compression results discussed in Chapter 4. A comparison was made between the experimental results for the wave moduli and those obtained from the modified model given in 6.18. This is shown in figures 6.9 and 6.10. As can be seen in the figures the model trends follow that reported by Masubichi et al. [7] experiments, but the magnitudes obtained from the model are higher than the experimental results. This might be attributed to the fact that the PC used by Masubichi et al. [7] was different from the Lexan 9034 used here.

## 6.6 Summary and conclusion

This chapter focuses on measuring and modeling the anisotropic elastic response observed in PC after plastic deformation at different temperatures. Uniaxial compression was used to prepare samples with different extents of plastic deformation at different temperatures, up to approximately 40% compression. Ultrasonic wave speed measurements were used to obtain the longitudinal wave speed moduli along the axis of compression and perpendicular to this axis. The transverse wave modulus increases while the axial wave

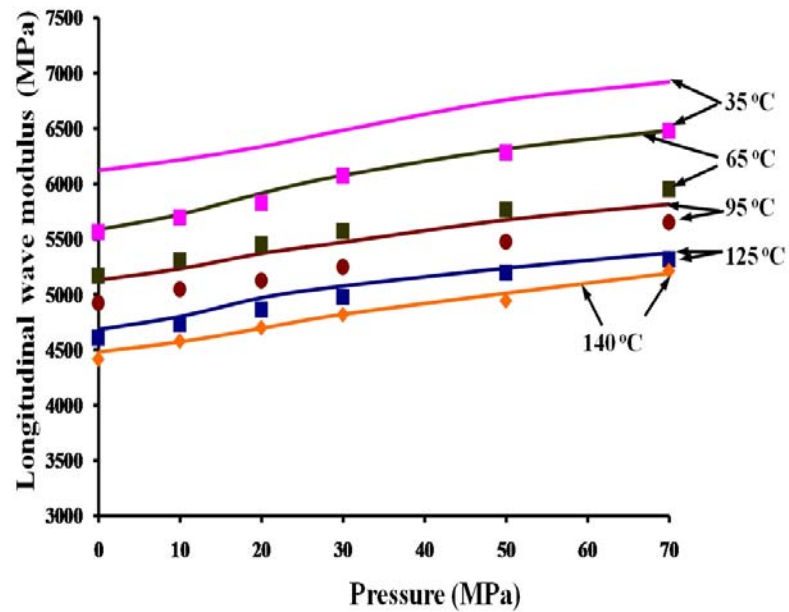


Figure 6.9: Comparison of model results with experimentally measured longitudinal wave moduli by Masubichi et al [7] in confined compression at different temperature and pressure.

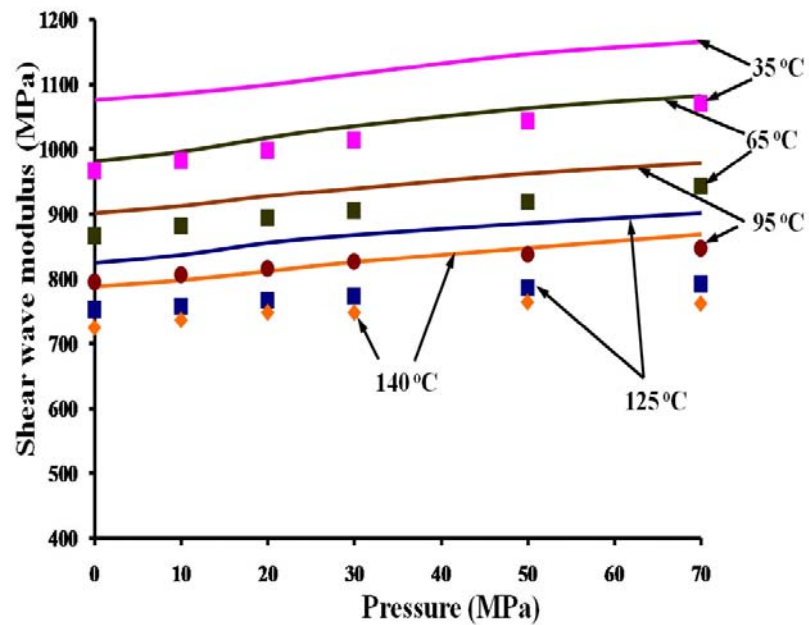


Figure 6.10: Comparison of model results with experimentally measured shear wave moduli Masubichi et al [7] in confined compression at different temperature and pressure.

modulus decreases with plastic compression, but with the increase in temperature both longitudinal and transverse wave moduli decreases. These experiments were the base for the model developed.

To capture the observed development of anisotropic elastic moduli, a model for the stress based on the elastic and plastic deformation gradients was constructed in the previous chapter. The model was extended here to fit the wave moduli in longitudinal and transverse direction at different temperatures using Arrhenius terms. In this process it was assumed that the isotropic bulk and shear parts are scaled similarly with temperature and behave differently from the anisotropic part. The experimental results and the constitutive model were in good agreement using these two Arrhenius functions as factors on the original model.

The two large deformation constitutive models, one constructed to fit the development of elastic anisotropy with plastic flow at different temperatures at zero load, and the another developed to reproduce the data of Masubichi et al. [7] under load, were combined together such that the final model reproduces the wave moduli we have measured for Lexan 9034 at zero load, but also includes some of the effect resulting from loading as reported by Masubichi et al [7].

## Chapter 7

# Experimentally evaluating equilibrium stress in uniaxial tests

### 7.1 Introduction

#### 7.1.1 Background

One group of models proposed for characterizing the mechanical response of glassy polymers is based on a structure that resembles finite plasticity. In most cases, a constitutive equation for stress is proposed, which depends on the elastic deformation gradient, supplemented by a flow rule for the plastic deformation, which depends on the “over stress”. The over stress is a properly invariant difference between the stress and the equilibrium stress, which is related to the back stress. The equilibrium stress represents conditions under which relaxation events stop and the material can carry an applied load indefinitely without a need to change the stress or strain. Questions that arise in using these models are whether such

an equilibrium stresses exist, how can it be evaluated, and what experiments can be used to characterize the flow rule. One challenge in accurately evaluating the locus of equilibrium conditions is the fact that the relaxation processes substantially slow down around equilibrium, and, therefore, a method that is more rapid and does not directly require holding at the equilibrium for long time intervals is desirable.

### **7.1.2 Method of approach**

We start from a model for stress that depends on the elastic and plastic deformation gradients and study its derivative with respect to time. In particular, we look at the derivative at equilibrium, where the internal parameter becomes constant. In this case the internal parameter is the plastic deformation gradient. We study the characteristics of the equilibrium and show that the tangent modulus and local Poisson's ratio at equilibrium are both rate independent for this modeling assumption. This fact is used to propose a method based on cyclic tests in uniaxial tension or compression to measure the equilibrium stress, and the associated point's tangent modulus and local Poisson's ratio. This method is based on evaluating the slope of stress-strain response under conditions of similar elastic and plastic strain, but different strain rates.

### **7.1.3 Results presented**

This method is used to characterize the equilibrium stress at room temperature for glassy polycarbonate. The results are studied in regard to the possible error for such a measurement. The added advantage of the proposed method is that we can get the associated values of tangent modulus and local Poisson's ratio at the equilibrium stress in

uniaxial tests, a quantity never measured to our best reading of the available results.

#### **7.1.4 Conclusions**

The method proposed looks promising in evaluating the equilibrium stress of glassy polymers. The method is faster than most other proposed methods for calculating the equilibrium stress, and provides additional measurements of parameters at equilibrium that are normally not obtained. This method is used to characterize the equilibrium stress and the associated point's tangent modulus and local Poisson's ratio for PC at different temperatures below the glass transition temperature.

## **7.2 Literature review**

Many models that are used to predict the response of metals and polymers at large deformations are based on internal parameters and take the form of plasticity-like models that use the back stress in evaluating the response of the material. Examples of such models are the models developed by Argon, Parks, Boyce, Arruda, and co-workers [49, 50, 51, 36, 52, 53, 54, 55, 56, 57, 58, 43, 59], those developed by Krempl and co-workers [60, 61, 62, 63], by Negahban [5], and others. These models all incorporate the idea of an equilibrium stress, that implies, thermodynamically, that there exist loading conditions under which the relaxation processes stop so the load may be held at constant strain indefinitely, and which, when away from equilibrium, the material response would normally tend toward this equilibrium. This is clearly observed above the glass-transition temperature for polymers, as is shown for PMMA in Figure 7.1, reproduced from Negahban

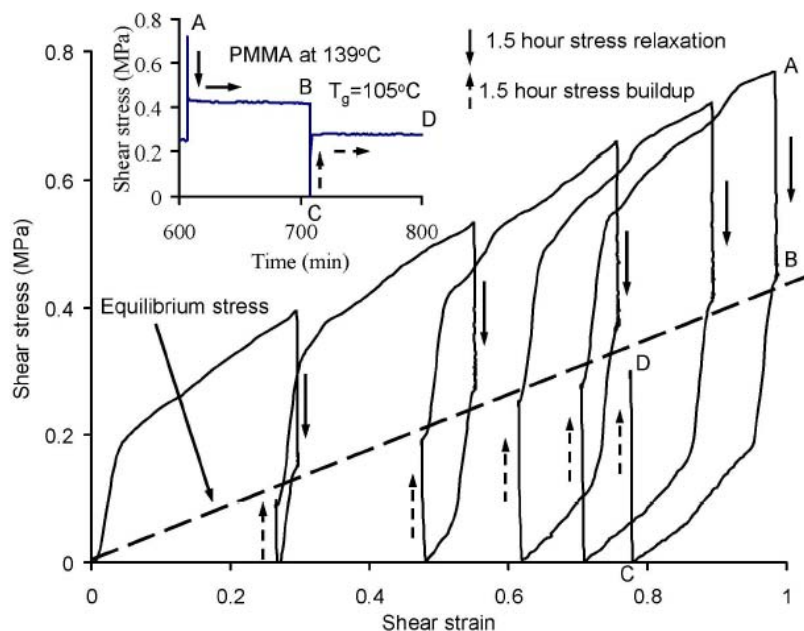


Figure 7.1: Stress buildup and stress relaxation seen in PMMA above its glass-transition temperature (From Negahban [5]).

[5]. This figure shows that at constant strain the stress either relaxes or increases toward the equilibrium response, depending on which side of the equilibrium response the process starts from, and then indefinitely stays there. Such simple experiments cannot be done for polymers below the glass-transition temperature that have very large relaxation times. As a result, for such cases identifying true equilibrium from standard experiments becomes difficult and the error is large.

In this chapter we have proposed a new method of calculating the equilibrium stress using cyclic loading in tension or compression. The method is based upon the theoretical characteristics of modeling stress and that of equilibrium, and is applied to the analysis of the response of polycarbonate. We also use the response of polycarbonate to evaluate the

estimated error in the response using the uncertainty in each of the measurements. The method was first conceived in 1995 by Negahban [5] applied to the shear response of PMMA and later applied by Negahban and coworkers [105, 106] for the shear response of polycarbonate. This is the first time it has been considered in a full three-dimensional context and for compression, and with the analysis of the associated error in the measurement. The method, in addition to equilibrium stress, provides values for the tangent modulus and local Poisson's ratio at equilibrium.

Several authors have looked at measuring the equilibrium stress. A review of the two main methods used for this can be found in an article by Neu and coworkers [71] in which they use a model proposed by McDowell to characterize the back stress in 60Sn-40Pb soldering material. As described in this article, there are essentially two methods proposed for measuring the equilibrium stress. One is that proposed by Ahlquist and Nix [72], where rapid unloading of the sample to different levels of stress is used to identify points of zero strain rate (the signature of equilibrium). The second method, proposed by Onat [73] and Sehitoglu [107], is based on finding the center of the yield points. Neu and coworkers use both the method of Ahlquist and Nix [72] and a modification of the method of Onat [73] and Sehitoglu [107]. There are others that have used these methods to calculate equilibrium stress. These are described and documented in the paper of Neu and coworkers [71].

The advantage of the method proposed here is that it is a faster method to obtain the values for the equilibrium stress, it provides the tangent modulus and the local Poisson's ratio at equilibrium, and also gives a measure of the error in each calculation. For clarification, the local Poisson's ratio refers to negative the transverse strain rate divided

by the axial strain rate, as opposed to the ratio of the total strains. The method proposed here, from our review of the literature, is the only method which also measures the tangent modulus and local Poisson's ratio at equilibrium.

### 7.3 Theoretical foundation

The proposed method for calculating the equilibrium stress, and associated tangent modulus and local Poisson's ratio, is based on the following theoretical derivation. The procedure will work for small and large deformations of initially isotropic materials, and for initially transversely isotropic materials with axis of transverse isotropy along the axis of loading. The material need not remain isotropic or transversely isotropic, as long as it is initially one of the two. The material needs to be characterizable by a stress that is a function of elastic and plastic deformation gradients, and the total deformation gradient should be given by a standard multiplicative relation in terms of the elastic and plastic deformation gradients. Infinitesimal formulations can take advantage of the additive approximation of the decomposition, but the final results are the same. Thermal effects can also be considered by adding the thermal deformation gradient, but in this chapter we have not considered this, assuming the deformations are isothermal. This addition simply provides additional terms that can be introduced into the method by an additional set of terms.

A typical model for Cauchy stress  $\mathbf{T}$  that can capture the developing anisotropy seen in the elastic response, which is seen for many polymers [67, 68, 69, 70, 108], can be written (see [108]) in the form

$$\mathbf{T} = \mathbf{T}^+(\mathbf{F}^e, \mathbf{F}^p), \quad (7.1)$$

where  $\mathbf{T}^+$  denotes the model used to evaluate the Cauchy stress from  $\mathbf{F}^e$  and  $\mathbf{F}^p$ .

For the case of uniaxial tension or compression along the third axis, the components of the stress will be assumed to be homogeneous and given by

$$\mathbf{T} = T_{33}\mathbf{e}_3 \otimes \mathbf{e}_3, \quad (7.2)$$

where  $T_{33}$  is the axial stress,  $\mathbf{e}_i$  denote base vectors for a fixed orthonormal base along the three directions, and “ $\otimes$ ” is the tensor product. The deformation gradient in this case is

$$\mathbf{F} = \lambda_t \mathbf{e}_1 \otimes \mathbf{e}_1 + \lambda_t \mathbf{e}_2 \otimes \mathbf{e}_2 + \lambda_a \mathbf{e}_3 \otimes \mathbf{e}_3, \quad (7.3)$$

where  $\lambda_a$  is the axial stretch and  $\lambda_t$  is the transverse stretch. It can be shown [102, 100] that in this case both the elastic and plastic deformation gradients are diagonal and have the same structure as the deformation gradient. That is,

$$\mathbf{F}^e = \lambda_t^e \mathbf{e}_1 \otimes \mathbf{e}_1 + \lambda_t^e \mathbf{e}_2 \otimes \mathbf{e}_2 + \lambda_a^e \mathbf{e}_3 \otimes \mathbf{e}_3, \quad (7.4)$$

$$\mathbf{F}^p = \lambda_t^p \mathbf{e}_1 \otimes \mathbf{e}_1 + \lambda_t^p \mathbf{e}_2 \otimes \mathbf{e}_2 + \lambda_a^p \mathbf{e}_3 \otimes \mathbf{e}_3, \quad (7.5)$$

with the relations obtained from the multiplicative decomposition written as

$$\lambda_a = \lambda_a^e \lambda_a^p, \quad \lambda_t = \lambda_t^e \lambda_t^p. \quad (7.6)$$

The stress rate can be evaluated from the constitutive equation for stress through the expression

$$\dot{\mathbf{T}} = \partial_{\mathbf{F}^e} (\mathbf{T}^+) : \dot{\mathbf{F}}^e + \partial_{\mathbf{F}^p} (\mathbf{T}^+) : \dot{\mathbf{F}}^p = \mathbf{E} : \dot{\mathbf{F}}^e + \mathbf{E}^b : \dot{\mathbf{F}}^p, \quad (7.7)$$

where  $\mathbf{E}$  is the fourth order tensor modulus associated with the elastic deformation gradient and  $\mathbf{E}^b$  is the fourth order tensor modulus associated with the plastic deformation gradient at

the current state. Here we use the standard tensor notation  $\partial_{\mathbf{A}}(\cdot)$  for the partial derivative and the notation “.” for double summation so that the component form of this equation is given by

$$\dot{T}_{ij} = \frac{\partial T_{ij}^+}{F_{kl}^e} \dot{F}_{kl}^e + \frac{\partial T_{ij}^+}{F_{kl}^p} \dot{F}_{kl}^p = E_{ijkl} \dot{F}_{kl}^e + E_{ijkl}^p \dot{F}_{kl}^p. \quad (7.8)$$

In the case of uniaxial tension or compression this will result in two distinct equations that are given as

$$\begin{aligned} \dot{T}_{11} = & \left( \frac{\partial T_{11}^+}{F_{11}^e} + \frac{\partial T_{11}^+}{F_{22}^e} \right) \dot{\lambda}_t^e + \frac{\partial T_{11}^+}{F_{33}^e} \dot{\lambda}_a^e + \left( \frac{\partial T_{11}^+}{F_{11}^p} + \frac{\partial T_{11}^+}{F_{22}^p} \right) \dot{\lambda}_t^p \\ & + \frac{\partial T_{11}^+}{F_{33}^e} \dot{\lambda}_a^p, \end{aligned} \quad (7.9)$$

$$\begin{aligned} \dot{T}_{33} = & \left( \frac{\partial T_{33}^+}{F_{11}^e} + \frac{\partial T_{33}^+}{F_{22}^e} \right) \dot{\lambda}_t^e + \frac{\partial T_{33}^+}{F_{33}^e} \dot{\lambda}_a^e + \left( \frac{\partial T_{33}^+}{F_{11}^p} + \frac{\partial T_{33}^+}{F_{22}^p} \right) \dot{\lambda}_t^p \\ & + \frac{\partial T_{33}^+}{F_{33}^e} \dot{\lambda}_a^p. \end{aligned} \quad (7.10)$$

In the experiments the total stretch is measured as opposed to the elastic stretch so that we use  $\lambda_a = \lambda_a^e \lambda_a^p$  and  $\lambda_t = \lambda_t^e \lambda_t^p$  to replace the elastic stretch rate using the equations

$$\begin{aligned} \dot{\lambda}_a^e &= \frac{1}{\lambda_a^p} \dot{\lambda}_a - \frac{\lambda_a}{\lambda_a^{p2}} \dot{\lambda}_a^p, \\ \dot{\lambda}_t^e &= \frac{1}{\lambda_t^p} \dot{\lambda}_t - \frac{\lambda_t}{\lambda_t^{p2}} \dot{\lambda}_t^p. \end{aligned} \quad (7.11)$$

This results in the two equations

$$\begin{aligned} \dot{T}_{11} = & \left( \frac{\partial T_{11}^+}{F_{11}^e} + \frac{\partial T_{11}^+}{F_{22}^e} \right) \left( \frac{1}{\lambda_t^p} \dot{\lambda}_t - \frac{\lambda_t}{\lambda_t^{p2}} \dot{\lambda}_t^p \right) + \frac{\partial T_{11}^+}{F_{33}^e} \left( \frac{1}{\lambda_a^p} \dot{\lambda}_a - \frac{\lambda_a}{\lambda_a^{p2}} \dot{\lambda}_a^p \right) \\ & + \left( \frac{\partial T_{11}^+}{F_{11}^p} + \frac{\partial T_{11}^+}{F_{22}^p} \right) \dot{\lambda}_t^p + \frac{\partial T_{11}^+}{F_{33}^e} \dot{\lambda}_a^p, \end{aligned} \quad (7.12)$$

$$\begin{aligned} \dot{T}_{33} = & \left( \frac{\partial T_{33}^+}{F_{11}^e} + \frac{\partial T_{33}^+}{F_{22}^e} \right) \left( \frac{1}{\lambda_t^p} \dot{\lambda}_t - \frac{\lambda_t}{\lambda_t^{p2}} \dot{\lambda}_t^p \right) + \frac{\partial T_{33}^+}{F_{33}^e} \left( \frac{1}{\lambda_a^p} \dot{\lambda}_a - \frac{\lambda_a}{\lambda_a^{p2}} \dot{\lambda}_a^p \right) \\ & + \left( \frac{\partial T_{33}^+}{F_{11}^p} + \frac{\partial T_{33}^+}{F_{22}^p} \right) \dot{\lambda}_t^p + \frac{\partial T_{33}^+}{F_{33}^e} \dot{\lambda}_a^p. \end{aligned} \quad (7.13)$$

We will organize this into the matrix equation

$$\begin{bmatrix} A_{11} & A_{12} \\ A_{21} & A_{22} \end{bmatrix} \begin{Bmatrix} \dot{\lambda}_t^p \\ \dot{\lambda}_a^p \end{Bmatrix} = \begin{bmatrix} B_{11} & B_{12} \\ B_{21} & B_{22} \end{bmatrix} \begin{Bmatrix} \dot{\lambda}_t \\ \dot{\lambda}_a \end{Bmatrix} - \begin{Bmatrix} \dot{T}_{11} \\ \dot{T}_{33} \end{Bmatrix}, \quad (7.14)$$

where

$$\mathbf{A} = \begin{bmatrix} A_{11} & A_{12} \\ A_{21} & A_{22} \end{bmatrix} = \begin{bmatrix} B_{11} \frac{\lambda_t}{\lambda_t^p} - \left( \frac{\partial T_{11}^+}{F_{11}^p} + \frac{\partial T_{11}^+}{F_{22}^p} \right) & B_{12} \frac{\lambda_a}{\lambda_a^p} - \frac{\partial T_{11}^+}{F_{33}^p} \\ B_{21} \frac{\lambda_t}{\lambda_t^p} - \left( \frac{\partial T_{33}^+}{F_{11}^p} + \frac{\partial T_{33}^+}{F_{22}^p} \right) & B_{22} \frac{\lambda_a}{\lambda_a^p} - \frac{\partial T_{33}^+}{F_{33}^p} \end{bmatrix}, \quad (7.15)$$

$$\mathbf{B} = \begin{bmatrix} B_{11} & B_{12} \\ B_{21} & B_{22} \end{bmatrix} = \begin{bmatrix} \left( \frac{\partial T_{11}^+}{F_{11}^e} + \frac{\partial T_{11}^+}{F_{22}^e} \right) \frac{1}{\lambda_t^p} & \frac{\partial T_{11}^+}{F_{33}^e} \frac{1}{\lambda_a^p} \\ \left( \frac{\partial T_{33}^+}{F_{11}^e} + \frac{\partial T_{33}^+}{F_{22}^e} \right) \frac{1}{\lambda_t^p} & \frac{\partial T_{33}^+}{F_{33}^e} \frac{1}{\lambda_a^p} \end{bmatrix}. \quad (7.16)$$

In a typical uniaxial test we measure  $(\lambda_a, \lambda_t, T_{33})$ , assuming  $T_{11} = T_{22} = 0$ . As a result we also can calculate  $(\dot{\lambda}_a, \dot{\lambda}_t, \dot{T}_{33})$  for isothermal conditions. An equilibrium condition is one for which the material can carry a given load without changing its shape. That is, equilibrium is a point for which the internal variable  $\mathbf{F}^p$  is constant so that  $\dot{\mathbf{F}}^p = \mathbf{0}$ . If we set  $\dot{\mathbf{F}}^p = \mathbf{0}$  in equation 7.14, we obtain an equation that is true when passing through equilibrium, and is given by

$$\begin{bmatrix} B_{11} & B_{12} \\ B_{21} & B_{22} \end{bmatrix} \begin{Bmatrix} \dot{\lambda}_t \\ \dot{\lambda}_a \end{Bmatrix} = \begin{Bmatrix} 0 \\ \dot{T}_{33} \end{Bmatrix}. \quad (7.17)$$

We can solve this to find

$$\nu_{eq} = -\frac{\dot{\lambda}_t}{\dot{\lambda}_a} = \frac{B_{12}}{B_{11}}, \quad (7.18)$$

$$E_{eq}^t = \frac{\dot{T}_{33}}{\dot{\lambda}_a} = B_{22} - \nu B_{21}, \quad (7.19)$$

where  $\nu_{eq}$  is the local Poisson's ratio at equilibrium and  $E_{eq}^t$  is the tangent modulus at equilibrium. The right hand side of both 7.18 and 7.19 are independent of the rate of stress

or stretch, so one can conclude that the condition of equilibrium is characterized by points that have  $\nu_{eq}$  and  $E_{eq}^t$  that are independent of how fast we pass through the equilibrium. We use this fact to propose a method for calculating the equilibrium stress, the tangent modulus and local Poisson's ratio at equilibrium in uniaxial tests.

## 7.4 Proposed experimental method

Figure 7.2 shows the basic idea of the proposed method. At the bottom of the figure is shown a schematic of a loading process that includes a cycle of unloading and loading. If we assume the plastic strain does not change substantially in this cycle, when we reach points of equal stress, we are reaching also points of approximately equal elastic strain, so that the state is approximately the same. In such a cycle, if we look at points on the unloading and loading that have the same slope (tangent modulus) we can consider them to represent a point of equilibrium since the tangent modulus has not changed even though the strain rate has changed sign. At the top of the figure is shown a typical plot of an unloading and subsequent loading cycle for polycarbonate at room temperature showing the tangent modulus as a function of the load. As can be seen, the point of intersection between the tangent modulus during unloading and loading provides the equilibrium stress.

The process of evaluating the equilibrium stress in this case is simple. We just need to design a cycle in which the difference between the unloading and loading is small enough so that we can assume there is little change in the plastic strain, but is different enough so that we can accurately evaluate the equilibrium stress from the point of equal tangent modulus. As will be shown, this can be done with reasonable accuracy for glassy

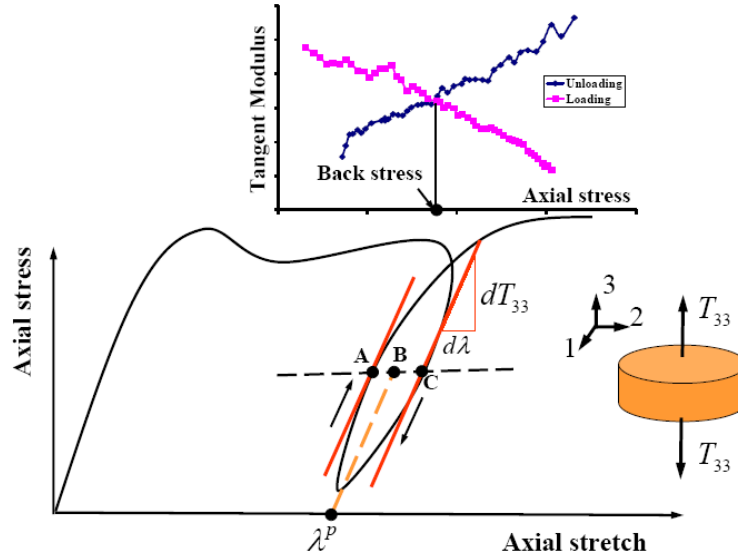


Figure 7.2: Schematic of proposed experiment to calculate the equilibrium stress and the associated tangent modulus (bottom), and a typical plot of the tangent modulus as a function of the axial stress in the cycle of unloading and loading for polycarbonate (top).

polymers, and may be possible for metals and other materials under certain conditions, and when using appropriate experimental setups.

Once we calculate the equilibrium stress, we can then obtain estimates of the axial and transverse strains at equilibrium, and also obtain estimates of the associated tangent modulus and local Poisson's ratio. Ideally, the difference between the unloading and loading should be small so that the associated elastic and plastic strains are the same for a given load. In reality, as shown in the schematic in Figure 7.2, the plastic stretch at the unloading and loading are not the same. This could be inferred from the fact that the equilibrium point obtained on unloading (point C in the figure) is not the same point as that obtained during loading (point A in the figure). A good estimate of the difference between the state of the materials (given by  $\mathbf{F}^e$  and  $\mathbf{F}^p$ ) during the unloading and loading parts of the cycle

is obtained from the difference in the strain at the two points (points A and C) since this is a good estimate of the difference in plastic strain at a given stress. We will show how we use this to estimate one part of the error in the calculation.

In the proposed procedure, once we evaluate the equilibrium stress, we designate it to the average point (point B shown in the figure) between the unloading and loading cycle. We do the same for the tangent modulus and local Poisson's ratio. We also designate to each point an error based on the uncertainty in each of the measurements and in the state of the material. A description of this is provided in the following section.

## 7.5 Materials and experimental setup

All tests were performed on Lexan 9034 sheets. Samples were cut from 12.5 mm thick sheets and tested without thermal conditioning.

All the experiments conducted were uniaxial compression experiments. Cylindrical samples with a height of 12.5 mm and a diameter of 19 mm were placed in a preheated environmental chamber and were left to stabilize for 15 minutes before compression. The samples were compressed on a MTS load frame with a maximum load of 100kN and axial and transverse strains were measured using ARAMIS, a stereo-optic surface strain measurement system. Typical results for the response of polycarbonate at room temperature are shown in Figure 7.3. The experiments were conducted at a loading unloading rate of approximately 0.001 1/s strain rate so as to eliminate thermal effects. In the figure is also shown the measured equilibrium stress and the calculated standard deviation on each data point. Figure 7.4 shows the transverse response observed in the entire test, the transverse strain at

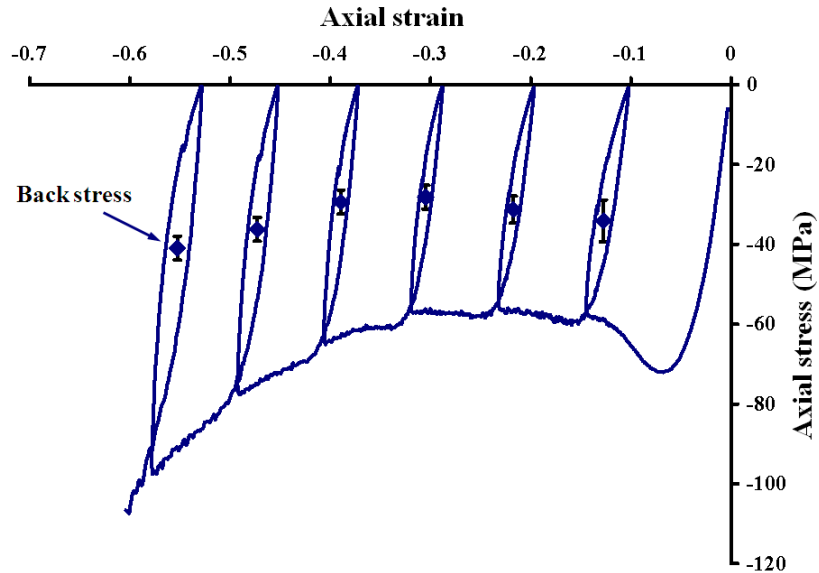


Figure 7.3: Typical cyclic loading in compression of polycarbonate at room temperature and the calculated back stress (from Goel et al. [10])

equilibrium, and the transverse strain for an incompressible material. Figures 7.5 and 7.6 show the measured tangent modulus and local Poisson's ratio, and the associated calculated standard deviations, all evaluated at the measured equilibrium. The stress response was a result of the strain history shown in Figure 7.7.

## 7.6 Error analysis

There are at least two distinct sources of error. First, in the experiment we measure axial load, axial strain, and transverse strain. Each of these three measurements include an uncertainty that contributes to the final measurements of equilibrium stress, tangent modulus and local Poisson's ratio. In addition, the method is based on assuming that there is little difference in the state of the material between the unloading and the loading. We

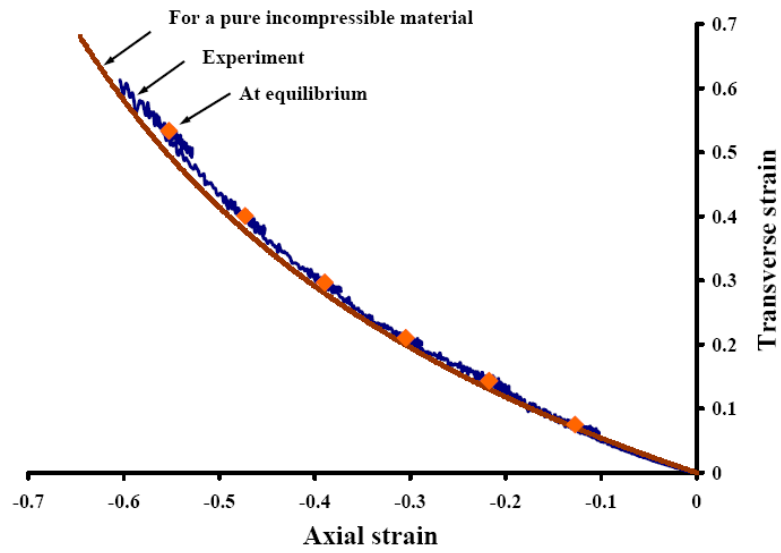


Figure 7.4: Typical transverse strain response obtained from the experiment (from Goel et al. [10]), the response that would result for an incompressible material, and the transverse strain measured at equilibrium.

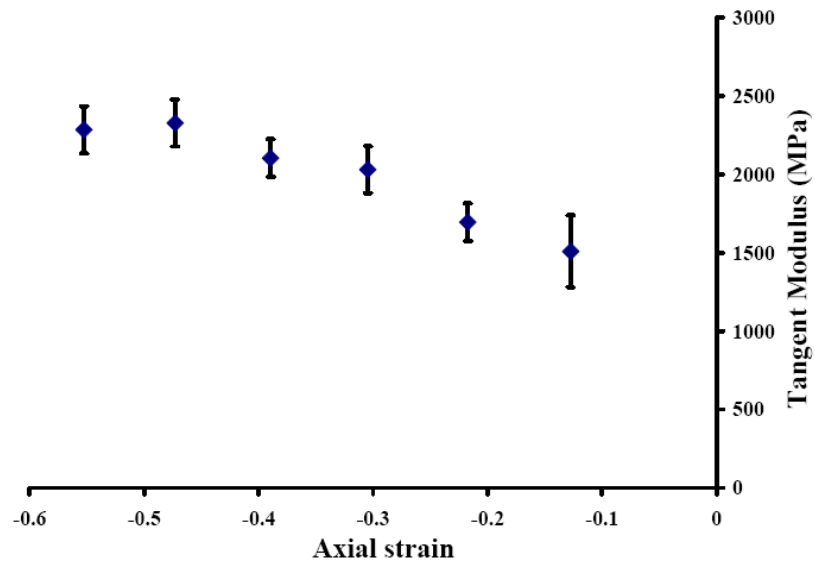


Figure 7.5: Tangent modulus of polycarbonate at equilibrium in compression at room temperature.

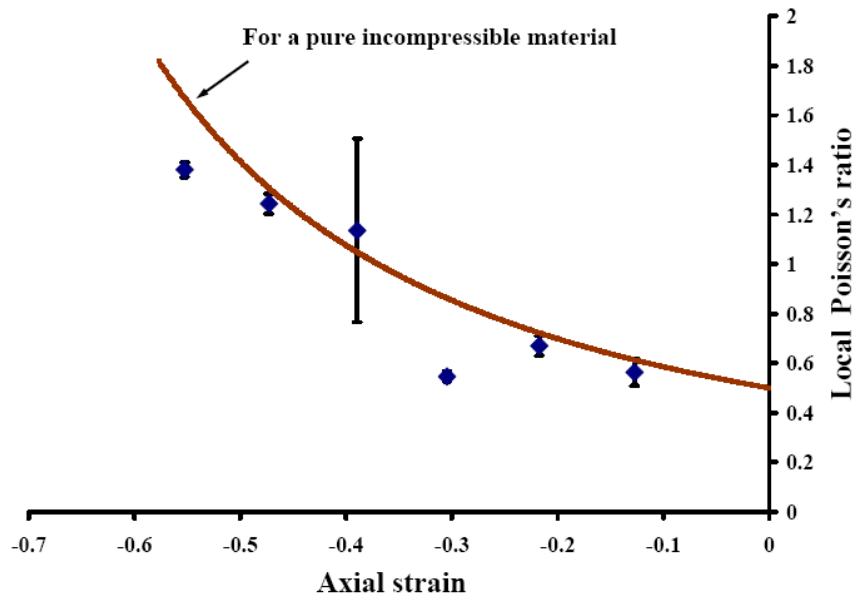


Figure 7.6: Local Poisson's ratio of polycarbonate at equilibrium in compression at room temperature.

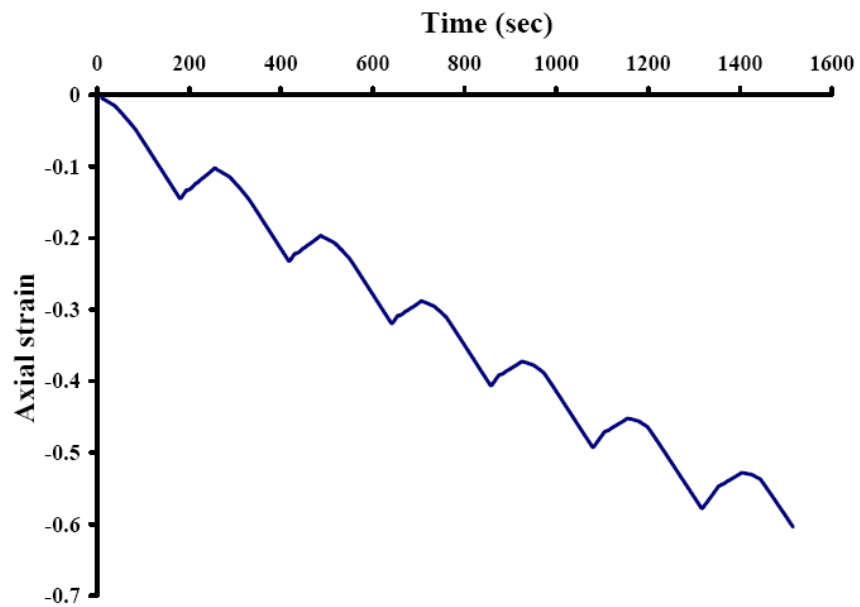


Figure 7.7: Strain history measured for polycarbonate in compression at room temperature (from Goel et al. [10]).

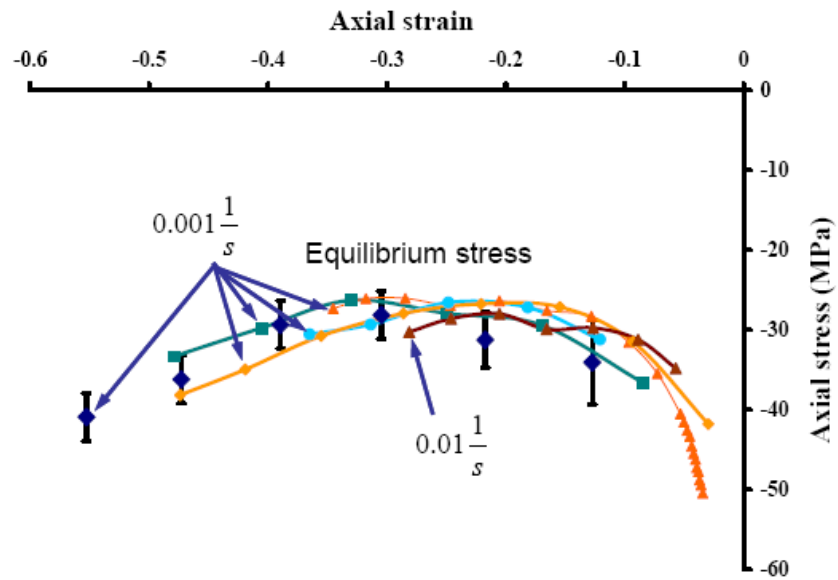


Figure 7.8: Comparison between calculated error for equilibrium stress and measurements calculated from multiple tests.

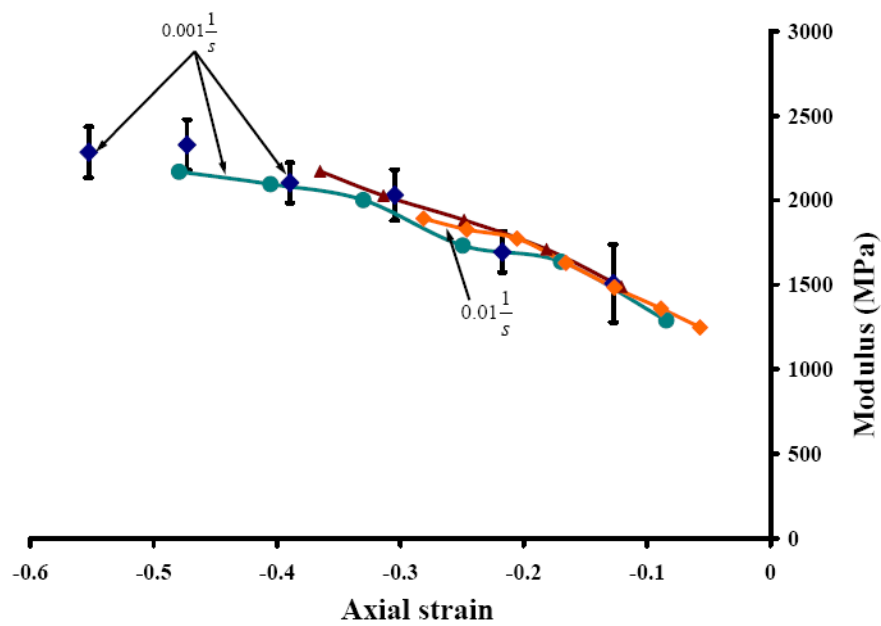


Figure 7.9: Comparison between calculated error for tangent modulus and measurements calculated from multiple tests.

estimate these two types of error differently.

We analyze each cycle of unloading and loading separately. In addition, we consider the unloading separately from the reloading, and we consider each part one segment of data. We used an ARAMIS dual stereo optical surface strain measurement system to measure the axial and transverse strains, and obtain the load from a load cell in series with the sample. We used the uncertainty in each measurement to create 20 random values for each data point using the uncertainty as the standard deviation in a normal distribution around the measured value. The uncertainty in strain was estimated to be 0.0005 and of stress to be 0.1 MPa. We then randomly selected from each set to generate data that was used to calculate the equilibrium stress, the tangent modulus and the local Poisson's ratio. We repeated this about 40,000 times until the average value and standard deviation became constant. A MATLAB program was written to generate the random sets, select from them, evaluate the values, and calculate the average and standard deviation.

To the standard deviation calculated from the uncertainty in each data we added an error associated with the fact that the unloading and loading do not truly represent the same state of the material. This error was estimated by evaluating the width of the strain (distance between point A and C in Figure 7.2) in each cycle divided by the average value of the strain (value at B in Figure 7.2). This is consistent with the fact that a small difference at large strains represents little error, but that the same difference at small strains could represent large relative differences in the plastic strain. As a result, the uncertainty of the method grows to infinity as the point of measurement is closer to the strain of the undeformed sample. As a result, the method in this particular setup provides much better

results at large strains.

## 7.7 Results for polycarbonate at different temperatures

Cyclic compression experiments were performed on PC cylinders at various strain rates and at different temperatures from room temperature to  $120^{\circ}\text{C}$ . To assess the quality of the calculated error, we compare the calculated error and the values obtained in tests conducted on several different samples. Figure 7.8 shows the equilibrium stress and the calculated standard deviation as done using the procedure described above, and the equilibrium stress calculated from a number of different samples. As can be seen, for some of the tests we evaluated the equilibrium stress for small strains. As discussed above, the error for these initial calculations are very large which indicates that the method is not suitable for small strains. Figure 7.9 shows the measured tangent moduli and calculated standard deviation as above, in addition to the tangent modulus at equilibrium calculated using a number of other samples. As can be seen from both figures, the calculated standard deviation is supported by the evaluation from multiple tests. Both Figure 7.8 and Figure 7.9 show one data set that was evaluated with a unloading/loading rate of approximately  $0.01\text{ 1/s}$  which is ten times faster than the other results at rates of  $0.001\text{ 1/s}$ . As can be seen, the change in the rate does not alter the final results.

In addition to the room temperature, equilibrium stress was calculated at  $60^{\circ}\text{C}$ ,  $80^{\circ}\text{C}$ ,  $100^{\circ}\text{C}$  and  $120^{\circ}\text{C}$  and is shown in Figure 7.10. The figure shows the associated uncertainty with each data point. Statistical analysis of the uncertainty shows a trend with temperature but not with strain rate. At any particular strain, as the temperature

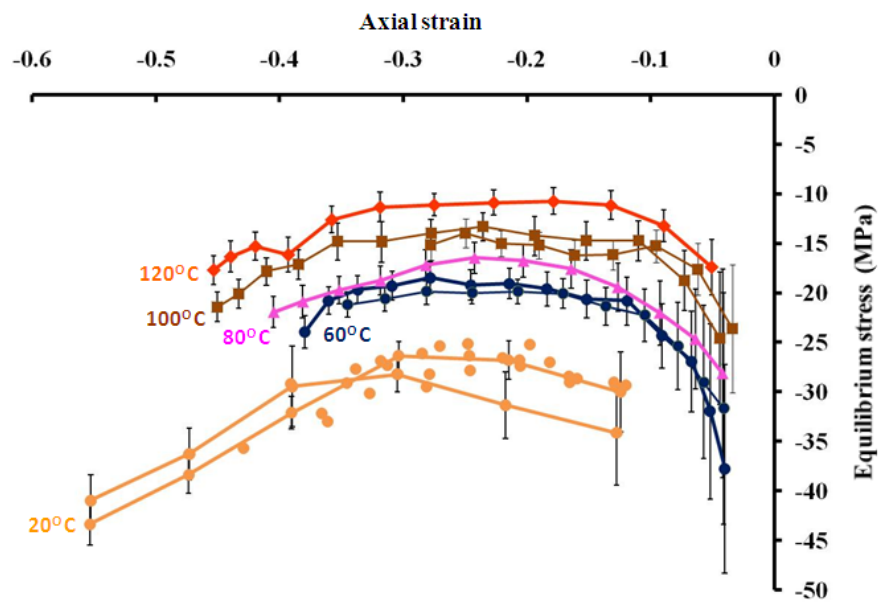


Figure 7.10: Equilibrium stress and error for different temperatures (from [11]).

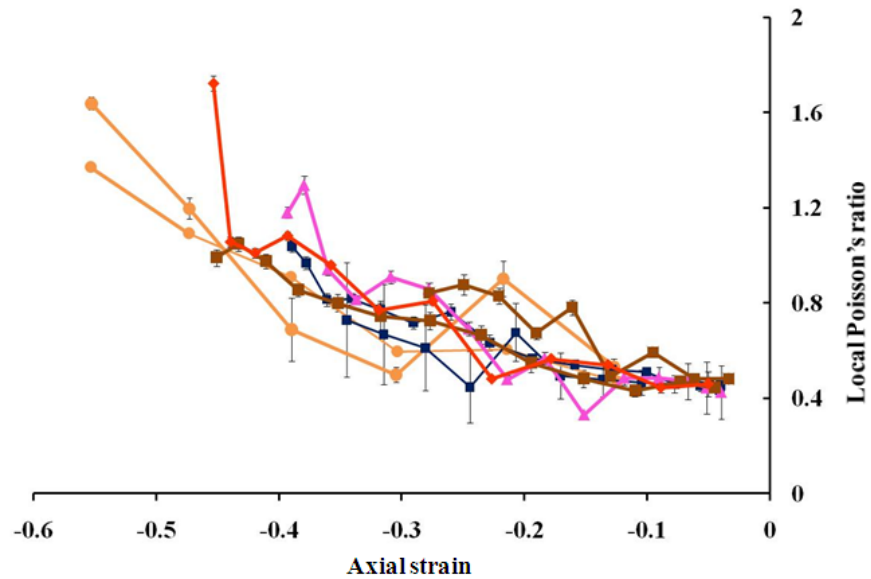


Figure 7.11: Local poisson's ratio at equilibrium for different temperatures (from [11]).

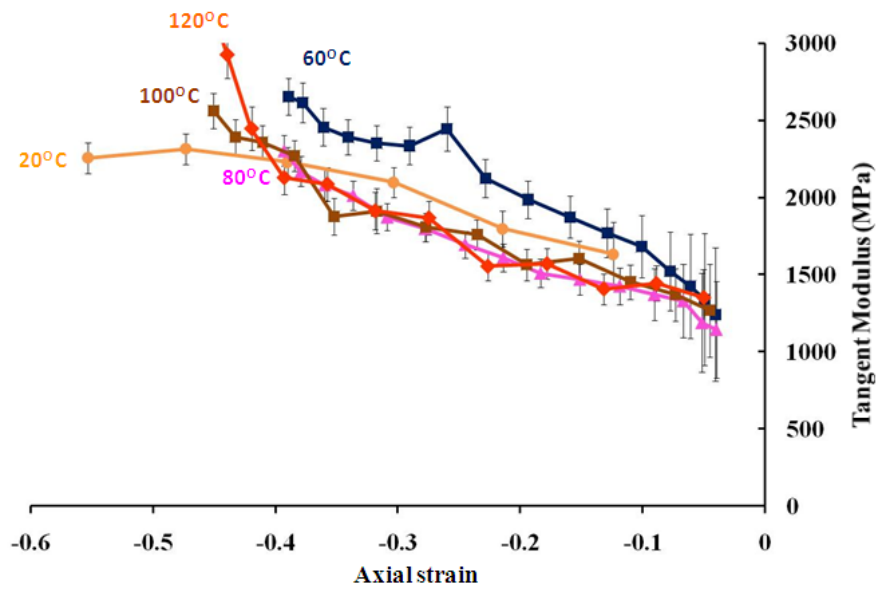


Figure 7.12: Tangent modulus at equilibrium for different temperatures (from [11]).

increases, the equilibrium stress decreases.

The local poisson's ratio at equilibrium is plotted with strain at different temperatures and is shown in figure 7.11. As the compressive strain increases, the local poisson's ratio increases. There is no particular trend between the local poisson's ratio and temperature.

The tangent modulus at equilibrium is plotted with strain at different temperatures and is shown in figure 7.12. As the compressive strain increases, the tangent's modulus increases.

## 7.8 Summary

Based on the theoretical form of the stress, we have proposed a method to calculate the equilibrium stress and the associated values of tangent modulus and local Poisson's ratio at the equilibrium stress in uniaxial tests at different temperatures. The method was evaluated for measuring the response of polycarbonate at different temperatures below the glass transition temperature and it was shown that both the calculated standard deviation and the variation observed in tests with multiple samples correlated well. This suggests that the calculated error can be used to evaluate the applicability of the method for evaluating these parameters for other materials. This is the first time we believe that the equilibrium stress has been measured in this test and the error in the measurement quantified. In addition, we believe this is the first time, to our knowledge, that both the tangent modulus and local Poisson's ratio at equilibrium have been measured for any material. The equilibrium stress, local poisson's ratio and tangent modulus at equilibrium were found to be independent of strain rate. At any particular strain, as the temperature increases, the equilibrium stress decreases but there is a weak trend of tangent modulus and local Poisson's ratio with temperature.

Finally, cyclic tests as we have proposed are not new. What is new is in how we use this test to evaluate the equilibrium stress, how we evaluate the error for this measurement, and the evaluation of the value and error of the associated tangent modulus and local poisson's ratio.

## Chapter 8

# Thermodynamically consistent model for back stress

In the last chapter we have discussed a new method based on uniaxial tests to measure the equilibrium stress, and the associated tangent modulus and local Poisson's ratio at equilibrium. The measured quantities have also been studied in regard to the possible error of such a measurement and this was reported at different temperatures. There are two purposes of this chapter, one is to partition the total stress to identify the contribution of the slow (corresponding to the standard linear solid element) and fast (corresponding to high relaxation element) relaxing elements. Another objective of this chapter is to develop a thermodynamically consistent model for back stress as a function of plastic deformation gradient and temperature. For modeling the back stress, we need to calculate the part of the response that will come from the slow relaxing element. Once this is evaluated, we use this information to model the back stress element of the slow relaxing element by appropriately

fitting the experimental results for the equilibrium stress.

## 8.1 Background

A significant part of the published work to model the back stress is based on "molecular" models and/or use the physics of polymer chain networks and statistical methods. The Neo Hookean model [24] is the simplest physically based model since it can be derived from molecular chain statistics. This model assumes that the material is constituted by a network of long chains linked by chemical bonds at junction points [25]. In 1942, Kuhn and Grun [26] used a non Gaussian theory to take into account the limiting extensibility of polymer chains and they derived the strain energy of the single chain. Later James and Guth [27], developed similar models where the network chains were distributed upon the principal stretch axis and Flory [28] and Treloar [29] assumed network chains are distributed upon four axis corresponding to the vertices of a regular tetrahedron. The Wang and Guth model [109], employed by Boyce, Parks and Argon [36], uses three non Gaussian chains arranged in a unit cube are used to predict the entropic forces associated with large deformation. This model was not capable of predicting the stress-stretch behavior so Arruda and Boyce [30] proposed a model with chains upon eight directions corresponding to the vertices of a cube inscribed in the unit sphere. The model they developed was quite similar to the three chain model but presents better agreement with experimental data for equibiaxial extension.

In the current work, we do not use the proposed models, but have directly modeled the free energy as a function of the strain invariants and fit them to experimental results.

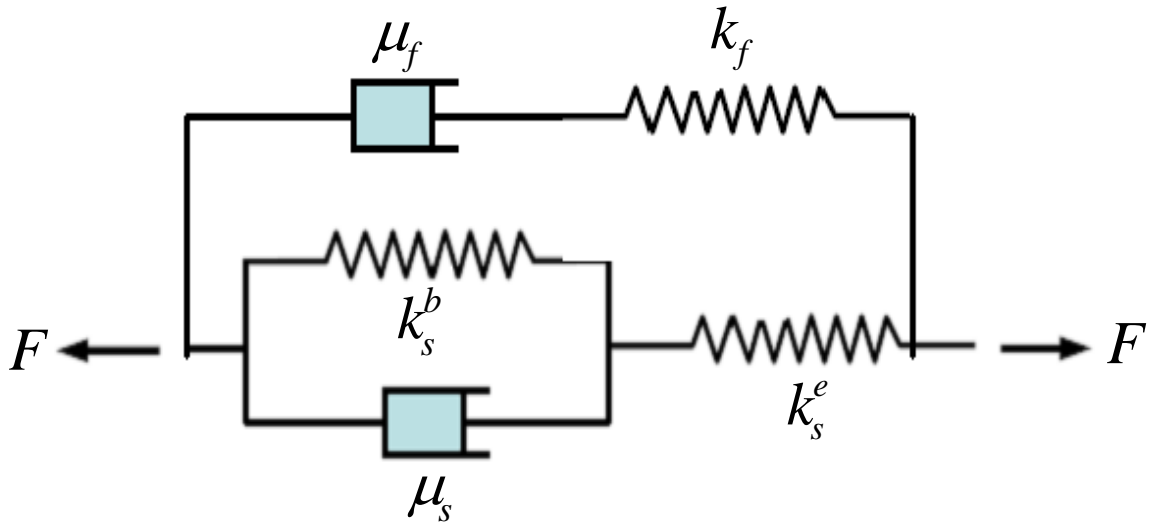


Figure 8.1: Mechanical analog of proposed constitutive model for rate dependent thermal plasticity.

## 8.2 Partitioning the stress of the slow and fast elements

In Chapter 3, we have introduced a mechanical analog on which we have developed our modeling structure. It contains a standard linear solid in parallel with a high relaxation rate element as shown in Figure 8.1. In this section we will consider how we can partition the stress to identify the separate contributions of these two elements. As described in Chapter 3, for a quasi-fast deformation at equilibrium, loading rates are faster than the quasistatic loading but slower than the high rate loading such that the high relaxation element is relaxed at all times and the entire response comes from the spring  $k_s^e$  since the spring-dashpot part of the slow relaxing element is locked as shown in Figure 8.2 and the total stress will be equal to  $\mathbf{T}_s$ . On the other hand, for ultrasonic tests, in which the time is not sufficient enough for the higher relaxation element to relax, due to rapid load, both dampers  $\mu_s$  and  $\mu_f$  will lock and the total stress will result from the two springs shown

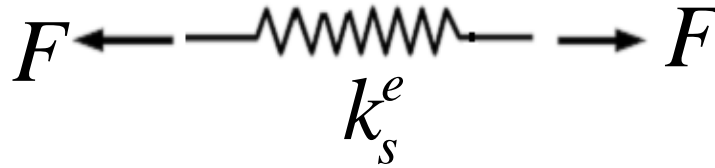


Figure 8.2: Mechanical analog corresponding to the quasi fast loading at equilibrium.

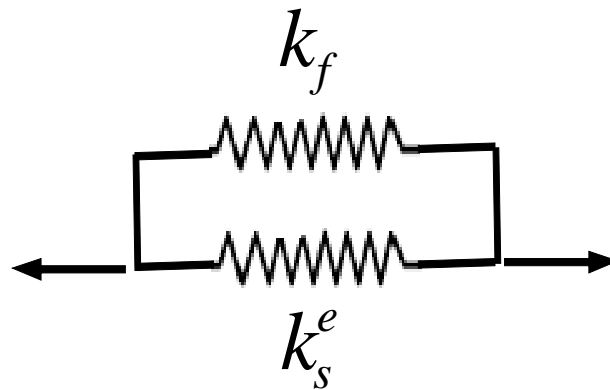


Figure 8.3: Mechanical analog corresponding to the ultrasonic testing.

in Figure 8.3 so that stress  $\mathbf{T}$  is the summation of  $\mathbf{T}_s$  and  $\mathbf{T}_f$ . The model developed in Chapter 7 captures the stress from ultrasonics measurements so the model represents the contribution of both  $\mathbf{T}_s$  and  $\mathbf{T}_f$ . We would like to separate these two parts since in this chapter we would like to focus on the slow relaxing element and need  $\mathbf{T}_s$  to obtain the information to model for back stress for this element. Therefore our first task is to take constitutive model developed for stress in Chapter 7 and extract the model of  $\mathbf{T}_s$ . This model was given as

$$\begin{aligned}
\mathbf{T} &= \mathbf{T}_s + \mathbf{T}_f = A_{iso} \left[ G \frac{1}{J J^{e\frac{2}{3}}} \left( \mathbf{B}^e - \frac{I_1}{3} \mathbf{I} \right) + \kappa \frac{J^e \ln(J^e)}{J} \mathbf{I} \right] \\
&+ A_{aniso} \left[ \rho_o \frac{\partial \psi}{\partial I_7^*} \frac{1}{J} \mathbf{F}^e [2(\mathbf{C}^p - \mathbf{I}) - (\mathbf{C}^e \mathbf{C}^p + \mathbf{C}^p \mathbf{C}^e - 2\mathbf{C}^e)] \right] \mathbf{F}^{eT} \\
&+ E_{comb} \left[ \frac{2}{J^{e\frac{2}{3}}} \left( \mathbf{B}^e - \frac{I_1}{3} \mathbf{I} \right) \ln^2(J^e) + 2 \ln(J^e) (I_1^* - 3) \right].
\end{aligned} \tag{8.1}$$

This separation will be done using the tangent modulus calculated at equilibrium in the previous chapter, assuming this is obtained under quasi-fast testing condition. We do this by assuming  $\mathbf{T}_s$  will produce the tangent modulus at equilibrium and thus stress  $\mathbf{T}_f$  is the additional stress which will result from the high relaxation element during ultrasonic measurements. We assume that the anisotropy is fully represented in the slow model, and only the other terms are split. A simple way to do this is achieved by selecting

$$\begin{aligned}
\mathbf{T}_s &= E_{quas} \left\{ A_{iso} \left[ G(\mathbf{F}_s^p) \frac{1}{J J_s^{e\frac{2}{3}}} \left( \mathbf{B}_s^e - \frac{tr(\mathbf{B}_s^e)}{3} \mathbf{I} \right) + \kappa(\mathbf{F}_s^p) \frac{J_s^e \ln(J_s^e)}{J} \mathbf{I} \right] \right. \\
&+ E_{comb} \left[ \frac{2}{J_s^{e\frac{2}{3}}} \left( \mathbf{B}_s^e - \frac{tr(\mathbf{B}_s^e)}{3} \mathbf{I} \right) \ln^2(J_s^e) + 2 \ln(J_s^e) \left( \frac{tr(\mathbf{C}_s^e)}{J_s^{e\frac{2}{3}}} - 3 \right) \right] \left. \right\} \\
&+ A_{aniso} \left[ \rho_o \frac{\partial \psi}{\partial I_7^*}(\mathbf{F}_s^p) \frac{1}{J} \mathbf{F}_s^e [2(\mathbf{C}_s^p - \mathbf{I}) - (\mathbf{C}_s^e \mathbf{C}_s^p + \mathbf{C}_s^p \mathbf{C}_s^e - 2\mathbf{C}_s^e)] \right] \mathbf{F}_s^{eT},
\end{aligned} \tag{8.2}$$

and

$$\begin{aligned}
\mathbf{T}_f &= (1 - E_{quas}) \left\{ A_{iso} \left[ G(\mathbf{F}_f^p) \frac{1}{J J_f^{e\frac{2}{3}}} \left( \mathbf{B}_f^e - \frac{tr(\mathbf{B}_f^e)}{3} \mathbf{I} \right) + \kappa(\mathbf{F}_f^p) \frac{J_f^e \ln(J_f^e)}{J} \mathbf{I} \right] \right. \\
&+ E_{comb} \left[ \frac{2}{J_f^{e\frac{2}{3}}} \left( \mathbf{B}_f^e - \frac{tr(\mathbf{B}_f^e)}{3} \mathbf{I} \right) \ln^2(J_f^e) + 2 \ln(J_f^e) \left( \frac{tr(\mathbf{C}_f^e)}{J_f^{e\frac{2}{3}}} - 3 \right) \right] \left. \right\}.
\end{aligned} \tag{8.3}$$

In equations 8.2 and 8.3,  $G(\mathbf{F}_s^p)$ ,  $\kappa(\mathbf{F}_s^p)$  and  $\rho_o \frac{\partial \psi}{\partial I_7^*}(\mathbf{F}_s^p)$  are functions evaluated at  $\mathbf{F}_s^p$  and  $G(\mathbf{F}_f^p)$  and  $\kappa(\mathbf{F}_f^p)$  are the same functions but evaluated at  $\mathbf{F}_f^p$ , respectively. The relationship between the deformation gradients, as explained in Chapter 3, is given by

$$\mathbf{F} = \mathbf{F}_s^e \mathbf{F}_s^p = \mathbf{F}_f^e \mathbf{F}_f^p. \tag{8.4}$$

The constitutive model for stress in equation 8.2 corresponds to the stress at equilibrium for quasi-fast test and can be used to calculate the tangent modulus at equilibrium. In the equations for  $\mathbf{T}_s$  and  $\mathbf{T}_f$ ,  $E_{quas}$  is the scalar material parameter which needs to be calculated such that we get the tangent modulus at equilibrium. For a given temperature, two quantities which are needed to calculate the modulus are  $\mathbf{F}_s^e$  and  $\mathbf{F}_s^p$ . For uniaxial tests the deformation gradient  $\mathbf{F}$  can be written as

$$\mathbf{F} = \lambda_t \mathbf{e}_1 \otimes \mathbf{e}_1 + \lambda_t \mathbf{e}_2 \otimes \mathbf{e}_2 + \lambda_a \mathbf{e}_3 \otimes \mathbf{e}_3, \quad (8.5)$$

where  $\lambda_t$  is the stretch in transverse direction and  $\lambda_a$  is the stretch in axial direction. A similar form will be taken by  $\mathbf{F}_s^p$  and is given by

$$\mathbf{F}_s^p = \lambda_{st}^p \mathbf{e}_1 \otimes \mathbf{e}_1 + \lambda_{st}^p \mathbf{e}_2 \otimes \mathbf{e}_2 + \lambda_{sa}^p \mathbf{e}_3 \otimes \mathbf{e}_3. \quad (8.6)$$

We will assume the plastic deformation is incompressible so that

$$J_s^p = \det(\mathbf{F}_s^p) = \lambda_{st}^{p2} \lambda_{sa}^p = 1, \quad (8.7)$$

so that  $\mathbf{F}_s^p$  can be simplified to

$$\mathbf{F}_s^p = \left( \frac{1}{\sqrt{\lambda_{sa}^p}} \right) \mathbf{e}_1 \otimes \mathbf{e}_1 + \left( \frac{1}{\sqrt{\lambda_{sa}^p}} \right) \mathbf{e}_2 \otimes \mathbf{e}_2 + \lambda_{sa}^p \mathbf{e}_3 \otimes \mathbf{e}_3. \quad (8.8)$$

The stress at equilibrium corresponding to the uniaxial tests is given by

$$\mathbf{T}_s = \sigma_{33}^b \mathbf{e}_3 \otimes \mathbf{e}_3, \quad (8.9)$$

where  $\sigma_{33}^b$  is the equilibrium stress ("back stress"). At equilibrium  $\lambda_a$  and  $\sigma_{33}^b$  are known, therefore,  $\lambda_t$  and  $\lambda_{sa}^p$  can be calculated using the equations of the stress in axial direction given to be the equilibrium stress and the stress in the transverse direction equals to zero

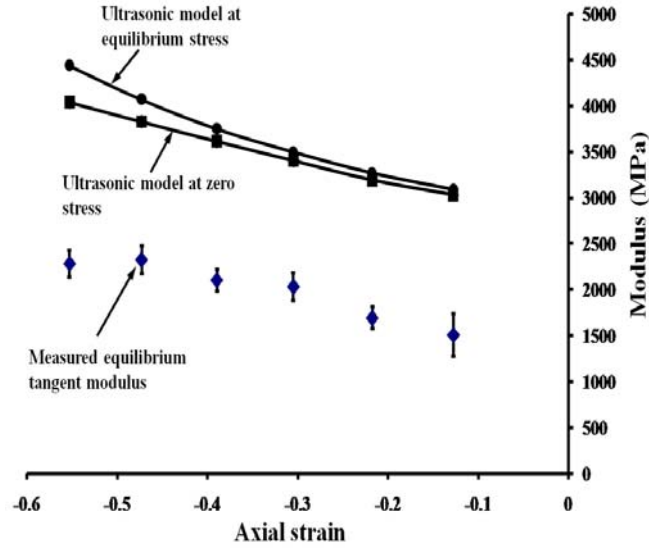


Figure 8.4: Comparison of tangent modulus from the ultrasonic model and measured from experimental cyclic loading.

$[\mathbf{T}_{s33} = \sigma_{33}^b \text{ and } \mathbf{T}_{s11} = 0]$ . Once  $\lambda_t$  and  $\lambda_{sa}^p$  are known, we know both  $\mathbf{F}_s^e$  and  $\mathbf{F}_s^p$  and can then be used to calculate the modulus at equilibrium.

Figure 8.4 shows the modulus for  $E_{quas} = 1$ , which is the modulus from ultrasonic tests, compared to that of the tangent modulus measured from the quasi-fast cyclic loading tests. As can be seen, the tangent modulus from the ultrasonic model overestimates the modulus calculated at equilibrium but both seems to have the same trend. Therefore, to fit the tangent modulus, material parameter  $E_{quas}$  is calculated to fit the experimental results. The value of  $E_{quas}$  calculated to fit the experimental equilibrium modulus is

$$E_{quas} = 0.6. \quad (8.10)$$

Figure 8.5 shows the model for the tangent modulus using  $\mathbf{T}_s$  with this  $E_{quas}$  compared to the experimentally evaluated tangent modulus at equilibrium. As can be seen, the model for  $\mathbf{T}_s$  provides similar results to the experimentally evaluated values.

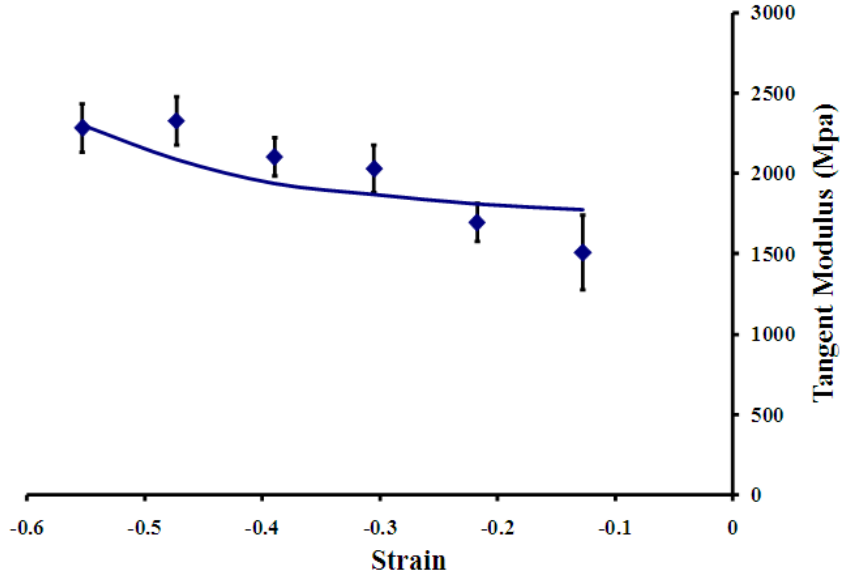


Figure 8.5: Comparison of quasistatic stress model with the cyclic experiments.

### 8.3 Combining the models for free energy

For a model to be thermodynamically consistent, models for stress and back stress should be calculated from a single free energy, as these models are respectively related to the derivatives of free energy with respect to the elastic and plastic deformation gradient. Therefore, the stress and the back stress can have terms that can come from the same term in the free energy. As discussed in Chapter 3, the total free energy is based on the form

$$\psi = \psi_s(\mathbf{F}_s^e, \mathbf{F}_s^p, \theta) + \psi_f(\mathbf{F}_f^e, \theta) + \psi_\theta(\theta), \quad (8.11)$$

where  $\psi_s(\mathbf{F}_s^e, \mathbf{F}_s^p, \theta)$  and  $\psi_f(\mathbf{F}_f^e, \theta)$  are, respectively, the free energy terms associated to slow and fast relaxation elements and  $\psi_\theta(\theta)$  is the free energy contribution just from the temperature. The stress models given by equations 8.2 and 8.3 can be used to calculate

the free energy. First let us see how we can calculate the free energy  $\psi_s(\mathbf{F}_s^e, \mathbf{F}_s^p, \theta)$  from the model of stress  $\mathbf{T}_s$  given by equation 8.2. The free energy contributions from slow strain rates  $\psi_s(\mathbf{F}_s^e, \mathbf{F}_s^p, \theta)$  are given by

$$\psi_s(\mathbf{F}_s^e, \mathbf{F}_s^p, \theta) = \psi_{s1}(\mathbf{F}_s^e, \theta) + \psi_{s2}(\mathbf{F}_s^p, \theta) + \psi_{s3}(\mathbf{F}_s^e, \mathbf{F}_s^p, \theta), \quad (8.12)$$

where  $\psi_{s1}$  and  $\psi_{s2}$  depend, respectively, upon the elastic and plastic deformation gradients and depend on temperature,  $\psi_{s3}$  is an additional free energy term that depends upon all three terms  $\mathbf{F}_s^e$ ,  $\mathbf{F}_s^p$  and  $\theta$ . For a thermodynamically consistent model, the expression for  $\mathbf{T}_s$  can be given by

$$\mathbf{T}_s^T = \rho \partial_{\mathbf{F}_s^e}(\psi_s) \mathbf{F}_s^{eT}. \quad (8.13)$$

Knowing the model of  $\mathbf{T}_s$ ,  $\partial_{\mathbf{F}_s^e}(\psi_s)$  can be written as

$$\partial_{\mathbf{F}_s^e}(\psi_s) = \frac{1}{\rho} \mathbf{T}_s^T \mathbf{F}_s^{e-T}, \quad (8.14)$$

which can be integrated to calculate  $\psi_s$  and is the summation of  $\psi_{s1}$ ,  $\psi_{s2}$  and  $\psi_{s3}$ . This can be written as

$$\begin{aligned} \psi_{s1}(\mathbf{F}_s^e, \theta) &= E_{quas} \left[ A_{iso} \left\{ \frac{G(\mathbf{F}_s^p)}{\rho_o} (I_1^*(\mathbf{F}_s^e) - 3) + \frac{\kappa(\mathbf{F}_s^p)}{\rho_o} \frac{\ln^2(J_s^e)}{2} \right\} \right. \\ &\quad \left. + \frac{E_{comb}}{\rho_o} (I_1^*(\mathbf{F}_s^e) - 3) \frac{\ln^2(J_s^e)}{2} \right], \\ \psi_{s2}(\mathbf{F}_s^p, \theta) &= \psi_{s2} [I_4^*(\mathbf{F}_s^p), I_5^*(\mathbf{F}_s^p), I_6^*(\mathbf{F}_s^p), \theta], \\ \psi_{s3}(\mathbf{F}_s^e, \mathbf{F}_s^p, \theta) &= \frac{A_{aniso}}{\rho_o} \left[ \rho_o \frac{\partial \psi}{\partial I_7^*} \left\{ I_7^*(\mathbf{F}_s^e, \mathbf{F}_s^p) - \frac{1}{2} I_8^*(\mathbf{F}_s^e, \mathbf{F}_s^p) \right\} \right]. \end{aligned} \quad (8.15)$$

In the above equation,  $G$ ,  $\kappa$  and  $\rho_o \frac{\partial \psi}{\partial I_7^*}$  are the function of  $\mathbf{F}_s^p$  and the invariants noted are given by

$$\begin{aligned} I_1^*(\mathbf{F}_s^e) &= \frac{tr(\mathbf{C}_s^e)}{J_s^{e\frac{2}{3}}}, & I_4^*(\mathbf{F}_s^p) &= \frac{tr(\mathbf{C}_s^p)}{J_s^{p\frac{2}{3}}}, \\ I_5^*(\mathbf{F}_s^p) &= \frac{tr(\mathbf{C}_s^{p2})}{tr^2(\mathbf{C}_s^p)}, & I_6^*(\mathbf{F}_s^p) &= J_s^p, \\ I_7^*(\mathbf{F}_s^e, \mathbf{F}_s^p) &= tr(\mathbf{C}_s^e \mathbf{C}_s^p) - tr(\mathbf{C}_s^e) - tr(\mathbf{C}_s^p) + 3, & I_8^* &= tr(\mathbf{C}_s^{e2} \mathbf{C}_s^p) - tr(\mathbf{C}_s^{e2}) - tr(\mathbf{C}_s^p) + 3. \end{aligned} \quad (8.16)$$

Also, the free energy term  $\psi_{s2}$  can be a function of three invariants  $I_4^*(\mathbf{F}_s^p)$ ,  $I_5^*(\mathbf{F}_s^p)$  and  $I_6^*(\mathbf{F}_s^p)$ . Similarly, the contribution from the fast relaxing element can be expressed as

$$\mathbf{T}_f^T = \rho \partial_{\mathbf{F}_f^e}(\psi_f) \mathbf{F}_f^{eT}. \quad (8.17)$$

The free energy contributions from this element can then be given by

$$\begin{aligned} \psi_f(\mathbf{F}_f^e, \theta) &= (1 - E_{quas}) \left[ A_{iso} \left\{ \frac{G(\mathbf{F}_f^p)}{\rho_o} (I_1^*(\mathbf{F}_f^e) - 3) + \frac{\kappa(\mathbf{F}_f^p) \ln^2(J_f^e)}{2} \right\} \right. \\ &\quad \left. + \frac{E_{comb}}{\rho_o} (I_1^*(\mathbf{F}_f^e) - 3) \frac{\ln^2(J_f^e)}{2} \right], \end{aligned} \quad (8.18)$$

where  $G$ ,  $\kappa$  and  $I_1^*$  are functions of noted arguments and where

$$I_1^*(\mathbf{F}_f^e) = \frac{tr(\mathbf{C}_f^e)}{J_f^{e\frac{2}{3}}}. \quad (8.19)$$

In the free energy terms in equation 8.11 and 8.12 there are two terms which are unknown. One is  $\psi_{s2}(\mathbf{F}_s^p, \theta)$ , which as will be explained in the next section can be derived from the model of back stress, and another term  $\psi_\theta$  which is the contribution from pure thermal behavior and is calculated in the next chapter.

## 8.4 Constitutive model for back stress

At equilibrium, stress in quasi-fast response it can be assumed that the response from high relaxation element will die out and there will be no stress coming from this element. Therefore, in calculating the back stress there will be no contribution in the free energy term corresponding to fast relaxing element. Therefore, free energy corresponds to the slow relaxing element along with the free energy corresponding to pure thermal behavior will be the only existing terms. This is given by

$$\psi \approx \psi_s(\mathbf{F}_s^e, \mathbf{F}_s^p, \theta) + \psi_\theta(\theta), \quad (8.20)$$

where  $\psi_s(\mathbf{F}_s^e, \mathbf{F}_s^p, \theta)$  is the summation of three terms  $\psi_{s1}(\mathbf{F}_s^e, \theta)$ ,  $\psi_{s2}(\mathbf{F}_s^p, \theta)$  and  $\psi_{s3}(\mathbf{F}_s^e, \mathbf{F}_s^p, \theta)$  and is given by equation 8.15. As discussed in Chapter 3, the model for back stress can be calculated as

$$\mathbf{T}_s^b = \rho \partial_{\mathbf{F}_s^p} (\psi_s) \mathbf{F}_s^{pT}. \quad (8.21)$$

Since  $\psi_\theta(\theta)$  is only a function of temperature, therefore taking the derivative of it with respect to  $\mathbf{F}_s^p$  will be  $\mathbf{0}$ . The expression of back stress can then be calculated as

$$\mathbf{T}^b = \rho \partial_{\mathbf{F}_s^p} (\psi_{s1} + \psi_{s2} + \psi_{s3}) \mathbf{F}_s^{pT}. \quad (8.22)$$

The individual term of back stress can then be calculated as

$$\rho \partial_{\mathbf{F}_s^p} (\psi_{s1}) \mathbf{F}_s^{pT} = E_{quas} \left[ A_{iso} \left\{ \partial_{\mathbf{F}_s^p} (G) (I_1^*(\mathbf{F}_s^e) - 3) + \partial_{\mathbf{F}_s^p} (\kappa) \frac{\ln^2(J_s^e)}{2} \right\} \right], \quad (8.23)$$

$$\rho \partial_{\mathbf{F}_s^p} (\psi_{s2}) \mathbf{F}_s^{pT} = \rho \left\{ \frac{2}{J_s^{p\frac{2}{3}}} \frac{\partial \psi_{s2}}{\partial I_4^*} \left[ \mathbf{B}_s^p - \frac{I_4(\mathbf{F}_s^p)}{3} \mathbf{I} \right] + \frac{4}{I_4^2} \frac{\partial \psi_{s2}}{\partial I_5^*} \mathbf{F}_s^p \mathbf{C} \left[ p - \frac{I_5(\mathbf{F}_s^p)}{I_4(\mathbf{F}_s^p)} \mathbf{I} \right] \mathbf{F}_1^{pT} + \ln(J_s^p) \frac{\partial \psi_{s2}}{\partial I_6^*} \mathbf{I} \right\}, \quad (8.24)$$

$$\begin{aligned} \rho \partial_{\mathbf{F}_s^p} (\psi_{s3}) \mathbf{F}_s^{pT} &= A_{aniso} \left\{ \partial_{\mathbf{F}_s^p} \left( \rho_o \frac{\partial \psi}{\partial I_7^*} \right) \left[ I_7^*(\mathbf{F}_s^e, \mathbf{F}_s^p) - \frac{1}{2} I_8^*(\mathbf{F}_s^e, \mathbf{F}_s^p) \right] \right. \\ &\quad \left. + \rho_o \frac{\partial \psi}{\partial I_7^*} \partial_{\mathbf{F}_s^p} \left[ I_7^*(\mathbf{F}_s^e, \mathbf{F}_s^p) - \frac{1}{2} I_8^*(\mathbf{F}_s^e, \mathbf{F}_s^p) \right] \right\}. \end{aligned} \quad (8.25)$$

The total back stress can be calculated by summing the equations 8.23, 8.24 and 8.25. It is to be noted that material parameters  $G$ ,  $\kappa$ ,  $\rho_o \frac{\partial \psi}{\partial I_7^*}$  in equations 8.23 to 8.25 are functions of plastic strain given by

$$G = 1072 - 159 \times [I_4^*(\mathbf{F}_s^p) - 3] \text{ MPa}, \quad (8.26)$$

$$\kappa = 4670 + 200 \times [I_4^*(\mathbf{F}_s^p) - 3] \text{ MPa}, \quad (8.27)$$

$$\rho_o \frac{\partial \psi}{\partial I_7^*} = -283 - 150 \times e^{-\frac{[I_4^*(\mathbf{F}_s^p) - 3]}{0.125}} + 433 \times e^{-\frac{[I_4^*(\mathbf{F}_s^p) - 3]}{0.004}} \text{ MPa}. \quad (8.28)$$

Therefore, the derivative of those material parameters with respect to  $\mathbf{F}_s^p$  can be calculated as

$$\partial_{\mathbf{F}_s^p} (G) = -159 \times \frac{2}{J_s^{p\frac{2}{3}}} \left[ \mathbf{B}_s^p - \frac{I_4(\mathbf{F}_s^p)}{3} \mathbf{I} \right], \quad (8.29)$$

$$\partial_{\mathbf{F}_s^p} (\kappa) = 200 \times \frac{2}{J_s^{p\frac{2}{3}}} \left[ \mathbf{B}_s^p - \frac{I_4(\mathbf{F}_s^p)}{3} \mathbf{I} \right], \quad (8.30)$$

$$\partial_{\mathbf{F}_s^p} \left( \rho_o \frac{\partial \psi}{\partial I_7^*} \right) = \left[ 150 \times \frac{1}{0.125} \times e^{-\frac{[I_4^*(\mathbf{F}_s^p) - 3]}{0.125}} - 433 \times \frac{1}{0.004} \times e^{-\frac{[I_4^*(\mathbf{F}_s^p) - 3]}{0.004}} \right] \frac{2}{J_s^{p\frac{2}{3}}} \left[ \mathbf{B}_s^p - \frac{I_4(\mathbf{F}_s^p)}{3} \mathbf{I} \right]. \quad (8.31)$$

Equations 8.23 and 8.25 are known from the model of stress and can be denoted by  $\mathbf{T}_{stress}^b$  therefore the model of back stress can be given by

$$\mathbf{T}^b = \mathbf{T}_{stress}^b + \rho \partial_{\mathbf{F}_s^p} (\psi_{s2}) \mathbf{F}_s^{pT}, \quad (8.32)$$

where

$$\mathbf{T}_{stress}^b = \rho \partial_{\mathbf{F}_s^p} (\psi_{s1}) \mathbf{F}_s^{pT} + \rho \partial_{\mathbf{F}_s^p} (\psi_{s3}) \mathbf{F}_s^{pT}. \quad (8.33)$$

The equation for the back stress can then be given by

$$\mathbf{T}_s^b = \mathbf{T}_{stress}^b + \rho \left\{ \frac{2}{J_s^{p\frac{2}{3}}} \frac{\partial \psi_{s2}}{\partial I_4^*} \left( \mathbf{B}_s^p - \frac{I_4}{3} \mathbf{I} \right) + \frac{4}{I_4^2} \frac{\partial \psi_{s2}}{\partial I_5^*} \mathbf{F}_s^p \left( \mathbf{C}_s^p - \frac{I_5}{I_4} \mathbf{I} \right) \mathbf{F}_s^{pT} + \ln(J_s^p) \frac{\partial \psi_{s2}}{\partial I_6^*} \mathbf{I} \right\}. \quad (8.34)$$

In the above equation there are three material parameters  $\frac{\partial \psi_{s2}}{\partial I_4^*}$ ,  $\frac{\partial \psi_{s2}}{\partial I_5^*}$  and  $\frac{\partial \psi_{s2}}{\partial I_6^*}$  which needs to be evaluated using the experimental results. The material parametres  $\frac{\partial \psi_{s2}}{\partial I_4^*}$  and  $\frac{\partial \psi_{s2}}{\partial I_5^*}$  correspond to the shear part of the plastic flow and  $\frac{\partial \psi_{s2}}{\partial I_6^*}$  corresponds to the volumetric part of the plastic flow. Considering the standard assumption that the plastic flow is incompressible, the equation for the back stress can be represented as

$$\mathbf{T}_s^b = \mathbf{T}_{stress}^b + \rho \left[ \frac{2}{J_s^{p\frac{2}{3}}} \frac{\partial \psi_{s2}}{\partial I_4^*} \left( \mathbf{B}_s^p - \frac{I_4}{3} \mathbf{I} \right) + \frac{4}{I_4^2} \frac{\partial \psi_{s2}}{\partial I_5^*} \mathbf{F}_s^p \left( \mathbf{C}_s^p - \frac{I_5}{I_4} \mathbf{I} \right) \mathbf{F}_s^{pT} \right] + p^b \mathbf{I}. \quad (8.35)$$

In the above equation there are two material functions  $\frac{\partial \psi_{s2}}{\partial I_4^*}$  and  $\frac{\partial \psi_{s2}}{\partial I_5^*}$  and an indeterminate constant  $p^b$ . Since  $\frac{\partial \psi_{s2}}{\partial I_4^*}$  and  $\frac{\partial \psi_{s2}}{\partial I_5^*}$  both corresponds to the shear part of the deformation, we have only selected  $\frac{\partial \psi_{s2}}{\partial I_4^*}$  as being nonzero and have evaluated this by fitting to the experimental value of the back stress. Using this simplification the model for back stress is given by

$$\mathbf{T}_s^b = \mathbf{T}_{stress}^b + \rho \frac{2}{J_s^{p\frac{2}{3}}} \frac{\partial \psi_{s2}}{\partial I_4^*} \left( \mathbf{B}_s^p - \frac{tr(\mathbf{B}_s^p)}{3} \mathbf{I} \right) + p^b \mathbf{I}. \quad (8.36)$$

## 8.5 Free energy assumption of the back stress

As a specific model let us consider a model for  $\psi_{s2}$  of the form

$$\begin{aligned} \psi_{s2}(\mathbf{F}_s^p, \theta) &= \frac{1}{2\rho_o} \left[ 2 \frac{\tau_o^{b2}}{(G_o^b - G_{\infty 1}^b)} \ln \left\{ \cosh \left( \sqrt{\frac{(G_o^b - G_{\infty 1}^b)^2}{\tau_o^{b2}} [I_4^*(\mathbf{F}_s^p) - 3]} \right) \right\} \right. \\ &\quad \left. + G_{\infty 1}^b (I_4^*(\mathbf{F}_s^p) - 3) + \frac{G_{\infty 2}^b}{2} [I_4^*(\mathbf{F}_s^p) - 3]^2 \right], \end{aligned} \quad (8.37)$$

where  $G_o^b, \tau_o^b, G_{\infty 1}^b$  and  $G_{\infty 2}^b$  are the material parameters,  $I_4^* = I_4 = tr(\mathbf{C}_s^p)$  and  $J_s^p = 1$ .

The back stress corresponding to this form of free energy can be calculated as

$$\mathbf{T}^b = \rho \partial_{\mathbf{F}_s^p} (\psi_{s2}) \mathbf{F}_s^{pT}. \quad (8.38)$$

This can be calculated to give

$$\mathbf{T}^b = \frac{1}{J} \left[ \left( G_o^b - G_{\infty 1}^b \right) \frac{\tanh \left( \sqrt{\frac{(G_o^b - G_{\infty 1}^b)^2}{\tau_o^{b2}} [I_4^*(\mathbf{F}_s^p) - 3]} \right)}{\sqrt{\frac{(G_o^b - G_{\infty 1}^b)^2}{\tau_o^{b2}} [I_4^*(\mathbf{F}_s^p) - 3]}} + G_{\infty 1}^b + G_{\infty 2}^b (I_4^*(\mathbf{F}_s^p) - 3) \right] \quad (8.39)$$

$$\left( \mathbf{B}_s^p - \frac{1}{3} tr(\mathbf{B}_s^p) \mathbf{I} \right).$$

To understand the model, let us consider its response in simple shear. Figure 8.6 shows the in-plane deformation for simple shear, the out-of-plane deformation is assumed to be zero. Let us assume that we are using similar rectangular coordinates for both reference and current configuration. The deformation associated with simple shear can be written as

$$x_1 = X_1 + \gamma X_2, \quad (8.40)$$

$$x_2 = X_2,$$

$$x_3 = X_3.$$

The deformation gradient in this case can be written as

$$\mathbf{F}_s = \mathbf{e}_1 \otimes \mathbf{e}_1 + \mathbf{e}_2 \otimes \mathbf{e}_2 + \mathbf{e}_3 \otimes \mathbf{e}_3 + \gamma_s \mathbf{e}_1 \otimes \mathbf{e}_2. \quad (8.41)$$

Let us assume that the plastic deformation gradient will be of similar structure and can be written as

$$\mathbf{F}_s^p = \mathbf{e}_1 \otimes \mathbf{e}_1 + \mathbf{e}_2 \otimes \mathbf{e}_2 + \mathbf{e}_3 \otimes \mathbf{e}_3 + \gamma_s^p \mathbf{e}_1 \otimes \mathbf{e}_2. \quad (8.42)$$

The left Cauchy stretch tensor  $\mathbf{B}_s^p$  is therefore given by

$$\mathbf{B}_s^p = (1 + \gamma_s^{p2}) \mathbf{e}_1 \otimes \mathbf{e}_1 + \mathbf{e}_2 \otimes \mathbf{e}_2 + \mathbf{e}_3 \otimes \mathbf{e}_3 + \gamma_s^p (\mathbf{e}_1 \otimes \mathbf{e}_2 + \mathbf{e}_2 \otimes \mathbf{e}_1). \quad (8.43)$$

Volume ratio  $J_s^p = 1$  and  $I_4^* = \frac{tr(\mathbf{B}_s^p)}{J_s^{p2/3}} = 3 + \gamma_s^{p2}$ . Using the values of  $J_s^p$  and  $I_4^*$ , the back stress in shear can be written as

$$\tau^b = \tau_o^b \tanh \left( \frac{(G_o^b - G_{\infty 1}^b)}{\tau_o^b} \gamma_s^p \right) + G_{\infty 1}^b \gamma_s^p + G_{\infty 2}^b \gamma_s^{p3}. \quad (8.44)$$

The slope (tangent modulus) from this equation for shear stress is given as

$$\frac{\partial \tau^b}{\partial \gamma_s^p} = (G_o^b - G_{\infty 1}^b) \sec h^2 \left( \frac{(G_o^b - G_{\infty 1}^b)}{\tau_o^b} \gamma_s^p \right) + G_{\infty 1}^b + 3G_{\infty 2}^b \gamma_s^{p2}, \quad (8.45)$$

where

$$\lim_{\gamma_s^p \rightarrow 0} \frac{\partial \tau^b}{\partial \gamma_s^p} = G_o^b, \quad \lim_{\gamma_s^p \rightarrow \infty} \frac{\partial \tau^b}{\partial \gamma_s^p} = G_{\infty 1}^b, \quad \text{if } G_{\infty 2}^b = 0. \quad (8.46)$$

Therefore, as plastic strain  $\gamma_s^p \rightarrow 0$ , the initial slope is given by  $G_o^b$  and for very large plastic strains, if material parameter  $G_{\infty 2}^b = 0$ ,  $G_{\infty 1}^b$  is given as the final slope, but if  $G_{\infty 2}^b$  is present then the slope will tend to infinity at large plastic strains. The plot of stress with respect to strain for  $G_{\infty 2}^b = 0$  is shown in figure 8.7, where  $G_o^b$  is the initial slope,  $G_{\infty}^b$  is a final slope and  $\tau_o^b$  is the stress which gives the transition from  $G_o^b$  to  $G_{\infty}^b$ .

The model discussed in this section can be combined together with equation 8.36 to give

$$\begin{aligned} \mathbf{T}_s^b = \mathbf{T}_{stress}^b + \frac{1}{J} & \left\{ (G_o^b - G_{\infty 1}^b) \frac{\tanh \left( \sqrt{\frac{(G_o^b - G_{\infty 1}^b)^2}{\tau_o^{b2}} [I_4^*(\mathbf{F}_s^p) - 3]} \right)}{\sqrt{\frac{(G_o^b - G_{\infty 1}^b)^2}{\tau_o^{b2}} [I_4^*(\mathbf{F}_s^p) - 3]}} \right. \\ & \left. + G_{\infty 1}^b + G_{\infty 2}^b [I_4^*(\mathbf{F}_s^p) - 3] \right\} \left( \mathbf{B}_s^p - \frac{1}{3} tr(\mathbf{B}_s^p) \mathbf{I} \right) + p^b \mathbf{I}. \end{aligned} \quad (8.47)$$

which will be used to fit the experimental results, where  $\mathbf{T}_{stress}^b$  is the terms coming from the model for stress.

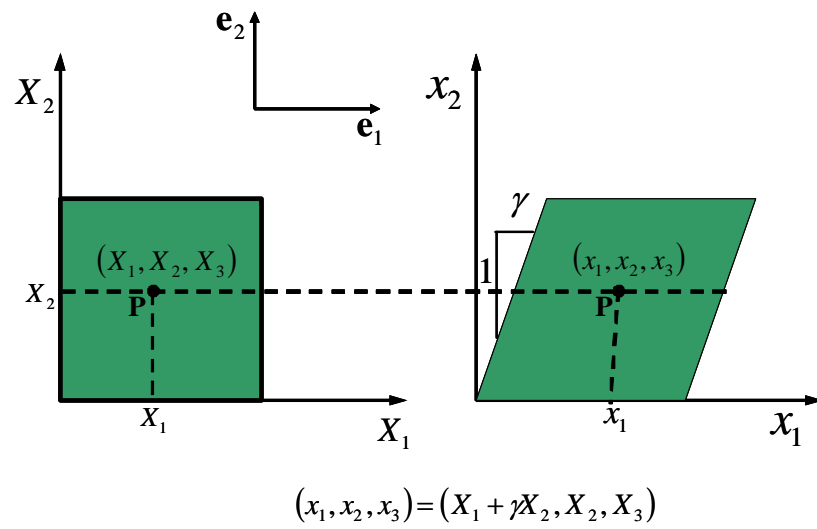
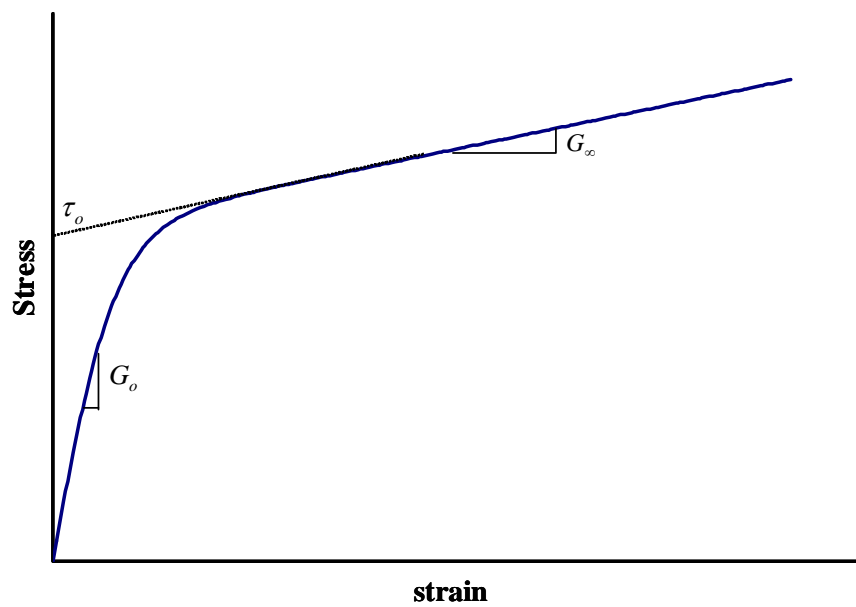


Figure 8.6: In plane deformation for simple shear

Figure 8.7: Stress strain curve response in shear from the model with  $G_\infty = G_{\infty 1}$  and  $G_{\infty 2} = 0$

## 8.6 Fitting the model to experimental results from compression

In last chapter we have calculated the location of stress at equilibrium and for large strains at different temperatures . The stress at equilibrium corresponding to the uniaxial tests will be

$$\mathbf{T}^{eq} = \sigma_{33}^{eq} \mathbf{e}_3 \otimes \mathbf{e}_3, \quad (8.48)$$

where  $\mathbf{T}^{eq}$  represents stresses at equilibrium and  $\sigma_{33}^{eq}$  is the component of equilibrium stress in the direction of compression. If the plastic flow is considered to be incompressible then the equilibrium stress can be considered to possibly be different from the back stress by a hydrostatic component. This can be fixed by assuming the model for back stress only characterizing the deviatoric part of this term. Therefore we take  $\mathbf{T}^b = \mathbf{S}^b$  where  $\mathbf{S}^b$  is the deviatoric part of the equilibrium stress and assume  $\mathbf{T}^{eq} = \mathbf{S}^b + p^b \mathbf{I}$ . In fitting the model, therefore the deviatoric part of the equilibrium stress is only considered. The slope  $G_o^b = 1000 \text{ MPa}$  is considered as the initial slope. This is arbitrarily taken since the value corresponding to the initial slope in shear for PC cannot be evaluated using the proposed method. The material parameter obtained from fitting the response shown in Figure 8.8 are

$$\begin{aligned} \tau_o^b &= 17 \text{ MPa}, \\ G_{\infty 1}^b &= 0 \text{ MPa}, \quad G_{\infty 2}^b = 5 \text{ MPa}. \end{aligned} \quad (8.49)$$

To obtain these values, first material parameter  $\tau_o^b$  is fitted assuming  $G_{\infty 1}^b$  and  $G_{\infty 2}^b$  equal to 0 and then  $G_{\infty 1}^b$  and  $G_{\infty 2}^b$  are used to fit the response at large strains. Figure 8.8 shows

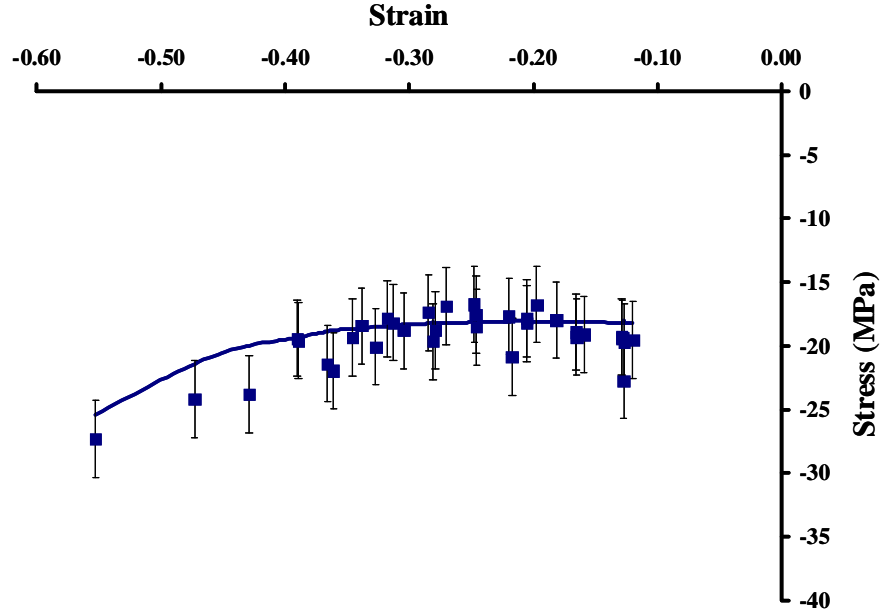


Figure 8.8: The experimental (from Goel et al. [11]) and the model for back stress at room temperature

the results of this fit and its comparison to the measured experimental results.

The model has been extended to higher temperature by including a factor  $\tau_o^b$  which depend upon temperature. By changing the value of  $\tau_o^b$  with respect to temperature the back stress location will be changed. The material parameter got for  $\tau_o^b$  as a function of temperature is

$$\tau_o^b = -0.119\theta + 51.795 \text{ MPa}, \quad (8.50)$$

where  $\theta$  is in  $K$ . The results of this fit are shown in Figure 8.9.

## 8.7 Summary and conclusion

In this chapter we have developed a thermodynamically consistent model for back stress at different temperatures. For model to be thermodynamically consistent, there will

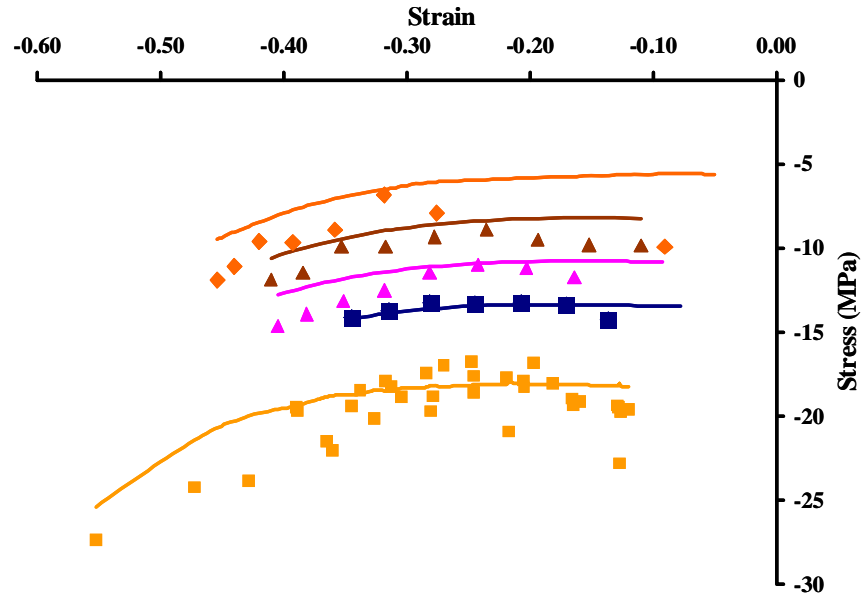


Figure 8.9: Comparison of experiment (from [11]) with model for back stress at different temperature

be some terms from stress which contribute to the back stress. These terms come from the terms in the equation for stress that introduce anisotropy in the elastic response as a result of plastic flow. To calculate the back stress, first the total stress is partitioned into the contribution from the slow and fast relaxing elements and then the model representing the slow relaxing element is fitted to the tangent modulus calculated from the cyclic experiments. The terms calculated in this way are then used for modeling the back stress, assuming that the incompressibility of the back stress element introduces an indeterminacy in the back stress model of the form of a hydrostatic stress. As a result, to fit the experimental results the deviatoric part of the equilibrium stress at different temperatures were considered and the material parameters were calculated.

## Chapter 9

# Heat generation and heat capacity

In the previous chapters we have developed the model for stress and back stress. These models for stress and back stress will correspond to the terms in free energy which will contribute to the slow and fast response depending upon the mechanical loading and are given by  $\psi_s(\mathbf{F}_s^e, \mathbf{F}_s^p, \theta)$  and  $\psi_f(\mathbf{F}_f^e, \theta)$ . The focus of this chapter is to calculate the part of the free energy which will represent pure thermal behavior and is given by  $\psi_\theta(\theta)$ . To calculate this free energy term, heat capacity is calculated for a material at zero stress and zero plastic strain. The free energy was then calculated using the heat capacity results from Differential Scanning Calorimetry (DSC).

## 9.1 Heat capacity for the sample at zero stress and zero elastic and plastic strain

The heat generation and flow at a point can be calculated using the expression of balance of work and energy given in Chapter 2 by

$$\rho \dot{e} = -\text{div}_{\mathbf{x}}(\mathbf{q}) + \rho r + \text{tr}(\mathbf{T}\mathbf{L}).$$

From this we have derived the specific heat capacity  $c$  which was given by

$$c = \frac{\dot{h}}{\dot{\theta}} = \frac{\dot{\eta}}{\dot{\theta}} - \frac{1}{\rho \dot{\theta}} \Delta \mathbf{T}^T : \mathbf{L}^p, \quad (9.1)$$

for a single internal variable and can be written in our case as

$$c = \frac{\dot{h}}{\dot{\theta}} = \frac{\dot{\eta}}{\dot{\theta}} - \frac{1}{\rho \dot{\theta}} \left[ \Delta \mathbf{T}_s^T : \mathbf{L}_s^p + \Delta \mathbf{T}_f^T : \mathbf{L}_f^p \right]. \quad (9.2)$$

For zero stress and at zero plastic strains, this leads to the expression of  $c$  as

$$c = \frac{\dot{\eta}}{\dot{\theta}}. \quad (9.3)$$

As can be seen  $\dot{\eta}$  is required to calculate  $c$ . The equation for  $\dot{\eta}$  as described in Chapter 2 can be written for the two internal parameters as

$$\dot{\eta} = \dot{\eta}_{\mathbf{L}} : \mathbf{L} + \dot{\eta}_{\dot{\theta}} \dot{\theta} + \dot{\eta}_{\mathbf{L}_s^p} : \mathbf{L}_s^p + \dot{\eta}_{\mathbf{L}_f^p} : \mathbf{L}_f^p, \quad (9.4)$$

where

$$\dot{\eta}_{\mathbf{L}} = \frac{1}{\rho} \partial_{\theta} (\mathbf{T}^T), \quad (9.5)$$

$$\dot{\eta}_{\dot{\theta}} = \partial_{\theta} (\eta) - \left[ \partial_{\mathbf{F}^{\theta}} (\psi) - \frac{1}{\rho} \mathbf{F}^{pT} \mathbf{F}^{eT} \partial_{\theta} (\mathbf{T}^T) \mathbf{F}^{p-T} \mathbf{F}^{\theta-T} \right] : \partial_{\theta} (\boldsymbol{\alpha}), \quad (9.6)$$

$$\dot{\eta}_{\mathbf{L}_s^p} = -\frac{1}{\rho} \partial_{\theta} (\mathbf{T}_s^T). \quad (9.7)$$

$$\dot{\eta}_{\mathbf{L}_f^p} = -\frac{1}{\rho} \partial_\theta (\mathbf{T}_f^T). \quad (9.8)$$

To calculate  $\dot{\eta}$ , the values of  $\dot{\eta}_{\mathbf{L}}$ ,  $\dot{\eta}_{\boldsymbol{\theta}}$ ,  $\dot{\eta}_{\mathbf{L}_s^p}$  and  $\dot{\eta}_{\mathbf{L}_f^p}$  needs to be calculated. That is, we need to evaluate from the free energy the equations 9.5, 9.6, 9.7 and 9.8. All these terms require us to calculate  $\partial_\theta (\mathbf{T}_s^T)$  and  $\partial_\theta (\mathbf{T}_f^T)$  at zero elastic and plastic strain. The equations for  $\mathbf{T}_s$  and  $\mathbf{T}_f$  were modeled as

$$\begin{aligned} \mathbf{T}_s = & E_{quas} \left\{ A_{iso} \left[ G(\mathbf{F}_s^p) \frac{1}{J J_s^{e\frac{2}{3}}} \left( \mathbf{B}_s^e - \frac{tr(\mathbf{B}_s^e)}{3} \mathbf{I} \right) + \kappa(\mathbf{F}_s^p) \frac{J_s^e \ln(J_s^e)}{J} \mathbf{I} \right] \right. \\ & + E_{comb} \left[ \frac{2}{J_s^{e\frac{2}{3}}} \left( \mathbf{B}_s^e - \frac{tr(\mathbf{B}_s^e)}{3} \mathbf{I} \right) \ln^2(J_s^e) + 2 \ln(J_s^e) \left( \frac{tr(\mathbf{C}_s^e)}{J_s^{e\frac{2}{3}}} - 3 \right) \right] \left. \right\} \\ & + A_{aniso} \left[ \rho_o \frac{\partial \psi}{\partial I_7^*}(\mathbf{F}_s^p) \frac{1}{J} \mathbf{F}_s^e [2(\mathbf{C}_s^p - \mathbf{I}) - (\mathbf{C}_s^e \mathbf{C}_s^p + \mathbf{C}_s^p \mathbf{C}_s^e - 2\mathbf{C}_s^e)] \right] \mathbf{F}_s^{eT}, \end{aligned} \quad (9.9)$$

and

$$\begin{aligned} \mathbf{T}_f = & (1 - E_{quas}) \left\{ A_{iso} \left[ G(\mathbf{F}_f^p) \frac{1}{J J_f^{e\frac{2}{3}}} \left( \mathbf{B}_f^e - \frac{tr(\mathbf{B}_f^e)}{3} \mathbf{I} \right) + \kappa(\mathbf{F}_f^p) \frac{J_f^e \ln(J_f^e)}{J} \mathbf{I} \right] \right. \\ & + E_{comb} \left[ \frac{2}{J_f^{e\frac{2}{3}}} \left( \mathbf{B}_f^e - \frac{tr(\mathbf{B}_f^e)}{3} \mathbf{I} \right) \ln^2(J_f^e) + 2 \ln(J_f^e) \left( \frac{tr(\mathbf{C}_f^e)}{J_f^{e\frac{2}{3}}} - 3 \right) \right] \left. \right\}, \end{aligned} \quad (10)$$

where  $G(\mathbf{F}_s^p)$ ,  $\kappa(\mathbf{F}_s^p)$  and  $\rho_o \frac{\partial \psi}{\partial I_7^*}(\mathbf{F}_s^p)$  are functions evaluated at  $\mathbf{F}_s^p$  and  $G(\mathbf{F}_f^p)$  and  $\kappa(\mathbf{F}_f^p)$  are the same functions but evaluated at  $\mathbf{F}_f^p$ . In this model only  $A_{iso}$ ,  $A_{aniso}$  and  $E_{comb}$  are functions of temperatures since the material parameters  $G(\mathbf{F}_s^p)$ ,  $\kappa(\mathbf{F}_s^p)$ ,  $\rho_o \frac{\partial \psi}{\partial I_7^*}$ ,  $G(\mathbf{F}_f^p)$  and  $\kappa(\mathbf{F}_f^p)$  are only a function of plastic strains. Taking the derivatives of  $\mathbf{T}_s$  and  $\mathbf{T}_f$  with respect to  $\theta$  and evaluating it at zero elastic and plastic strain will give us

$$[\partial_\theta (\mathbf{T}_s^T)]_{\mathbf{F}_s^e=\mathbf{I}, \mathbf{F}_s^p=\mathbf{I}} = 0 \quad , \quad [\partial_\theta (\mathbf{T}_f^T)]_{\mathbf{F}_f^e=\mathbf{I}, \mathbf{F}_f^p=\mathbf{I}} = 0. \quad (9.11)$$

Free energy  $\psi$  is independent of  $\mathbf{F}^\theta$ , therefore

$$\partial_{\mathbf{F}^\theta} (\psi) = 0. \quad (9.12)$$

Using the above two equations  $\dot{\eta}_{\mathbf{L}} = \mathbf{0}$ ,  $\dot{\eta}_{\mathbf{L}_s^p} = \mathbf{0}$  and  $\dot{\eta}_{\mathbf{L}_f^p} = \mathbf{0}$  and since  $\dot{\boldsymbol{\eta}}_{\boldsymbol{\theta}} = \partial_{\theta}(\boldsymbol{\eta})$ , the expression in 9.4 one can be written as

$$\dot{\boldsymbol{\eta}} = \partial_{\theta}(\boldsymbol{\eta}) \dot{\boldsymbol{\theta}}. \quad (9.13)$$

The specific heat capacity  $c$  can thus be calculated as

$$c = \frac{\dot{\boldsymbol{\eta}}}{\dot{\boldsymbol{\theta}}} \boldsymbol{\theta} = \theta \partial_{\theta}(\boldsymbol{\eta}) = -\theta \frac{\partial^2 \psi}{\partial \theta^2}. \quad (9.14)$$

The total form of free energy is given as

$$\psi = \psi_s(\mathbf{F}_s^e, \mathbf{F}_s^p, \theta) + \psi_f(\mathbf{F}_f^e, \theta) + \psi_{\theta}(\theta), \quad (9.15)$$

where

$$\psi_s(\mathbf{F}_s^e, \mathbf{F}_s^p, \theta) = \psi_{s1}(\mathbf{F}_s^e, \theta) + \psi_{s2}(\mathbf{F}_s^p, \theta) + \psi_{s3}(\mathbf{F}_s^e, \mathbf{F}_s^p, \theta). \quad (9.16)$$

The expression of  $\psi_{s1}(\mathbf{F}_s^e, \theta)$ ,  $\psi_{s2}(\mathbf{F}_s^p, \theta)$ ,  $\psi_{s3}(\mathbf{F}_s^e, \mathbf{F}_s^p, \theta)$  and  $\psi_f(\mathbf{F}_f^e, \theta)$  have already been calculated from the two models for stress and the model for back stress in the previous chapter and are written as

$$\psi_{s1}(\mathbf{F}_s^e, \theta) = E_{quas} \left[ A_{iso} \left\{ \frac{G(\mathbf{F}_s^p)}{\rho_o} (I_1^*(\mathbf{F}_s^e) - 3) + \frac{\kappa(\mathbf{F}_s^p)}{\rho_o} \frac{\ln^2(J_s^e)}{2} \right\} + \frac{E_{comb}}{\rho_o} (I_1^*(\mathbf{F}_s^e) - 3) \frac{\ln^2(J_s^e)}{2} \right], \quad (9.17)$$

$$\psi_{s2}(\mathbf{F}_s^p, \theta) = \frac{1}{2\rho_o} \left[ 2 \frac{\tau_o^{b2}}{(G_o^b)} \ln \left\{ \cosh \left( \sqrt{\frac{(G_o^b)^2}{\tau_o^{b2}} [I_4^*(\mathbf{F}_s^p) - 3]} \right) \right\} + \frac{G_{\infty 2}^b}{2} [I_4^*(\mathbf{F}_s^p) - 3]^2 \right], \quad (9.18)$$

$$\psi_{s3}(\mathbf{F}_s^e, \mathbf{F}_s^p, \theta) = \frac{A_{aniso}}{\rho_o} \left[ \rho_o \frac{\partial \psi}{\partial I_7^*} (I_7^*(\mathbf{F}_s^e, \mathbf{F}_s^p) - \frac{1}{2} I_8^*(\mathbf{F}_s^e, \mathbf{F}_s^p)) \right], \quad (9.19)$$

$$\begin{aligned} \psi_f(\mathbf{F}_f^e, \theta) = & (1 - E_{quas}) \left[ A_{iso} \left\{ \frac{G(\mathbf{F}_f^p)}{\rho_o} (I_1^*(\mathbf{F}_f^e) - 3) + \frac{\kappa(\mathbf{F}_f^p)}{\rho_o} \frac{\ln^2(J_f^e)}{2} \right\} \right. \\ & \left. + \frac{E_{comb}}{\rho_o} (I_1^*(\mathbf{F}_f^e) - 3) \frac{\ln^2(J_f^e)}{2} \right]. \end{aligned} \quad (9.20)$$

As can be shown using these expressions, at zero elastic and plastic strains we have

$$\left[ \frac{\partial^2 \psi_s}{\partial \theta^2} \right]_{\mathbf{F}_s^e = \mathbf{I}, \mathbf{F}_s^p = \mathbf{I}} = \left[ \frac{\partial^2 \psi_f}{\partial \theta^2} \right]_{\mathbf{F}_f^e = \mathbf{I}, \mathbf{F}_f^p = \mathbf{I}} = 0. \quad (9.21)$$

Therefore, the specific heat capacity can be calculated from

$$c = -\theta \frac{\partial^2 \psi_\theta}{\partial \theta^2}. \quad (9.22)$$

Therefore, knowing the specific heat allows us to calculate  $\psi_\theta$  by integrating twice.

## 9.2 Experimental results and fitting the model

Differential Scanning Calorimetry (DSC) was used to calculate the heat capacity of the polycarbonate sample at zero stress and before plastic deformation. This was measured from  $-46^\circ C$  to just above the glass transition temperature. The results from DSC are shown in figure 9.1. For the range of temperature shown in the figure, the specific heat is increasing linearly with temperature. Therefore, heat capacity can be put in the form

$$c = c(298K) + \left. \frac{dc}{d\theta} \right|_{298K} (\theta - 298), \quad (9.23)$$

where temperature is in Kelvin, and  $c(298K)$  and  $\left. \frac{dc}{d\theta} \right|_{298K}$  are respectively, the heat capacities and its derivative at  $298^\circ K$ . For polycarbonate, the constants are given as

$$c(298K) = 1.2676 \frac{J}{g \text{ } ^\circ C}, \quad \left. \frac{dc}{d\theta} \right|_{298K} = 0.004017 \frac{J}{g \text{ } ^\circ C^2}, \quad (9.24)$$

where  $J$  in the units refers to Joules (not the volume ratio). Using equation 9.22 and the

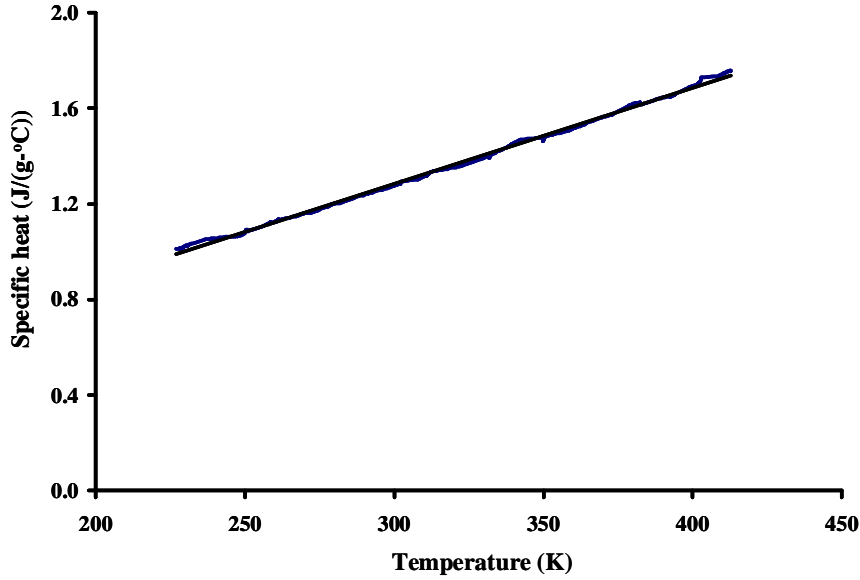


Figure 9.1: Specific heat for polycarbonate at different temperature (from [12]).

specific heat expression from the experiments one can get

$$\frac{\partial^2 \psi_\theta}{\partial \theta^2} = -\frac{1}{\theta} \left[ c(298K) + \left. \frac{dc}{d\theta} \right|_{298K} (\theta - 298) \right].$$

The above equation can be integrated twice to get the free energy term

$$\psi_\theta(\theta) = - \left[ c(298K) - 298 \left. \frac{dc}{d\theta} \right|_{298K} \right] (\theta \ln(\theta) - \theta) - \left. \frac{dc}{d\theta} \right|_{298K} \frac{\theta^2}{2} + K_1 \theta + K_2, \quad (9.25)$$

where  $K_1$  and  $K_2$  are integration constants. At absolute zero, we take the free energy equal to zero, so that the constant of integration  $K_2 = 0$ . The constant of integration  $K_1$  is arbitrary. As  $\psi_\theta$  only depends on temperature, this term will not have any effect on the calculation of stress and back stress. The other quantity that can be calculated using this form of free energy is enthalpy resulting from this term. This can be obtained by the equation

$$h = \psi + \eta_\theta \theta. \quad (9.26)$$

Using the expression of free energy, entropy can be calculated

$$\eta_{\theta} = -\frac{\partial\psi_{\theta}}{\partial\theta} = \left[ c(298K) - 298 \left. \frac{dc}{d\theta} \right|_{298K} \right] \ln(\theta) + \theta \frac{dc}{d\theta} - K_1. \quad (9.27)$$

Substituting the value of entropy in the enthalpy expression we get

$$\begin{aligned} h &= \psi_{\theta} + \eta_{\theta}\theta & (9.28) \\ &= - \left[ c(298K) - 298 \left. \frac{dc}{d\theta} \right|_{298K} \right] (\theta \ln(\theta) - \theta) - \left. \frac{dc}{d\theta} \right|_{298K} \frac{\theta^2}{2} + K_1\theta \\ &\quad + \left[ c(298K) - 298 \left. \frac{dc}{d\theta} \right|_{298K} \right] \theta \ln(\theta) + \theta^2 \left. \frac{dc}{d\theta} \right|_{298K} - K_1\theta \\ &= \left[ c(298K) - 298 \left. \frac{dc}{d\theta} \right|_{298K} \right] \theta + \left. \frac{dc}{d\theta} \right|_{298K} \frac{\theta^2}{2}. \end{aligned}$$

As can be seen in the equation, the enthalpy does not depend on  $K_1$ .

### 9.3 Results and conclusion

In this chapter the free energy contribution from the pure thermal behavior is calculated. The heat capacity expressions is calculated using thermodynamic process for a material under zero stress and zero plastic strain. The free energy was then calculated using DSC experimental results for polycarbonate from 46°C to 150°C. The resulting expression for this part of the free energy was obtained to be

$$\psi_{\theta}(\theta) = - \left[ c(298K) - 298 \left. \frac{dc}{d\theta} \right|_{298K} \right] (\theta \ln(\theta) - \theta) - \left. \frac{dc}{d\theta} \right|_{298K} \frac{\theta^2}{2} + K_1\theta, \quad (9.29)$$

for an arbitrary  $K_1$ . As was explained in the calculation of enthalpy,  $K_1$  is arbitrary and for PC

$$c(298K) = 1.2676 \frac{J}{g -^{\circ}C} \quad , \quad \left. \frac{dc}{d\theta} \right|_{298K} = .004017 \frac{J}{g -^{\circ}C^2}. \quad (9.30)$$

## Chapter 10

# Flow rule for glassy polycarbonate

In the previous chapters we have developed the model for stress from ultrasonics wave speeds at different temperatures and high loads and separated the response of stress into two parts, one contributes to the slow response and the additional term corresponding to the fast response. Then we have developed a thermodynamically consistent model for back stress at different temperatures. We have also discussed constructing a single free energy that is used to model stress, back stress and heat capacity. In this chapter we will discuss the evolution equations, also known as flow rules, which describes how the internal variables  $\mathbf{F}_s^p$  and  $\mathbf{F}_f^p$  will change.

### 10.1 Flow rule and second law of thermodynamics

From the second law of thermodynamics shown in Chapter 2 the flow rule for plastic flow needs to satisfy the inequality

$$-\Delta \mathbf{T}^T : \mathbf{L}^p \leq 0, \quad (10.1)$$

where  $\Delta \mathbf{T}$  is the overstress and  $\mathbf{L}^p$  is the plastic velocity gradient. The restriction imposed by the second law of thermodynamics on the two internal variables proposed here can be satisfied by requiring that

$$-\Delta \mathbf{T}_s^T : \mathbf{L}_s^p \leq 0, \quad (10.2)$$

$$-\Delta \mathbf{T}_f^T : \mathbf{L}_f^p \leq 0, \quad (10.3)$$

where  $\mathbf{L}_s^p$  and  $\mathbf{L}_f^p$  are, respectively, the plastic velocity gradient corresponding to  $\mathbf{F}_s^p$  and  $\mathbf{F}_f^p$ , and are given by the equations

$$\mathbf{L}_s^p = \dot{\mathbf{F}}_s^p \mathbf{F}_s^{p-1}, \quad (10.4)$$

$$\mathbf{L}_f^p = \dot{\mathbf{F}}_f^p \mathbf{F}_f^{p-1}. \quad (10.5)$$

Normally the plastic flow is close to incompressible, this seems to also be true for the internal parameter proposed. To construct the flow rules for the two internal parameters we will use the associated deviatoric overstress

$$\Delta \mathbf{S}_s^T = \Delta \mathbf{T}_s - (\Delta T_{ave})_s \mathbf{I}, \quad (10.6)$$

$$\Delta \mathbf{S}_f^T = \Delta \mathbf{T}_f - (\Delta T_{ave})_f \mathbf{I}, \quad (10.7)$$

where  $(\Delta T_{ave})_s$  and  $(\Delta T_{ave})_f$  are, respectively, the hydrostatic part of overstress  $\Delta \mathbf{T}_s$  and  $\Delta \mathbf{T}_f$ . The simplest flow rules that both satisfy the thermodynamic constraints and the assumption that  $\mathbf{F}_s^p$  and  $\mathbf{F}_f^p$  are volume preserving deformations can be written as

$$\dot{\mathbf{F}}_s^p = \beta_s \Delta \mathbf{S}_s^T \mathbf{F}_s^p, \quad (10.8)$$

$$\dot{\mathbf{F}}_f^p = \beta_f \Delta \mathbf{S}_f^T \mathbf{F}_f^p. \quad (10.9)$$

where  $\beta_s$  and  $\beta_f$  are appropriately selected positive valued scalar functions. These can also be written in terms of the velocity gradients as

$$\dot{\mathbf{L}}_s^p = \beta_s \Delta \mathbf{S}_s^T, \quad (10.10)$$

$$\dot{\mathbf{L}}_f^p = \beta_f \Delta \mathbf{S}_f^T, \quad (10.11)$$

## 10.2 Experimental results on monotonic compression

Uniaxial compression tests were performed on glassy polycarbonate at various temperatures and strain rates. The experiments from 0.0001 1/s to 0.01 1/s were performed in our lab at University of Nebraska Lincoln (UNL) by Kyle, the experiments from  $-40^\circ\text{C}$  to  $100^\circ\text{C}$  at strain rates from 0.1 1/s to 100 1/s were performed by Army research lab(ARL) and the experiments at strain rates from 500 1/s to 1500 1/s from room temperature to  $100^\circ\text{C}$  were performed at UNL using Hopkinson bar tests by Jason. The experimental results are shown and summarized in the figures from Figure 10.1 to Figure 10.6. Figure 10.1 to 10.3 shows the results at three different temperatures for different strain rates and Figure 10.4 to 10.6 shows the comparison of the response at different temperatures for one particular strain rate. All the curves indicate the expected feature of the material response, which as described in Chapter 1, can be distributed in three regions: initial nonlinear elasticity with rate dependence, strain softening and hardening which is rate and temperature dependent.

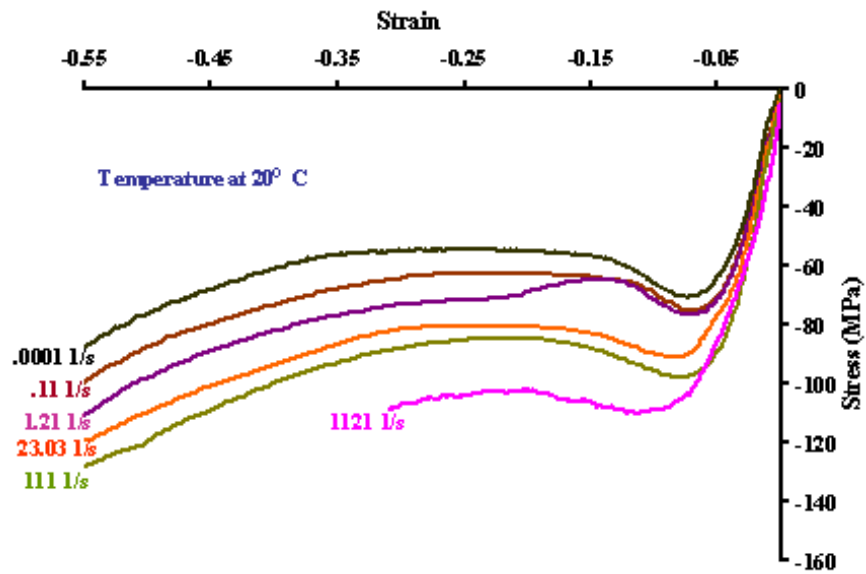


Figure 10.1: Monotonic compression experiments for different strain rates at room temperature (from [1, 2, 3]).

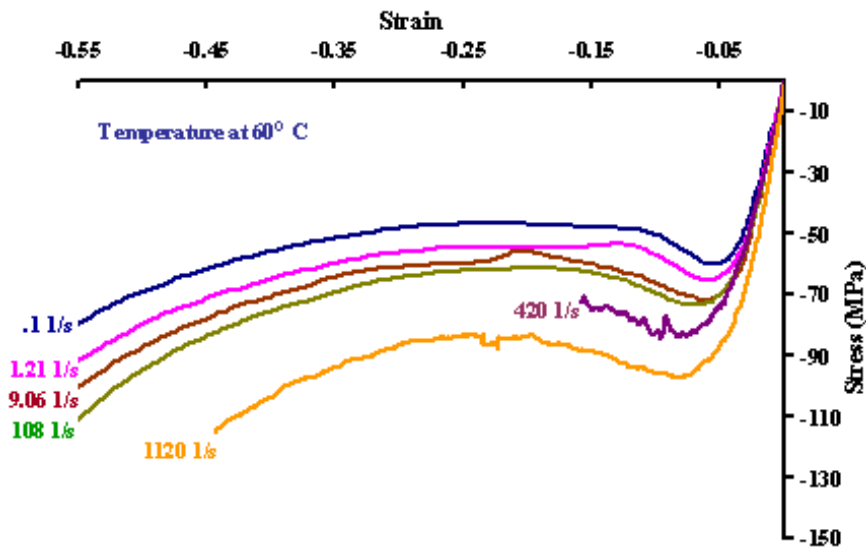


Figure 10.2: Monotonic compression experiments for different strain rates at 60°C (from [1, 2, 3]).

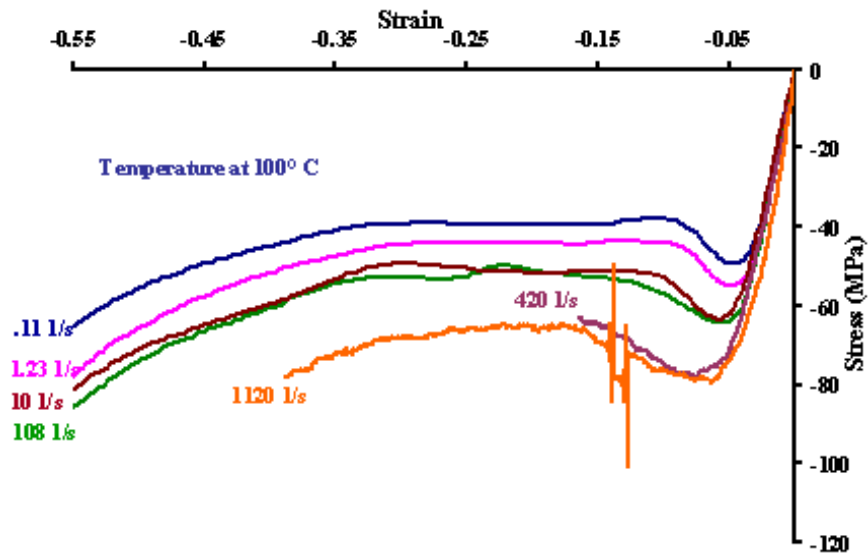


Figure 10.3: Monotonic compression experiments for different strain rates at 100°C (from [1, 2, 3]).

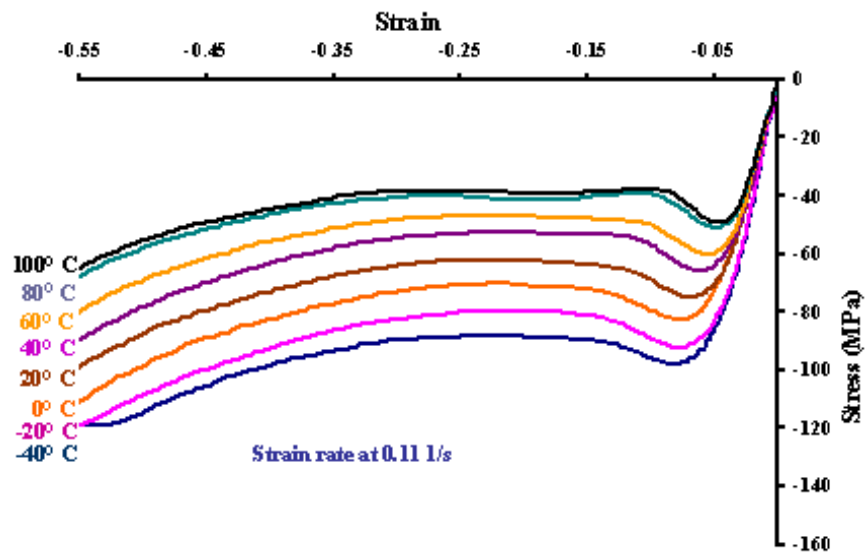


Figure 10.4: Monotonic compression experiments for different temperatures at 0.11 s<sup>-1</sup> (from [2]).

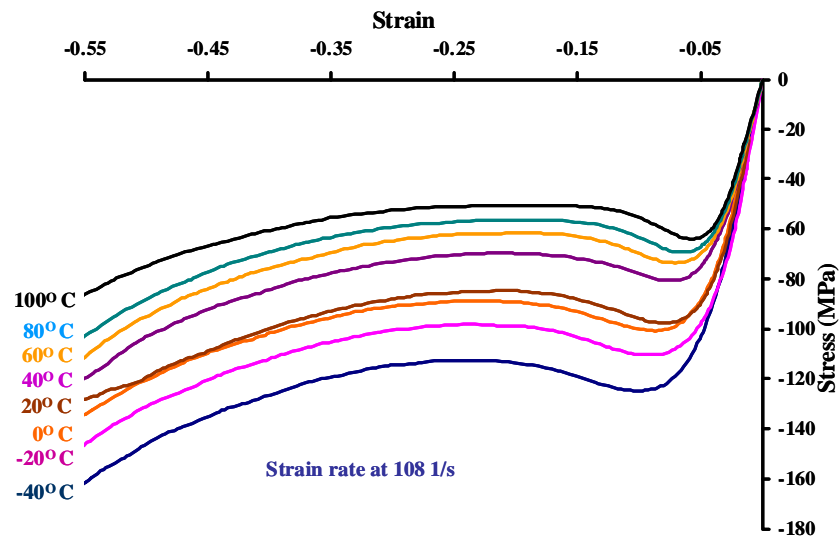


Figure 10.5: Monotonic compression experiments for different temperatures at  $100 \text{ s}^{-1}$  (from [2]).

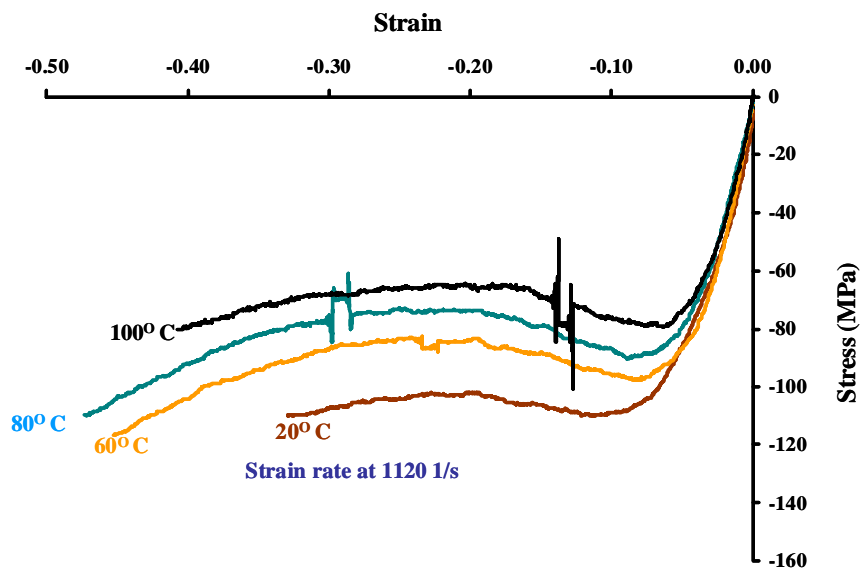


Figure 10.6: Monotonic compression experiments for different temperatures at  $1120 \text{ s}^{-1}$  (from [3]).

### 10.3 Conversion of plastic work to heat

As discussed in the previous section, like other glassy polymers the response of PC depends upon the strain, strain rate as well as temperature. It has been known that the mechanical energy of plastic deformation transform into heat which can cause temperature rise under adiabatic consideration. Mulliken and Boyce have pointed to this fact in a paper published in 2006 [95]. The monotonic compression experiments at a very low strain rate of 0.0001 1/s probably corresponds to an isothermal condition in since the time is sufficient enough that the heat can move out of the system and one can assume the response to be isothermal. For a very high strain rate, the response probably corresponds to adiabatic conditions, that should result in temperature increasing during the experiments. Rittel [77] and Lerch [13] have performed a compression experiments under high strain rate ( $10^3$  1/s and  $10^4$  1/s) and have indicated that the temperature can increase as much as  $60^\circ C$  for 80% plastic strain. Lerch et al. have performed a dynamic compression tests on PC for strain rate in the range of 500 to 2000  $s^{-1}$  using a Split Hopkinson Pressure bar and temperature measurement was carried out using an infrared optical pyrometer which could measure the surface temperature rise of a specimen during the tests. The results extracted from the paper for the temperature in this test are shown in Figure 10.8 for a strain rate of  $1800s^{-1}$ .

To look at the temperature rise from the model at high strain rates, we considered adiabatic flow and assumed that the majority of heat generated is due to plastic flow. If we consider this assumption then the balance of energy can be approximately written as

$$\rho c_p \dot{\theta} = tr(\Delta \mathbf{T}_s \mathbf{L}_s^p) + tr(\Delta \mathbf{T}_f \mathbf{L}_f^p), \quad (10.12)$$

where  $\rho$  is the density in the current configuration,  $c_p$  is the specific heat,  $\Delta \mathbf{T}_s$  and  $\Delta \mathbf{T}_f$  are

the overstress for slow and fast relaxing element,  $\mathbf{L}_s^p$  and  $\mathbf{L}_f^p$  are the plastic velocity gradients and  $\dot{\theta}$  is the temperature rise. The left hand side of the equation gives the amount of heat generated due to increase in temperature and the right hand side gives the amount of heat generated due to plastic flow. For this comparison we have considered the experimental results for monotonic compression at a strain rate of  $1200s^{-1}$  and assumed adiabatic flow. We have already measured and modeled the equilibrium stress and the specific heat as a function of temperature. Having experimental results for the stress and the axial and transverse strain histories, they can be used to calculate  $\mathbf{L}_s^p$  and  $\mathbf{L}_f^p$ . From the model for back stress and the model for stress, the overstress can be calculated. The stress and the backstress are shown in Figure 10.7. For the large deformation considered, we can assume that both the internal variables have a value approximately the same so that we can write the balance of energy as

$$\rho c_p \dot{\theta} = tr(\Delta \mathbf{T} \mathbf{L}^p),$$

when we have assumed  $\mathbf{L}^p = \mathbf{L}_s^p = \mathbf{L}_f^p$ . Using this equation the temperature rate  $\dot{\theta}$  can be calculated using the experimental results and the proposed model. This temperature rise is compared with the experimental results obtained from Lerch in Figure 10.8. As can be seen from the plot, the results are in close agreement with the experimental results until 50% strain. The accuracy of the temperature rise primarily depends upon  $\Delta \mathbf{T}$  so the close agreement of the directly measured temperature rise in the experiment of Lerch and that calculated through model gives an indication that we are correctly measuring the equilibrium stress and hence supports the new method which has been introduced in Chapter 6 to calculate the equilibrium stress. The same procedure is used to calculate the

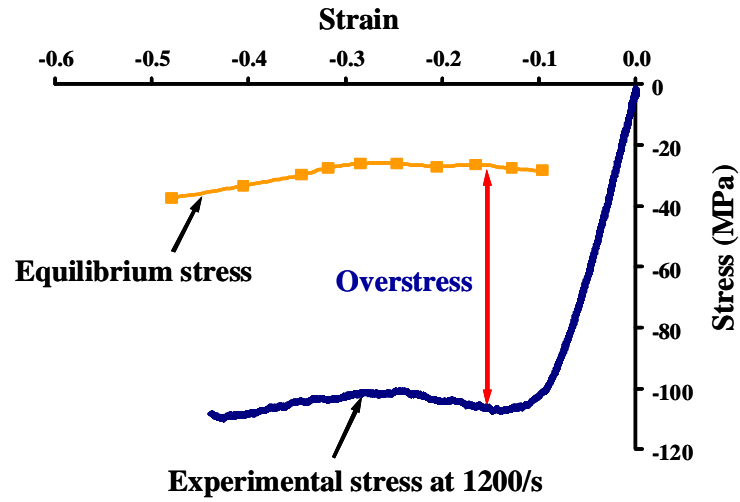


Figure 10.7: Schematic of the stress and equilibrium stress.

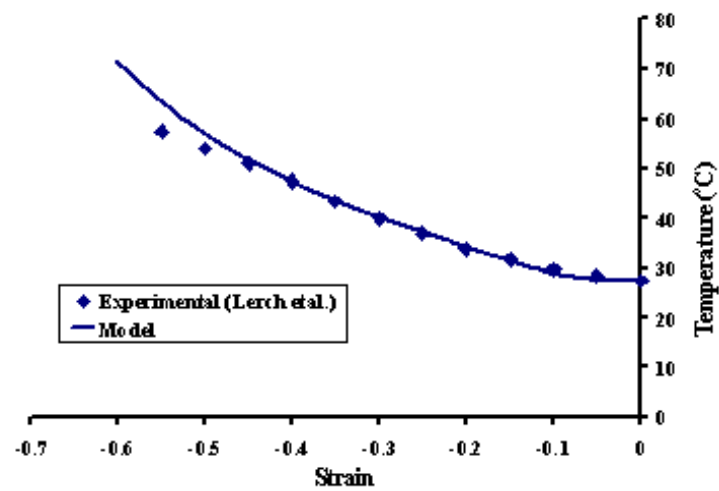


Figure 10.8: Comparison of model prediction and experimentally evaluated temperature rise from Lerch et al. [13].

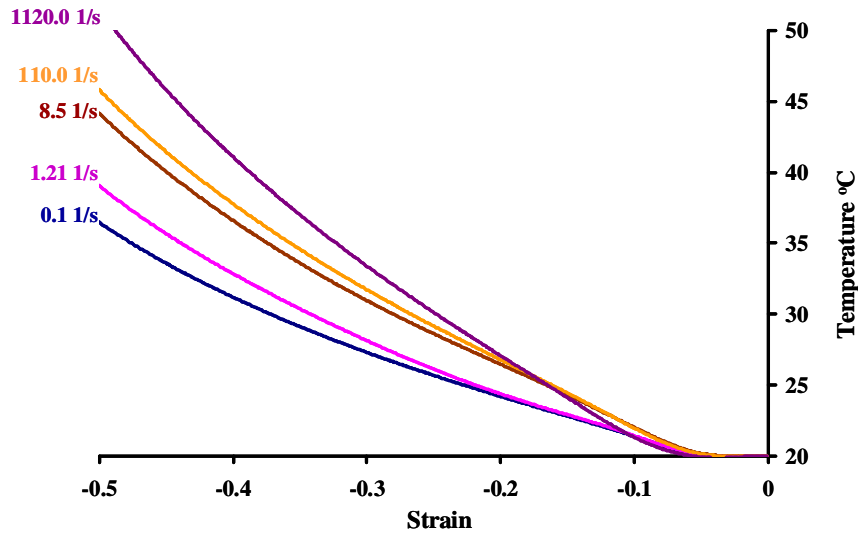


Figure 10.9: Comparison of temperature rise from model at room temperature for different strain rates assuming adiabatic deformations.

temperature rise for all the experiments performed at strain rates from  $0.1s^{-1}$  to  $1200s^{-1}$  and at different temperature. The plot of temperature rise for different strain rates at  $20^{\circ}C$ ,  $60^{\circ}C$  and  $100^{\circ}C$  are shown in the figures.

As can be seen in Figures 10.9 to 10.11, the temperature does not rise significantly until 10% strain, beyond which it rises considerably. For each starting temperature, the temperature rise depends upon the strain rate and it increases with the increase in strain rate. Using this information, the stresses for true isothermal compression can be calculated by interpolating the stresses between the predicted temperatures. The results of this calculation to obtain the isothermal response at  $0.11\ 1/s$  is shown in Figure 10.12 The same method was used to calculate the true isothermal responses for the different strain rates and temperatures. The results are shown in figures 10.13 and 10.14. As can be seen, due to the temperature rise in the experiments one observes lower stresses, but corrected by

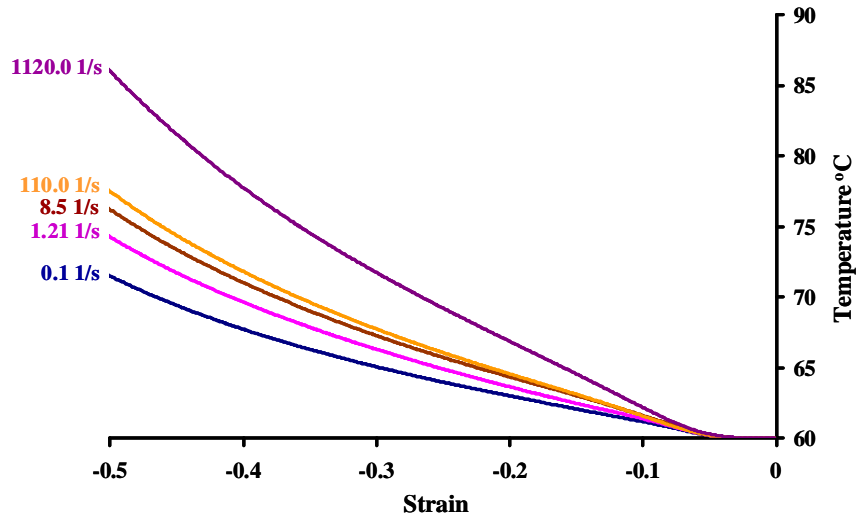


Figure 10.10: Comparison of temperature rise from model at  $60^{\circ}\text{C}$  for different strain rates assuming adiabatic deformations.

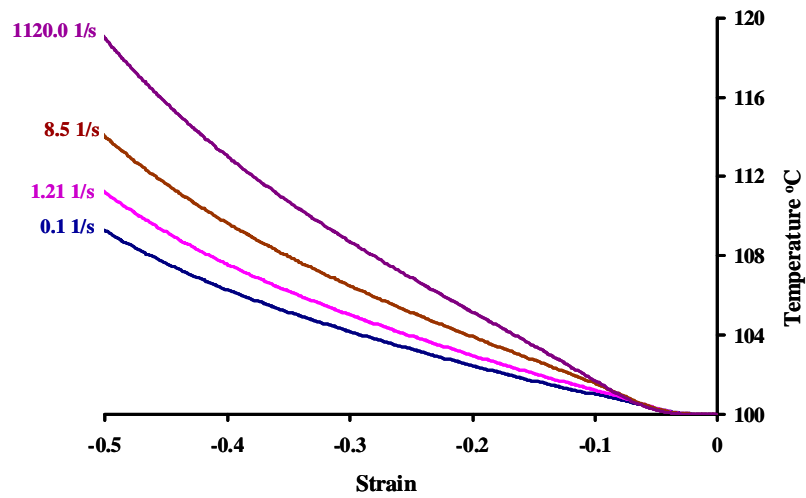


Figure 10.11: Comparison of temperature rise from model at  $100^{\circ}\text{C}$  for different strain rates assuming adiabatic deformations.

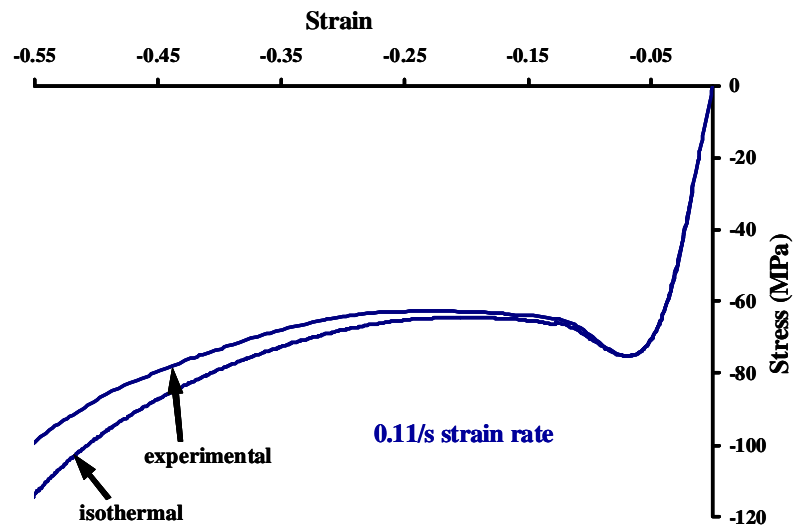


Figure 10.12: Comparison of experimental (from [2]) and model under isothermal condition for 0.11 1/s and at room temperature.

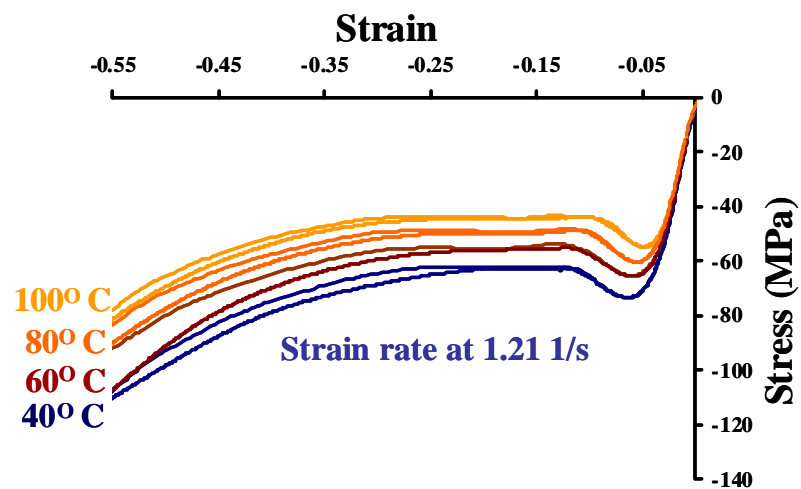


Figure 10.13: Experimental (from [2]) and model isothermal monotonic compression results for 1.21 1/s and at different temperatures.

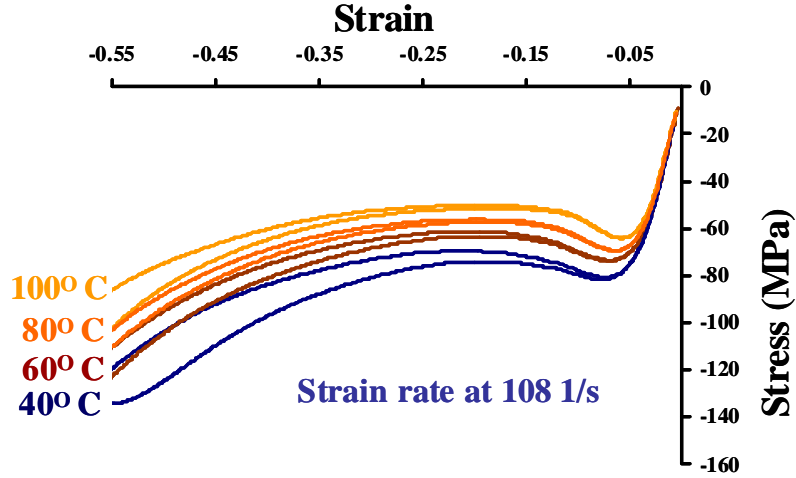


Figure 10.14: Experimental (from [2]) and model isothermal monotonic compression results for 108 1/s and at different temperatures.

knowing the overstress. For very low strain rate response (0.0001 1/s-0.11/s), as the time is sufficient enough for heat flow out of the system, the experimental results measured probably correspond to isothermal condition and need to be modified. But, for higher strain rate response (100-1000 1/s) the response is probably adiabatic, and needs to be corrected to obtain the corresponding isothermal response.

## 10.4 Modeling the flow rules

To fit the monotonic compression results, we need to evaluate the flow rules to calculate the internal parameter  $\mathbf{F}_s^p$  and  $\mathbf{F}_f^p$ . According to the mechanical analog the total deformation gradient is given by

$$\mathbf{F} = \mathbf{F}_s^e \mathbf{F}_s^p = \mathbf{F}_f^e \mathbf{F}_f^p. \quad (10.13)$$

The total Cauchy stress  $\mathbf{T}$  can be written as

$$\mathbf{T} = \mathbf{T}_s + \mathbf{T}_f, \quad (10.14)$$

where  $\mathbf{T}_s$  is the stress corresponds to the low strain rates and  $\mathbf{T}_f$  comes into effect when strain rates becomes higher. The overstress  $\Delta\mathbf{T}_s$  and  $\Delta\mathbf{T}_f$  can be written as

$$\Delta\mathbf{T}_s = \mathbf{F}_s^{e-1} \mathbf{T}_s \mathbf{F}_s^e - \mathbf{T}_s^b, \quad (10.15)$$

where  $\mathbf{T}_s^b$  is the back stress.

$$\Delta\mathbf{T}_f = \mathbf{F}_f^{e-1} \mathbf{T}_f \mathbf{F}_f^e. \quad (10.16)$$

A flow rule that satisfies the second law of thermodynamics and does not induce volumetric changes in the internal variables can be written as

$$\dot{\mathbf{F}}_s^p = \beta_s \Delta \mathbf{S}_s^T \mathbf{F}_s^p, \quad (10.17)$$

$$\dot{\mathbf{F}}_f^p = \beta_f \Delta \mathbf{S}_f^T \mathbf{F}_f^p, \quad (10.18)$$

for strictly positive scalar functions  $\beta_s$  and  $\beta_f$ .

#### 10.4.1 Models used for stress and back stress

The stress contribution, as discussed in earlier chapters, is splited into two parts, one part that is related to the slow relaxing element and is given by  $\mathbf{T}_s$  and the additional stress which comes from the high relaxation element and is given by  $\mathbf{T}_f$  such that the total

stress  $\mathbf{T} = \mathbf{T}_s + \mathbf{T}_f$ . These two models are given as

$$\begin{aligned} \mathbf{T}_s = & E_{quas} \left\{ A_{iso} \left[ G(\mathbf{F}_s^p) \frac{1}{J J_s^{e\frac{2}{3}}} \left( \mathbf{B}_s^e - \frac{tr(\mathbf{B}_s^e)}{3} \mathbf{I} \right) + \kappa(\mathbf{F}_s^p) \frac{J_s^e \ln(J_s^e)}{J} \mathbf{I} \right] \right. \\ & + E_{comb} \left[ \frac{2}{J_s^{e\frac{2}{3}}} \left( \mathbf{B}_s^e - \frac{tr(\mathbf{B}_s^e)}{3} \mathbf{I} \right) \ln^2(J_s^e) + 2 \ln(J_s^e) \left( \frac{tr(\mathbf{C}_s^e)}{J_s^{e\frac{2}{3}}} - 3 \right) \right] \left. \right\} \\ & + A_{aniso} \left[ \rho_o \frac{\partial \psi}{\partial I_7^*}(\mathbf{F}_s^p) \frac{1}{J} \mathbf{F}_s^e [2(\mathbf{C}_s^p - \mathbf{I}) - (\mathbf{C}_s^e \mathbf{C}_s^p + \mathbf{C}_s^p \mathbf{C}_s^e - 2\mathbf{C}_s^e)] \right] \mathbf{F}_s^{eT}, \end{aligned} \quad (10.19)$$

and

$$\begin{aligned} \mathbf{T}_f = & (1 - E_{quas}) \left\{ A_{iso} \left[ G(\mathbf{F}_f^p) \frac{1}{J J_f^{e\frac{2}{3}}} \left( \mathbf{B}_f^e - \frac{tr(\mathbf{B}_f^e)}{3} \mathbf{I} \right) + \kappa(\mathbf{F}_f^p) \frac{J_f^e \ln(J_f^e)}{J} \mathbf{I} \right] \right. \\ & + E_{comb} \left[ \frac{2}{J_f^{e\frac{2}{3}}} \left( \mathbf{B}_f^e - \frac{tr(\mathbf{B}_f^e)}{3} \mathbf{I} \right) \ln^2(J_f^e) + 2 \ln(J_f^e) \left( \frac{tr(\mathbf{C}_f^e)}{J_f^{e\frac{2}{3}}} - 3 \right) \right] \left. \right\}. \end{aligned} \quad (10.20)$$

During slow tests  $\mathbf{T}_f$  can be taken to be approximately zero. As a result, the tangent moduli measures at equilibrium will be assumed to be only from  $\mathbf{T}_s$ .

Back stress contribution is associated with only the slow element. This back stress is given by

$$\begin{aligned} \mathbf{T}_s^b = & \mathbf{T}_{stress}^b + \frac{1}{J} \left[ \left( G_o^b - G_{\infty 1}^b \right) \frac{\tanh \left( \sqrt{\frac{(G_o^b - G_{\infty 1}^b)^2}{\tau_o^{b2}} (I_4^*(\mathbf{F}_s^p) - 3)} \right)}{\sqrt{\frac{(G_o^b - G_{\infty 1}^b)^2}{\tau_o^{b2}} (I_4^*(\mathbf{F}_s^p) - 3)}} \right. \\ & \left. + G_{\infty 1}^b + G_{\infty 2}^b (I_4^*(\mathbf{F}_s^p) - 3) \right] \left( \mathbf{B}_s^p - \frac{1}{3} tr(\mathbf{B}_s^p) \mathbf{I} \right), \end{aligned} \quad (10.21)$$

where the material parameter obtained by fitting the response is given by

$$\tau_o^b = -0.119\theta + 51.795 \text{ MPa} \quad \theta \text{ is in } K, \quad (10.22)$$

$$G_{\infty 1}^b = 0, \quad G_{\infty 2}^b = 5 \text{ MPa}.$$

The initial slope  $G_o^b = 1000 \text{ MPa}$  was considered as the initial slope in shear, as the back

stress calculated from the method is not good for a very small strains. Since the slow element is active for all rates, the back stress from this element will also be active.

Knowing the stresses and back stresses, the overstress  $\Delta \mathbf{T}_s$  and  $\Delta \mathbf{T}_f$  can be written as

$$\begin{aligned}\Delta \mathbf{T}_s &= \mathbf{F}_s^{e-1} \mathbf{T}_s \mathbf{F}_s^e - \mathbf{T}_s^b, \\ \Delta \mathbf{T}_f &= \mathbf{F}_f^{e-1} \mathbf{T}_f \mathbf{F}_f^e.\end{aligned}\tag{10.23}$$

#### 10.4.2 Calculation of plastic flow at low strain rates

Initially let us consider the case for a very low strain rates. For a very low strain rate it is assumed that the monotonic compression experiments performed are isothermal since the time during the test is sufficient enough so that heat can move out of the sample. At room temperature we have considered strain rates from  $0.00011/s$ ,  $0.11/s$  and  $1.21s^{-1}$ . In fitting the response at low strain rates, it is assumed that the stress  $\mathbf{T}_f = \mathbf{0}$ .

To model the experimental results we assume the conditions are that of homogeneous uniaxial compression with zero transverse stresses as shown in Figure 10.15. The stress under such a condition can be given by

$$\boldsymbol{\sigma} = \sigma_a \mathbf{e}_3 \otimes \mathbf{e}_3,\tag{10.24}$$

where  $\sigma_a$  is the axial stress and the expression for deformation gradient would be

$$\mathbf{F} = \lambda^* \mathbf{e}_1 \otimes \mathbf{e}_1 + \lambda^* \mathbf{e}_2 \otimes \mathbf{e}_2 + \lambda \mathbf{e}_3 \otimes \mathbf{e}_3.\tag{10.25}$$

where  $\lambda$  is the stretch in the axial direction and  $\lambda^*$  is the stretch in the transverse direction.

Under the same assumptions, a reasonable expression for  $\mathbf{F}_s^p$ , considering its incompress-

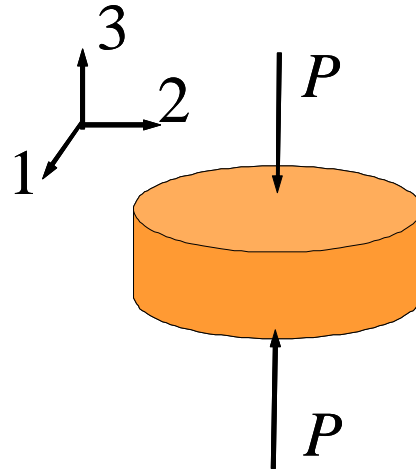


Figure 10.15: Schematic for uniaxial compression for polycarbonate sample

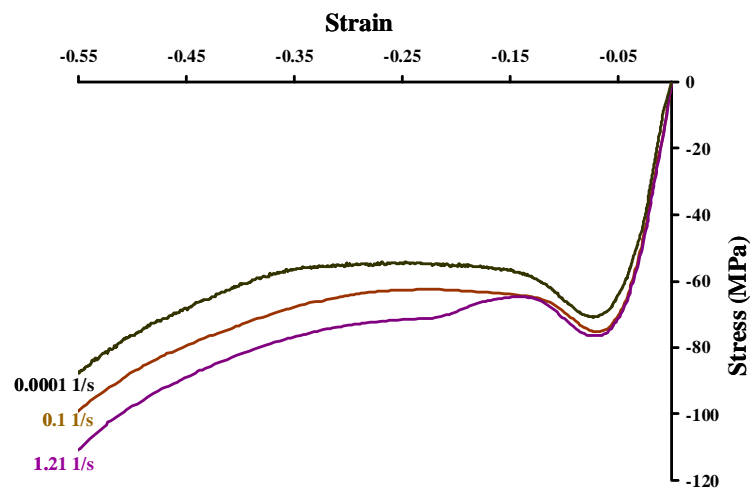


Figure 10.16: Experimental monotonic compression experiments (from [1, 2]) at room temperature.

ibility, is

$$\mathbf{F}_s^p = \left( \frac{1}{\sqrt{\lambda_s^p}} \right) \mathbf{e}_1 \otimes \mathbf{e}_1 + \left( \frac{1}{\sqrt{\lambda_s^p}} \right) \mathbf{e}_2 \otimes \mathbf{e}_2 + \lambda_s^p \mathbf{e}_3 \otimes \mathbf{e}_3. \quad (10.26)$$

In the experiments we measure  $\lambda$ ,  $\lambda^*$  and  $T_{33} = \sigma_a$ , and we know that  $T_{11} = 0$ . Since the incompressibility of  $\mathbf{F}_s^p$  model does not allow to independently calculate both the axial and transverse plastic stretches, we select to use the measured axial stretch of  $\lambda$  in the two equations  $T_{33} = \sigma_a$  and  $T_{11} = 0$  to calculate  $\lambda_s^p$  and  $\lambda^*$ . In this way we obtain  $\mathbf{F}_s^e$  and  $\mathbf{F}_s^p$  without violating the assumption of incompressibility of  $\mathbf{F}_s^p$ . The back stress tensor can then be calculated from these. Subsequently the overstress  $\Delta \mathbf{T}_s = \mathbf{F}_s^{e-1} \mathbf{T}_s \mathbf{F}_s^e - \mathbf{T}_s^b$  and deviatoric part of the overstress  $\Delta \mathbf{S}_s = \Delta \mathbf{T}_s - (\Delta T_s)_{ave} \mathbf{I}$  can be calculated. From the expression of flow rule we can then calculate  $\beta_s$  from

$$\beta_s = \frac{\sqrt{(\Delta \mathbf{S}_s^T \mathbf{F}_s^p) : (\Delta \mathbf{S}_s^T \mathbf{F}_s^p)}}{\sqrt{(\dot{\mathbf{F}}_s^p) : (\dot{\mathbf{F}}_s^p)}}. \quad (10.27)$$

In this way we can obtain from the experimental results both a value of  $\mathbf{F}_s^p$  and the value of  $\beta_s$  using its associated flow rule. To model  $\beta_s$  we note that it can be a function of many different combination of state variable which may include ( $\mathbf{T}_s$ ,  $\Delta \mathbf{T}_s$ ,  $\Delta \mathbf{S}_s$ ,  $\mathbf{F}_s^p$ ,  $\mathbf{T}_s \mathbf{F}_s^p$ ,  $\Delta \mathbf{S}_s \mathbf{F}_s^p$ , ...etc.). We consider  $\beta_s$  to be formed from three parts

$$\beta_s = \beta_{s1} \beta_{s2} \beta_{s3}, \quad (10.28)$$

where they can be modeled as follows:

1. We assume  $\beta_s$ , comes from the "steady state" large deformation response just after yielding and that it only depends on the overstress. We select  $\Delta S_s = \sqrt{\Delta \mathbf{S}_s : \Delta \mathbf{S}_s}$  to represent this overstress and assume  $\beta_{s1}$  depends on it. We use the response between strain

rates of 0.0001 1/s to 1.21 1/s to fit this to the evaluated values of  $\beta_s$  for a strain of 20% (see Figures 10.1 to Figure 10.6). The result of this fit are shown in Figure 10.17.

2. Function  $\beta_{s2}$  is assumed to characterize the effect of large plastic deformation. After calculating  $\beta_{s1}$  as a function of  $\Delta S_s$ , the measured value of  $\beta_s$  is divided by  $\beta_{s1}$  for each  $\Delta S_s$  and the value obtained is denoted as  $\beta_{s2}$ . This is plotted with respect to the invariant  $\varepsilon_s^p = tr(\mathbf{C}_s^p - 3)$  of the plastic deformation gradient. The value of  $\beta_{s2}$  as a function of  $\varepsilon_s^p$  is fit to the large deformation response at the strain rate of 0.11 1/s and the result is plotted in Figure 10.18.

3. The function  $\beta_{s3}$  is assumed to capture the effect of temperature. After calculating material parameters  $\beta_{s1}$  and  $\beta_{s2}$  as shown in Figure 10.20, the value of  $\beta_{s3}$  is then obtained by scaling the room temperature model  $\dot{\mathbf{F}}_s^p = \beta_s \Delta \mathbf{S}_s^T \mathbf{F}_s^p$  with temperature. The modeled value of  $\beta_{s3}$  is shown in Figure 10.19. The expression of  $\beta_s$  for PC can be fit as the product of  $\beta_{s1}$ ,  $\beta_{s2}$  and  $\beta_{s3}$  given by

$$\beta_{s1} = 7.43E^{-10} \times e^{(0.52 \times \Delta S_s)}, \quad (10.29)$$

$$\beta_{s2} = 25.8 \times e^{(-11.66 \times \varepsilon_s^p)}, \quad (10.30)$$

$$\beta_{s3} = 2.453E^{-16} \times e^{(0.122 \times \theta)}, \quad (10.31)$$

where  $\Delta S_s = \sqrt{\Delta \mathbf{S}_s : \Delta \mathbf{S}_s}$ ,  $\varepsilon_s^p = tr(\mathbf{C}_s^p - 3)$  and  $\theta$  is given in degree Kelvin.

### 10.4.3 Calculation of plastic flow at high strain rates

As discussed before, high strain rate curve corresponds to an adiabatic deformation and we thus use response to get the isothermal results. For calculating the material parameter  $\beta_f$  three different strain rates in the range of 23 – 1200 1/s are used. Again we

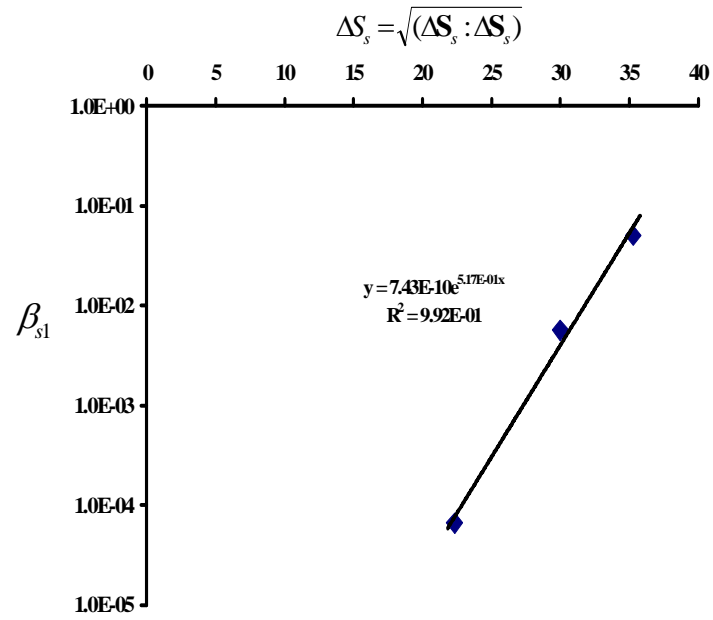


Figure 10.17: The material parameter  $\beta_{s1}$  with respect to  $\Delta S_s$  at 20% axial strain for strain rates 0.00011/s, 0.11/s and 1.21 1/s.

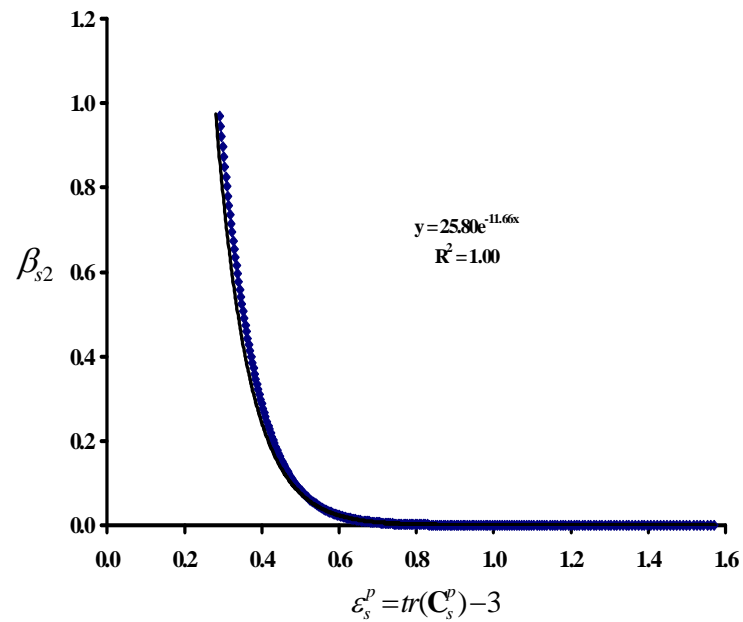


Figure 10.18: The material parameter  $\beta_{s2}$  with respect to  $\epsilon_s^p$  for strain rate 0.11 1/s.

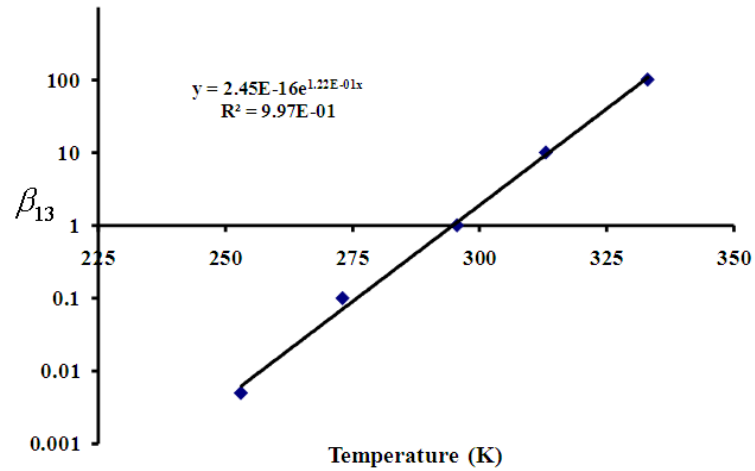


Figure 10.19: Change of  $\beta_{s3}$  with temperature.

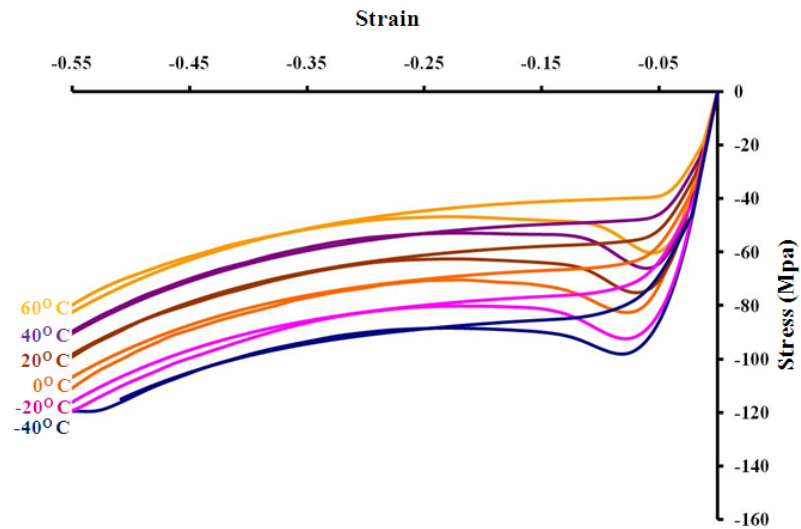


Figure 10.20: Comparison between the experimental response (from [2]) and the model results at 0.11 1/s at different temperatures.

have considered  $\beta_f$  to have three parts :  $\beta_{f1}(\Delta S_f)$  where  $\Delta S_f = \sqrt{\Delta \mathbf{S}_f : \Delta \mathbf{S}_f}$ ,  $\beta_{f2}(\varepsilon_f^p)$  where  $\varepsilon_f^p = tr(\mathbf{C}_f^p) - 3$  and  $\beta_{f3}(\theta)$ . As before, for fitting  $\beta_{f1}$  the value of  $\Delta S_f$  at 20% strain is used for different strain rates. The value of  $\beta_{f2}$  is fit to the response at strain rate of 1200 1/s for large strains. The function  $\beta_{f3}$  is then used to fit the results to higher temperature. Figure 10.21, 10.22 and 10.23 show how  $\beta_{f1}$ ,  $\beta_{f2}$  and  $\beta_{f3}$  are changing with respect to  $\Delta S_f$ ,  $\varepsilon_f^p$  and  $\theta$ . The combined expression of  $\beta_f$  can then be written as

$$\beta_f = \beta_{f1}\beta_{f2}\beta_{f3}, \quad (10.32)$$

where  $\beta_{f1}$ ,  $\beta_{f2}$  and  $\beta_{f3}$  are given by the expressions

$$\beta_{f1} = 3.5 \times e^{(0.154 \times \Delta S_f)}, \quad (10.33)$$

$$\beta_{f2} = 1.2 \times e^{(-3 \times \varepsilon_f^p)},$$

$$\beta_{f3} = 0.0634 \times \theta - 17.91, \quad (10.34)$$

where  $\Delta S_f = \sqrt{\Delta \mathbf{S}_f : \Delta \mathbf{S}_f}$ ,  $\varepsilon_f^p = tr(\mathbf{C}_f^p) - 3$  and  $\theta$  is in degree Kelvin.

The models for  $\beta_s$  and  $\beta_f$  along with the models for  $\mathbf{T}_s$ ,  $\mathbf{T}_s^b$  and  $\mathbf{T}_f$  are now complete and can be used to compare the monotonic compression results. This is done for strain rates at 0.11 1/s, 23.03 1/s and 1194 1/s at room temperature in Figure 10.25. There are several conclusions which can be drawn by looking at this figure.

1. Modulus at zero strain from the model will correspond to the ultrasonic modulus as the initial effect from the load will correspond to the combined effect from both the elastic springs (see mechanical analog in Figure 8.3), but the tangent modulus at different strain rates for very small strains (0.3% and 0.5%) is shown in Figure 10.26. For both of these strains, for very low strain rates the tangent model corresponds to a quasistatic

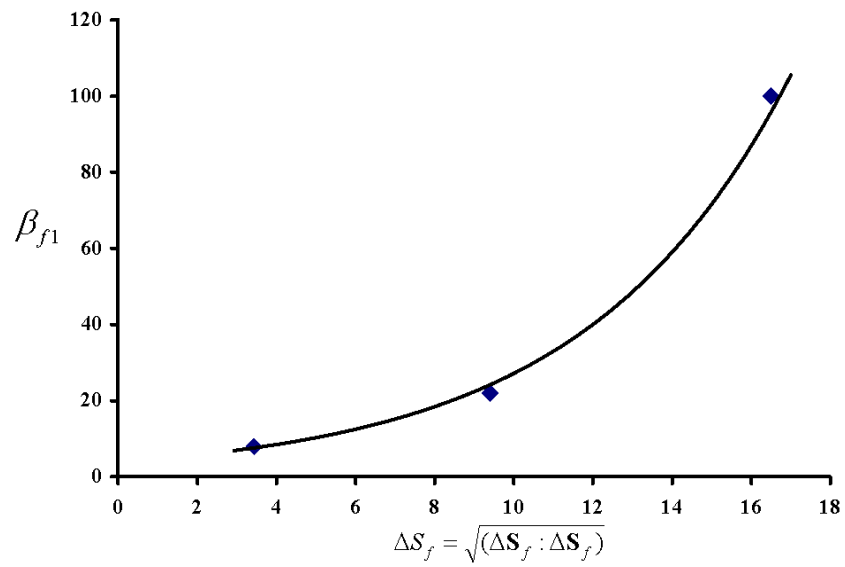


Figure 10.21: The material parameter  $\beta_{f1}$  with respect to  $\Delta S_f$  at 20% axial strain for strain rates 23 1/s, 108 1/s and 1120 1/s.

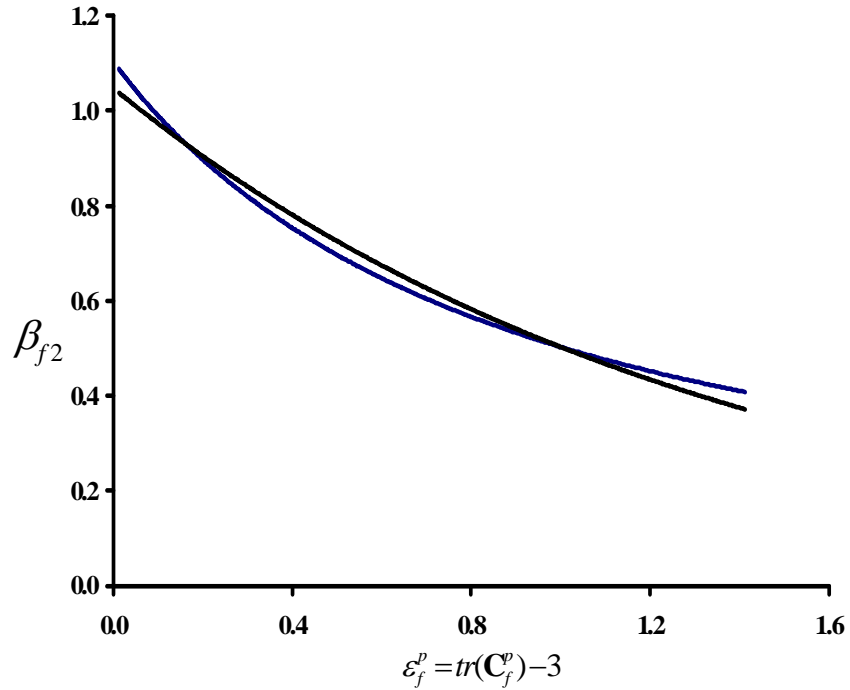


Figure 10.22: The material parameter  $\beta_{f2}$  with respect to  $\epsilon_f^p$  for strain rate 1120 1/s.

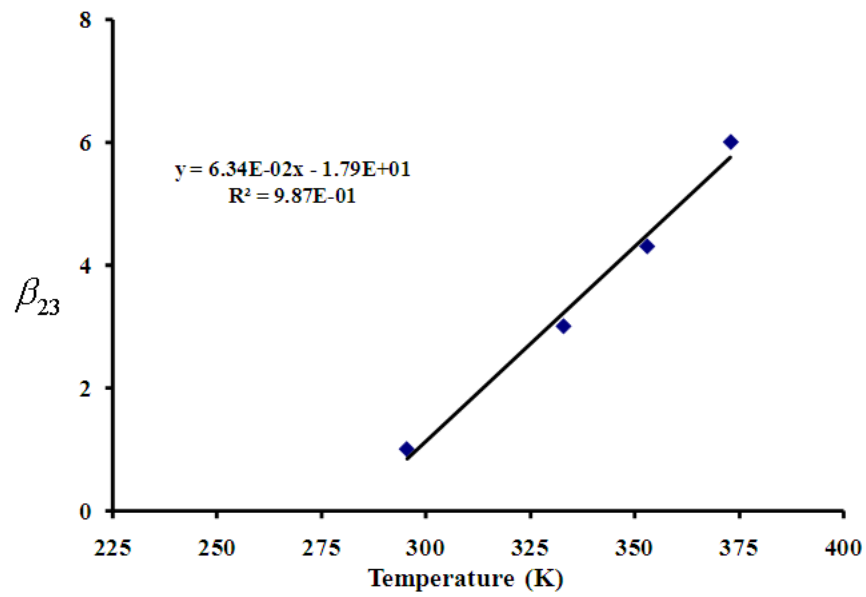


Figure 10.23: Change of  $\beta_{f3}$  with temperature.

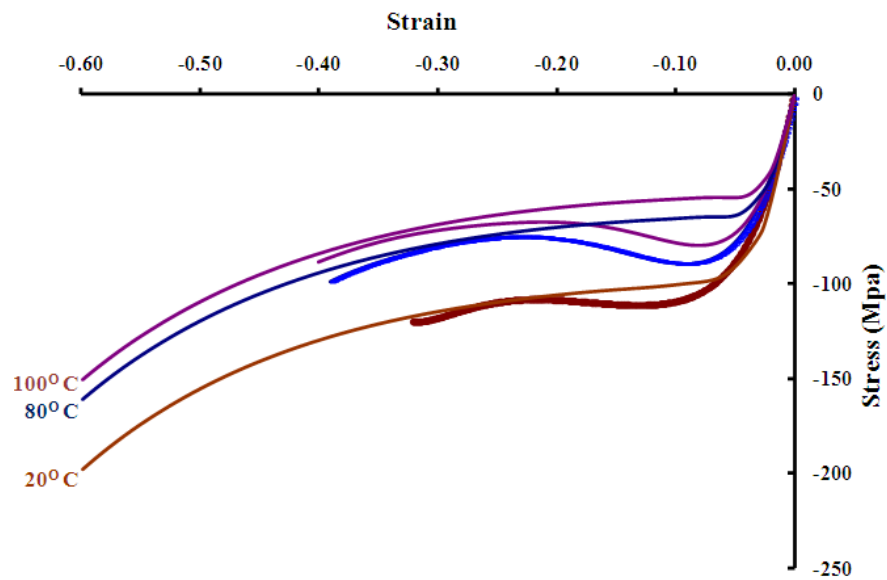


Figure 10.24: Comparison between the correction of experimental response (from [3]) to get an isothermal response and the model results at 1194 1/s at different temperatures.

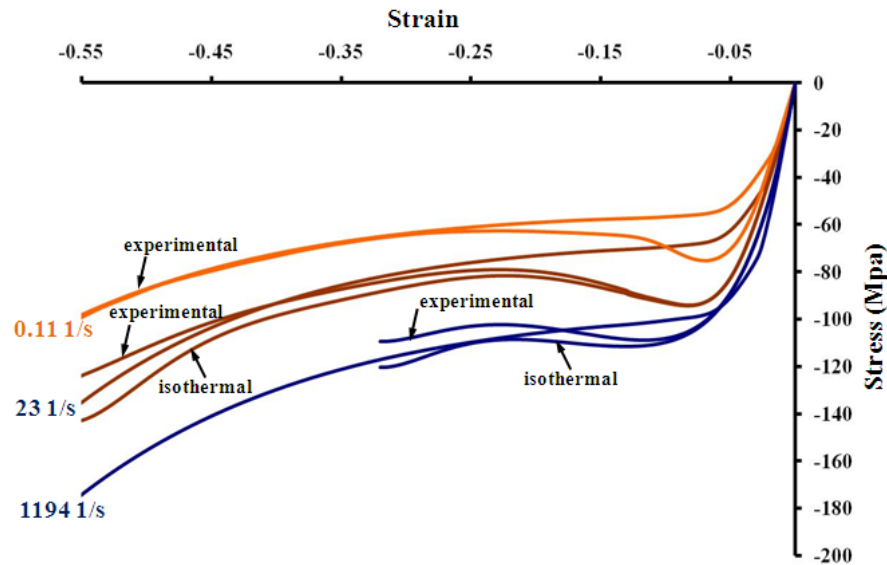


Figure 10.25: Comparison between experimental (from [2, 3]) and model results at room temperature and at different strain rates.

modulus and for very high strain rates modulus corresponds to an ultrasonic modulus and for intermediate rate there will be a transition between the two modulus values.

2. The region 3, strain higher than 20-25%, for a low strain rate the response matches the experimental results and to the corrected response to get isothermal response at a very high strain rates. At the intermediate strain rate the response from the model is between the experimental and isothermal response, as can be expected.

3. In calculating the value of  $\beta$  region 2 was not considered. This region corresponds to strain softening. Two events are happening in this region, one is strain rate effect and another is associate with aging. Firstly, care needs to be taken to separate both the effects and then use region 2 to fit the response. The experiments are in process to separate these effects, which will give us the idea of modeling region 2.

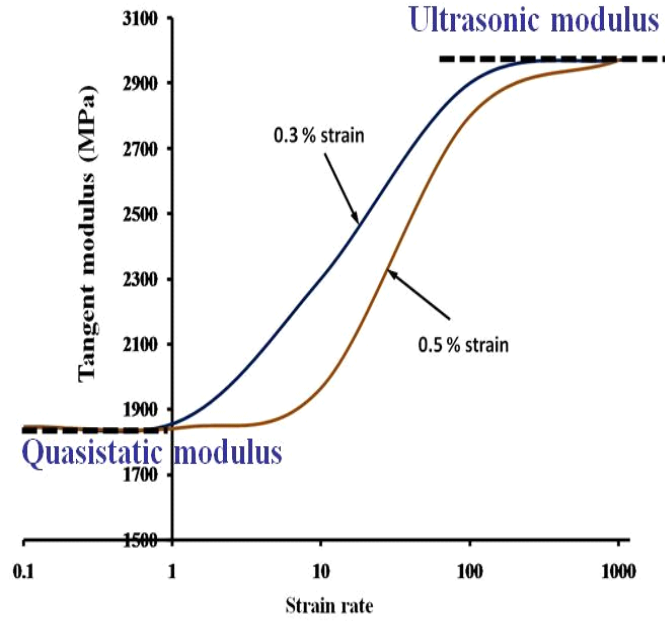


Figure 10.26: Tangent modulus from model at different strain rates under monotonic compression at two particular strains (0.3% strain and 0.5% strain).

## 10.5 Summary and conclusion

This chapter is focused on modeling the rule for the change of the internal variables  $\mathbf{F}_s^p$  and  $\mathbf{F}_f^p$ . As has been described, we have selected a constitutive equation for each that preserves the volume and has written these two forms as

$$\dot{\mathbf{F}}_s^p = \beta_s \Delta \mathbf{S}_s^T \mathbf{F}_s^p, \quad (10.35)$$

$$\dot{\mathbf{F}}_f^p = \beta_f \Delta \mathbf{S}_f^T \mathbf{F}_f^p, \quad (10.36)$$

where  $\beta_s$  and  $\beta_f$  are positive scalar valued functions to satisfy the constraint imposed by the second law of thermodynamics. These factor are selected as a product of three functions and written as

$$\beta_s = \beta_{s1}(\Delta S_s) \beta_{s2}(\varepsilon_s^p) \beta_{s3}(\theta), \quad (10.37)$$

$$\beta_f = \beta_{f1}(\Delta S_s)\beta_{f2}(\varepsilon_s^p)\beta_{f3}(\theta), \quad (10.38)$$

where  $\Delta S_s = \sqrt{\Delta \mathbf{S}_s : \Delta \mathbf{S}_s}$ ,  $\Delta S_f = \sqrt{\Delta \mathbf{S}_f : \Delta \mathbf{S}_f}$ ,  $\varepsilon_s^p = \text{tr}(\mathbf{C}_s^p - \mathbf{3})$ ,  $\varepsilon_f^p = \text{tr}(\mathbf{C}_f^p) - 3$  and  $\theta$  is given in degree Kelvin.

Before we could fit these models we needed to take into account that, even though the slow strain rate tests can be considered close to isothermal, the higher strain rate test are more close to adiabatic response. To use the higher rate loading results, we needed to find a method to consider the temperature rise. To do this we first showed that one can accurately predict the temperature changes observed by Lerch et al. [13] with the developed model for stress and back stress. Once this was established, we used the models to predict the temperature rise for the faster, loading rates and used interpolation to predict the isothermal response. Once this correction to the data was made, we fit the  $\beta_s$  and  $\beta_f$  systematically using the experimental results, first extracting the dependence on overstress ( $\Delta S_s$  or  $\Delta S_f$ ), then extracting the effect of large plastic deformation ( $\varepsilon_s^p$  or  $\varepsilon_f^p$ ), and finally the effect of temperature. The results of these fits can be summarized as

$$\beta_{s1} = 7.43E^{-10} \times e^{(0.52 \times \Delta S_s)}, \quad (10.39)$$

$$\beta_{s2} = 25.8 \times e^{(-11.66 \times \varepsilon_s^p)}, \quad (10.40)$$

$$\beta_{s3} = 2.453E^{-16} \times e^{(0.122 \times \theta)}, \quad (10.41)$$

$$\beta_{f1} = 3.5 \times e^{(0.154 \times \Delta S_f)}, \quad (10.42)$$

$$\beta_{f2} = 1.2 \times e^{(-3 \times \varepsilon_f^p)},$$

$$\beta_{f3} = 0.0634 \times \theta - 17.91. \quad (10.43)$$

It should be noted that the model should be good for the temperature from  $-40^{\circ}\text{C}$  to  $100^{\circ}\text{C}$ , strain rates from  $10^{-4}$ 1/s to  $10^3$ 1/s and plastic strain upto 50% compression. It should also be noted that the effects of aging are not included.

## Chapter 11

# Conclusion and scope for future work

### 11.1 Conclusion

This dissertation is primarily focused on characterizing the rate dependent mechanical behavior for glassy polymers at large strains and different temperatures below the glass transition temperature. This work uses a diverse set of experiments which includes monotonic compression experiments at different strain rates and temperatures, ultrasonic wave speed measurement and uniaxial cyclic tests to develop a large deformation thermodynamically consistent constitutive model which can potentially capture the response at large strains and different strain rates and temperatures. The significant contributions made in this process are listed below.

1. We have studied and modeled the anisotropic elastic response developed in ini-

tially isotropic polycarbonate as a result of plastic flow. Uniaxial compression was used to prepare samples with different extents of plastic deformation and then they were ultrasonically tested to measure wave moduli in longitudinal and shear along the axis of compression and perpendicular to this axis (The experiments were performed by other people in my group) . The transverse wave moduli, both longitudinal and shear, increased with plastic compression, while in the axial direction the longitudinal wave modulus decreased and the shear wave modulus stayed constant. The difference in the wave moduli between axial and transverse directions for PC is substantial, indicating that ignoring this could result in substantial error in the predictions of the resulting models. This fact is frequently ignored and not reflected in the models that are developed. To capture the observed development of anisotropic elastic moduli, a model for the free energy based on the elastic and plastic deformation gradients was constructed. Since the PC used was initially isotropic, representations for this model were provided for an initially isotropic material. This model was then simplified and fit to the experimental data. The resulting fits were in good agreement with the experimentally observed moduli, and predicted similar trends to experimental results reported in tension.

2. A large deformation thermo-elastic model was developed for glassy PC to capture the thermo-elastic effects of temperature and loads using confined compression experiments performed by Masubichi et al. measuring ultrasonic velocity under load in a PVT machine. This model was then combined with the model developed to predict the development of anisotropic ultrasonic response after plastic flow.

3. We have introduced a new technique based on cyclic compression to calculate

the equilibrium stress for temperatures below the glass transition temperature. The method was evaluated for measuring the response of polycarbonate at different temperatures and the standard deviation was calculated. This is the first time we believe that the equilibrium stress has been measured and at the same time the error in the measurement quantified. In addition, we believe, this is the first time, to our knowledge, that both the tangent modulus and local Poisson's ratio at equilibrium have been measured for any material. The method may be used for other materials showing an equilibrium stress.

4. A coupled free energy is constructed from the model developed for the stress and the results obtained for the equilibrium stress that provide the two as appropriate derivatives of the free energy.

5. Noting that the high strain rate tests corresponds to an adiabatic deformation due to heating in the samples, we evaluated the temperature rise using the model and obtained isothermal response by interpolation. The calculated temperature rise was supported by comparison to existing experiments. The calculated isothermal plots were used to develop flow rules for the internal parameters.

The entire dissertation can be summarized using the experimental protocol shown in Figure 11.1 and shows that first from the plastic compression followed by ultrasonic wave moduli evaluation we are calculating the material parameters for the model for stress as a function of elastic and plastic deformation gradient, then using cyclic compression we calculate the material parameters in the model for back stress and finally using monotonic compression at different strain rates we calculate the material parameters in the flow rules. In addition we have added the effects of temperature for each part and incorporated ultra-

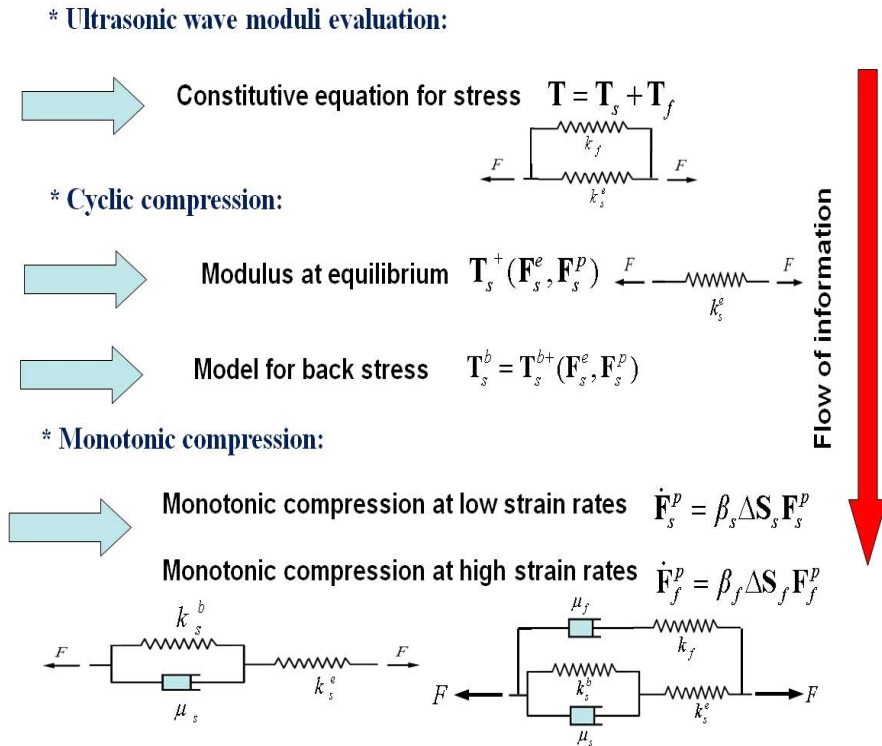


Figure 11.1: Experimental protocol used to develop a large deformation constitutive model.

sonics under load using published results by Masubichi et al.

## 11.2 Constitutive model

The summary of the constitutive model developed in the dissertation is as follows.

### 11.2.1 Constitutive model for stress

The constitutive model for stress is split into two parts, one corresponding to the slow relaxation element  $\mathbf{T}_s$  and the other corresponds to the fast relaxation element  $\mathbf{T}_f$

such that the total stress  $\mathbf{T}$  can be given as

$$\mathbf{T} = \mathbf{T}_s + \mathbf{T}_f \quad (11.1)$$

where  $\mathbf{T}_s$  and  $\mathbf{T}_f$  are given by

$$\begin{aligned} \mathbf{T}_s = & E_{quas} \left\{ A_{iso} \left[ G(\mathbf{F}_s^p) \frac{1}{J J_s^{e\frac{2}{3}}} \left( \mathbf{B}_s^e - \frac{tr(\mathbf{B}_s^e)}{3} \mathbf{I} \right) + \kappa(\mathbf{F}_s^p) \frac{J_s^e \ln(J_s^e)}{J} \mathbf{I} \right] \right. \\ & + E_{comb} \left[ \frac{2}{J_s^{e\frac{2}{3}}} \left( \mathbf{B}_s^e - \frac{tr(\mathbf{B}_s^e)}{3} \mathbf{I} \right) \ln^2(J_s^e) + 2 \ln(J_s^e) \left( \frac{tr(\mathbf{C}_s^e)}{J_s^{e\frac{2}{3}}} - 3 \right) \right] \left. \right\} \\ & + A_{aniso} \left[ \rho_o \frac{\partial \psi}{\partial I_7^*}(\mathbf{F}_s^p) \frac{1}{J} \mathbf{F}_s^e [2(\mathbf{C}_s^p - \mathbf{I}) - (\mathbf{C}_s^e \mathbf{C}_s^p + \mathbf{C}_s^p \mathbf{C}_s^e - 2\mathbf{C}_s^e)] \right] \mathbf{F}_s^{eT}, \end{aligned} \quad (11.2)$$

and

$$\begin{aligned} \mathbf{T}_f = & (1 - E_{quas}) \left\{ A_{iso} \left[ G(\mathbf{F}_f^p) \frac{1}{J J_f^{e\frac{2}{3}}} \left( \mathbf{B}_f^e - \frac{tr(\mathbf{B}_f^e)}{3} \mathbf{I} \right) + \kappa(\mathbf{F}_f^p) \frac{J_f^e \ln(J_f^e)}{J} \mathbf{I} \right] \right. \\ & + E_{comb} \left[ \frac{2}{J_f^{e\frac{2}{3}}} \left( \mathbf{B}_f^e - \frac{tr(\mathbf{B}_f^e)}{3} \mathbf{I} \right) \ln^2(J_f^e) + 2 \ln(J_f^e) \left( \frac{tr(\mathbf{C}_f^e)}{J_f^{e\frac{2}{3}}} - 3 \right) \right] \left. \right\}. \end{aligned} \quad (11.3)$$

where  $\mathbf{B}_s^e$  and  $\mathbf{B}_f^e$  are elastic right Cauchy stretch tensor corresponds to  $\mathbf{F}_s^e$  and  $\mathbf{F}_f^e$  and given by ,respectively, the  $\mathbf{B}_s^e = \mathbf{F}_s^e \mathbf{F}_s^{eT}$  and  $\mathbf{B}_f^e = \mathbf{F}_f^e \mathbf{F}_f^{eT}$ . The volume ratio  $J_s^e$  and  $J_f^e$  are ,respectively, the elastic volume ratio corresponds to  $\mathbf{F}_s^e$  and  $\mathbf{F}_f^e$  and given by  $J_s^e = \det(\mathbf{F}_s^e)$  and  $J_f^e = \det(\mathbf{F}_f^e)$  and the total volume ratio  $J$  are given by  $J = J_s^e J^\theta = J_f^e J^\theta$  since due to assumption of incompressibility in plastic flow, plastic volume ratio  $J_s^p$  and  $J_f^p$  is equal to one. The material parameter  $E_{quas}, A_{iso}, A_{aniso}, E_{comb}, G, \kappa$  and  $\rho_o \frac{\partial \psi}{\partial I_7^*}$  in the equations are given by

$$E_{quas} = 0.6, \quad (11.4)$$

$$A_{iso} = 2.28 \times e^{-\left(\frac{\theta}{357}\right)}, \quad (11.5)$$

$$A_{aniso} = 6.04 \times e^{-\left(\frac{\theta}{166}\right)}, \quad (11.6)$$

$$E_{comb} = 60500 \text{ MPa} \quad , \quad (11.7)$$

$$\kappa = 4670 + 200 \times (I_4^* - 3) \text{ MPa}, \quad (11.8)$$

$$G = 1072 - 159 \times (I_4^* - 3) \text{ MPa}, \quad (11.9)$$

$$\rho_o \frac{\partial \psi}{\partial I_7^*} = -283 - 150 \times e^{-\frac{(I_4^*-3)}{0.125}} + 433 \times e^{-\frac{(I_4^*-3)}{0.004}} \text{ MPa}, \quad (11.10)$$

where  $\theta$  are in Kelvin and  $I_4^*$  is defined by  $tr(\mathbf{C}_s^p)$  or  $tr(\mathbf{C}_f^p)$  depending upon the model of stress.

### 11.2.2 Constitutive model for back stress

In the mechanical analog presented in Chapter 3, there is one back stress element corresponding to the standard linear solid. The constitutive model for back stress corresponding to that element can be summarized as

$$\begin{aligned} \mathbf{T}_s^b = \mathbf{S}_s^b = \mathbf{T}_{stress}^b + \frac{1}{J} & \left[ \left( G_o^b - G_{\infty 1}^b \right) \frac{\tanh \left( \sqrt{\frac{(G_o^b - G_{\infty 1}^b)^2}{\tau_o^b} [I_4^*(\mathbf{F}_s^p) - 3]} \right)}{\sqrt{\frac{(G_o^b - G_{\infty 1}^b)^2}{\tau_o^b} [I_4^*(\mathbf{F}_s^p) - 3]}} \right. \\ & \left. + G_{\infty 1}^b + G_{\infty 2}^b \{I_4^*(\mathbf{F}_s^p) - 3\} \right] \left( \mathbf{B}_s^p - \frac{1}{3} tr(\mathbf{B}_s^p) \mathbf{I} \right). \end{aligned} \quad (11.11)$$

where  $\mathbf{T}_{stress}^b$  corresponds to the terms coming from model of stress and material parameters  $E_{quas}$ ,  $A_{iso}$ ,  $A_{aniso}$ ,  $G$ ,  $\kappa$  and  $\rho_o \frac{\partial \psi}{\partial I_7^*}$  are given by equations 11.4 to 11.10,  $G_o^b$ ,  $G_{\infty 1}^b$ ,  $G_{\infty 2}^b$  and  $\tau_o^b$  are given as

$$G_o^b = 1000 \text{ MPa}, \quad (11.12)$$

$$G_{\infty 1}^b = 0, \quad G_{\infty 2}^b = 5 \text{ MPa}, \quad (11.13)$$

$$\tau_o^b = -0.119\theta + 51.795 \text{ MPa}, \quad (11.14)$$

where  $\theta$  is in  $K$ .

### 11.2.3 Over stress contribution for low and high strain rates

The overstress  $\Delta \mathbf{T}_s$  and  $\Delta \mathbf{T}_f$  can be related to an appropriate difference between stress and back stress and are given by

$$\begin{aligned}\Delta \mathbf{T}_s &= \mathbf{F}_s^{e-1} \mathbf{T}_s \mathbf{F}_s^e - \mathbf{T}_s^b, \\ \Delta \mathbf{T}_f &= \mathbf{F}_f^{e-1} \mathbf{T}_f \mathbf{F}_f^e.\end{aligned}\tag{11.15}$$

### 11.2.4 Flow rule

The flow rule for each element is given by

$$\dot{\mathbf{F}}_s^p = \beta_s \Delta \mathbf{S}_s^T \mathbf{F}_s^p,\tag{11.16}$$

$$\dot{\mathbf{F}}_f^p = \beta_f \Delta \mathbf{S}_f^T \mathbf{F}_f^p,\tag{11.17}$$

where  $\Delta \mathbf{S}_s$  and  $\Delta \mathbf{S}_f$  are the deviatoric part of the overstress  $\Delta \mathbf{T}_s$  and  $\Delta \mathbf{T}_f$  and are given by

$$\Delta \mathbf{S}_s = \Delta \mathbf{T}_s - (\Delta T_s)_{ave} \mathbf{I},\tag{11.18}$$

$$\Delta \mathbf{S}_f = \Delta \mathbf{T}_f - (\Delta T_f)_{ave} \mathbf{I},\tag{11.19}$$

and the material parameters  $\beta_s$  and  $\beta_f$  are strictly positive functions given by

$$\beta_s = \beta_{s1} \beta_{s2} \beta_{s3},\tag{11.20}$$

where  $\beta_{s1}$ ,  $\beta_{s2}$  and  $\beta_{s3}$  are given by the expressions

$$\beta_{s1} = 7.43 E^{-10} \times e^{(0.52 \times \sqrt{\Delta \mathbf{S}_s : \Delta \mathbf{S}_s})},\tag{11.21}$$

$$\beta_{s2} = 25.8 \times e^{(-11.66 \times tr(\mathbf{C}_s^p) - 3)},\tag{11.22}$$

$$\beta_{s3} = 2.453E^{-16} \times e^{(0.122 \times \theta)}, \quad (11.23)$$

where  $\theta$  is in  $K$ . The material parameter  $\beta_f$  is given by

$$\beta_f = \beta_{f1}\beta_{f2}\beta_{f3}, \quad (11.24)$$

where  $\beta_{f1}$ ,  $\beta_{f2}$  and  $\beta_{f3}$  are given by the expressions

$$\beta_{f1} = 3.5 \times e^{(.154 \times \sqrt{\Delta \mathbf{S}_f : \Delta \mathbf{S}_f})}, \quad (11.25)$$

$$\beta_{f2} = 1.2 \times e^{(-3 \times \text{tr}(\mathbf{C}_f^p) - 3)}, \quad (11.26)$$

$$\beta_{f3} = 0.0634 \times \theta - 17.91, \quad (11.27)$$

where  $\theta$  is in  $K$ .

### 11.3 Future work

There are some issues which needs to be addressed in future.

**1. Modeling the influence of aging:** Amorphous glassy polymers pass through a non equilibrium state when cooled from the rubbery state. This transformation of glassy polymers with time at temperatures below the glass-transition temperature is known as aging. This condition is characterized by excess thermodynamic quantities (volume, enthalpy and entropy etc.) and appears to be a non-equilibrium state of matter. The influence of aging on the thermomechanical response of glassy polymers is very strong. Therefore, proper modeling of the thermomechanical response of polymers needs to include the influence of aging, which was not considered in this work.

**2. Modeling the strain softening:** The constitutive model developed does not capture the strain softening seen in region 2 of the stress strain curve. The effect of aging on strain softening needs to be studied to separate the aging effect and possibly model the effects not captured by aging.

**3. Incorporation of the model into finite element software:** In general, the solution of boundary value problems in continuum mechanics implies integrating a set of nonlinear partial differential equations. These boundary value problems, often involve complex geometries, highly nonlinear material behavior and sophisticated boundary conditions. For such problems, analytical solutions remain exceptional and numerical solutions are necessary for their solution. The constitutive model developed needs to be incorporated into finite element software. The model needs to be evaluated for impact conditions and the response needs to be compared with the experimental results.

**4. Development of large deformation constitutive model for other polymers:** From the literature it is seen that several commonly used polymers, other than PC, which exhibits development of elastic anisotropy includes polyvinyl chloride, PDMS and PET, although PC shows a more significant development of anisotropy. Up to now, according to our information, the constitutive models developed for these polymers are assumed to be isotropic and remain isotropic with plastic flow. The constitutive modeling structure developed for polycarbonate can also be used for others glassy polymers to develop more accurate models which then can be used for studying practical applications.

Work is currently in progress in our research group to address some of these issues.

## Chapter 12

# Appendix

## 12.1 Appendix A: Calculation of derivatives of invariants

Given the invariants  $I_1^* - I_{10}^*$ , the time derivative of these are given by

$$\begin{aligned}
I_1^* &= \frac{\mathbf{F}^e : \mathbf{F}^e}{J^e \frac{2}{3}} \rightarrow \dot{I}_1^* = \frac{2\mathbf{F}^e : \dot{\mathbf{F}}^e}{J^e \frac{2}{3}} - \frac{2}{3} \frac{\mathbf{F}^e : \mathbf{F}^e}{J^e \frac{5}{3}} J^e \mathbf{F}^{e-T} : \dot{\mathbf{F}}^e = \frac{2}{J^e \frac{2}{3}} \left[ \mathbf{F}^e - \frac{1}{3} (\mathbf{F}^e : \mathbf{F}^e) \mathbf{F}^{e-T} \right] : \dot{\mathbf{F}}^e, \\
I_2^* &= \frac{\mathbf{C}^e : \mathbf{C}^e}{(\mathbf{F}^e : \mathbf{F}^e)^2} \rightarrow \dot{I}_2^* = \frac{2\mathbf{C}^e : \dot{\mathbf{C}}^e}{(\mathbf{F}^e : \mathbf{F}^e)^2} - 4 \frac{\mathbf{C}^e : \mathbf{C}^e}{(\mathbf{F}^e : \mathbf{F}^e)^3} \mathbf{F}^e : \dot{\mathbf{F}}^e = \frac{4}{(\mathbf{F}^e : \mathbf{F}^e)^2} \mathbf{F}^e \left( \mathbf{C}^e - \frac{\mathbf{C}^e : \mathbf{C}^e}{\mathbf{F}^e : \mathbf{F}^e} \mathbf{I} \right) : \dot{\mathbf{F}}^e, \\
I_3^* &= \det(\mathbf{F}^e) \rightarrow \dot{I}_3^* = J^e \mathbf{F}^{e-T} : \dot{\mathbf{F}}^e, \\
I_4^* &= \frac{\mathbf{F}^p : \mathbf{F}^p}{J^p \frac{2}{3}} \rightarrow \dot{I}_4^* = \frac{2\mathbf{F}^p : \dot{\mathbf{F}}^p}{J^p \frac{2}{3}} - \frac{2}{3} \frac{\mathbf{F}^p : \mathbf{F}^p}{J^p \frac{5}{3}} J^p \mathbf{F}^{p-T} : \dot{\mathbf{F}}^p = \frac{2}{J^p \frac{2}{3}} \left[ \mathbf{F}^p - \frac{1}{3} (\mathbf{F}^p : \mathbf{F}^p) \mathbf{F}^{p-T} \right] : \dot{\mathbf{F}}^p, \\
I_5^* &= \frac{\mathbf{C}^p : \mathbf{C}^p}{(\mathbf{F}^p : \mathbf{F}^p)^2} \rightarrow \dot{I}_5^* = \frac{2\mathbf{C}^p : \dot{\mathbf{C}}^p}{(\mathbf{F}^p : \mathbf{F}^p)^2} - 4 \frac{\mathbf{C}^p : \mathbf{C}^p}{(\mathbf{F}^p : \mathbf{F}^p)^3} \mathbf{F}^p : \dot{\mathbf{F}}^p = \frac{4}{(\mathbf{F}^p : \mathbf{F}^p)^2} \mathbf{F}^p \left( \mathbf{C}^p - \frac{\mathbf{C}^p : \mathbf{C}^p}{\mathbf{F}^p : \mathbf{F}^p} \mathbf{I} \right) : \dot{\mathbf{F}}^p, \\
I_6^* &= \det(\mathbf{F}^p) \rightarrow \dot{I}_6^* = J^p \mathbf{F}^{p-T} : \dot{\mathbf{F}}^p, \\
I_7^* &= \mathbf{C}^e : \mathbf{C}^p - \mathbf{F}^e : \mathbf{F}^e - \mathbf{F}^p : \mathbf{F}^p + 3 \rightarrow \dot{I}_7^* = \dot{\mathbf{C}}^e : \mathbf{C}^p + \mathbf{C}^e : \dot{\mathbf{C}}^p - 2\mathbf{F}^e : \dot{\mathbf{F}}^e - 2\mathbf{F}^p : \dot{\mathbf{F}}^p \\
&= 2\mathbf{F}^e (\mathbf{C}^p - \mathbf{I}) : \dot{\mathbf{F}}^e + 2\mathbf{F}^p (\mathbf{C}^e - \mathbf{I}) : \dot{\mathbf{F}}^p, \\
I_8^* &= \mathbf{C}^{e2} : \mathbf{C}^p - \mathbf{C}^e : \mathbf{C}^e - \mathbf{F}^p : \mathbf{F}^p + 3 \\
\rightarrow \dot{I}_8^* &= \left( \dot{\mathbf{C}}^e \mathbf{C}^e + \mathbf{C}^e \dot{\mathbf{C}}^e \right) : \mathbf{C}^p + \mathbf{C}^{e2} : \dot{\mathbf{C}}^p - 2\mathbf{C}^e : \dot{\mathbf{C}}^e - 2\mathbf{F}^p : \dot{\mathbf{F}}^p \\
&= 2\mathbf{F}^e (\mathbf{C}^p \mathbf{C}^e + \mathbf{C}^e \mathbf{C}^p - 2\mathbf{C}^e) : \dot{\mathbf{F}}^e + 2\mathbf{F}^p (\mathbf{C}^{e2} - \mathbf{I}) : \dot{\mathbf{F}}^p, \\
I_9^* &= \mathbf{C}^e : \mathbf{C}^{p2} - \mathbf{F}^e : \mathbf{F}^e - \mathbf{C}^p : \mathbf{C}^p + 3 \\
\rightarrow \dot{I}_9^* &= \dot{\mathbf{C}}^e : \mathbf{C}^{p2} + \mathbf{C}^e : \left( \dot{\mathbf{C}}^p \mathbf{C}^p + \mathbf{C}^p \dot{\mathbf{C}}^p \right) - 2\mathbf{F}^e : \dot{\mathbf{F}}^e - 2\mathbf{C}^p : \dot{\mathbf{C}}^p \\
&= 2\mathbf{F}^e (\mathbf{C}^{p2} - \mathbf{I}) : \dot{\mathbf{F}}^e + 2\mathbf{F}^p (\mathbf{C}^e \mathbf{C}^p + \mathbf{C}^p \mathbf{C}^e - 2\mathbf{C}^p) : \dot{\mathbf{F}}^p, \\
I_{10}^* &= \mathbf{C}^{e2} : \mathbf{C}^{p2} - \mathbf{C}^e : \mathbf{C}^e - \mathbf{C}^p : \mathbf{C}^p + 3 \\
\rightarrow \dot{I}_{10}^* &= 2\mathbf{F}^e (\mathbf{C}^e \mathbf{C}^{p2} + \mathbf{C}^{p2} \mathbf{C}^e - 2\mathbf{C}^e) : \dot{\mathbf{F}}^e + 2\mathbf{F}^p (\mathbf{C}^{e2} \mathbf{C}^p + \mathbf{C}^p \mathbf{C}^{e2} - 2\mathbf{C}^p) : \dot{\mathbf{F}}^p.
\end{aligned} \tag{12.1}$$

## 12.2 Appendix B: Calculation of stress and its rate

The expression for Cauchy stress derived in Chapter 5 can also be written as

$$\begin{aligned} \mathbf{T} = & \rho \left\{ \frac{2}{J^{e\frac{2}{3}}} \frac{\partial \psi}{\partial I_1^*} \left( \mathbf{B}^e - \frac{I_1}{3} \mathbf{I} \right) + \frac{4}{I_1^2} \frac{\partial \psi}{\partial I_2^*} \mathbf{F}^e \left( \mathbf{C}^e - \frac{I_2}{I_1} \mathbf{I} \right) \mathbf{F}^{eT} + J^e \frac{\partial \psi}{\partial I_3^*} \mathbf{I} \right. \\ & + \frac{\partial \psi}{\partial I_7^*} \mathbf{F}^e [2(\mathbf{C}^e - \mathbf{I}) - \mathbf{C}^p (\mathbf{C}^e - \mathbf{I}) - (\mathbf{C}^e - \mathbf{I}) \mathbf{C}^p] \mathbf{F}^{eT} \\ & \left. + \frac{\partial \psi}{\partial I_9^*} \mathbf{F}^e [2(\mathbf{C}^e - \mathbf{I}) - \mathbf{C}^{p2} (\mathbf{C}^e - \mathbf{I}) - (\mathbf{C}^e - \mathbf{I}) \mathbf{C}^{p2}] \mathbf{F}^{eT} \right\}. \end{aligned} \quad (12.2)$$

It should be noted that the terms in the curly brackets “{}” add to zero at zero elastic deformation (i.e.  $\mathbf{F}^e = \mathbf{I}$ ). This is also true for all the terms in the round brackets “( )”. Taking the derivative of  $\mathbf{T}$  and evaluating it at  $\mathbf{F}^e = \mathbf{I}$ , assuming plastic deformation gradients are constant, and after eliminating terms that are multiplied  $\frac{\partial \psi}{\partial I_3^*}$ , “{}” and “( )” we find

$$\begin{aligned} \dot{\mathbf{T}} \Big|_{\mathbf{F}^e=\mathbf{I}} = & \rho \left\{ \frac{2}{J^{e\frac{2}{3}}} \frac{\partial \psi}{\partial I_1^*} \left( \overline{\mathbf{B}^e - \frac{I_1}{3} \mathbf{I}} \right) + \frac{4}{9} \frac{\partial \psi}{\partial I_2^*} \left( \overline{\mathbf{C}^e - \frac{I_2}{I_1} \mathbf{I}} \right) \mathbf{F}^{eT} + \frac{\dot{\partial \psi}}{\partial I_3^*} \mathbf{I} \right. \\ & \left. + \frac{\partial \psi}{\partial I_7^*} \mathbf{F}^e [2\dot{\mathbf{C}}^e - \mathbf{C}^p \dot{\mathbf{C}}^e - \dot{\mathbf{C}}^e \mathbf{C}^p] + \frac{\partial \psi}{\partial I_9^*} [2\dot{\mathbf{C}}^e - \mathbf{C}^{p2} \dot{\mathbf{C}}^e - \dot{\mathbf{C}}^e \mathbf{C}^{p2}] \right\}_{\mathbf{F}^e=\mathbf{I}}. \end{aligned} \quad (12.3)$$

This shows that the derivative of the free energy with respect to the invariants  $I_1^*$  and  $I_2^*$  always appear in the same combination. Therefore, measurements that use stress rate at  $\mathbf{F}^e = \mathbf{I}$  can only be used to evaluate the given combination of these derivatives. Next, let us consider the term

$$\frac{\dot{\partial \psi}}{\partial I_3^*} \Big|_{\mathbf{F}^e=\mathbf{I}} = \frac{\partial^2 \psi}{\partial I_i^* \partial I_3^*} \dot{I}_i \Big|_{\mathbf{F}^e=\mathbf{I}}, \quad (12.4)$$

$$\begin{aligned} \frac{\dot{\partial \psi}}{\partial I_3^*} \Big|_{\mathbf{F}^e=\mathbf{I}} = & \left\{ \frac{\partial}{\partial I_3^*} \left( \frac{\partial \psi}{\partial I_3^*} \right) \mathbf{I} : \dot{\mathbf{F}}^e + 2 \left[ \frac{\partial}{\partial I_7^*} \left( \frac{\partial \psi}{\partial I_3^*} \right) + 2 \frac{\partial}{\partial I_8^*} \left( \frac{\partial \psi}{\partial I_3^*} \right) \right] (\mathbf{C}^p - \mathbf{I}) : \dot{\mathbf{F}}^e \right. \\ & \left. + 2 \left[ \frac{\partial}{\partial I_9^*} \left( \frac{\partial \psi}{\partial I_3^*} \right) + 2 \frac{\partial}{\partial I_{10}^*} \left( \frac{\partial \psi}{\partial I_3^*} \right) \right] (\mathbf{C}^p - \mathbf{I}) : \dot{\mathbf{F}}^e \right\}_{\mathbf{F}^e=\mathbf{I}}. \end{aligned} \quad (12.5)$$

We now note that if we change the order of the derivatives in the square brackets “[ ]”, both become zero as a result of the general conditions (11) imposed on the relation between the derivatives of the free energy. We, thus, conclude that the expression for the stress rate evaluated at zero elastic deformation is given by

$$\begin{aligned} \dot{\mathbf{T}} \mid_{\mathbf{F}^e=\mathbf{I}} = & \rho \left\{ 2 \left( \frac{\partial \psi}{\partial I_1^*} + \frac{2}{9} \frac{\partial \psi}{\partial I_2^*} \right) \left[ \dot{\mathbf{F}}^e + \dot{\mathbf{F}}^{eT} - \frac{2}{3} (\mathbf{I} : \dot{\mathbf{F}}^e) \mathbf{I} \right] + \frac{\partial}{\partial I_3^*} \left( \frac{\partial \psi}{\partial I_3^*} \right) (\mathbf{I} : \dot{\mathbf{F}}^e) \mathbf{I} \right. \\ & \left. + \frac{\partial \psi}{\partial I_7^*} \mathbf{F}^e \left[ 2\dot{\mathbf{C}}^e - \mathbf{C}^p \dot{\mathbf{C}}^e - \dot{\mathbf{C}}^e \mathbf{C}^p \right] + \frac{\partial \psi}{\partial I_9^*} \left[ 2\dot{\mathbf{C}}^e - \mathbf{C}^{p2} \dot{\mathbf{C}}^e - \dot{\mathbf{C}}^e \mathbf{C}^{p2} \right] \right\}_{\mathbf{F}^e=\mathbf{I}}, \end{aligned} \quad (12.6)$$

where we note that

$$\dot{\mathbf{C}}^e \mid_{\mathbf{F}^e=\mathbf{I}} = \dot{\mathbf{F}}^e + \dot{\mathbf{F}}^{eT}. \quad (12.7)$$

In component form this can be written as

$$\begin{aligned} \dot{T}_{ij} \mid_{\mathbf{F}^e=\mathbf{I}} = & \rho \left\{ 2 \left( \frac{\partial \psi}{\partial I_1^*} + \frac{2}{9} \frac{\partial \psi}{\partial I_2^*} \right) \left[ \dot{F}_{ij}^e + \dot{F}_{ji}^e - \frac{2}{3} \dot{F}_{kk}^e \delta_{ij} \right] + \frac{\partial}{\partial I_3^*} \left( \frac{\partial \psi}{\partial I_3^*} \right) \dot{F}_{kk}^e \delta_{ij} \right. \\ & + \frac{\partial \psi}{\partial I_7^*} \left[ 2 \left( \dot{F}_{ij}^e + \dot{F}_{ji}^e \right) - C_{ik}^p \left( \dot{F}_{kj}^e + \dot{F}_{jk}^e \right) - \left( \dot{F}_{ik}^e + \dot{F}_{ki}^e \right) C_{kj}^p \right] \\ & \left. + \frac{\partial \psi}{\partial I_9^*} \left[ 2 \left( \dot{F}_{ij}^e + \dot{F}_{ji}^e \right) - C_{ik}^{p2} \left( \dot{F}_{kj}^e + \dot{F}_{jk}^e \right) - \left( \dot{F}_{ik}^e + \dot{F}_{ki}^e \right) C_{kj}^{p2} \right] \right\}_{\mathbf{F}^e=\mathbf{I}}. \end{aligned} \quad (12.8)$$

From this we can calculate the tangent modulus at zero elastic strain as

$$\begin{aligned} E_{ijmn} = & \rho \left\{ 2 \left( \frac{\partial \psi}{\partial I_1^*} + \frac{2}{9} \frac{\partial \psi}{\partial I_2^*} \right) \left[ \delta_{im} \delta_{jn} + \delta_{jm} \delta_{in} - \frac{2}{3} \delta_{mn} \delta_{ij} \right] + \frac{\partial}{\partial I_3^*} \left( \frac{\partial \psi}{\partial I_3^*} \right) \delta_{mn} \delta_{ij} \right. \\ & + \frac{\partial \psi}{\partial I_7^*} \left[ 2 (\delta_{im} \delta_{jn} + \delta_{jm} \delta_{in}) - C_{ik}^p (\delta_{km} \delta_{jn} + \delta_{jm} \delta_{kn}) - (\delta_{im} \delta_{kn} + \delta_{km} \delta_{in}) C_{kj}^p \right] \\ & \left. + \frac{\partial \psi}{\partial I_9^*} \left[ 2 (\delta_{im} \delta_{jn} + \delta_{jm} \delta_{in}) - C_{ik}^{p2} (\delta_{km} \delta_{jn} + \delta_{jm} \delta_{kn}) - (\delta_{im} \delta_{kn} + \delta_{km} \delta_{in}) C_{kj}^{p2} \right] \right\}_{\mathbf{F}^e=\mathbf{I}} \quad (12.9) \\ = & \rho \left\{ 2 \left( \frac{\partial \psi}{\partial I_1^*} + \frac{2}{9} \frac{\partial \psi}{\partial I_2^*} \right) \left[ \delta_{im} \delta_{jn} + \delta_{jm} \delta_{in} - \frac{2}{3} \delta_{mn} \delta_{ij} \right] + \frac{\partial}{\partial I_3^*} \left( \frac{\partial \psi}{\partial I_3^*} \right) \delta_{mn} \delta_{ij} \right. \\ & + \frac{\partial \psi}{\partial I_7^*} \left[ 2 (\delta_{im} \delta_{jn} + \delta_{jm} \delta_{in}) - \left( C_{im}^p \delta_{jn} + C_{in}^p \delta_{jm} + \delta_{im} C_{nj}^p + \delta_{in} C_{mj}^p \right) \right] \\ & \left. + \frac{\partial \psi}{\partial I_9^*} \left[ 2 (\delta_{im} \delta_{jn} + \delta_{jm} \delta_{in}) - \left( C_{im}^{p2} \delta_{jn} + C_{in}^{p2} \delta_{jm} + \delta_{im} C_{nj}^{p2} + \delta_{in} C_{mj}^{p2} \right) \right] \right\}_{\mathbf{F}^e=\mathbf{I}}. \quad (12.10) \end{aligned}$$

Reorganizing this yields

$$\begin{aligned}
E_{ijmn} = & \rho \left\{ 2 \left( \frac{\partial \psi}{\partial I_1^*} + \frac{2}{9} \frac{\partial \psi}{\partial I_2^*} + \frac{\partial \psi}{\partial I_7^*} + \frac{\partial \psi}{\partial I_9^*} \right) (\delta_{im} \delta_{jn} + \delta_{jm} \delta_{in}) \right. \\
& + \left[ \frac{\partial}{\partial I_3^*} \left( \frac{\partial \psi}{\partial I_3^*} \right) - \frac{4}{3} \left( \frac{\partial \psi}{\partial I_1^*} + \frac{2}{9} \frac{\partial \psi}{\partial I_2^*} \right) \right] \delta_{mn} \delta_{ij} \\
& - \frac{\partial \psi}{\partial I_7^*} \left( C_{im}^p \delta_{jn} + C_{in}^p \delta_{jm} + \delta_{im} C_{nj}^p + \delta_{in} C_{mj}^p \right) \\
& \left. - \frac{\partial \psi}{\partial I_9^*} \left( C_{im}^{p2} \delta_{jn} + C_{in}^{p2} \delta_{jm} + \delta_{im} C_{nj}^{p2} + \delta_{in} C_{mj}^{p2} \right) \right\}_{\mathbf{F}^e = \mathbf{I}}. \quad (12.11)
\end{aligned}$$

Denoting by

$$\begin{aligned}
A &= 2\rho \left( \frac{\partial \psi}{\partial I_1^*} + \frac{2}{9} \frac{\partial \psi}{\partial I_2^*} + \frac{\partial \psi}{\partial I_7^*} + \frac{\partial \psi}{\partial I_9^*} \right)_{\mathbf{F}^e = \mathbf{I}}, \quad (12.12) \\
B &= \rho \left[ \frac{\partial}{\partial I_3^*} \left( \frac{\partial \psi}{\partial I_3^*} \right) - \frac{4}{3} \left( \frac{\partial \psi}{\partial I_1^*} + \frac{2}{9} \frac{\partial \psi}{\partial I_2^*} \right) \right]_{\mathbf{F}^e = \mathbf{I}}, \\
C &= -\rho \frac{\partial \psi}{\partial I_7^*} \Big|_{\mathbf{F}^e = \mathbf{I}}, \\
D &= -\rho \frac{\partial \psi}{\partial I_9^*} \Big|_{\mathbf{F}^e = \mathbf{I}},
\end{aligned}$$

we note that

$$\begin{aligned}
E_{ijmn} = & A (\delta_{im} \delta_{jn} + \delta_{jm} \delta_{in}) + B \delta_{mn} \delta_{ij} + C (C_{im}^p \delta_{jn} + C_{in}^p \delta_{jm} \\
& + \delta_{im} C_{nj}^p + \delta_{in} C_{mj}^p) + D (C_{im}^{p2} \delta_{jn} + C_{in}^{p2} \delta_{jm} + \delta_{im} C_{nj}^{p2} + \delta_{in} C_{mj}^{p2}). \quad (12.13)
\end{aligned}$$

Where  $A$ ,  $B$ ,  $C$ , and  $D$  are functions of the ten invariants evaluated at zero elastic deformation. We note that at zero elastic deformation the invariants take the values

$$\begin{aligned}
I_1^* &= 3, & I_2^* &= \frac{1}{3}, & I_3^* &= 1, & I_4^* &= \frac{I_4}{J^{\frac{2}{3}}}, & I_5^* &= \frac{I_5}{I_4^2}, & I_6^* &= J^p, \quad (12.14) \\
I_7^* &= 0, & I_8^* &= 0, & I_9^* &= 0, & I_{10}^* &= 0,
\end{aligned}$$

so that it can be stated that  $A$ ,  $B$ ,  $C$ , and  $D$  can be considered scalar functions of the three isotropic invariants of the plastic right Cauchy stretch given by  $I_4^*$ ,  $I_5^*$ ,  $I_6^*$ . It is also noted

that the equation for stress can be written as

$$\mathbf{T} = 2A\varepsilon^e + B \text{tr}(\varepsilon^e) \mathbf{I} + 2C(\mathbf{C}^p \varepsilon^e + \varepsilon^e \mathbf{C}^p) + 2D(\mathbf{C}^{p2} \varepsilon^e + \varepsilon^e \mathbf{C}^{p2}), \quad (12.15)$$

in terms of the infinitesimal elastic strain defined in the standard way by the equation

$$\varepsilon^e = \frac{1}{2}(\mathbf{H}^e + \mathbf{H}^{eT}), \quad (12.16)$$

where  $\mathbf{H}^e = \mathbf{F}^e - \mathbf{I}$  is the elastic displacement gradient and

$$\dot{\varepsilon}^e = \frac{1}{2}(\dot{\mathbf{F}}^e + \dot{\mathbf{F}}^{eT}). \quad (12.17)$$

The four moduli that we have measured are

$$E_a = E_{3333} = 2A + B + 4C_{33}^p C + 4C_{33}^{p2} D, \quad (12.18)$$

$$E_t = E_{1111} = 2A + B + 4C_{11}^p C + 4C_{11}^{p2} D,$$

$$G_a = E_{1313} = A + (C_{11}^p + C_{33}^p)C + (C_{11}^{p2} + C_{33}^{p2})D,$$

$$G_t = E_{1212} = A + (C_{11}^p + C_{22}^p)C + (C_{11}^{p2} + C_{22}^{p2})D.$$

This can be written in a matrix equation for the four unknowns as

$$\begin{bmatrix} 2 & 1 & 4C_{33}^p & 4C_{33}^{p2} \\ 2 & 1 & 4C_{11}^p & 4C_{11}^{p2} \\ 1 & 0 & (C_{11}^p + C_{33}^p) & (C_{11}^{p2} + C_{33}^{p2}) \\ 1 & 0 & (C_{11}^p + C_{22}^p) & (C_{11}^{p2} + C_{22}^{p2}) \end{bmatrix} \begin{bmatrix} A \\ B \\ C \\ D \end{bmatrix} = \begin{bmatrix} E_a \\ E_t \\ G_a \\ G_t \end{bmatrix}. \quad (12.19)$$

For uniaxial compression we have  $C_{11}^p = C_{22}^p$  and  $C_{11}^{p2} = C_{22}^{p2}$  so that we can write

$$\begin{bmatrix} 2 & 1 & 4C_{33}^p & 4C_{33}^{p2} \\ 2 & 1 & 4C_{11}^p & 4C_{11}^{p2} \\ 1 & 0 & (C_{11}^p + C_{33}^p) & (C_{11}^{p2} + C_{33}^{p2}) \\ 1 & 0 & 2C_{11}^p & 2C_{11}^{p2} \end{bmatrix} \begin{bmatrix} A \\ B \\ C \\ D \end{bmatrix} = \begin{bmatrix} E_a \\ E_t \\ G_a \\ G_t \end{bmatrix}. \quad (12.20)$$

By examination it can be seen that the coefficient matrix for this system is singular. Therefore, the solution to the unknowns  $A, B, C$  and  $D$  cannot be obtained from this expression for experiments in uniaxial compression.

# Bibliography

- [1] “Experiments on Polycarbonate Conducted by Mr. Kyle Strabala with Collaboration with Professor Mehrdad Negahban, Engineering Mechanics Department, University of Nebraska, Lincoln,” 2004-2008.
- [2] “Experiments on Polycarbonate Conducted by Army Research Lab, Aberdeen, Maryland with Collaboration with Professor Mehrdad Negahban, Engineering Mechanics Department, University of Nebraska, Lincoln,” 2004-2008.
- [3] “Experiments on Polycarbonate Conducted by Mr. Jason Vogeler with Collaboration with Professor Mehrdad Negahban and Professor Ruqiang Feng, Engineering Mechanics Department, University of Nebraska, Lincoln,” 2004-2008.
- [4] Ward, I. M., *Mechanical Properties of Solid Polymers*, Wiley, 1979.
- [5] Negahban, M., “Preliminary Results on an Effort to Characterize Thermo-Mechanical Response of Amorphous Polymers in the Glass-Transition Range,” *ASME MD/AMD Volume: Mechanics of Plastics and Plastic Composites, MD-vol. 68/AMD*, Vol. 215, 1995, pp. 133–152.

- [6] Negahban, M., *The Mechanical and Thermodynamical Theory of Plasticity*, CRC, 1st ed., September 2009.
- [7] Masubuchi, Y., Matsuoka, H., and Takimoto, J., "Measurement of Young's Modulus and Poisson's Ratio of Polymers under High Pressure," *Materials Science Research International*, Vol. 4, No. 3, 1998, pp. 223–226.
- [8] Goel, A., Strabala, K., Negahban, M., and Turner, J., "Modeling the Development of Elastic Anisotropy with Plastic Flow for Glassy Polycarbonate," *Polymer Engineering and Science*, 2008, Accepted.
- [9] Strabala, K., Oliviera, N., Goel, A., Negahban, M., and Turner, J., "Measuring the Influence of Temperature on the Development of Elastic Anisotropy with Compressive Plastic Flow for Glassy Polycarbonate," *Journal of Engineering Materials and Technology*, Submitted.
- [10] Goel, A., Strabala, K., Negahban, M., and Feng, R., "Experimentally Evaluating Equilibrium Stress in Uniaxial Tests," *Experimental Mechanics*, Accepted.
- [11] "Experiments on Polycarbonate Conducted by " Mr. Kyle Strabala, Mr. Nathan Oliveira and Mr. Jonathan Hein" with Collaboration with Professor Mehrdad Negahban, Engineering Mechanics Department, University of Nebraska, Lincoln," 2004-2008.
- [12] "Experiments on Polycarbonate Conducted by Mr. Pierre Delabarre with Collaboration with Professor Mehrdad Negahban, Engineering Mechanics Department, University of Nebraska, Lincoln," .

- [13] Lerch, V., Gary, G., and Herve, P., “Thermomechanical Properties of Polycarbonate under Dynamic Loading,” *Journal De Physique IV*, Vol. 110, 2003, pp. 159–164.
- [14] Lu, J. and Ravi-Chandar, K., “Inelastic Deformation and Localization in Polycarbonate under Tension,” *International Journal of Solids and Structures*, Vol. 36, 1999, pp. 391–425.
- [15] Mooney, M., *Journal of Applied Physics*, Vol. 11, 1940, pp. 582.
- [16] Rivlin, R., *Philos. Trans. Roy. Soc. London A*, Vol. 240, 1948, pp. 459.
- [17] Rivlin, R., *Philos. Trans. Roy. Soc. London A*, Vol. 241, 1948, pp. 379.
- [18] Biderman, V., *Rascheti na Prochnost*, Vol. 40, 1958.
- [19] James, A., Green, A., and Simpson, G., *Journal of Applied Polymer Science*, Vol. 19, 1975, pp. 2033.
- [20] Hill, R., *Advanced Applied Mathematics*, Vol. 18, 1978, pp. 1.
- [21] Rivlin, R. and Saunders, D., *Philos. Trans. Roy. Soc. London A*, Vol. 243, 1951, pp. 251.
- [22] Gent, A. and Thomas, A., *Journal of Polymer Science*, Vol. 28, 1958, pp. 625.
- [23] Hart-Smith, L. and Angew, Z., *Math. Phys.*, Vol. 17, 1966, pp. 608.
- [24] Treloar, L., *Trans. Faraday Soc.*, Vol. 39, 1943, pp. 241.
- [25] Treloar, L., *The Physics of Rubber Elasticity*, Oxford University Press, Oxford, UK, 1975.

- [26] Kuhn, W. and Grun, F., *Kolloideitschrift*, Vol. 101, 1942, pp. 248.
- [27] James, H. and Guth, E., *Journal of Chem. Phys.*, Vol. 11, 1943, pp. 455.
- [28] Flory, P., *Journal of Chemical Review*, Vol. 35, 1944, pp. 51.
- [29] Treloar, L., *Trans. Faraday Society*, Vol. 42, 1946, pp. 77.
- [30] Arruda, E. and Boyce, M., "A Three Dimensional Constitutive Model for Large Stretch Behavior of Rubber Materials," *Journal Mech. Phys. Solids*, Vol. 41, 1993, pp. 389–412.
- [31] Rosen, S., *Fundamental Principals of Polymer Materials*, John Wiley and Sons, New York, 1982.
- [32] Cessna, L. J. and Sternstein, S., *Viscoelasticity and Plasticity Considerations in the Fracture of Glasslike High Polymers*, Vol. 4, Plenum Press, New York, 1967.
- [33] Miller, E., *Introduction to Plastics and Composites*, Marcel Dekker, Inc., New York, 1996.
- [34] Amoedo, J., *Rate-Dependent Constitutive Equations and Process Modeling of Polymer Materials*, Ph.D. thesis, Rensselaer Polytechnic Institute, Troy, New York, 1990.
- [35] James, H. and Guth, E., "Theory of the Elastic Properties of Rubber," *J. Chem. Phys.*, Vol. 11, 1943, pp. 455–481.
- [36] Boyce, M. C., Parks, D. M., and Argon, A. S., "Large Inelastic Deformation of Glassy Polymers. Part I: Rate Dependent Constitutive Model," *Mechanics of Materials*, Vol. 7, 1988, pp. 15–33.

- [37] Argon, A., “A Theory for the Low Temperature Plastic Deformation of Glassy Polymers,” *Phil. Mag*, Vol. 28, 1973, pp. 839–865.
- [38] Wu, P. and der Giessen, E. V., “On Improved Network Models for Rubber Elasticity and their Applications to Orientation Hardening in Glassy Polymers,” *Journal Mech. Phys Solids*, Vol. 41, 1993, pp. 427–456.
- [39] Raha, S. and Bowden, P., “Birefringence of Plastically Deformed Poly (Methyl Methacrylate),” *Polymer*, Vol. 13, 1972, pp. 174–183.
- [40] Botto, P., Duckett, R., and Ward, I., “The Yield and Thermoelastic Properties of Oriented Poly (Methyl Methacrylate),” *Polymer*, Vol. 28, 1987, pp. 257–262.
- [41] Tomita, Y. and Tanaka, S., “Prediction of Deformation Behavior of Glassy Polymers Based on Molecular Chain Network Model,” *Internation J. Solids Structures*, Vol. 32, 1995, pp. 3423–3434.
- [42] Tomita, Y., Adachi, T., and Tanaka, S., “Modeling and Application of Constitutive Equation for Glassy Polymer Based on Nonaffine Network Theory,” *Eur. J. Mech A/Solids*, Vol. 16, 1997, pp. 745–755.
- [43] Hasan, O., Boyce, M. C., Li, X. S., and Berko, S., “Constitutive Model for the Non-linear Viscoelastic Viscoplastic Behavior of Glassy Polymers,” *Polymer Engineering and Science*, Vol. 35, No. 4, 1995, pp. 331–344.
- [44] Qian, Z. and Liu, S., *Unified Constitutive Modeling from Viscoelasticity and Viscoplasticity of Polymer Matrix Composites*, Technomic Publishing Co., Lancaster, PA, 1997.

- [45] Bordonaro, C., *Rate Dependent Mechanical Behavior of High Strength Plastics: Experiment and Modeling*, Ph.D. thesis, Rensselaer Polytechnic Institute, Troy, New York, 1995.
- [46] Krempl, E., McMahon, J., and Yao, D., “Viscoplasticity Based on Overstress with a Differential Growth Law for the Equilibrium Stress,” *Mechanics of Materials*, Vol. 5, 1986, pp. 35.
- [47] Valisetty, R. and Teply, J., “Overall Instantaneous Viscoplastic Properties of Composites,” *Journal of Composite Materials*, Vol. 26, 1992, pp. 1708–1724.
- [48] Zhang, C. and Moore, I., “Nonlinear Mechanical Response of High Density Polyethylene. Part II: Uniaxial Constitutive Model,” *Polymer Engineering Science*, Vol. 37, 1997, pp. 414–420.
- [49] Argon, A., “Plastic Deformation in Glassy Polymers,” *Polymer Materials: Relationship Between Structure and Mechanical Behavior*, American Society for Materials, 1975, pp. 411–486.
- [50] Argon, A. and Bessonov, M., “Plastic Flow in Glassy Polymers,” *Polymer Engineering and Science*, Vol. 17, No. 3, March 1977.
- [51] Argon, A. and Bessonov, M., “Plastic Deformation in Polyimides, with New Implications on the Theory of Plastic Deformation of Glassy Polymers,” *Philosophical Magazine*, Vol. 35, No. 4, 1977, pp. 917–933.
- [52] Boyce, M. C., Parks, D. M., and Argon, A. S., “Plastic Flow in Oriented Glassy Polymers,” *International Journal of Plasticity*, Vol. 5, 1989, pp. 593–615.

- [53] Boyce, M. C. and Arruda, E. M., “An Experimental and Analytical Investigation of the Large Strain Compressive and Tensile Response of Glassy Polymers,” *Polymer Engineering and Science*, Vol. 30, No. 20, 1990, pp. 1288–1298.
- [54] Arruda, E. M. and Boyce, M. C., “Evolution of Plastic Anisotropy in Amorphous Polymers During Finite Stretch,” *International Journal of Plasticity*, Vol. 9, 1993, pp. 697–721.
- [55] Arruda, E. M. and Boyce, M. C., “Strain Rate and Temperature Dependence in Amorphous Polymers at Finite Strain,” *ASME MD Volume: Use of Plastics and Plastic Composites: Materials and Mechanical Issues*, Vol. 46, 1993, pp. 697–721.
- [56] Arruda, E. M., Boyce, M. C., and Quintus-Bosz, H., “Effects of Initial Anisotropy on the Finite Strain Deformation Behavior of Glassy Polymers,” *International Journal of Plasticity*, Vol. 9, 1993, pp. 783–811.
- [57] Boyce, M. C., Arruda, E. M., and Jayachandran, R., “The Large Strain Compression, Tension, and Simple Shear of Polycarbonate,” *Polymer Engineering and Science*, Vol. 34, No. 9, 1994, pp. 716–725.
- [58] Boyce, M. C., Arruda, E. M., and Jayachandran, R., “Effects of Strain Rate, Temperature and Thermomechanical Coupling on the Finite Strain Deformation of Glassy Polymers,” *Mechanics of Materials*, Vol. 19, 1995, pp. 193–212.
- [59] Arruda, E. M., Boyce, M. C., and Jayachandran, R., “Effects of Strain Rate, Temperature and Thermo-Mechanical Coupling on the Finite Strain Deformation of Glassy Polymers,” *Mechanics of Materials*, Vol. 19, 1995, pp. 193.

- [60] Krempl, E. and Ho, K., "Overstress Model for Solid Polymer Deformation Behavior Applied to Nylon 66," *Polymer Engineering and Science*, Vol. 35, 1995, pp. 310–316.
- [61] Krempl, E. and Bordonaro, C. M., "State Variable Model for High Strength Polymers," *ASTM Special Technical Publication*, 2000, pp. 118–137.
- [62] Krempl, E. and Khan, F., "Rate (Time)-Dependent Deformation Behavior: An Overview of some Properties of Metals and Solid Polymers," *International Journal of Plasticity*, Vol. 19, 2003, pp. 1069–1095.
- [63] Krempl, E. and Khan, F., "Pre-Necking and Post-Necking Relaxation and Creep Behavior of Polycarbonate: A Phenomenological Study," *Polymer Engineering and Science*, Vol. 44, 2004, pp. 1783–1791.
- [64] Hennig, V., "Anisotropie Des Dynamischen Elastizitätsmoduls in Einachsigen Verstreckten Amorphen Hochpolymeren," *Kolloidzeitschrift*, Vol. 200, 1964, pp. 46–47.
- [65] Rawson, F. F. and Rider, J. G., "The Elastic Constants of Oriented Polyvinyl Chloride," *Journal of Physics D*, Vol. 7, 1974, pp. 41–49.
- [66] Wright, H., Faraday, C. S. N., White, E., and Treloar, L., "The Elastic Constants of Oriented Glassy Polymers," *Journal of Physics D*, Vol. 4, 1971, pp. 2002–2014.
- [67] Kashiwagi, M., Folkes, M. J., and Ward, I., "The Measurement of Molecular Orientation in Drawn Poly (Methyl Methacrylate) by Broad Line Nuclear Magnetic Resonance," *Polymer*, Vol. 12, 1971, pp. 697–710.
- [68] Kausch, H. H., *Journal of Applied Physics*, Vol. 38, 1967, pp. 4213.

- [69] Kausch, H. H., *Polymer Fracture*, Springer-Verlag, Berlin, 1978.
- [70] Robertson, R. and Buenker, R., “Some Elastic Moduli of Bisphenol A Polycarbonate,” *Journal of Polymer Science, A2*, Vol. 2, 1964, pp. 4889–4901.
- [71] Neu, R., Scott, D., and Woodmansee, M., “Measurement and Modeling of Back Stress at Intermediate to High Homologous Temperatures,” *International Journal of Plasticity*, Vol. 16, 2000, pp. 283–301.
- [72] Ahlquist, C. and Nix, W., “A Technique for Measuring Mean Internal Stress During High Temperature Creep,” *Scripta Metallurgica*, Vol. 3, 1969, pp. 679.
- [73] Onat, E., “Representation of Inelastic Behavior,” Tech. Rep. ORNL/Sub/3863-2, Yale University Subcontract Report to Oak Ridge National Laboratory, 1976.
- [74] Farren, W. and Taylor, G., “The Heat Developed During Plastic Extension of Metals,” *Proc. R. Soc.*, Vol. CVII, 1925, pp. 422–451.
- [75] Taylor, G. and Quinney, H., “The Latent Energy Remaining in a Metal After Cold Working,” *Proc. R. Soc. Ser. A*, Vol. 143, 1934, pp. 307–326.
- [76] Hodowany, J., Ravichandran, G., Rosakis, A., and Rosakis, P., “Partition of Plastic Work Into Heat and Stored Energy in Metals,” *Experimental Mechanics*, Vol. 40, No. 2, 2000, pp. 113–123.
- [77] Rittel, D., “On the Conversion of Plastic Work to Heat During High Strain Rate Deformation of Glassy Polymers,” *Mechanics of Materials*, Vol. 31, 1999, pp. 131–139.

- [78] Cristescu, N. and Suliciu, I., *Viscoplasticity*, Martinus Nijhoff Publishers, 1982.
- [79] Hill, R., *The Mathematical Theory of Plasticity*, Oxford University Press, 1950.
- [80] Lubliner, J., *Plasticity Theory*, Macmillan Publishing Company, 1990.
- [81] Kachanov, L., *Fundamentals of the Theory of Plasticity*, Mir Publishers, 1974.
- [82] Cristescu, N., *Dynamic Plasticity*, North Holland Publishing Company - Amsterdam and John Wiley Sons, Inc.- New York, 1967.
- [83] Maugin, G., *The Thermodynamics of Plasticity and Fracture*, Cambridge University Press, 1992.
- [84] Khan, A. and Huang, S., *Continuum Theory of Plasticity*, John Wiley Sons, Inc., 1995.
- [85] Simo, J. and Hughes, T., *Computational Inelasticity (Interdisciplinary Applied Mathematics, Vol. 7)*, Springer Verlag, 1998.
- [86] Lubarda, V., *Elastoplasticity Theory*, CRC Press, 2002.
- [87] Bertram, A., *Elasticity and Plasticity of Large Deformations, An Introduction*, Springer, 2005.
- [88] Truesdell, C. and Noll, W., *The Nonlinear Field Theories of Mechanics*, Springer Verlag, Berlin, 1965.
- [89] Chadwick, P., *Continuum Mechanics*, Dover Publications, Inc., Mineola, 1999.
- [90] Ferry, J., *Viscoelastic Properties of Polymers*, Wiley, New York, 3rd ed., 1980.

- [91] Kroner, E., "Allgemeine Kontinuumstheorie der Versetzungen und Eigenspannungen," *Archive for Rational Mechanics and Analysis*, Vol. 4, 1960, pp. 273–334.
- [92] Lee, E., "Elastic Plastic Deformation at Finite Strain," *ASME Journal of Applied Mechanics*, Vol. 36, 1969, pp. 1–6.
- [93] Govaert, L., Timmermans, P., and Brekelmans, W., "The Influence of Intrinsic Strain Softening on Strain Localization in Polycarbonate: Modeling and Experimental Validation," *Journal of Engineering Materials and Technology*, Vol. 122, 2000, pp. 177–185.
- [94] Anand, L. and Gurtin, M., "A Theory of Amorphous Solids Undergoing Large Deformations, with Application to Polymer Glasses," *International Journal of Solids and Structures*, Vol. 40, 2003, pp. 1465–1487.
- [95] Mulliken, A. and Boyce, M., "Mechanics of the Rate-Dependent Elastic-Plastic Deformation of Glassy Polymers from Low to High Strain Rates," *International Journal of Solids and Structures*, Vol. 43, 2006, pp. 1331–1356.
- [96] Kuttruff, H., *Ultrasonics Fundamentals and Applications*, Elsevier Science Publishers Co. Inc, New York, 1991.
- [97] Shutilov, V., *Fundamentals Physics of Ultrasound*, Gordon and Breach Science Publishers, Amsterdam, 1988.
- [98] Nishiwaki, N., Cui, A., Kohno, M., and Hori, S., *Proceedings of Polymer Processing Society Annual Meeting*, 1994, pp. 182.

- [99] Spencer, A., *Theory of Invariants in Continuum Physics: Volume 1- Mathematics*, Academic Press, 1971.
- [100] Negahban, M., “A Study of Thermodynamic Restrictions, Constraint Conditions, and Material Symmetry in Fully Strain-Space Theories of Plasticity,” *International Journal of Plasticity*, Vol. 11, 1995, pp. 679–724.
- [101] Workman, G., Kishoni, D., and Moore, P., *Nondestructive Testing Handbook, Chapter 7, Ultrasonic Testing*, ASNT, Columbus, 2007.
- [102] Negahban, M. and Wineman, A., “The Evolution of Anisotropies in the Elastic Response of an Elastic-Plastic Material,” *International Journal of Plasticity*, Vol. 8, 1992, pp. 519– 542.
- [103] Negahban, M. and Wineman, A., “The Evolution of Material Symmetry in the Elastic Response of a Fully Strain Space Theory of Plasticity,” *Applied Mechanics Division publication, AMD*, Vol. 158, 1993, pp. 19–24.
- [104] Zheng, Q., “On Transversely Isotropic, Orthotropic and Relative Isotropic Functions of Symmetric Tensors, Skew Symmetric Tensors and Vectors. Part I: Two Dimensional Orthotropic and Relative Isotropic Functions and Three Dimensional Relative Isotropic Functions,” *International Journal of Engineering Science*, Vol. 31, No. 10, 1993, pp. 1399–1409.
- [105] Negahban, M., Goel, A., Delabarre, P., Feng, R., and Dimick, A., “Experimentally Evaluating the Equilibrium Stress in Shear of Glassy Polycarbonate,” *ASME Journal of Engineering Materials and Technology*, Vol. 128, 2006, pp. 537–542.

- [106] Negahban, M., Strabala, K., Delabarre, P., Goel, A., Feng, R., and Grenet, J., “Temperature Dependence of the Back-Stress in Shear for Glassy Polycarbonate,” *Macromolecular Symposia*, Vol. 258, 2007, pp. 142–151.
- [107] Sehitoglu, H., “Changes in State Variables at Elevated Temperatures,” *Journal of Engineering Materials and Technology*, Vol. 111, 1989, pp. 192.
- [108] Negahban, M., Goel, A., and Zhang, L., “Evaluating the Development of Elastic Anisotropy with Plastic Flow,” *Acta Mechanica*, (accepted).
- [109] Wang, M. and Guth, E., “Statistical Theory of Networks of Non-Gaussian Flexible Chains,” *Journal of Chemical Physics*, Vol. 20, 1952, pp. 1144.